Appendix 8
Hazard Analysis

Introduction

This appendix includes several components. First is an overall discussion of the Hazard Analysis modeling effort, describing the surge (ADCIRC) and wave (WAM, STWAVE) modeling. That first section is followed by a subsidiary section labeled Appendix 8-1 that defines the many acronyms used in the modeling discussion. This is followed by a major section labeled Appendix 8-2 consisting of the Whitepaper of Donald T. Resio, ERDC-CHL, which forms the basis of the storm statistics and JPM methods discussed in the main body of the report. Owing to its prominence in the discussion, it has, for convenience, been referred to as R2007. Note that R2007, itself, includes several appendices; these are identified as Appendices A-G within Appendix 8-2. Finally, a discussion of the rainfall model is included here as Appendix 8-3.

Hazard Analysis

The hazard analysis required for the risk assessment was based upon the hurricane modeling conducted by a team of Corps of Engineers, FEMA, NOAA, private sector and academic researchers working toward the definition of a new system for estimating hurricane surges and waves. Following is a discussion of the processes used by this team and the steps taken by the risk team to incorporate the results into the risk analysis.

The hurricane hazard definition required as input to the risk analysis involved several steps:

1. Selection of the methodology to be used for estimating surges and waves
2. Determination of hurricane probabilities
3. Production of the ADCIRC grid models for the different HPS configurations.
4. Production of the computer system for development of the large number of hydrographs required by the risk model.
5. Formatting of the ADCIRC/STWAVE hydrographs for input to the risk computer model
6. Determination of the rainfall volumes expected for each hurricane

The hurricane modeling resulted in a total of 152 storms that were used in the risk analysis. Of these storms, frequencies were developed by the storm team for only 77 storms. The storm parameters and there frequency of occurance are shown in Table 8-1.

Methodology for Hurricane Modeling

At least five methods have been applied in past studies of environmental extremes due to hurricanes in the United States:

1. Formulation of design storm events
2. Estimates based only on historical storms
3. The empirical simulation technique (EST)
4. The joint probability method (JPM) and
5. The Empirical Track Model

All of the methods referenced above have different strengths and weaknesses for various applications. Appendix 2 (R2007) includes a complete discussion of each of these methods. It considers includes the following topics:

1. Potential extensions of probabilistic methods to future hurricane surges,
2. The JPM with Optimal Sampling (JPM-OS); and
3. A computational methodology for effective simulation of storm surges for hurricane inundation studies.

In each method, it is important to understand that two different statistical measures are required to characterize the expected extremes over an interval of time. The first of these is the measure of the expected values of the distribution and the second is a measure of expected dispersion around these central values.

Hydrograph Production System

Overview

On-going projects for storm-surge and inundation mapping along the US Gulf of Mexico coast require the computation of many simulations using state-of-the-art numerical models and high-performance computational facilities. In this context, the storm-surge model ADCIRC and spectral wave model STWAVE are used in a “coupled” scenario to improve upon the storm surge solutions provided by ADCIRC. Coupling of the models is done through input/output file exchange between the numerical models. The water level and wind field from ADCIRC are provided in the appropriate form for the spectral wave model STWAVE. STWAVE computes the high-frequency wave field, including the wave radiation stress associated with the storm (wind) and simulated water level. This wave radiation stress is then passed to the next ADCIRC simulation as an additional forcing term, in conjunction with the storm wind and pressure field. This model communication through file I/O achieves a first-order coupling of the non-linear interaction between the wind-induced storm-surge and the wind-driven higher frequency wave fields.

The primary difficulty with the large number of compute-resource-intensive simulations required by these projects is ensuring that each simulation uses the correct files and that the compute-jobs run to completion with as little intervention as possible. Avoiding human interaction is critical to prevent errors in file input, compute-job staging, and post-processing. To address this problem, a software system has been developed to prepare each required simulation and submit each simulation to the compute-resource job manager. Basic graphics/visualizations and archiving are included to aid in QA/QC procedures and permanent storage of the computed results.

This document describes the software production system developed for coupled ADCIRC/STWAVE simulations. The software manages the gathering and preparation of input files for the ADCIRC/STWAVE models, and writes the job control script that the user submits to the host machine job manager (e.g., LSF, PBS, LoadLeveler). The production management software is written in the scripting languages ***perl*** and ***bash***. Technical details of the script procedures and operations are reported in a separate technical report.

The primary requirements for the production system are independently verified and validated numerical models; tested and verified model grids; and runtime inputs to the models (forcing functions). Input files that provide initial conditions and forcing functions to the ADCIRC/STWAVE system are required to be pre-computed. This includes the storm realization (wind and pressure fields computed by the Ocean Weather PBL model) and the wave energy spectra for each storm (computed by the WAM model and interpolated onto the STWAVE model boundaries).

Computer system

The components of the production system are independent of the UNIX HPC computer system used, and can be set up on any system with accessible processing elements, large disk and storage capacity, and a job controller (Load Sharing Facility, Portable Batch System, LoadLeveler, etc). The scripting language ***perl*** and shell language ***bash*** must exist on the computer system (which is generally the case on Linux-based systems). Additional software packages (GNUplot, GMT) are used to facilitate post-simulation graphical analysis of the solutions.

The production system has been developed on the ERDC Cray XT3 (Sapphire) and the University of Texas Dell cluster LoneStar. However, the system is easily portable to other high-performance computing facilities with minor changes to the scripts and job controller/manager configurations. This has been tested several times on the following system/job scheduler combinations: NAVO IBM P5 (*Babbage*)/LSF, LONI IBM P5 (*Neptune*)/LoadLeveler, Cray Research Cray XT3 (*Salmon*)/PBS.

For the 2005, 2007, and 2010 (LACPR) simulations, the ERDC Cray XT3 *Sapphire* and University of Texas Dell cluster *LoneStar* were used for the computations. The only required changes to the scripts and setup are the specification of different job control parameters and a different home directory for the system. The basic computer system characteristics for *Sapphire* and *LoneStar* are shown in Table A.

Table A: Basic configurations of the High-Performance Computer systems used for the LACPR storm-surge simulations. On 9 April, 2007, the ERDC Cray XT3 Sapphire returned to service after a major hardware upgrade and several related software changes. Its current configuration is indicated in parentheses in the table.

System	ERDC Cray XT3 *Sapphire*	University of Texas Dell *LoneStar*
Operating System	SUSE Linux & UNICOS/lc	CentOS Linux
Compute-Nodes	AMD Opteron 2.6GHz single-core, single-processor (dual core, single-processor)	Intel Xeon 5100 series 2.66GHz dual-core, dual-processor
Number of Nodes/Processors	4176/4176 (4096/8192)	1300/5200
Parallel Filesystem (/work)	Lustre	Lustre
Compute-Job Controller	LSF (PBS)	LSF
Website	*www.erdc.hpc.mil*	*www.tacc.utexas.edu*

Numerical Models in the Production System

The "coupled" approach to the required storm-surge solutions uses the shallow-water finite element surge model ADCIRC (Luettich and Westerink, 2004) in conjunction with the steady-state spectral wave model STWAVE (Smith et al, 2001). Software versions are 46_48 and greater, and ep_110306 and greater, for ADCIRC and STWAVE respectively. Figure A shows the extents of the three models' grids. The ADCIRC grids (boundary drawn in black) cover the western North Atlantic Ocean, with the only open boundary at 60 deg west. All ADICRC grids in this project use the same footprint and general coverage. Only the details in the Louisiana and surrounding regions differ. The Ocean Weather PBL model boundary is shown in red, covering the Gulf of Mexico and 0.05 degrees resolution. ADCIRC interpolates the PBL grid to the ADCIRC grid and pads the far-field extent with background values. The STWAVE grid boundaries (blue) are shown along the Louisiana, Alabama, and Mississippi coasts. The Lake Pontchartrain domain is barely visible at this scale.

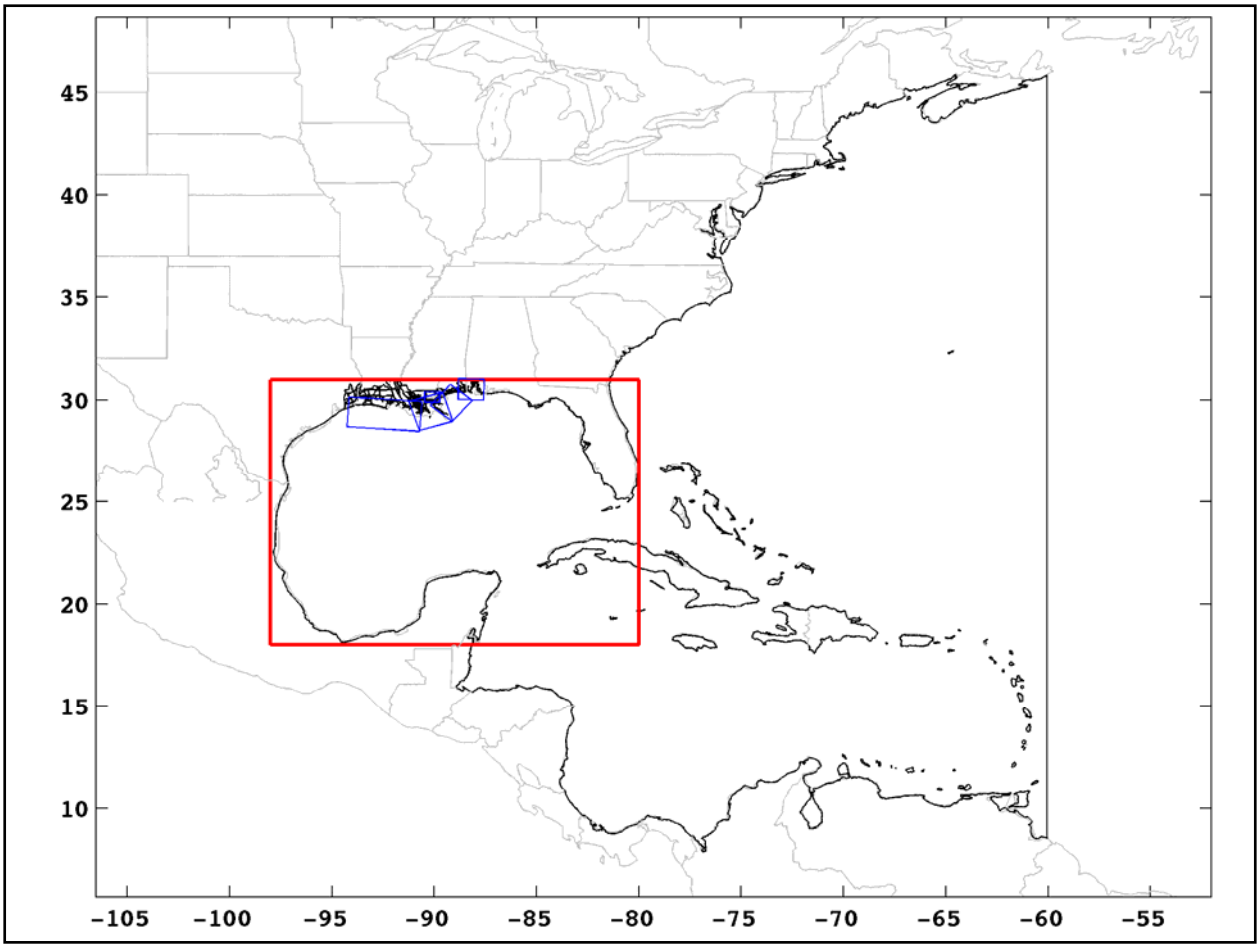

Figure A. Footprints of the various model domains for the coupled ADCIRC/STWAVE system. ADCIRC, OWI/PBL, and STWAVE grid boundaries are shown in black, red, and blue respectively.

Surge Model – ADCIRC

The storm surge model ADCIRC is a state-of-the-art model that solves the generalized wave-continuity equation on linear triangular elements. The depth-integrated (2D) implementation is used, where the water level and depth-averaged velocity are solved for at each triangle vertex (node), after complete specification of the initial conditions and time history of the boundary conditions (forcing). The finite element grids used in this project are the SL15 grid sequence for the 2005, 2007, and 2010 levee configurations. There are approximately 2.1 million horizontal nodes and 4.2 million elements in this sequence of grids. Ninety percent of the computational grid nodes are within the region shown in Figure B1. The computational domain is decomposed into 256 sub-domains, and each sub-domain problem is allocated to a separate computing processor. Inter-domain communication of boundary data is handled through MPI. Each solution is computed with a timestep of 1 second. A detail of the finite element grid is shown in Figure B2 for the New Orleans East area.

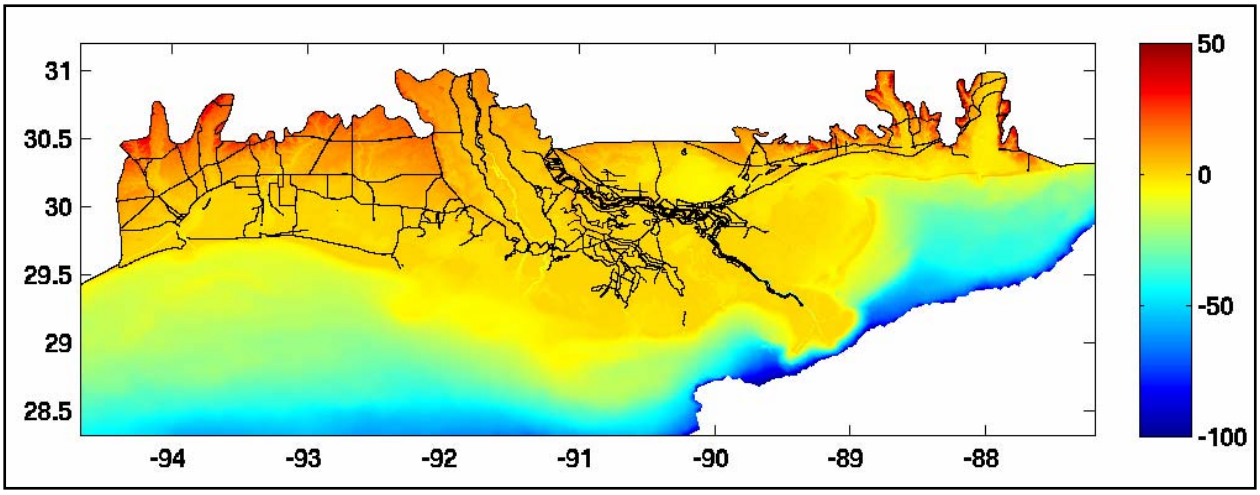

Figure B1. ADCIRC bathymetry (in meters) for the SL15 grids along the northern Gulf of Mexico coast. In this image, the bathymetry is clipped at -100 meters for display purposes. Each of the SL15 grids, for the 2005, 2007, and 2010 simulation sets has details that are not discernable at this scale shown.

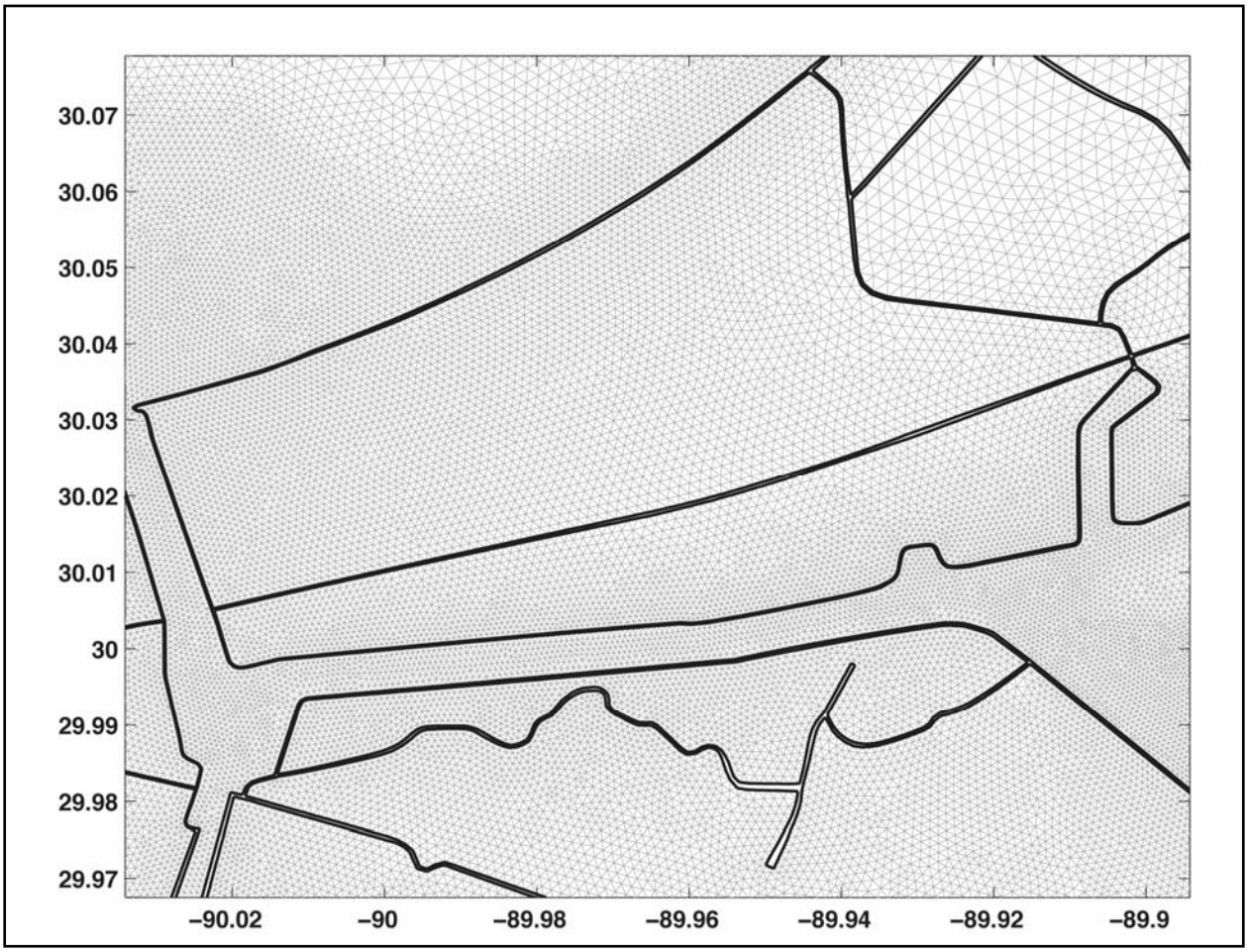

Figure B2. ADCIRC grid detail in the New Orleans East area. The solution is computed at the vertex of each triangle, and the thick black line is the model boundary. Weir boundary conditions are applied at the boundaries shown in this image.

Wave model – STWAVE

Five STWAVE grids are used in the current production system implementation covering the Louisiana, Mississippi and Alabama coastal region. (The "west" W grid is not used for the LA EAST simulations.) The boundaries of the domains are shown in Figure C. The spatial resolution of each STWAVE grid is 200 meters, and the temporal resolution is set to 30 minutes. The parallel STWAVE implementation is used in this system. In this version, each wave field snapshot is solved for on a separate processing element (cpu). The half-plane STWAVE is used for the South (S), Mississippi-Alabama (MS-AL), Southeast (SE) and West (W) grids. The full-plane STWAVE model is used for the Lake Pontchartrain domain.

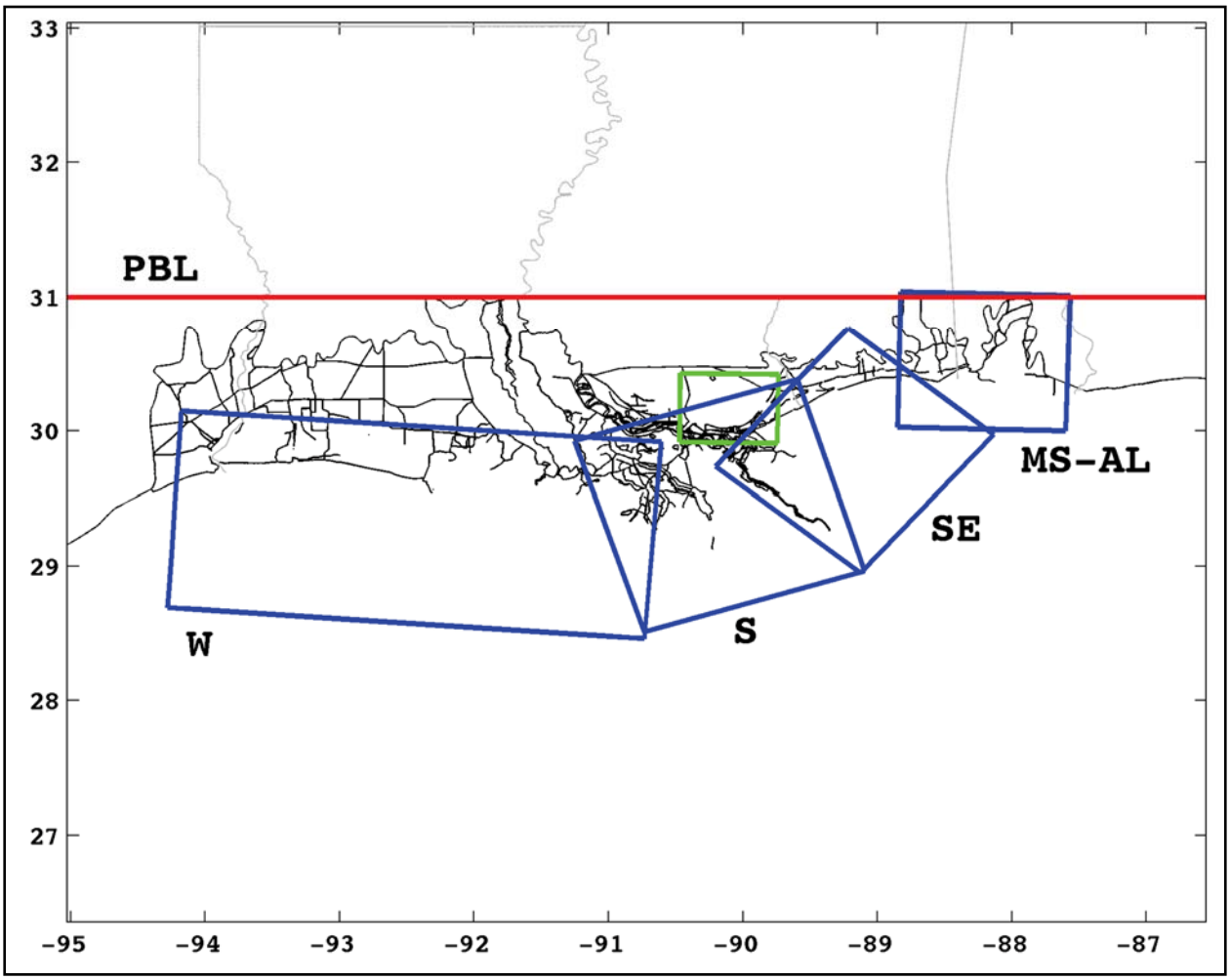

Figure C. Boundaries of the five STWAVE model domains and the PBL wind model northern extent (red) used in the current implementation of the production simulation system. The ADCIRC grid boundary is also shown (black) for one of the production grids. The Lake Pontchartrain (in green and not labeled) simulations use the full-plane STWAVE version; the other domains use the half-plane STWAVE. The "W" west grid is used in the LAWEST simulations, but not in the LAEAST simulations. The actual STWAVE grids to use for a specific simulation are a configurable part of the system.

Initial Condition to Storm Simulations (River Spinup)

The initial condition for the storm-surge simulations is an ADCIRC solution that provides a background river discharge on the Mississippi and Atchafalaya Rivers. River inflow to the Mississippi River at Baton Rouge and to the Atchafalaya River at Simmesport is specified as a flux per unit width as defined by a wave radiation boundary. The radiation condition is based on the relationship between the normal flow and elevation at the boundary. The river condition is spun up for 2.0 simulation days, with forcing of normal flow specified at the head of the rivers. A two-day spin up period with a half-day hyperbolic ramping function is applied to the river boundary forcing prior to any additional model forcing. While the solution has not quite reached a steady state after this period, the subsequent wind-driven solutions continue this river spinup, and the river stages reach steady state over the next simulation day. The water elevations at the default sampling locations within the two rivers are shown in Figure D. This initial condition is a pre-computed requirement to each storm-driven simulation.

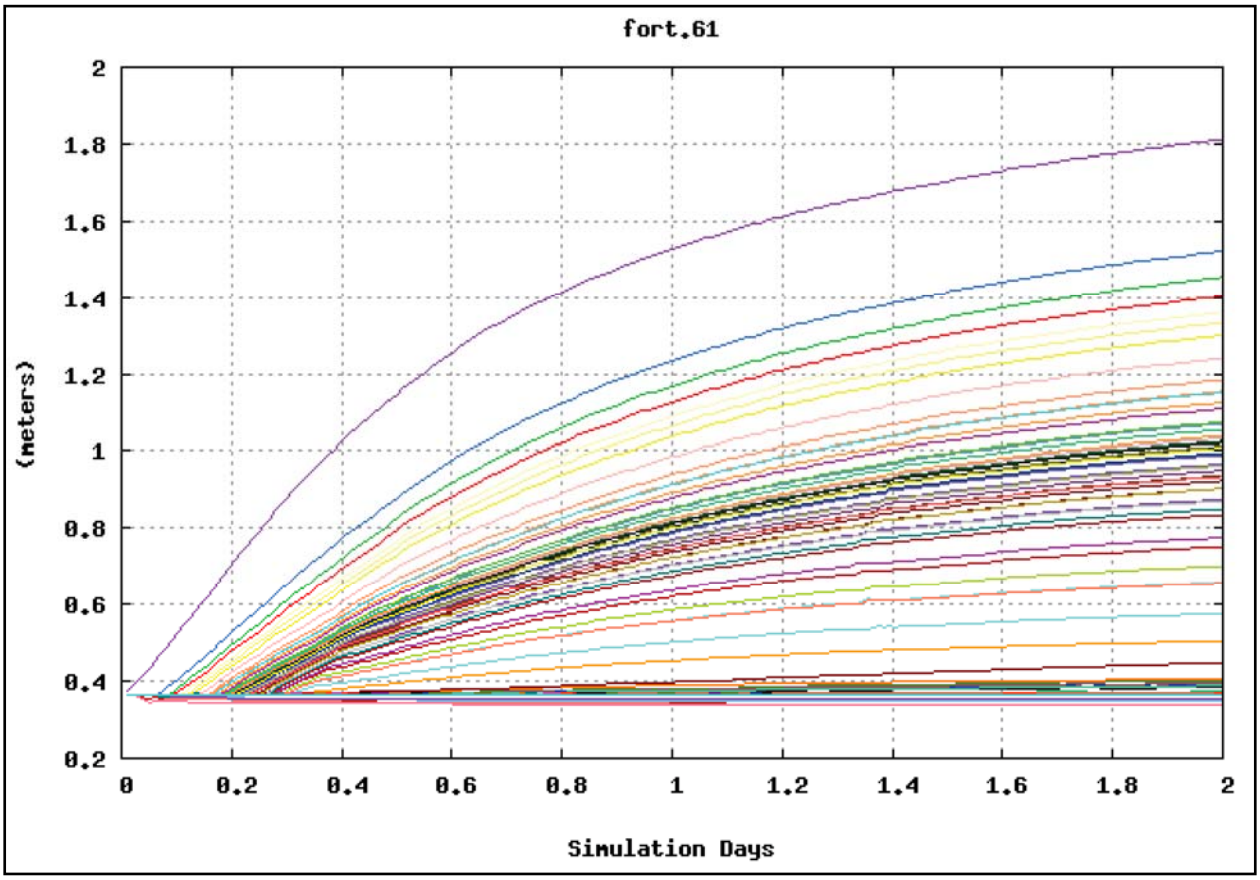

Figure D. Water elevations along the Mississippi and Atchafalaya Rivers showing the spinup of the initial condition. This solution is driven by volume fluxes across the open boundary on the two rivers. The discharge is ramped up over the first 0.5 days. The maximum elevation reached at the top of the Mississippi River is 1.84 meters.

Wind Fields for Storms

The primary inputs to the production system are the wind and pressure fields generated by application of the Ocean Weather Planetary Boundary Layer (PBL) model. The boundary of this domain is shown in Figure A1. Each storm/simulation must be represented by wind and pressure field files (WND/pre) in PBL format, ready to read by ADCIRC and as specified by the parameter NWS=+/-12,212 in the fort.15 file. For the LACPR storms, the WND/pre fields were pre-computed, external to the production system and assumed to exist as input to the system. An example of the WND/pre fields is shown in Figure E for LACPR storm number 042 (TPOC: Jay Ratcliff, USACE/MVN).

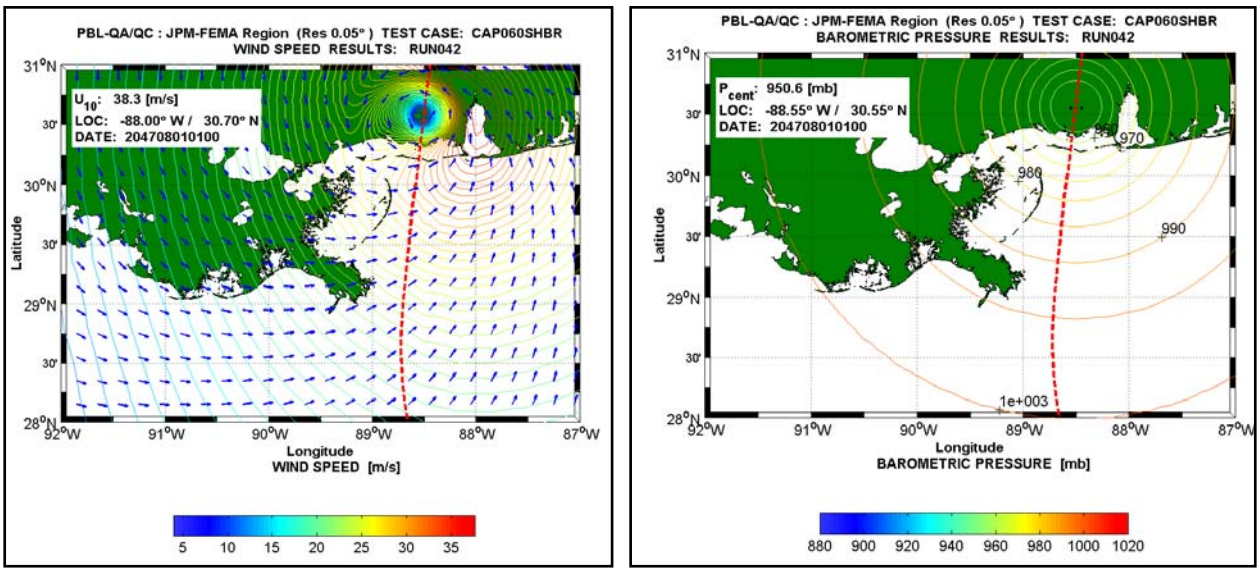

Figure E. Wind (left) and pressure (right) fields for LACPR storm 042 at landfall. The storm track is shown with the dashed, red line. The fields are computed with the Ocean Weather Planetary Boundary Layer (PBL) model, and are used to drive the far-field wave model WAM and ADCIRC. The wind field information is passed to STWAVE through the ADCIRC global output wind file fort.74.

The WND/pre files must be placed in the $PSHOME/winds directory to be detected by the production system. In the USACE/LACPR specification of the production system, the landfall date is YYYYMMDDHHMN, where the year is arbitrary and MMDDHHMN is 08010200 (2AM on 01 August). This landfall date is conveyed to the production system scripts by specifying it in system control file (ProdSysDef.pm). It is also assumed that the storm center continues past landfall time for 24 hours. The pre-landfall time length is arbitrary. A graphic timeline is shown at the top of Figure F.

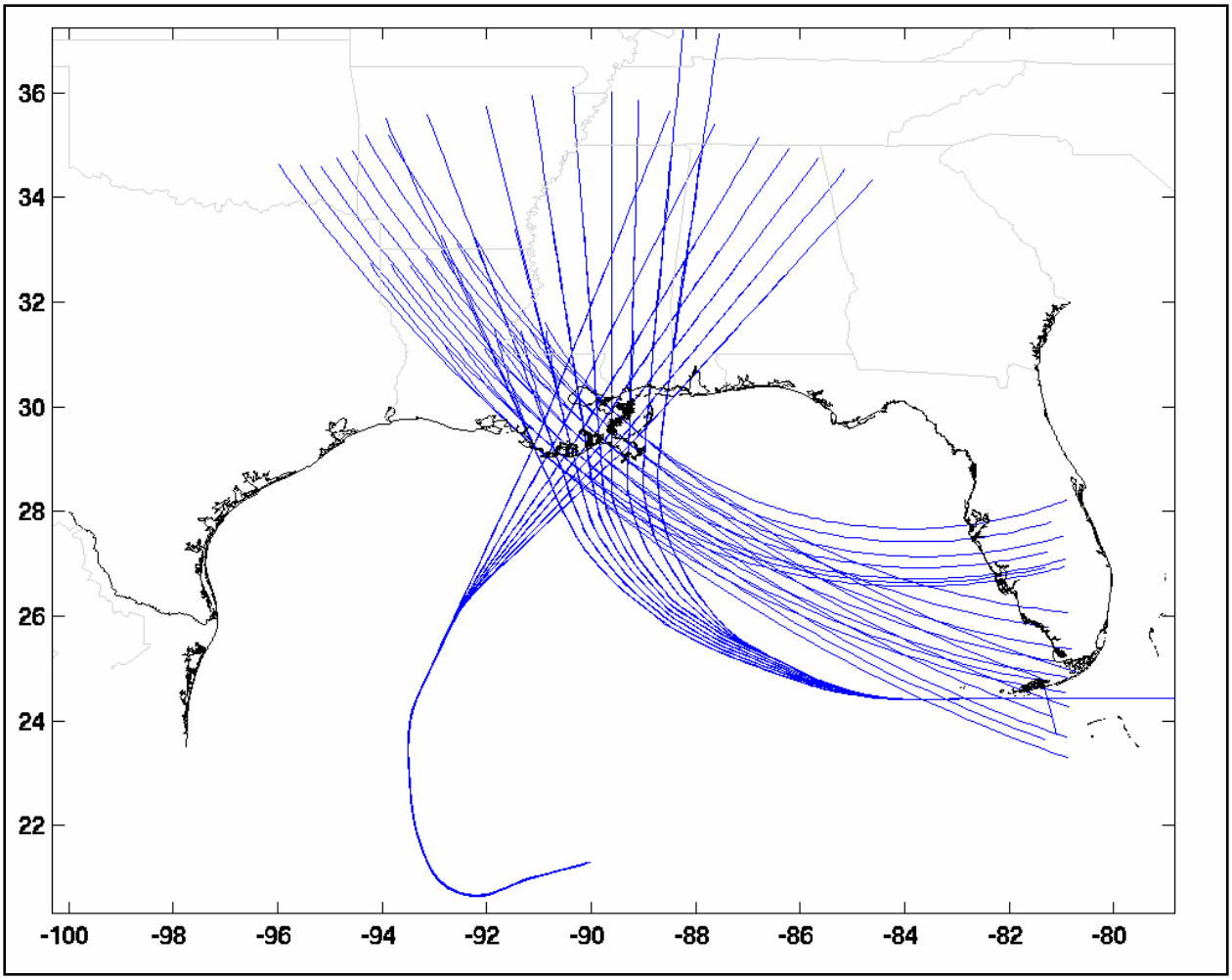

Figure F. Tracks used to define the 152 LACPR storms. Hurricane parameters vary along the tracks, and provide the input to the Ocean Weather PBL wind/pressure field model. This provides the storm forcing required for each production system simulation.

There are 152 storms defined, each of which has a corresponding PBL WND/pre field. The storms are specified by variations of the hurricane parameters along the tracks shown in Figure F. The details of the storm parameter specification are described elsewhere in the technical documentation for this project.

Wave Field Boundary Conditions for STWAVE

All of the half-plane STWAVE grids (the full-plane STWAVE version is used for Lake Pontchartrain) require specification of the wave spectral characteristics on the open boundary. These boundary condition sets are pre-computed by running the WAM ocean wave model for each storm and extracting the wave energy spectra from the WAM solutions at the STWAVE open boundary node locations. The WAM-to-STWAVE procedure is applied for each of the storm wind/pressure fields, and the results are made available to the production system (WAM TPOC: Robert Jensen, USACE/ERDC-CHL).

Solution Sampling Locations

Each ADCIRC storm-surge simulation produces water level timeseries, both for the global model domain and for pre-defined station locations. In the current system implementation, the pre-defined sampling locations are shown in Figure G. There are three sets of points; for LACPR (blue), MSCIP (magenta), and IPET (red). The IPET locations correspond to reach locations as defined in the IPET risk model system definition files. The station output from each solution can be visualized using the post-processing code plotofort61.pl. This ***perl*** script generates a timeseries plot using ***GNUplot*** to be used for quick inspection of the fort.61 results. The timeseries plot for the ADCIRC3 (step 4) part of the process is shown in Figure G for storm 042.

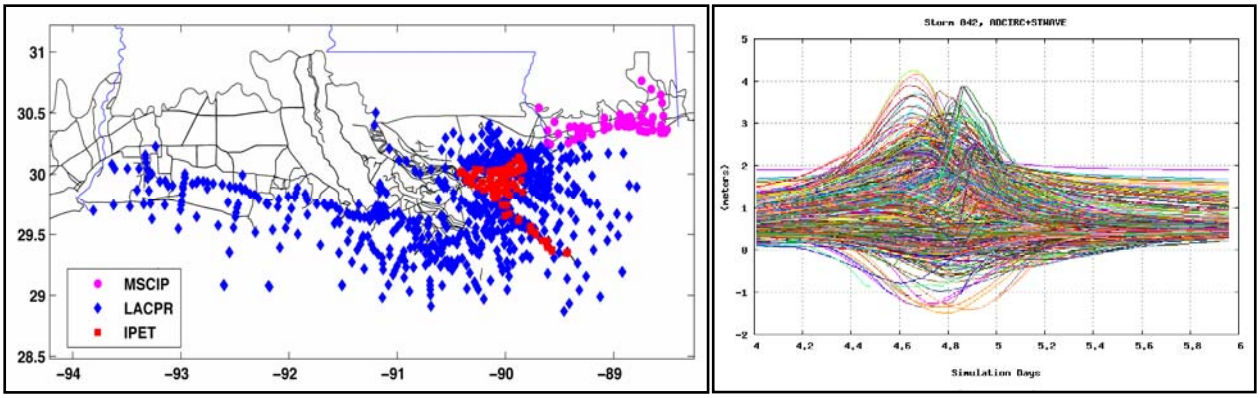

Figure G. Left) ADCIRC solution sampling points that define the station output in the fort.61 file. The global model solution is interpolated to these locations and output for visualization and analysis. Right) Hydrograph plot generated by plotfort61.pl, for the ADCIRC3 step of the production system, for LACPR storm 042.

Solution Procedure (Process Management)

Each simulation is performed in four computational parts, as shown in the "Production Steps" part of Figure H. The initial conditions (River Spinup), PBL wind and pressure fields, and the wave energy spectra boundary conditions (as computed by WAM) are all required inputs to the system.

1. **ADCIRC1:** Each simulation is started from the River Spinup (ADCIRC0). ADCIRC is run from the start of the PBL wind field to 24 hours prior to landfall of the storm (ADCIRC1, River+Winds). The model state is output to disk to provide initial conditions for continuation of the simulation (step 2), and for the subsequent rerun of step 2 that includes wave radiation stresses from STWAVE (step 3).

2. **ADCIRC2:** The ADCIRC1 solution (River+Winds) is then continued to the termination of the PBL wind/pressure fields. The ADCIRC2 global water level (fort.63) and wind field (fort.74) are output for QA/QC as well as to provide to STWAVE as input.

3. **STWAVE:** The ADCIRC2 solution in step 2 is interpolated to the STWAVE domains, and each STWAVE domain is executed to generate wave radiation stress gradients for input back to ADCIRC in step 4.

4. **ADCIRC3:** ADCIRC2 is re-run over the same time period as in step 2, but including the wave radiation stress gradient computed by STWAVE and interpolated onto the ADCIRC grid. This is the River+Winds+RadStress solution and is also referred to as the ADCIRC+STWAVE step.

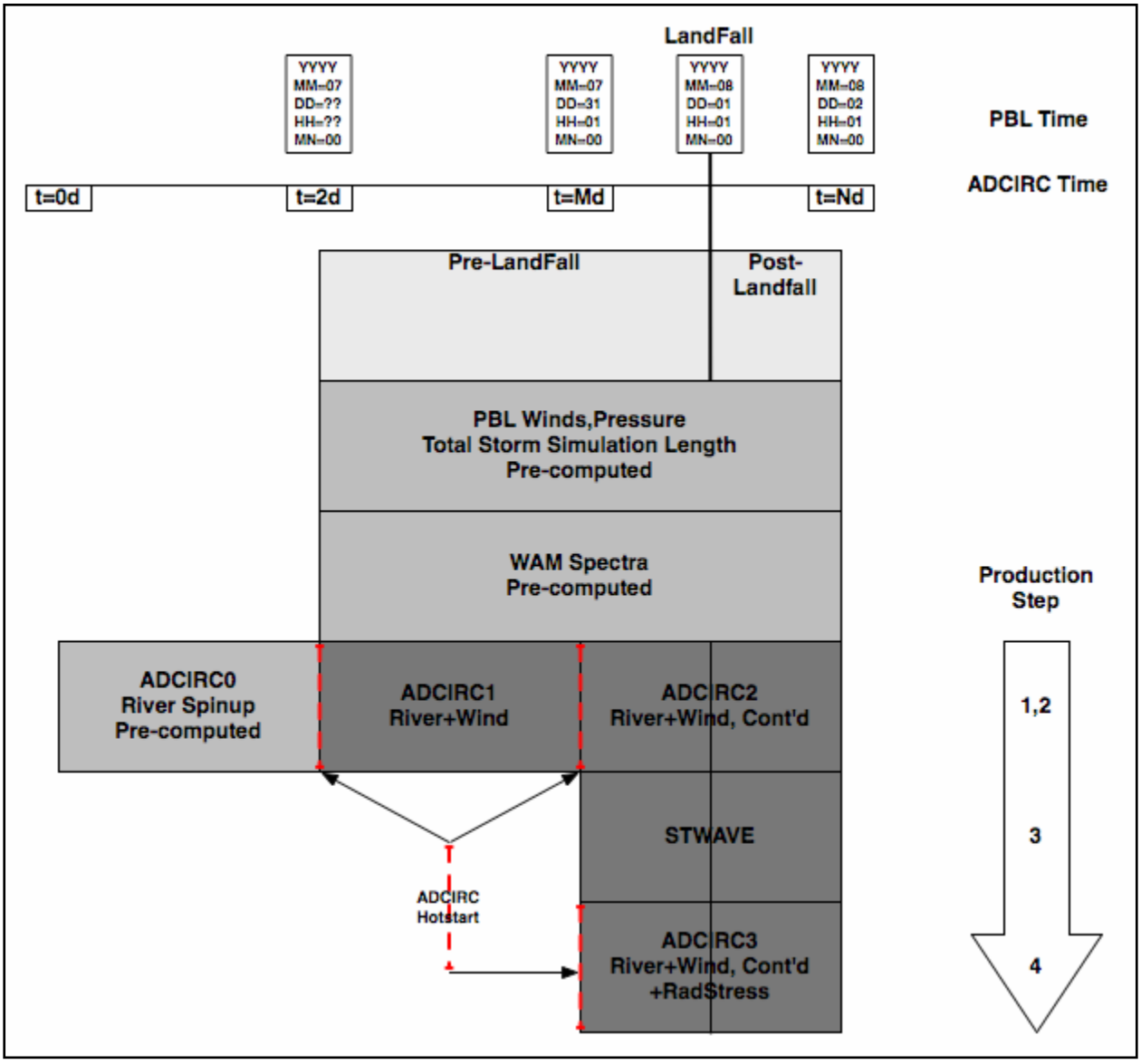

Figure H. Timeline for Production System simulations. The timeline for the wind forcing (PBL) is shown at the top. PBL winds and pressures are used to drive both the WAM wave model and the ADCIRC/STWAVE simulations. Specification of the PBL and WAM fields is a required input to the Production System.

These four steps are coordinated by a ***perl*** script (prep_prod_sim.pl) that organizes the directory structure for each run, gathers the needed input files (grids, initial conditions), edits the files for the specifics of the current simulation, and writes a job control file for the high-performance computer system job controller (PBS on the ERDC Cray Sapphire and LSF on the Uni. of Texas Lonestar Dell cluster). The data file flow controlled by this script is shown in

Figure I. To stage a specific simulation, this script is executed with the storm number specified on the command line.

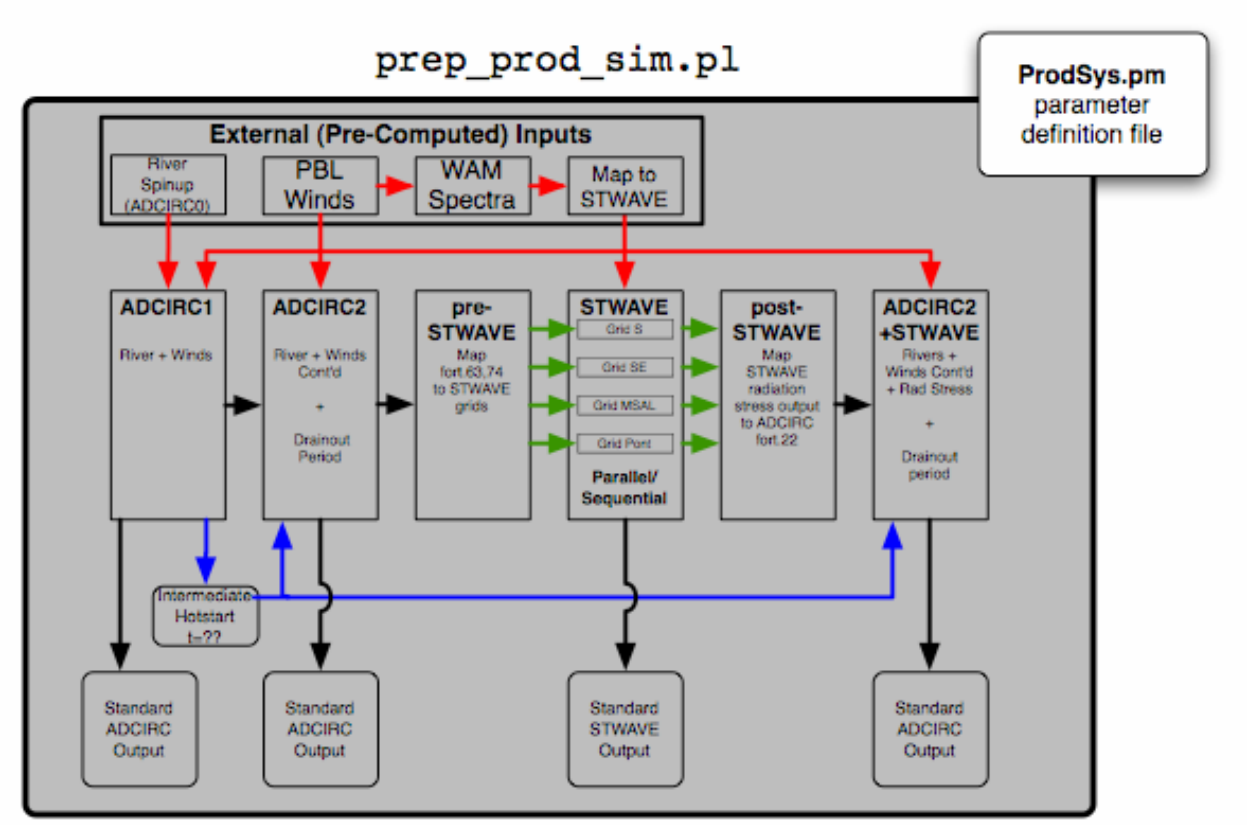

Figure I. Data flow controlled by the production system script prep_prod_sim.pl. Pre-computed inputs are shown at the top with red arrows. The middle row of boxes corresponds to the four steps, where the STWAVE step includes interpolation from ADCIRC to the STWAVE grids, the STWAVE simulations, and the interpolation back to ADCIRC. ADCIRC2+STWAVE is the "ADCIRC3" step. Blue lines indicate the ADCIRC hotstart file process. Parameters that are the same for all simulations are defined in the ProdSysDef.pm file and read by prep_prod_sim.pl at runtime.

Katrina Simulation with PBL Wind Field

A comparison of the observed high-water marks (HWMs) to ADCIRC+STWAVE solutions is shown in Figure J, for the surge that accompanied hurricane Katrina. Two ADCIRC solutions are shown.

The verification solution, forced by the Ocean Weather 95% best-estimate winds, is compared to the observed HWMs (in blue). The overall agreement is very good, with the best-estimate winds solution explaining 94% of the observed HWM variance (r^2=.94, S_e=1.5). The ADCIRC3 solution forced by the Ocean Weather PBL wind and pressure field is shown in red. The agreement is also very good (r^2=.88, S_e=2.1).

For each solution, the best-fit line is shown, colored the same as the data points, as well as the 95% confidence region about the data.

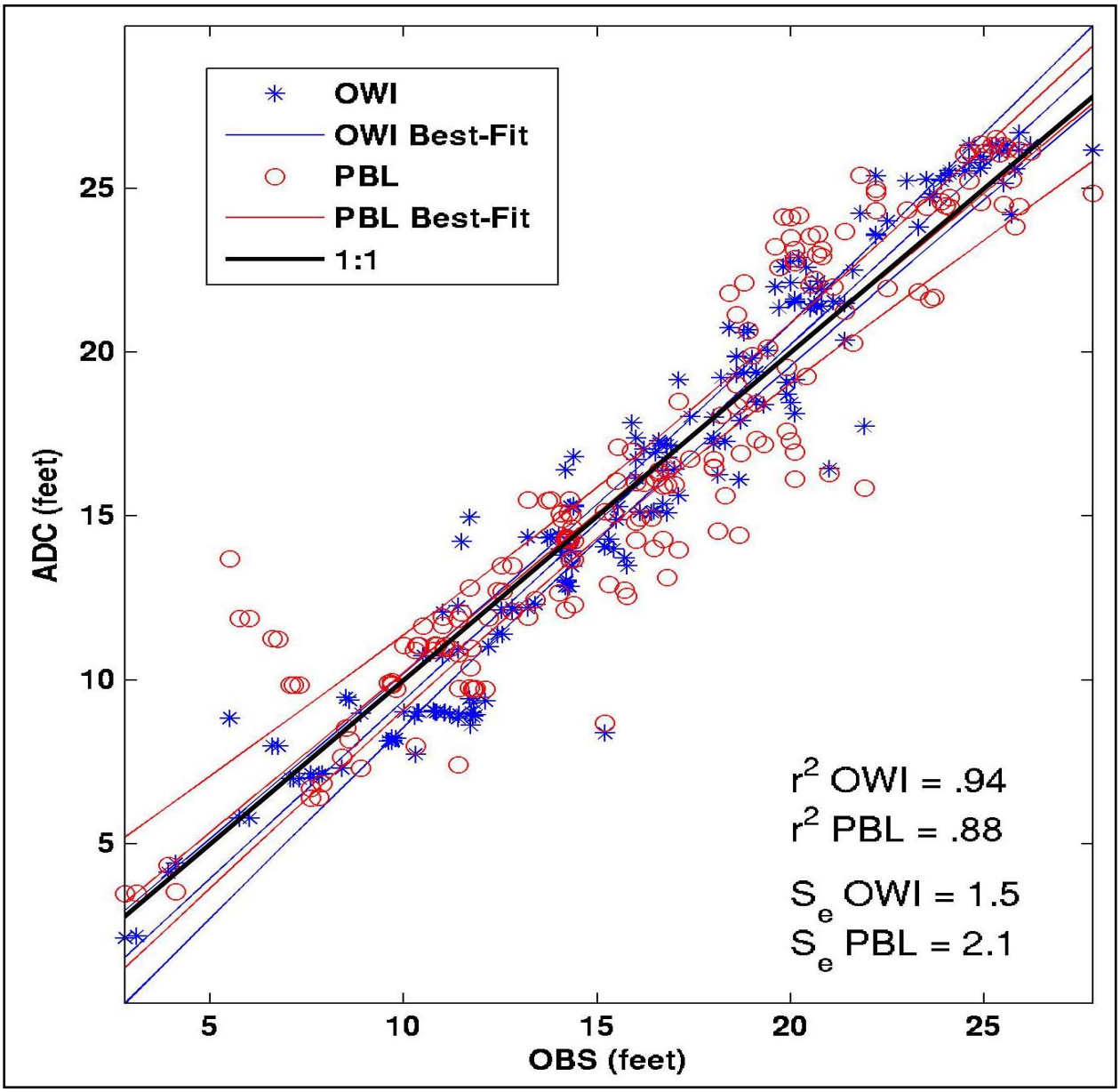

Figure J. Comparison of observed High Water Marks (HWM) for hurricane Katrina, and the Production System Katrina simulation using the PBL wind and pressure fields (red). Also shown is the comparison between the observed HWMs and the verification solution forced by the Ocean Weather 95% wind and pressure field (blue). Observations are on the abscissa, and the ADCIRC3 values are on the ordinate.

References

Luettich, R., and J. Westerink. *Formulation and Numerical Implementation of the 2D/3D ADCIRC, Finite Element Model Version 44.XX*, 2004. *http://adcirc.org/adcirc_theory_2004_12_08.pdf*

Smith, J., A. Sherlock, and D. Resio. *STWAVE: Steady-State Spectral Wave Model User's Manual for STWAVE Version 3.0,* Tech Report ERDC/CHL SR-01-1, 2001. *http://chl.erdc.usace.army.mil/Media/2/4/4/erdc-chl-sr-01-11.pdf*

Appendix 8-1
Acronyms

ADCIRC	ADvanced CIRCulation model for shallow seas
CHL	Coastal Hydraulics Laboratory
ERDC	Engineer Research and Development Center
GMT	Generic Mapping Tools; open-source plotting package used for post-processing graphics generation
HWM	High-water mark
HPC	High-performance computing
I/O	Computer input and output
IPET	Interagency Performance Evaluation Task force
LACPR	Louisiana Coastal Protection and Restoration project
LONI	Louisiana Optical Network Initiative
LSF	Platform Computing's Load Sharing Facility (LSF) job scheduler
MPI	Message-passing interface; parallel programming model used by ADCIRC and STWAVE
NAVO	NAVal Oceanographic computing facility
PBL	Planetary boundary layer model of Ocean Weather Inc.
PBS	Portable Batch System job scheduler
QA/QC	Quality assurance/quality control
STWAVE	STeady-state spectral WAVE model
WAM	NOAA large-scale wave model

Appendix 8-2 (R2007)
(May 27, 2007)
White Paper on Estimating Hurricane Inundation Probabilities

Written by: Donald T. Resio, Senior Scientist, U.S. Army Corps of Engineers, ERDC-CHL
Incorporating contributions, discussions, data, and comments by: (in alphabetic order) Stanley J. Boc (ERDC-CHL), Leon Borgman (private consultant), Vincent J. Cardone, (Oceanweather, Inc), Andrew Cox (Oceanweather, Inc.), William R. Dally (Surfbreak Engineering), Robert G. Dean (U. of Florida), David Divoky (Watershed Concepts), Emily Hirsh (FEMA), Jennifer L. Irish (Texas A&M University), David Levinson (NOAA's National Climatic Data Center), Alan Niedoroda (URS Corporation), Mark D. Powell (NOAA's Hurricane Research Division, AOML), Jay J. Ratcliff (USACE-MVN), Vann Stutts (USACE-MVN), Joseph Suhada (URS Corporation), Gabriel R. Toro (Risk Engineering), Peter J. Vickery (Applied Research Associates), and Joannes Westerink (U. of Notre Dame)

Introduction

Over the last several months, a team of Corps of Engineers, FEMA, NOAA, private sector and academic researchers have been working toward the definition of a new system for estimating hurricane inundation probabilities. This White Paper is an attempt to capture the findings and recommendations of this group into a single document.

At least five methods have been applied in past studies of environmental extremes due to hurricanes in the United States:

1. Formulation of design storm events
2. Estimates based only on historical storms
3. The empirical simulation technique (EST)
4. The joint probability method (JPM) and
5. The Empirical Track Model

In each method, it is important to understand that two different statistical measures are required to characterize the expected extremes over an interval of time. The first of these is the measure of the expected values of the distribution and the second is a measure of expected dispersion around these central values.

All of the methods referenced above have different strengths and weaknesses for various applications. To help understand these, a brief discussion of conventional applications of these methods in the past will be given before moving on to a discussion of the approach recommended for future hurricane surge applications. This will be followed by sections that treat the following:

1. Potential extensions of probabilistic methods to future hurricane surges,
2. The JPM with Optimal Sampling (JPM-OS); and
3. A computational methodology for effective simulation of storm surges for hurricane inundation studies.

As will be discussed in this paper, two methods, the EST (or some other variation of the historical storm method) and the JPM, were both considered viable at the outset of our investigations. Based on all of the available advantages and disadvantages in these different methods that are discussed here, it was initially recommended that a modified version of the JPM be used for estimating probabilities of hurricane surge inundation, rather than the EST approach. Since the original selection of the JPM-based methods for application along the U.S. Gulf coast, two papers have had the opportunity to examine the relative performance of the EST and JPM for this purpose (Divoky and Resio, 2007; Agbley and Basco, 2008). Both of these papers present substantial evidence that the JPM provides much more stable estimates of hurricane inundation probabilities than the EST, which provides additional confirmation for the selected methodology.

Formulation of Design Storm Events

An example of this approach applied to coastal inundation is the Standard Project Hurricane. This approach was adopted by the Corp of Engineers in the 1960's to estimate potential surge hazards along many U.S. coastlines. Due to the paucity of data, it would have been very difficult, if indeed possible, to investigate detailed characteristics of landfalling hurricanes prior to 1960; consequently, the Corps requested that NOAA prepare an estimate of a storm with characteristics that were expected relatively infrequently within some stretch of coastline. Unfortunately, the period prior to 1960 (the input to the statistical analyses performed by NOAA) was a period of relatively low hurricane activity in the Gulf of Mexico; consequently, the SPH, as specified in those earlier studies, is not representative of the characteristics of extreme storms that have occurred in the Gulf since 1960.

In the past, the design storm approach has typically utilized a single storm to characterize environmental factors for design at a given location. This effectively reduces the number of degrees of freedom in storm behavior to one parameter, typically the intensity of the storm. All other storm parameters (for example: storm size, forward storm speed, and track location) are deterministically related to storm intensity. The major problem with this is that, if a second factor (such as angle of storm approach to the coast, storm duration or river stage) significantly affects design conditions and/or considerations, the design storm approach cannot accurately capture all aspects of the storm that affect the design. An extrapolation of the single design storm concept is to define a small set of storms with some range of additional parameters considered. This defines a set of storms that can be used to examine various design alternatives in an efficient manner, while retaining some additional degrees of freedom within the analysis. Because of their use in this context, these storms are often termed "screening storms" rather than design storms.

Estimates Based only on Historical Storms

If at least one sample from a population of interest occurs within each year, it might be possible to apply statistical methods that utilize annual maxima to formulate the stage-frequency curves at a site. However, it is clear that such a situation cannot be well characterized by conventional asymptotic methods which assume many samples in a population occur annually. Since hurricanes are both relatively infrequent and relatively small in terms of the amount of coastline affected by these storms each year, the frequency of storms affecting a site is typically significantly less than 1 storm per year. As an example of this, Figure 1 provides an estimate for the frequency of severe hurricanes (greater than Category 2 intensity) per 1-degree by 1-degree (area) per year for the Gulf of Mexico.

Another sampling problem related to the use of historical storms for specifying extremes is the tendency for intense storms to behave differently than weaker storms. To compensate for this sampling inhomogeneity, many oil-industry groups have adopted the "Peaks Over Threshold," or POT method for estimating extremes. In this approach, only storms above some threshold value are considered within a statistical analysis of extremes. By screening small storms from the analyzed sample, the effect of small storms on the parameters of fitted distributions (e.g. the parameters of the Gumbel, Frechet, Weibull, Lognormal, Log Pearson or other distributions of choice) is minimized. This approach is inherently parametric due to the need to assume/specify a distribution (or class of distributions such as the Generalized Extreme Value method).

Another potentially more serious problem with the reliance only on historical storms for estimating coastal inundation is related to the small sample of storms at any site. As can be seen from Figure 1, even in the vicinity of New Orleans, the frequency of major storms passing within a given 60 nautical mile region (1-degree) is only about once every 20-25 years. Since we have limited records beyond the middle of the 20th century and since the frequency of storms in the latter half of the century may be markedly different than the frequency of storms in the early part of the century, the historical record for a direct hit (taken here for simplicity as ±30nm of a site) would include on the average only about 2-3 storms. Given this small potential sample size, sampling variability can lead to very unrealistic variations in storm frequency and intensities along the coast. For this reason, methods for estimating coastal inundation based solely on historical analyses should not be used for coastal hazard assessment. This point is also pertinent to arguments that the use of historical records for extremal estimation is also difficult to justify in many other, non-coastal applications.

The Empirical Simulation Technique (EST)

Statistics of Expected Extremes

Conventionally, the EST was used as an approach for estimating the expected extremal distribution for surges based on a variation of the "historical record" approach (Borgman *et al.*, 1992; Scheffner *et al.* 1993). In this approach a set of storms above some threshold affecting a particular area are hindcast, similar to the approach used within the POT method. The primary difference is that typically the largest 1 or 2 storms is re-run over a number of track variations in

order to distribute the effects of the storm over a wider area. Unfortunately, the rules for this re-distribution of tracks were developed only after some preliminary applications of this approach and tend to be somewhat arbitrary. Results from computer simulations at each point of interest are then ranked and assigned a cumulative distribution value via a formula that links the rank to the cumulative distribution function, F(x), which is be abbreviated as CDF is subsequent discussions,

$$F(x) = \frac{m}{N+1} \tag{1}$$

where m is the rank of the storm (with m=1 as the smallest) and N is the total sample number. This is converted to a measure of recurrence via the use of a Poisson frequency parameter, λ

$$T(x) = \frac{1}{\lambda[1-F(x)]} \tag{2}$$

where T(x) is the expected return period for x. For example, if we hindcast 50 storms from an interval of 100 years, the value of λ would be 0.5; and the estimates of T(x) would span the range from slightly over 100 years to slightly over 2 years.

In the interior of the ranked points, the EST assumes that the best estimate of the expected distribution is the sample itself and does not fit any parametric distribution to the central distribution in order to obtain a "smoothed" distribution. Thus, within this interior range, the distribution is nonparametric. If one is interested in return intervals outside of the range covered by the ranked sample points, it is necessary to invoke some sort of empirical (parametric) function for extrapolation. This is a severe limitation of the conventionally applied EST, since it restricts the non-parametric estimates to approximately the number of years covered by the hindcasts, just as in any other method that relies only on historical storms. In fact, the conventional EST, as used in most past studies, is very similar to the so-called peaks over threshold (POT) method based on historical hindcasts, with three notable exceptions discussed below.

First, the POT method typically uses a parametric fit in the interior region of the distribution, rather than just in the region beyond the largest storms. It can be shown via Monte Carlo simulations that, if the entire sample is drawn from a single parent distribution, the POT method would provide a more stable estimate of the actual distribution in the interior than would the EST. However, in many situations in nature, the interior distribution can consist of samples from several different parent populations. An example of multiple populations would be the case of storm surges due to "direct hits" of hurricanes vs. storm surges due to bypassing storms. Surges from these two sources could have relatively different probability characteristics at a fixed coastal location, as shown in Figure 2. Consequently, the use of nonparametric estimates within the central portion of the distribution seems more appropriate for most coastal flooding applications.

Second, the POT method uses a "fit" to the entire sample to extrapolate into longer return periods. In this case, the problem of mixed populations could potentially introduce serious problems into extrapolations, if the more that one population persists into the region above the "cut-off" threshold. However, many POT methods carefully choose the threshold value to try to restrict the sample to a single population. In some situations this is possible and in others this may not be possible due to lack of sample size (i.e. there may only be 1 or two direct "hits" by hurricanes). On the other hand, the EST uses an empirical "spline" fit to some small number of points near the high end of the distribution combined with a set of secondary restrictions that tend to limit excessive curvature in the extremes. Extrapolations in such situations tends to be subject to considerable judgment, since there is no underlying distribution used as the basis for estimating values larger than those included within the sample.

Third, in hurricane surge studies with the EST, it was observed that a single intense storm could introduce an anomalously large value into a small spatial region, while other areas had much lower maximum surge values. Since there is no reason to believe that all future hurricanes would strike only points included in the historical data set, some applications of the EST introduced a set of hypothetical storms intended to distribute the effects of large storms throughout the region being studied. In this approach, the largest storm was usually assigned a number of offset tracks and the probability of that storm was distributed over that set of tracks. However, each of these "cloned" storms had exactly the same characteristics as the original storm. In this approach, the extent of the offsets was rather arbitrary, in spite of the fact that the degree of smoothing (distance over which the storm track is replicated) can significantly affect estimated local extremes. Also, only characteristics of storms that fell within the area being analyzed were included in an analysis. Thus, a storm such as Katrina (a large, very intense storm) is difficult to reliably predict from a local sample that does not contain this type of storm within its sample.

Both the POT method and the EST use various statistical methods to incorporate tidal effects into their estimates of water levels at the coast. In a sense, these could be considered as hypothetical storms, since they represent storms that struck the coast at a different tidal phase.

From this discussion, it can be seen that a major problem with the conventional EST is the same as encountered in any approach to hurricane flooding based on local data only: lack of sample. The relatively small spatial extent of hurricanes combined with the small number of storms affecting a given section of coast during the period of reliable records and the apparent existence of long term cycles and trends makes the sampling variability in historical records very large along U.S. coastlines. This same variability affects all estimates of coastal flooding since they all rely on historical data; however, this variability can be greatly exacerbated when only local data is considered. It is perhaps fair to say that the application of the EST requires more experience and judgment than an application of the JPM.

Measures of Variability in Expected Extremes

Since the EST does not contain an underlying theoretical distribution, no theoretical estimates of variability (confidence limits) are possible. Instead, the EST uses a "re-sampling" method to obtain estimates of expected variations in extremes over an interval of time. This

method, rather than its methodology for estimating expected extremes, is the strength of the EST. The combination of the re-sampling with the nonparametric distribution provides a sound basis for estimating the variability of the estimated extremes.

The Joint Probability Method (JPM)

Statistics of Expected Extremes

The JPM was developed in the 1970's (Myers, 1975; Ho and Meyers, 1975) and subsequently extended by a number of investigators (Schwerdt *et al.*, 1979; Ho *et al.*, 1987) in an attempt to circumvent problems related to limited historical records. In this approach, information characterizing a small set of storm parameters was analyzed from a relatively broad geographic area. In applications of this method in the 1970's and 1980's, the JPM assumed that storm characteristics were constant along the entire section of coast from which the sample was drawn. Recent analyses suggest that this assumption is inconsistent with the actual distribution of hurricanes within the Gulf of Mexico.

The JPM used a set of parameters, including 1) central pressure, 2) radius of maximum wind speed, 3) storm forward speed, 4) storm landfall location, and 5) the angle of the storm track relative to the coast, to generate parametric wind fields. Furthermore, initial applications of the JPM assumed that the values of these five parameters varied only slowly in storms approaching the coast; therefore, the values of these parameters at landfall could be used to estimate the surge at the coast. Recent data shows that this is not a good assumption (Figure 3). Kimball (2006) has shown that such decay is consistent with the intrusion of dry air into a hurricane during its approach to land. Other mechanisms for decay might include lack of energy production from parts of the hurricane already over land and increased drag in these areas. In any event, the evidence appears rather convincing that major hurricanes begin to decay before they make landfall, rather than only after landfall as previously assumed.

The conventional JPM used computer simulations of straight-line tracks with constant parametric wind fields to define the maximum surge value for selected combinations of the basic five storm parameters. Each of these maximum values was associated with a probability

$$p(c_p, R_{\max}, v_f, \theta_l, x)$$

where

c_p is the central pressure,

$R_{\max}$ is the radius of maximum wind speed

v_f is the forward velocity of the storm

θ_l is the angle of the track relative to the coast at landfall

x is the distance between the point of interest and the landfall location

These probabilities were treated as discrete increments and the CDF was defined as

$$F(x) = \sum p_{ijklm} \mid x_{ijklm} < x \tag{3}$$

where the subscripts denote the indices of the 5 parameters used to characterize the hurricanes. Similar to the EST, this method is nonparametric; however, the conventional JPM included a range of parameter combinations that typically made extrapolation beyond the range of simulations unnecessary. This is an advantage over the conventional EST, since it removes the need to assume a particular parametric form for the CDF in critical ranges of values.

Another potential advantage of the JPM over methods which depend heavily on historical storms was that the JPM considered storms that might happen; whereas, the EST considered only storms that did happen. Assuming that, for the purpose of surge generation, storm characteristics can be represented adequately by the set of parameters used, it is possible to construct a Katrina-like storm (high intensity combined with large size) even if one has not happened previously. Likewise, it is possible to interpolate between re-curved storms such as Opal and Wilma to understand possible hurricane impacts in the Tampa area, even though neither of these storms produced significant surges in the Tampa area.

Perhaps the biggest controversy in JPM applications during the 1970's and 1980's centered on the definition of this 5-dimension joint-probability function. The lack of data on historical storms prior to 1950 made it very difficult to derive representative distributions, even for extended sections of coast. For example, information on storm size (radius of maximum wind speed was lacking for most historical storms; consequently, a statistical estimate of $r_{\max}$ (as a function of latitude and central pressure) was frequently substituted for actual values in the probability distribution. One wind field factor not considered in early JPM applications was the variable peakedness of hurricane wind fields. This term is represented in terms of the Holland B parameter in recent hurricane wind models and will be discussed in a subsequent section of this white paper.

One point of interest that should not be lost here is the importance of capturing the mean statistical behavior of any time-varying properties used in JPM applications. For example, surges derived from previous JPM applications, under the assumption of that storm characteristics near the coast were constant, may have been biased low, since they were based on statistics at landfall. Since storms are consistently more intense off the coast (as shown in Figure 3), the modeled offshore storms are less intense than the actual offshore storms, under this assumption. Of course, some calibration was performed in these studies, so this might have been somewhat accounted for via calibration procedures; however, calibration tends to somewhat storm specific, so such calibration could still leave considerable residual bias in the final results.

JPM Measures of Variability in Expected Extremes

Most applications of the JPM only considered the definition of the mean CDF from the simulations, and little attention was paid to quantifying the dispersion (uncertainty) of what could happen within a particular time sample. This is potentially a major shortfall in the JPM as it was originally applied.

The Empirical Track Model

Vickery *et al.* (2000) presents a method for modeling hurricane risk in the United States. This method has been adopted for the development of design wind speed maps within the U.S. (American National Standards Institute (ANSI), ASCE 1990, 1996). This method uses a Monte Carlo approach to sample from empirically derived probability and joint probability distributions. The central pressure is modeled stochastically as a function of sea surface temperature along with storm heading, storm size, storm speed, and the Holland B parameter. This method has been validated for several regions along U.S. coastlines and provides a rational means for examining hurricane risks associated with geographically distributed systems such as transmission lines and insurance portfolios.

A key requirement for the application of the Empirical Track Model within its Monte Carlo framework is the ability to efficiently execute storms over many, many years (20,000 years in the Vickery *et al.* (2000) application). Whereas this is not too demanding for an efficiently written PBL wind model, it is well beyond the range of possibility in large, high-resolution ocean and coastal response models (wave models and surge models). For this reason, the Empirical Track Model was not considered for application to coastal inundation; however, it provides an excellent source for validating the statistical characteristics of the winds used for inundation modeling.

Potential Extensions of Probabilistic Methods to Future Hurricane Surges

As noted in the earlier section on the design storm approach, the design storm approach suppresses much of the real variability in storm characteristics and should be used only for screening alternatives and not for final design of critical coastal structures. However, it is sometimes informative to examine the relative return period of specific historical storms. Appendix A provides an estimation method along these lines which estimates the return periods for both Hurricanes Katrina and Rita (found to be 397 and 89 years, respectively).

It should be clear from the previous section that both the EST and the JPM in older applications suffered from a paucity of historical data. Also, older applications did not include many of the modeling advances that are now regarded as necessary for accurate simulations, for example: inclusion of numerically simulated wave set-up, use of detailed grids to capture high-resolution bathymetric effects, and the application of improved near-coast meteorological models for hurricane evolution and wind-field behavior. Many of these effects were recognized and improved methods for treating them were developed during the forensic study of Hurricane Katrina by the Interagency Performance Evaluation Task Force (IPET).

Recognition that waves can play a substantial role in coastal surge levels introduces a key difference between older JPM applications and the applications being considered today. In the older methods, the assumption of constant parameters was intended to span an interval of about 12 – 24 hours, essentially the primary period for direct wind forcing of coastal surges in historical hurricanes. Waves contribute to coastal surges primarily in nearshore areas; however

they are generated over a span of days during the approach of the storm to land. Thus, consideration of wave contributions to surges requires some knowledge of the storm behavior 1-4 days prior to landfall. Treatment of hurricanes in terms of straight tracks with constant size and intensity over such a period is a bad assumption, since such tracks would not retain the wave-generation characteristics produced by the curved tracks within the historical record.

This brings us to a crucial point in considering what statistical approach should be used in future applications, i.e. whether to use an approach based strictly on re-sampling historical storms (essentially a modification/extension of the EST) or an approach based on parameterized wind fields over longer tracks (essentially a modification/extension of the JPM). On one hand, it is clear that each historical storm has many, many factors which vary throughout its history which influence hurricane wind fields. For example, eye-wall replacement cycles, interactions with large-scale wind systems, asymmetries within the eye-wall, and complicated track curvatures can all create significant perturbations within the structure of hurricane wind fields. It is not clear however that such modifications to the winds affect the total wave generation process so much, since the nature of this process integrates the wind input over several 10's of hours. In fact, numerical experimentation with hurricane Katrina showed that all of the versions of the wind field (PBL alone, HWIND, and the most recent Oceanweather version) created minimal variations in the wave field (in the range of 5-7% differences in wave height) in the area off of Mississippi.

In a sense, the critical factor that must be considered here is the number of primary dimensions required for representing wind fields with sufficient accuracy that they provide reasonable, relatively unbiased skill when used to drive coastal wave and surge models. For the case of extratropical storms, there is no known simple set of parameters that meets this criterion and some extension of the EST or POT method may be the suitable choice for such applications. For the case of hurricanes, dynamic models of hurricane wind fields (Thompson and Cardone, 1996; Vickery et al., 2000) can be shown to capture a substantial portion of the wind field structure, when driven with the parameters listed above plus the so-called "Holland B" (Holland, 1980) parameter.

Each hurricane will tend to exhibit some degree of deviation from the theoretical PBL-model estimates. At any fixed time, such deviations could be produced by strong storm asymmetries, variations in $R_{\max}$ around the storm, enhanced spiral bands, etc. Hence, a "best-estimate" wind field crafted by experts to assimilate all the observations in a given hurricane will typically represent the details of that particular storm much more faithfully than possible via a parameterized theoretical model. Such wind fields today are produced primarily by Mark Powell and others at the Hurricane Research Division of the National Hurricane Center of NOAA or by analysts at Oceanweather, Inc. These wind fields are absolutely essential for advancing our understanding of hurricane winds relative to wave and surge forcing in offshore and coastal areas.

It is obvious that "best-estimate" wind fields contain an extremely large number of degrees of freedom in their formulation. Given the relatively small number of historical hurricanes, it is unlikely that we can understand/quantify the probabilistic nature of all the interrelated detailed factors creating these deviations. If these details were absolutely critical to coastal wave and

surge estimation, we would be able to represent a past hurricane very accurately but would know little about the probability of future hurricanes unless we retained the same number of the degrees of freedom, including their expected variability in estimates of future storm surge and wave estimates. To demonstrate this point, in the definition of surge probabilities via numerical models, we are considering a relationship of the form

$$p(\eta) = \int ... \int p(x_1, x_2, ..., x_n) \delta[\Psi(x_1, x_2, ..., x_n) - \eta] dx_1 dx_2 ... dx_n \quad (4)$$

where η (= $\eta_{\max}$ for each individual storm at a fixed spatial location) is the storm surge level, $\delta[.]$ is the Dirac delta function and $\Psi(x_1, x_2, ..., x_n)$ is a numerical model or system of models that operate on the set of parameters ($x_1, x_2, ..., x_n$) to provide an estimate of the surge level at a fix location. This can be directly integrated to yield the CDF for surge levels

$$F(\eta) = \int ... \int p(x_1, x_2, ..., x_n) H[\eta - \Psi(x_1, x_2, ..., x_n)] dx_1 dx_2 ... dx_n \quad (5)$$

where $H[.]$ is the Heaviside function. If we retained a sufficient number of degrees of freedom to resolve the wind fields exactly, if our numerical codes were also "exact," and if our specification of the joint probability function $p(x_1, x_2, ..., x_n)$ were known exactly, we could treat this equation as an exact integral for the CDF, with no uncertainty in its expected value. The sampling variability could then be estimated by re-sampling methods along the lines of the EST.

The CDF integral (equation 5) shows that the number of dimensions required for an exact representation of the surge CDF must equal the number of degrees of freedom contained within the system (for practical purposes determined by the number of degrees of freedom contained in the wind fields). Since we recognize that all wind fields, wave models, and surge models remain inexact and that our estimates of joint probabilities are greatly hampered by lack of sample size, it is clear that the actual representation of this integral should be written as

$$F(\eta) = \int ... \int p(x_1, x_2, ..., x_n, \varepsilon) H[\eta - \Psi(x_1, x_2, ..., x_n) + \varepsilon] dx_1 dx_2 ... dx_n d\varepsilon \quad (6)$$

where ε is an "error" term due to wind field deficiencies, model deficiencies, unresolved scales, etc. In this form, we see that there is a trade-off between modeling accuracy and the magnitude of the error term, ε. There is also a similar trade-off between errors/uncertainties in the probability estimates and the overall accuracy in estimates of the surge CDF. These errors will increase substantially if we attempt to split a small sample (for example the historical hurricane record in the Gulf of Mexico) into information for too many dimensions. Following this reasoning, it seems advisable to limit the number of parameters considered in the JPM probability integral and to include an approximation for all of the neglected terms within the error term, ε. As noted previously, PBL models provide a relatively accurate representation of the broad-scale structure within hurricanes. Furthermore, wind fields from PBL models have a very long history of providing accurate wave estimates in Gulf of Mexico hurricanes (Cardone *et*

al., 1976). Consequently, the logical choice appears to be to limit the number of dimensions in the JPM integral to the number of parameters contained within such PBL models

$$F(\eta) = \int ... \int p(c_p, R_p, v_f, \theta_l, x, B) p(\varepsilon) H[\eta - \Psi(x_1, x_2, ..., x_n) + \varepsilon] dx_1 dx_2 ... dx_n d\varepsilon \quad (7)$$

where the error term has been separated from the rest of the probability distribution. In this form, the "error" term allows us to include additional effects on water levels, such as tides (albeit in an uncoupled, linear fashion). Also, in this equation, we have replace $R_{\max}$ with R_p, since the latter term is used in the PBL model selected for application here (see Appendix B) for details.

During the last several months considerable effort has gone into re-analyzing hurricane characteristics and hurricane wind fields. One of the significant findings of this effort is that the Holland B parameter in mature storms within the Gulf of Mexico tended to fall within the range of 0.9 – 1.6. Furthermore, numerical sensitivity tests of both wind fields and coastal surges suggest that the adoption of a constant value of 1.27 for storms centered more than 90 nm from the coast provided a reasonable first approximation to both the wind fields and the surges. Thus, if we add the effects of B-variations into the "error" term, we can reduce the CDF equation to

$$F(\eta) = \int ... \int p(c_p, R_p, v_f, \theta_l, x) p(\varepsilon \mid \eta) H[\eta - \Psi(x_1, x_2, ..., x_n) + \varepsilon] dx_1 dx_2 ... dx_n d\varepsilon \quad (8)$$

In this form, ε is considered to include, at a minimum, the following terms:

1. tides,
2. random variations in B,
3. track variations not captured in storm set,
4. model errors (including errors in bathymetry, errors in model physics, etc.), and
5. errors in wind fields due to neglect of variations not included in the PBL winds.

It is evident that we can only approximate the overall distribution of ε from ancillary information on errors in comparisons to High Water Marks and comparisons of results from runs with the "best-estimate" wind fields and PBL wind fields. Tides can be factored into this analysis assuming linear superposition, with some degree of error introduced. Based on the best available approximations to all of these terms, assuming that all the "error" contributions are independent, and a loose application of the Central Limit Theorem, we will assume that the "error" term can be represented as a Gaussian distribution with a mean of zero (assuming that the model suite is calibrated to this condition) and a standard deviation equal to some percentage of the modeled surge.

If we were to try to extend the EST to include shifting actual historical storms from one landfall site to another, we would implicitly be holding all the "details" constant by assuming exactly the same storm will occur in the future at different locations. This constrains all future hurricanes to have the same detailed characteristics as the single historical storm upon which it is based. It seems more logical to approach this in two stages as described above, an initial stage to capture the broad-scale wind characteristics and a second stage to understand/quantify the impact

of deviations around these broad-scale winds on coastal surges. In this way, the probability analysis can be kept within a sufficiently small number of dimensions to allow reasonable approximation from historical records.

In our own work investigating modifying the EST, we began by making the same assumption as the older JPM application, i.e. that we could take some section of coast and treat it at though it were homogeneous with respect to expected storm parameters. With this assumption, we felt that it would be appropriate to move a storm some distance along the coast without affecting its characteristics. Unfortunately, when we tested this approach, we saw that historical tracks did not translate well spatially. We found that all of the large storms affecting U.S. Gulf of Mexico coastlines entered the Gulf through either the gap between Cuba and the Yucatan Peninsula or through the southern Florida to Cuba area. A simple geometric displacement of a particular storm track made that track intersect with land in areas that are not suitable for their origin. For example, such a displacement to allow a storm such as Hurricane Opal to strike the western portion of Louisiana would intersect with land at a point slightly south of the border between the United States and Mexico. It is essentially impossible for such a track to generate a storm of Opal's strength. Another example would be the simple translation of Katrina's track to a point farther east. It is highly unlikely that such a track would be able to support a storm of Katrina's size and intensity. Thus, any concept that involves a simple geometric translation of a historical storm track to a position very far from where it actually occurred was found to be very naïve, at least in a meteorological/climatological sense. Still another example of problems associated with the use of a detailed track would be the simplistic shifting of a track with a loop in it, such as Hurricane Elena along the panhandle of Florida. The implication of using this exact track and associated wind field is that all future storms of this type will exhibit exactly this same loop and associated intensity, size, asymmetry, and other detailed characteristics during its approach to land. The probability of this actually occurring is very near zero.

An additional problem in our initial attempt to modify the EST for storm surge application relates to the definition of storm probability. We found that, due to the geographic constraints of entry points for intense storms into the Gulf, it was a very bad assumption to treat any extended section of coast as though it were a homogeneous area in terms of expected hurricane characteristics. Instead, several independent analyses have shown that the statistical properties of hurricanes vary continuously and substantially throughout the Gulf of Mexico. This means that it is not advisable to shift a storm track from one section of coast to another and treat it as an equivalent sample to a storm that actually occurred in that section of coast. A related problem in attempting to modify the EST for hurricane surge applications is assigning the probability of exceedance of some characteristic in a particular storm. For example, most critical reviews conducted recently have advocated limiting the period of record to be used in climatological estimates of hurricane characteristics to a period from no earlier than the mid-1940's to the present. Thus, if we adopt the conventional plotting position, Katrina will represent somewhere in the neighborhood of a 60 year event. We can probably increase this a little by spreading Katrina over some section of coast; but as noted above, this is not a simple exercise. The degree of spreading, the reasonableness of the tracks, and the spatial variation of statistical properties all make this a procedure that should not be trivialized.

The final point worth noting is that prior to 2005, there was no Katrina in the historical record. Straightforward estimates of surges using the EST method prior to Katrina suggest that such a surge only occurs once every 1200 years, or so. Most analyses suggest that this is a substantial overestimation of the return period for such a surge. The problem here is that, prior to Katrina, no historical storm combined both intensity and size in a fashion equivalent to Katrina. Thus, Katrina was outside the sample range of the EST. Although this particular deficiency in the sample has been remedied for at least some of the Gulf coast (since Katrina has now occurred there), one must ask what other gaps in the sample of historical storms might exist. Given this point along with all the other discussion points in this section, it was decided that it would be more straightforward to modify the JPM for hurricane surge applications than to modify the EST. As noted previously, both of the methods are nonparametric in the interiors of their cumulative distribution functions.

The Modified JPM Method (JPM-OS)

In this section, a method for estimating storm surges via a modified JPM will be developed, including estimation of some key climatological characteristics of hurricane tracks, intensities, and sizes. The term JPM-OS will be used here to denote this new methodology, since the underlying concept of this methodology is to provide a good estimate of the surges in as small a number of dimensions as possible, while retaining the effects of additional dimensions by including the ε term within the estimated CDF for surges. This approach will also attempt to minimize the number of runs required by improving methods used for interpolating between combinations of variables in different simulations.

Estimation of Spatially Varying Probabilities

In our new approach, the recommended treatment of geographic variation is to use the Chouinard et al. (1997) method for determining optimal spatial size for estimating hurricane statistics. In this method, the optimal size for spatial sampling is estimated in a manner that balances the opposing effects of spatial variability and uncertainties related to sample size. Although the final, definitive statistics are still being developed, a brief description of the method is included here, along with the preliminary results.

We begin by estimating the omni-directional statistical properties for storm frequency and intensity. Work performed by Gabriel Toro of Risk Engineering showed that the optimal spatial sample (kernel) size was in the range of 160 km for frequency analyses, but found that the optimal spatial size for intensities reached a plateau above about 200 km and did not drop off substantially at higher spatial kernel sizes. For our purposes, we took the basic data set of 22 hurricanes, which had central pressures less than 955 mb, shown in Figures A3 through A5 and defined their locations and intensities along the line shown in Figure A2. Although this line includes the west coast of the Florida peninsula for completeness within the analysis, results will only be presented for the section of coast west of this peninsula. Our hurricane sample covers the interval 1941 through 2005. Appendix C provides a synopsis of some work supporting the selection of this period of record.

For our frequency analysis, we selected a "line-crossing" methodology, rather than an 'area-crossing" (such as used in the Toro analysis presented in Figure 1) since the frequency of landfalling storms is inherently better posed in this context. The location of this line is shown in Figure A2 and distance in this system will be referenced in this white paper via an "increment number." This "increment number" is based on integer values of the distance in degrees (longitude at 29.5 degrees latitude) as explained in the figure caption in Figure A2.

After a number of sensitivity studies we were able to show that the results for spatial samples for spatial kernels above 250 km or so did not vary markedly and settled on a sample size of ±3 degrees (333 km) along this line. Results from this analysis are converted into an estimate of the frequency of hurricanes (which attain a minimum central pressure of 955 mb or less) making landfall within contiguous 1-degree increments along the reference line. Figure 4 gives the results of this analysis. As can be seen here, the "line-crossing" frequency estimate is fairly consistent with the spatial-area frequency estimates obtained by Toro in Figure 1. It should be noted that the Toro analysis was based on 52 storms (all storms above Category 2 intensity within the Gulf of Mexico) rather than the 22-storm subset used here.

For each 1-degree increment along the coast, pressure differentials at the time of landfall for all storms making landfall within the ±3-degree distance along the reference line were used to define a best-fit (conditional) Gumbel distribution, i.e. the distribution of hurricane intensity given that a hurricane (with central pressure less than 955 mb) does occur. The Gumbel coefficients for the pressure differentials are shown in Figure 5. Combining the storm frequency estimates with these values we can estimate the omni-directional probability of intensity along the Gulf coast at the time of landfall.

Figure 6 shows the (smoothed) distribution of the 50-year, 100-year, and 500-year central pressures based on the Oceanweather information. Also shown in this Figure is the estimates using the same derivation methodology, but based on the official NOAA values for landfalling central pressures. As can be seen here, the two methods yield very similar results, except for some divergence as the Louisiana-Texas border is approached. This curious aspect of the otherwise excellent agreement was found to be related to a single spurious value in the Oceanweather files for Hurricane Audrey. Once this was fixed, the region of good agreement extended across the entire region.

Interpretation of these values to "off-coast" values should refer to Figure 3, which suggests that the off-coast central pressures should be on the average around 10-15 mb lower that these values. For comparison, return periods based on independent analyses performed by David Levinson (National Climate Center) suggest that the 100-year central pressure offshore was in the range of 894-908 for a broad portion of the central Gulf of Mexico, which is reasonably in agreement with the values derived here, based on 1-degree increments of coast. However, in performing this comparison, it is essential to bear in mind that the estimates are appropriate for the recurrence within a 1-degree section of coastline. To compare the estimates in Figure 6 with values for the entire Gulf of Mexico, Peter Vickery performed an independent analysis of extremes based on 1) a statistical combination of all of the coastal segments and 2) an extremal analysis of the NOAA's landfalling pressures. As can be seen in Figure 7a, the estimates of landfalling central pressures shown in Figure 6 can be used to provide a very consistent estimate

for landfalling central pressures along the U.S. coast from Texas to the northwest Florida coast. And, as can be seen in Figure 7b, a similar analysis for a single 1-degree increment shows, as expected, a little more randomness for this (smaller) set of points but a similar good general agreement in the tail of the distribution. Figure 7c shows a comparison of another independent check on the probability distribution based on a comparison to the results of Toro's analysis performed for FEMA Region 4, along the Mississippi coast. These tests confirm the general estimation methodology used here is quite robust for hurricanes along the U.S. Gulf of Mexico coasts.

Several independent analyses over the last several months have shown that storm size is not independent of storm intensity; and recently, Shen (2006) has shown that the potential intensity achievable by a hurricane is very sensitive to the size of a hurricane eye. Figures 8a and 8b show the relationships between R_p and central pressure from Oceanweather analyses of all storms exceeding Category 2 within the Gulf of Mexico at their time of maximum strength (52 storms – shown in Figure 8a) and the 22-storm sample of landfalling storms (Figure 8b). Equation A3 in Appendix A gives an estimate of the conditional probability of storm size as a function of central pressure. Figure 8 gives the mean angle of storm heading as a function of distance along the reference line shown in Figure A2, along with the standard deviation of the heading angles around this mean value. The direction convention used here is that a heading of due north represents an angle of zero degrees. Storms heading more westerly than due north will have positive angles, while storms heading more easterly will have negative angles. These estimates were derived by the same spatial averaging procedure used in deriving the central pressures and frequencies. A circular normal distribution is used here to represent the storm heading probability distribution as a function of location along the reference line.

Figure 10 presents the estimated forward storm speed as a function of central pressure. This figure suggests that storm intensity and the forward speed of the storm are approximately independently distributed. However, if we plot forward storm speed as a function of storm heading at landfall for the 14 storm subset that intersect with the 29.5-degree latitude portion of the reference line in Figure A2 and for the entire 22-storm sample of landfalling storms (shown in Figures 11a and 11b), we see that there is a tendency for higher forward speeds to be associated with lower storm heading angle (a correlation of 0.52 which is significant at the 0.05 level of signficance with 21 degrees of freedom in a "Student's *t*" test). This is consistent with the expected behavior of re-curving storms that become swept up in stronger westerly circulations. The primary exception to the overall relationship is Hurricane Betsy, represented by the point in the upper right-hand corner of this Figure. This storm moved very fast into the New Orleans area after crossing the lower portion of the Florida peninsula.

Putting all of the pieces of information together, for any point in our five-dimensional parameter space (retaining appropriate interrelationships among parameters), we see that the final estimates of joint probability densities can be written as

$$p(c_p, R_p, v_f, \theta_l, x) = \Lambda_1 \cdot \Lambda_2 \cdot \Lambda_3 \cdot \Lambda_4 \cdot \Lambda_5$$

$$\Lambda_1 = p(c_p \mid x) = \frac{\partial F[a_0(x), a_1(x)]}{\partial c_p} = \frac{\partial}{\partial x}\left\{\exp\left\{-\exp-\left[\frac{c_p - a_0(x)}{a_1(x)}\right]\right\}\right\} \text{ (Gumbel Distribution)}$$

$$\Lambda_2 = p(R_p \mid c_p) = \frac{1}{\sigma(\Delta P)\sqrt{2\pi}} e^{-\frac{(\bar{R}_p(\Delta P) - R_p)^2}{2\sigma^2(\Delta P)}}$$

$$\Lambda_3 = p(v_f \mid \theta_l) = \frac{1}{\sigma\sqrt{2\pi}} e^{-\frac{(\bar{v}_f(\theta_l) - v_f)^2}{2\sigma^2}}$$

$$\Lambda_4 = p(\theta_l \mid x) = \frac{1}{\sigma(x)\sqrt{2\pi}} e^{-\frac{(\bar{\theta}_l(x) - \theta_l)^2}{2\sigma^2(x)}}$$

$$\Lambda_5 = \Phi(x)$$

where the overbars denote average values of the dependent variable for a specified value of an independent variable in a regression equation, $a_0(x)$ and $a_1(x)$ are the Gumbel coefficients for the assumed Gumbel form of the central pressures, and $\Phi(x)$ is the frequency of storms per year per specified distance along the coast (taken as one degree in examples presented here).

Figures 12-14 show three sets of synthesized tracks that are being used in the ongoing New Orleans area study. These central tracks (Figure12) essentially mimic the behavior of intense landfalling historical storms in the record, while preserving the geographic constraints related to land-sea boundaries. These storms preserve the historical pattern of the tracks better than simply shifting the same storm tracks east or west along the coast, since they capture the observed variations in mean storm angles along the coast.

Estimation of the ε Term

Although there may be some degree of nonlinearity in the superposition of tides and storm surges, numerical experiments have shown that for the most part linear superposition provides a reasonable estimate of the (linearly) combined effects of tides and surges. Thus, the tidal component of the ε term, represents the percentage of time occupied by a given tidal stage and can be directly derived from available tidal information along the coast.

Careful analyses appropriate for formulating Holland B parameters for ocean response modeling have shown that this parameter falls primarily in the range of 1.1 - 1.6 offshore and 0.9 - 1.2 at the coast (Appendix E). For Gulf of Mexico hurricanes, a mean value of 1.27 in offshore areas is assumed with a standard deviation of 0.15, while at the coast the corresponding mean and standard deviation is 1.0 and 0.10, respectively. Via numerical experiments, the maximum storm surge generated by a hurricane has been found to vary approximately linearly with variations in the Holland B parameter, at least for changes of the Holland B parameter in the range of 10-20%.

Off-coast track variations affect surges at the coast primarily through the effects of these track variations on wave fields, rather than by their effects on direct wind-driven surges. As noted previously, wave fields tend to integrate wind field inputs over 10's of hours; consequently, off-coast track variations tend to shift the wave fields somewhat while maintaining the general form and magnitude of the wave height contours. Near-coast radiation stresses are approximately proportional to gradients in wave energy fluxes, which, in turn, can be related to the square of the wave height gradient. In shallow water, where contributions of radiation stresses to surges are most important, wave heights tend to be depth limited. It is only in the incremental region, where larger waves make additional contributions due to increased energy losses offshore, that larger wave conditions affect the total wave set-up at the coast. Numerical sensitivity studies suggest that once incident waves become much larger than about 10 meters, most of the additional energy loss is in depths that do not contribute very much to wave set up. For this reason plus the fact that in general the wave set-up term tends to be only about 15-30% of the total surge, we expect the effect of storm track variations on wave set-up at the coast to be fairly small (due to the fact that surge response is on a much faster scale than wave generation, where we noted that the "straight-track" approximation was not very good). We will assume that the deviations around the mean surge will be approximately Gaussian. A standard deviation of 20% of the calculated wave-set up contributions to the total surge (determined by subtracting the direct wind-only surge from the total surge due to winds and waves combined) will be used within this distribution.

Model errors combined in calibration/verification runs of ADCIRC have shown that this combination of model and forcing in the Louisiana-Mississippi coastal area provides relatively unbiased results with a standard deviation in the range of 1.75-2.50 feet. Relative errors associated with the use of PBL winds increase the value of the standard deviation to 2.00 to 3.50 feet. This is not to surprising, since the accuracy of HWM's (the primary measurements to which the model results are compare) are quite variable in and of itself.

Combining all of these terms, under the assumption that they are each independently distributed, gives

$$p(\varepsilon) = \iint\iint \delta(\varepsilon_1 + \varepsilon_2 + \varepsilon_3 + \varepsilon_4 - \varepsilon) p(\varepsilon_1) p(\varepsilon_2) p(\varepsilon_3) p(\varepsilon_4) d\varepsilon_1 d\varepsilon_2 d\varepsilon_3 d\varepsilon_4$$

where

ε_1 is the deviation between a storm at a random tide phase and a zero tide level;
ε_2 is the deviation created by variation of the Holland B parameter;
ε_3 is the deviation created by variations is tracks approaching the coast; and
ε_4 is the deviation created primarily by errors in models and grids.

Three of the terms $\varepsilon_1, \varepsilon_3,$ and ε_4 are treated here as though they are approximately independent of the magnitude of the surge, while the remaining term, ε_2 has been found to depend essentially linearly with the magnitude of the surge. For a monochromatic tide, the tidal

elevation distribution, ε_1, is known to be bimodal distributed around its zero value; however, in nature, the effect of combining several tidal components with varying phases is to force the distribution toward a unimodal distribution. The probabilities of terms ε_3 and ε_4 are assumed to be normally distributed; thus, the probability distribution of the sum of these two terms will also be a normal distribution with the variance given by the sums of the individual variances of the two terms.

Figure 15 gives a numerical example of the combination of all four terms assuming a storm surge of 15 feet, as might be associated with a particular deterministic model execution based on a set of track and PBL parameters. As can be seen in this figure, the overall magnitude of these effects can add or subtract substantially to the total water depth. In this case, the distribution appears similar to a Gaussian distribution, since it is dominated by the term with the largest variance (deviations due to the omission of the Holland B parameter); however, the other terms have been included within the integral for $p(\varepsilon)$. Table 1 shows an example of the effect of adding this term on expected surge levels for selected return periods. In this example, a Poisson frequency of 1/16 was used in combination with a Gumbel distribution, with parameters a_0 = 9.855 and a_1 = 3.63. For this example, the effect of adding the ε-term is less than ½ foot for return periods up to 175 years and only exceeds1 foot at return periods greater than 400 years. However, for risk-based calculations which often include very large return periods (1,000-10,000 years), this term can become as large as 2-3 feet, even for the case where the effects of all neglected factors are assumed to be distributed around a mean deviation of zero. The effect could of course be larger if the deviations were biased.

From Table 1 and the above discussion, we see that the effect of the ε-term becomes much more pronounced at large return periods. Thus, older applications of the JPM that neglected this term were probably reasonably accurate at the 100-year return period, but were likely to have been progressively biased low at higher return periods. The important points to stress here are twofold. First, any neglect or suppression of natural variability in a procedure to estimate extremes will lead to some degree of underestimation of the estimated extremes, whether using a JPM or an EST approach; therefore, it is important to recognize and attempt to quantify all significant factors affecting surge heights at the coast. Second, to avoid making the number of dimensions in the JPM unmanageable, the estimated effects of the neglected factors contributing to extreme surges should be addressed statistically, such as we have done here via the addition of the ε-term to the JPM integral.

Treatment of Subsidence and Sea-Level Rise

Rather than treat subsidence and sea-level rise within the ε-term, it is simpler to include this in a separate analysis. For purposes of design, as a first approximation to the non-overtopping situations, estimates of subsidence and sea-level rise can be added linearly to the expected surge levels. Thus, (as a purely hypothetical scenario) if two feet of local subsidence is anticipated along with one-foot of sea-level rise over a design lifetime (say 100 years as an example), a levee design set for 20 feet would need to "evolve" to 23 feet in order to provide the same level of protection at the end of the design lifetime. Other options might be to overbuild the design at the outset to account for anticipated subsidence and sea-level rise. In either case, it will be

critical to constantly monitor the changing water levels to ensure that the design level of protection is maintained.

Sampling of Storm Parameters for the JPM-OS

In the conventional JPM each simulation was typically treated as representative of its entire discrete probability range (i.e. all of the probability for each multi-dimensional box centered on its mean position). In these applications, the computational burden was considerably less than what is considered appropriate for surge simulations today (see subsequent section on the computational effort recommended for today's applications). Even in the original JPM, however, a scaling relationship between the pressure differential of a storm and computed surge levels was used to reduce the number of computer runs. This relationship, based on theoretical considerations and confirmed numerically in several studies, shows that surges are linearly proportional to the pressure differential of a storm at all areas close to the area of maximum storm impact. This information can be used effectively to interpolate between two different numerical results within the JPM integral. Such an interpolation provides added resolution along the pressure differential axis in this integral, which is very important due to the highly nonlinear characteristics of the probability of pressure differentials [$p(\Delta P)$].

In addition to the scaling relationship between surge levels and pressure differentials, the JPM-OS attempts to sample the parameter space in a fashion that can be used to estimate surges (develop the response surface) in an optimal manner. This method has been developed via hundreds of simulations on relatively straight coasts, as well as on coasts with other simple geometries, and is in the process of being extended to more complex coasts. It attempts to alleviate the need for very closely spaced parameter values in numerical simulations (essentially track spacing and number of storm sizes, forward speeds, and track angles considered); thereby potentially greatly reducing the total number of computer runs required for JPM execution. The initial set of runs for the New Orleans area consists of 152 hurricanes traveling along tracks shown in Figures 12-14. To put this number of runs in perspective, since a major storm only affects each one-degree section of coast once per 16 years and the section of coast being studied is only about 2.5 degrees, this number of hurricanes would only be expected in the simulated area every 853 years. Consequently, unless we have selected these storms in a very unrepresentative fashion, we expect this number of storms (combined with an accurate methodology for surge simulation) to provide a fairly accurate description of the general characteristics of hurricane surges at least up to the 500-year return period. A description of the parameters of these storms is given in Appendix D, along with a discussion of some scaling relationships between storm parameters and surges that have been found in our numerical studies.

Specification of Variations in Pre-landfalling Hurricanes

Whereas the original JPM considered storm size, intensity, and wind field distribution to be constant in storms approaching the coast, the new JPM uses information from recent storms to estimate the rate of change of these parameters for pre-landfall conditions. In general these trends show that storms tend to fill by about 10-15 millibars (Figure 3), become slightly

(15-30%) larger (Figure 16) and have less peaked wind speed distributions (Holland B parameter decreasing from about 1.27 to around 1.0) over the last 90 nautical miles of coastal water before landfall. Since all of our probabilities have been developed based on landfalling characteristics, the offshore characteristics must be estimated from a generalized transform

$$p(\Delta P, R_p, v_f, \theta_l, x)_{offshore} = p(\Delta P, R_p, v_f, \theta_l, x)_{landfall} J^{-1}$$

where J is the Jacobian for the transform from nearshore to offshore conditions. However, since 1) storm heading during approach to the coast is relatively constant, 2) the forward speeds are assumed to be constant during approach to land and 3) the points of intersection (x) are identical for each offshore and landfall case, the transform can be viewed in only two dimensions, ΔP and R_p. Details will be given in Appendix D.

A Computational Methodology for Effective Simulation of Storm Surges for Hurricane Inundation Studies

For completeness, we include here a brief description of the computational methodology that has been adopted for calculating inundation levels/probabilities. The first step in this procedure is to develop appropriate surge and wave model grids and verify them. The second step is to use both "best available" winds and best PBL winds to verify the modeling system performance within the area of interest. The "best available" winds, which include all appropriate data assimilation and expert analyses, are used to verify the model and grid and to provide calibration guidance, if required. The second set of runs with winds from the PBL model are used to establish any additional tuning required and to determine the actual modeling error term to be used in the ε-term in the JPM integration. Following this procedure, the complete production system is exercised for all of the selected combinations of storm tracks and wind parameters required for the JPM-OS application. A schematic diagram of this system is shown in Figure 17.

Step 1

As seen here, for each defined storm (a track and its time-varying wind field parameters) the Oceanweather PBL model (Thompson and Cardone, 1996) is used to construct 15-minute snapshots of wind and pressure fields for driving surge and wave models.

Step 2

Using "warm-start" condition with all major rivers already "spun up," initiate ADCIRC (version 46.50 or higher as they come online) for simulation of direct wind-driven surge component (assuming zero tide). In parallel with the initial ADCIRC runs, execute a large-domain,discrete, time-dependent spectral wave model (WAM or WAVEWATCH) to calculate directional wave spectra that serve as boundary conditions for local-domain, near-coast wave model runs in Step 3.

Step 3

Using initial water levels from ADCIRC, winds that include the effects of sheltering due to land boundaries, and spectral boundary conditions from the large-domain wave model, execute either STWAVE or SWAN model runs (again using the PBL winds) to produce a wave fields and estimated radiation stress fields.

Step 4

Using the radiation stress fields from Step 3 added to the PBL-estimated wind stresses, rerun the ADCIRC model for the time period during which the radiation stresses potentially make a significant contribution to the water levels. In this step, care must be taken to "match" the grids in the wave model and ADCIRC model.

Step 5

Using the water levels from Step 4, in locations adjacent to structures, a method based on Boussinesq modeling (either direct application or interpolations from generic runs) is used to provide estimates of the following key information along man-made structures and steep-sided natural flood barriers: incremental contribution to the water level at the structure (which should be considered as the final water level for inundation efforts at these locations); estimated total overtopping at structure; and estimated velocities on the front face, crest, and rear face of the structures. The boundary conditions for driving the Boussinesq-based runs are taken from the closest points in the nearshore grids used in Step 3.

Summary

Some of the key issues addressed in this paper, along with relevant conclusions, are as follows:

1. The Joint Probability Method (JPM) provides a sound method for estimating inundation probabilities. However, given the number of degrees of freedom in hurricanes characteristics affecting coastal surges and the computational burdens associated with coastal surge simulations, it is critical to reduce the number of factors considered to a minimum, while maintaining sufficient detail to properly model hurricane wind fields for surge prediction.

2. After a discussion of various alternatives, it is recommended that the same five parameters used in older JPM studies (storm intensity, storm size, forward speed of the storm, angle of the storm track with the coast, and track location) be used to characterize storms for simulating coastal surges. With this number of dimensions within the JPM integral, it is essential 1) to allow these characteristics to exhibit observed variations during their approach to land and 2) to retain and quantify a statistical "error" term that adds the suppressed variability back into the estimated extremes. Previous applications of the JPM did not consider this term.

3. Similar to the Empirical Simulation Technique (EST), it is recommended that uncertainty in the stage-frequency relationships be estimated via re-sampling methods.

4. As discussed in Appendix C and as has been noted in many journal publications, it appears that a 40-year cycle is a dominant feature within the recent hurricane record. We have experienced one full "high-activity" portion of a cycle and about 2/3 of a second "high-activity" portion of a cycle. It is recommended that a comparable proportion of "low-activity" years be included within the record being used for estimating inundation probabilities. Following this logic, we will use the full "low-activity" interval (approximately 30 years) between the two recent "high-activity" intervals plus a period equivalent to 2/3 of the recent "low-activity" interval within our sample period. This yields 1941 through 2005 as our period of record for coastal inundation analyses.

5. The topic of future climatic variability has been dealt with in a recent manuscript by Resio and Orelup. In this manuscript, it is shown that the hurricane record within the Gulf of Mexico does not exhibit a strong secular trend, in contrast to the record in the Atlantic Basin. The Resio and Orelup manuscript showed that the "high-activity" intervals dominated the extreme surge population for return periods greater than 50 years or so. As a sensitivity study, they investigated the consequences of a doubling of "high-activity" years, even though there is no evidence that such a doubling is imminent. Results of this study showed that such a climate scenario would produce about a 12% increase in surge levels at the 100-year level, with decreasing effects at longer return periods.

6. Historically, the storms which appear to have had the most impact on coastal areas within the Gulf of Mexico have all moved along the central paths shown in Figure 12. Theses storms include Rita, Ivan, Camille, Katrina, and Andrew in the historical record from 1941 through 2005; thus the set of tracks in this figure have been nicknamed the RICK-fan.

7. The JPM-OS represents an attempt to combine statistical information over an interval of the coastline in order to gain more confidence in information relevant to the definition of extreme surges at a point. This approach also allowed us to incorporate information on the general behavior of storms in coastal areas (such as storm decay and variations in storm size and the peakedness of the wind distribution along a transect) into our simulations of extreme events.

References, Tables, and Figures for R2007

Agbley, S. K., and Basco, D. R. 2008. "An evaluation of storm surge frequency of occurrence estimators; Solutions to Coastal Disasters 2008," ASCE Conference Proc., 185-197.

ASCE, 1990: Minimum design loads for buildings and other structures, ASCE 7-88, New York.

ASCE 1996: Minimum design loads for buildings and other structures, ASCE 7-95, New York.

Borgman, L.E, Miller, M., Butler, L. and R. Reinhard, 1992: Empirical simulation of future hurricane storm histories as a tool in engineering and economic analysis, Proc. Fifth Intn'l, Conf. on Civil Engr. In the Ocean, ASCE, November, College Station, Texas.

Cardone, V.J., Pierson. W.J., and E.G. Ward, 1976: Hindcasting the directional spectra of hurricane generated waves, J. Petrol. Technol., 28, 385-394.

Collins, J.I., and M.J.Viehmann, 1971: A simplified model for hurricane wind fields, Paper 1346, Offshore Technology Conference, Houston, TX.

Chouinard, L.E., Liu, C. and C.K. Cooper, 1997: A model for the severity of hurricanes in the Gulf of Mexico, J. Waterways, Harbor and Coastal Engr., ASCE, 123, 113-119.

Chow, S., 1971: A study of the wind field in the planetary boundary layer of a moving tropical cyclone, M.S. Thesis, New York University.

Divoky, D., and Resio, D. T. 2007. Performance of the JPM and EST methods in storm surge studies, Proc. 10th Workshop on Wave Forecasting and Hindcasting and Coastal Hazards, Session K, *www.waveworkshop.org*.

Ho, F.P and V.A. Myers, 1975: Joint Probability Method of Tide Frequency Analysis applied to Apalachicola Bay and St. George Sound, Florida, NOAA Tech. Rep. NWS 18, 43p.

Ho, F.P., Su, J.C., Hanevich, K.L., Smith, R.J. and F.P. Richards, 1987: Hurricane Climatology for the Atlantic and Gulf Coasts of the United States, NOAA Tech. Rep. NWS 38, completed under agreement EMW-84-E-1589 for FEMA, 194 p.

Holland, G.J., 1980: An analytic model of the wind and pressure profiles in hurricanes, Mon. Wea. Rev. 108, 1212-1218.

Irish, Resio, & Ratcliff, 2006: The influence of hurricane size on coastal storm surges, submitted to J. Phys. Oceanogr.

Kimball, S.K., 2006: A modeling study of hurricane landfalls in a dry environment, Mon. Wea. Rev., 134, 1901-1918.

Myers, V.A., 1954: Characteristics of United States hurricanes pertinent to levee design for Lake Okeechobee, Florida, Hydromet. Rep. No. 32, U.S. Weather Bureau, Washington, D.C.

Myers, V.A., 1975: Storm Tide Frequencies on the South Carolina Coast, NOAA Tech. Rep. NWS-16, 79 p.

Resio, D.T. and E.A. Orelup, 2006: Potential effects of climatic variability in hurricane characteristics on extreme waves and surges in the Gulf of Mexico, submitted to J. Climate.

Scheffner, N., Borgman, L. and D. Mark, 1993: Empirical simulation technique applications to a tropical storm surge frequency analysis fo the coast of Delaware, Proc. Third Intn'l Conf. on Estuarine and Coastal Modeling.

Schwerdt, R.W., Ho, F.P., and R.R. Watkins , 1979: Meteorological criteria for Standard Project Hurricane and Probable Maximum Hurricane Windfields, Gulf and East Coasts of the United States, Tech. Rep. NOAA-TR-NWS-23, National Oceanic and Atmospheric Administration.

Shen, W., 2006: Does the size of hurricane eye matter with its intensity?, Geophys. Res. Let., 33, L18813.

Thompson, E.F. and V.J. Cardone, 1996: Practical modeling of hurricane surface wind fields, ASCE J. Waterway, Port, Coastal, and Ocean Engineering, 122, No. 4, 195-205.

Vickery, P.J., Skerjl, P.F., and L.A. Twisdale, 2000: Simulation of hurricane risk in the U.S. using empirical track model, *J.Struct. Engr.*, 1222-1237.

Table 1.
Example of Expected Surge Values as a Function of Return Period With and Without ε-Term Included

Return Period (years)	Without ε-Term (feet)	With ε-Term (feet)
50	11.98	12.06
75	13.64	13.90
100	14.82	15.21
125	15.74	16.22
150	16.49	17.04
175	17.12	17.74
200	17.67	18.35
225	18.15	18.88
250	18.59	19.36
275	18.98	19.79
300	19.33	20.18
325	19.66	20.55
350	19.97	20.88
375	20.25	21.20
400	20.52	21.49
425	20.76	21.76
450	21.00	22.02
475	21.22	22.27
500	21.43	22.50

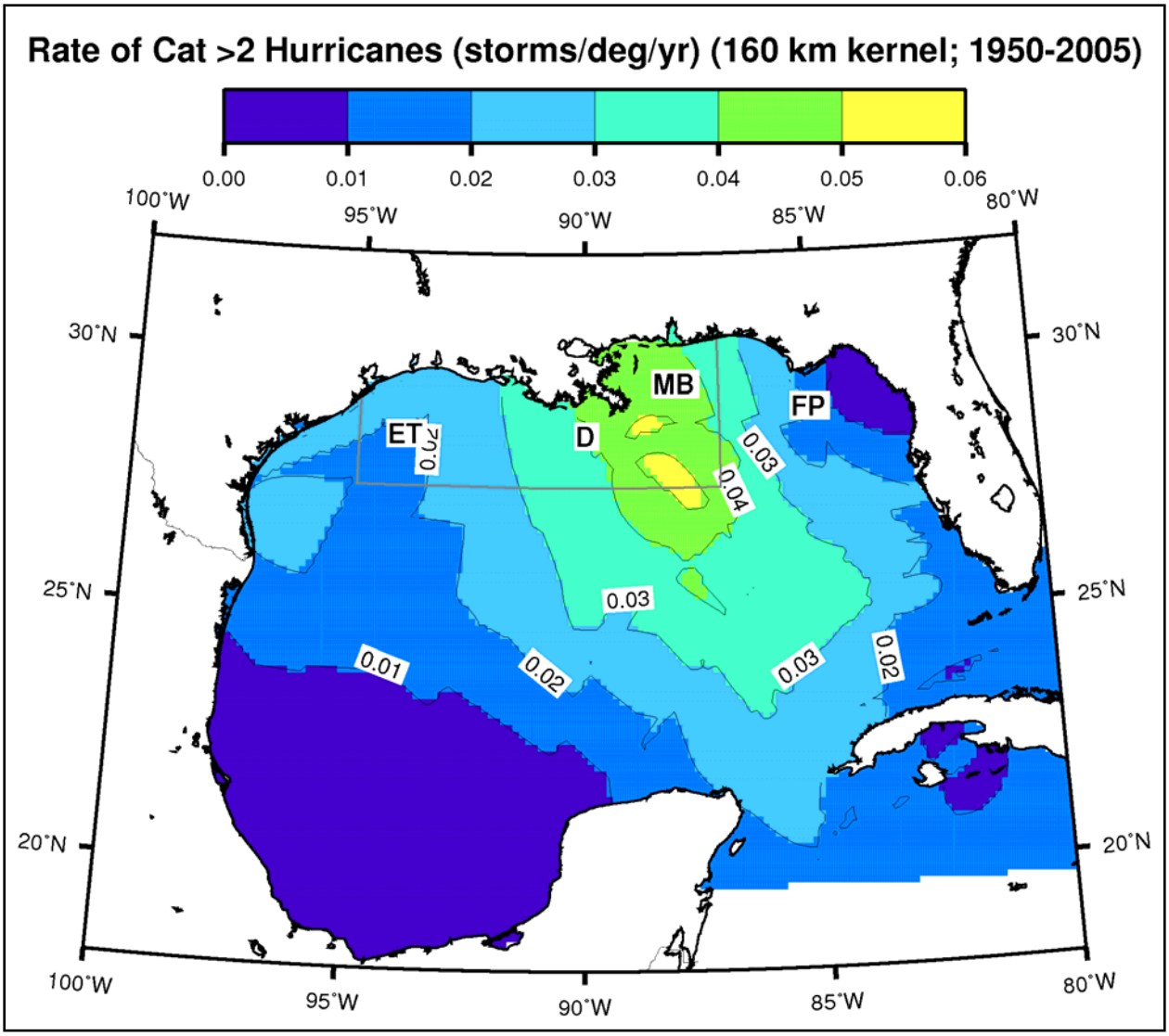

Figure 1. Analysis of hurricane frequency from Toro (Risk Engineering) from an analysis using an optimized spatial kernel.

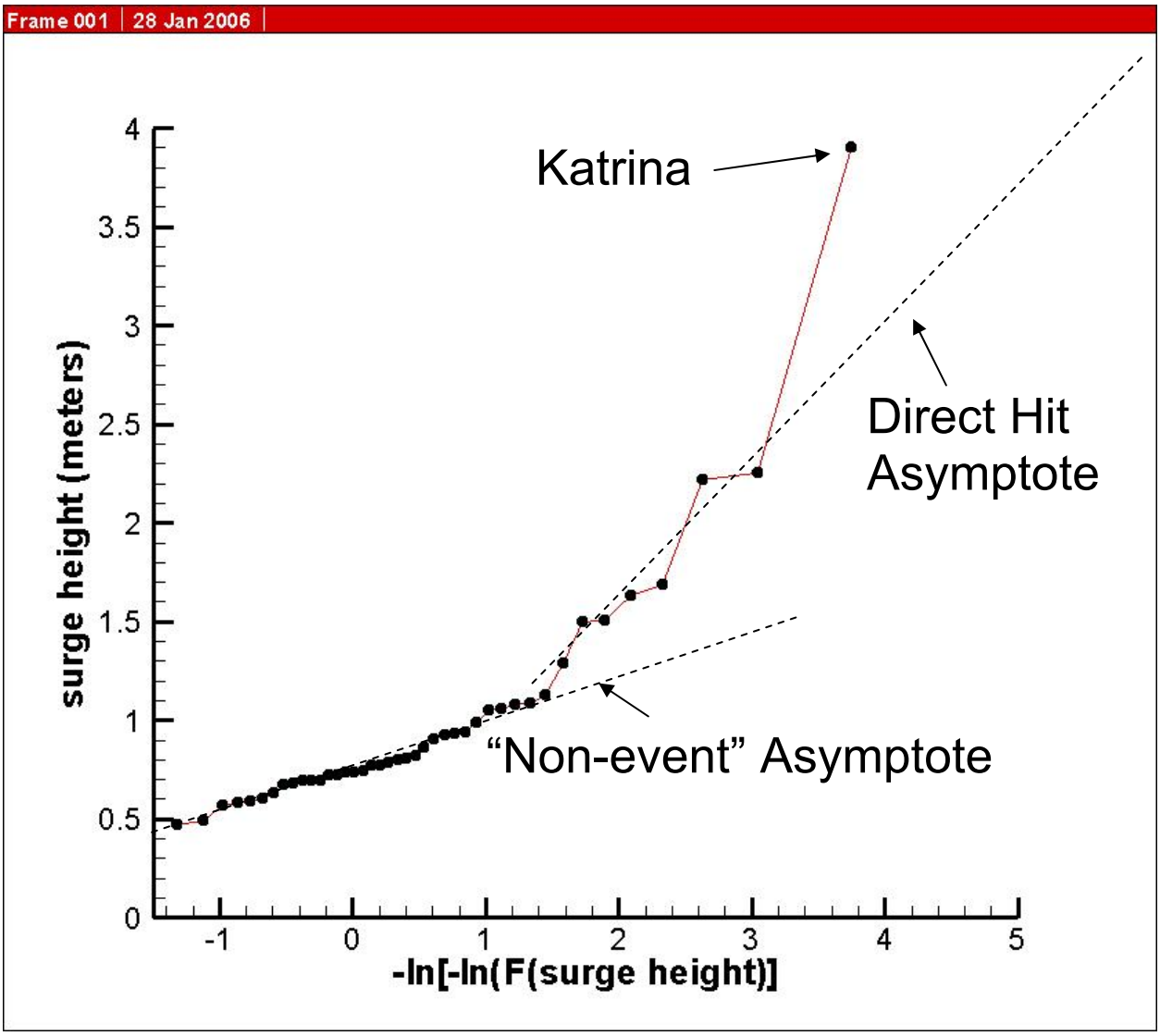

Figure 2. Distribution of the maximum surge heights from ADCIRC simulations for a site in Lake Pontchartrain. Storms within the "non-event" asymptote consist of storms which do not make landfall close to the site of interest; whereas, storms within the "direct-hit" asymptote represent storms that pass very close to the site of interest. The different slopes of these line segments suggests that it may not be justifiable to combine these points into an analysis that treats all of the points as though they are drawn from a single analysis.

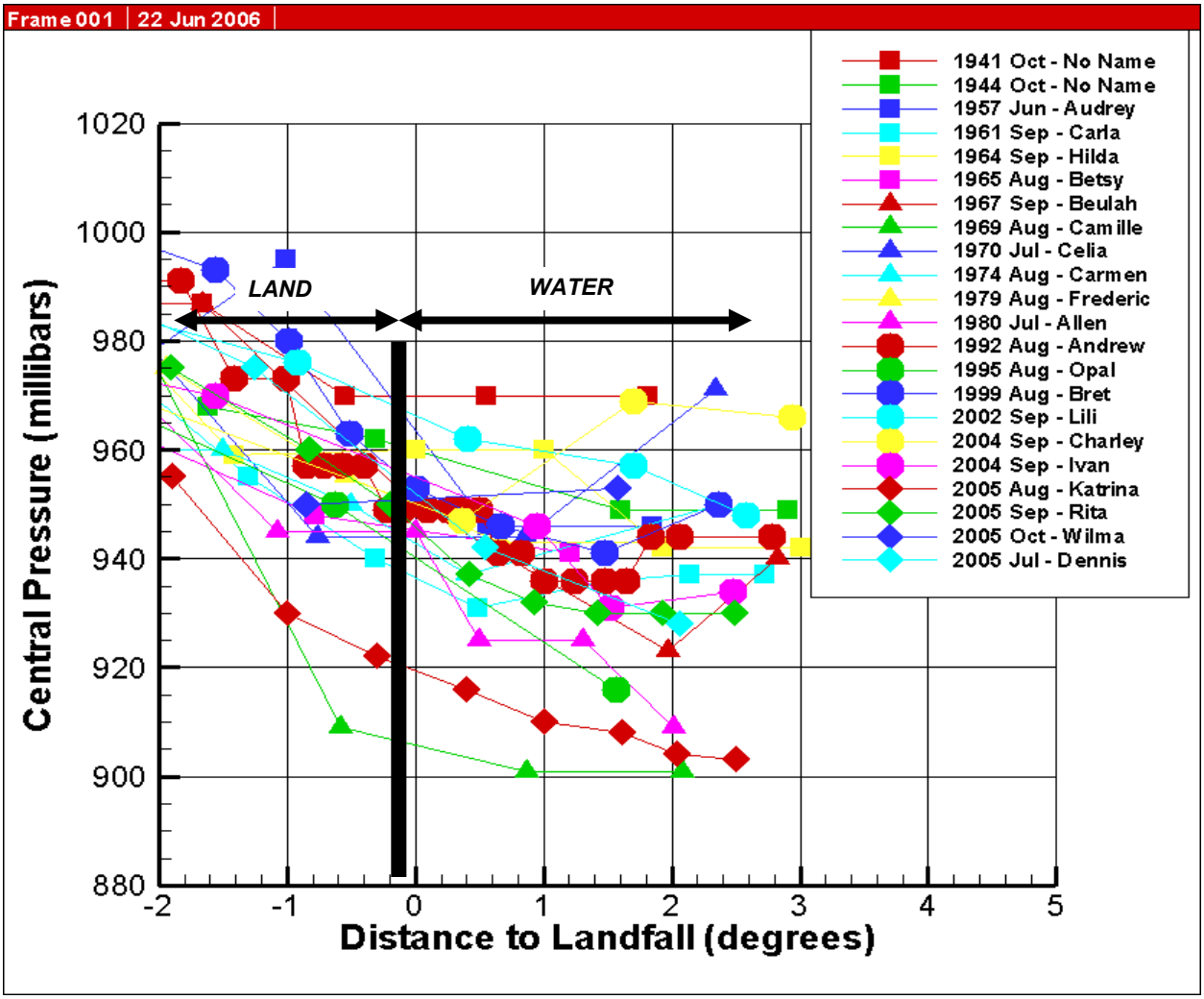

Figure 3. Central pressure in landfalling storms plotted against distance from the coast. Previously it was believed that storm decay began only after landfall. These data from Oceanweather, Inc. show clearly that decay begins offshore.

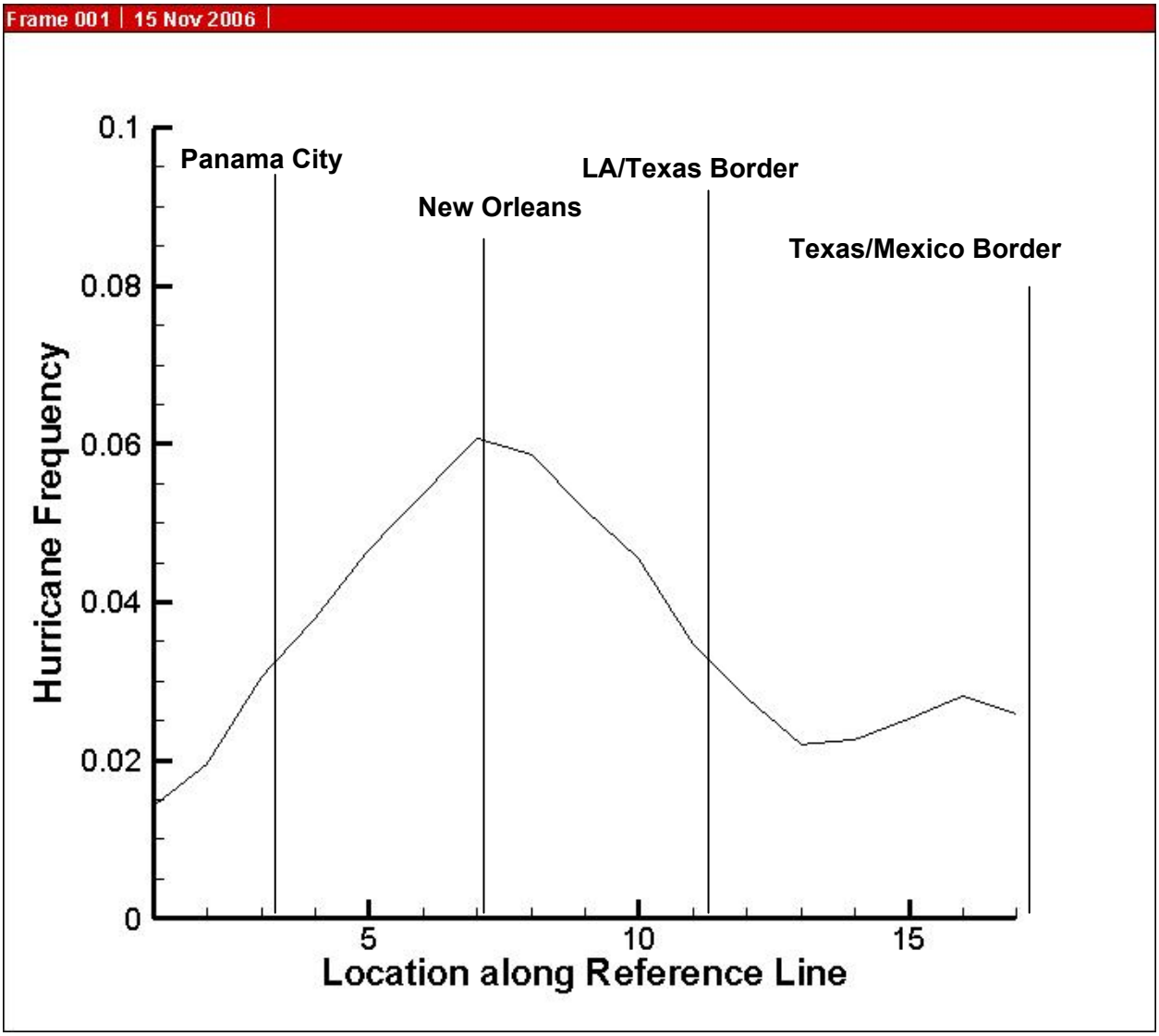

Figure 4. Frequency of hurricanes along reference line with annotated geographic locators, based on 22-storm sample. Location along this line can be taken as equivalent to 1-degree increments along the coast, with the New Orleans area falling within increment 7.

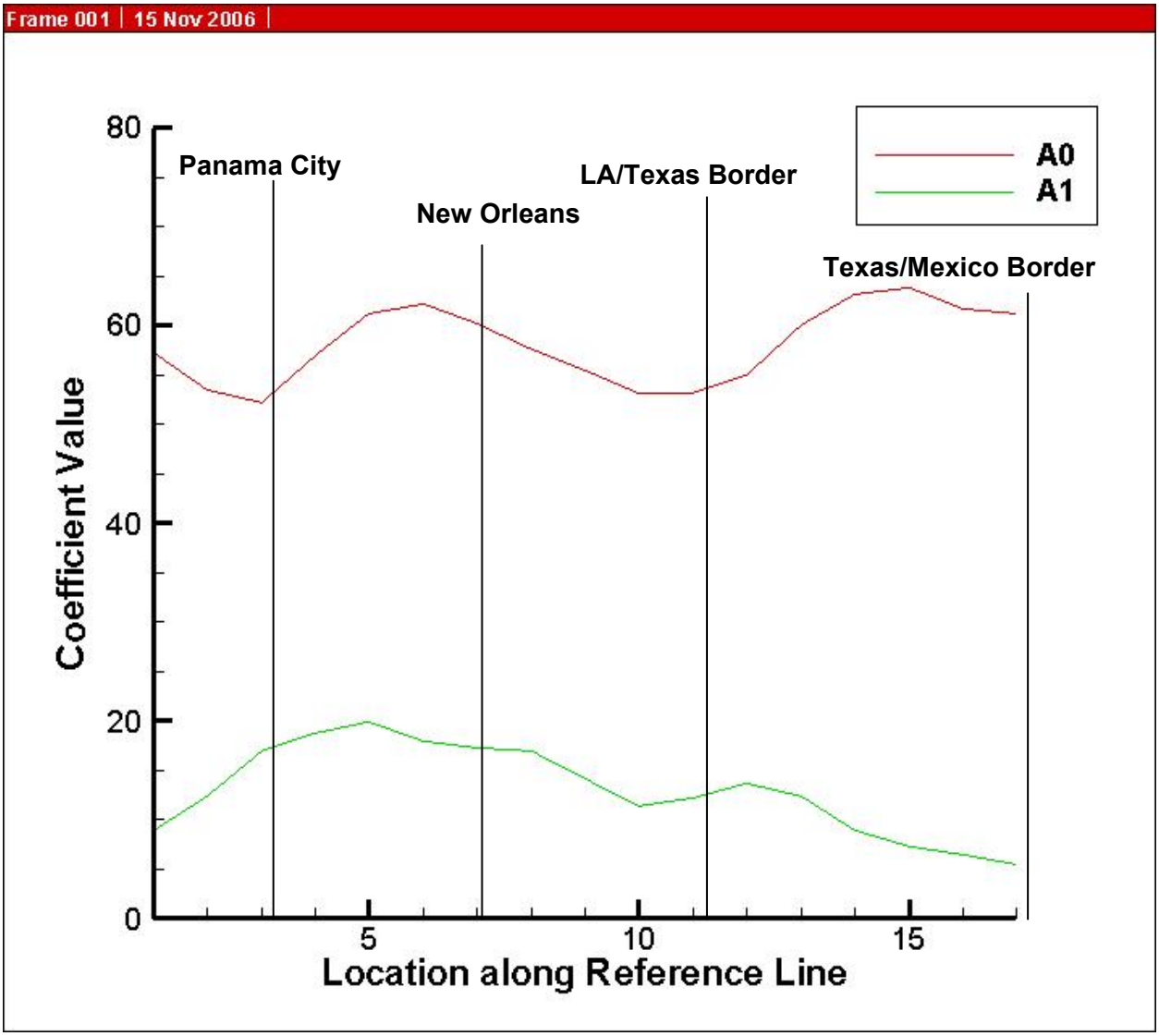

Figure 5. Gumbel coefficients for locations along reference line, based on 22-storm sample. For reference, the Gumbel equation is reproduced here in terms of its explicit dependence on x, $F(\Delta P \mid x) = \exp -\left\{\exp -\left[\frac{\Delta P - a_0(x)}{a_1(x)}\right]\right\}$, where ΔP is the pressure differential (peripheral pressure minus central pressure). It should be recognized that the frequency is assumed to be equal to 1 in this equation. Location along this line can be taken as equivalent to 1-degree increments along the coast, with the New Orleans area falling within increment 7.

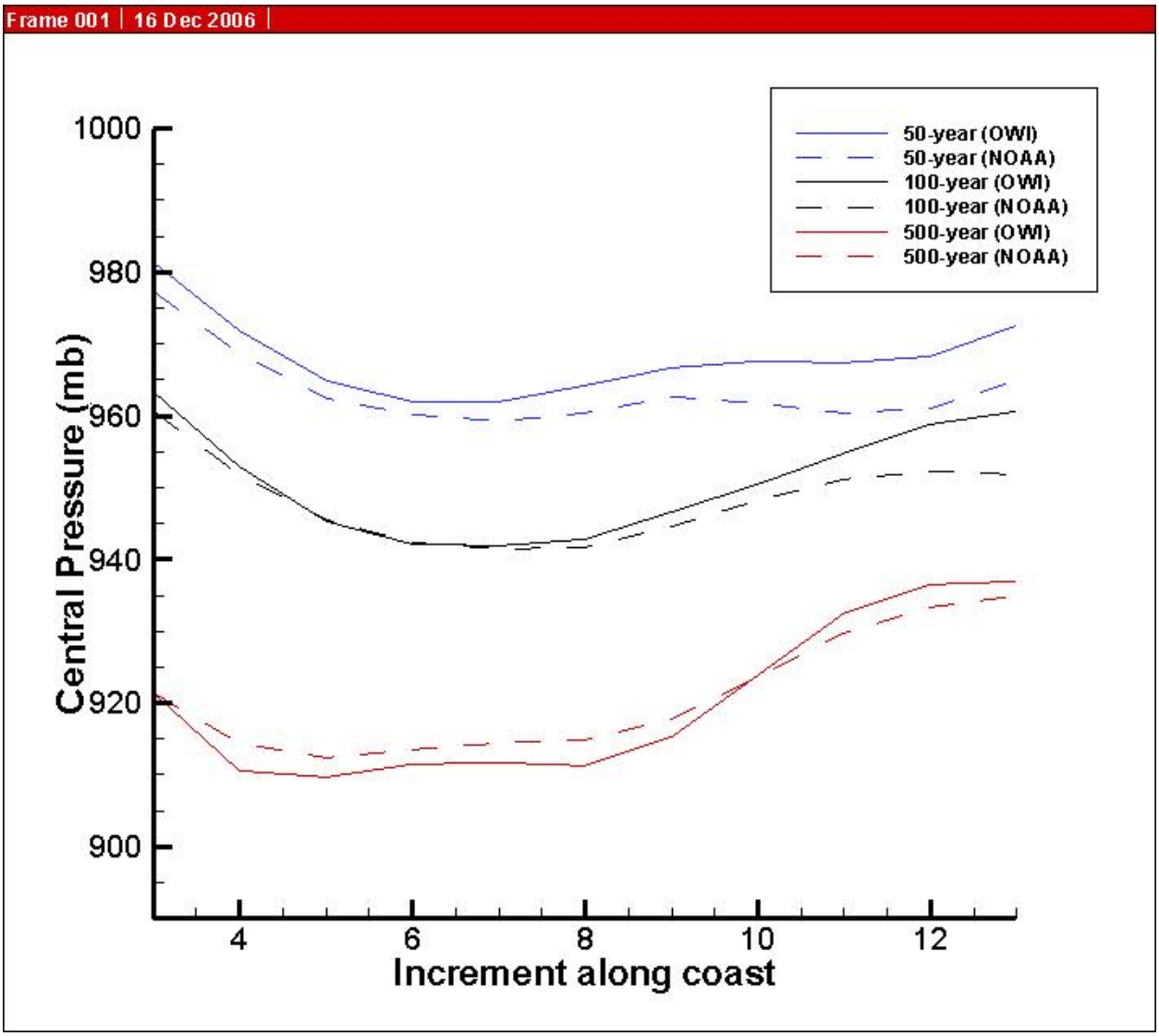

Figure 6. Distribution of 50-year, 100-year, and 500-year central pressures along the reference line shown in Figure A2, using both Oceanweather, Inc. (OWI) data and official NOAA values. Location along this line can be taken as equivalent to 1-degree increments along the coast, with the New Orleans area falling within increment 7.

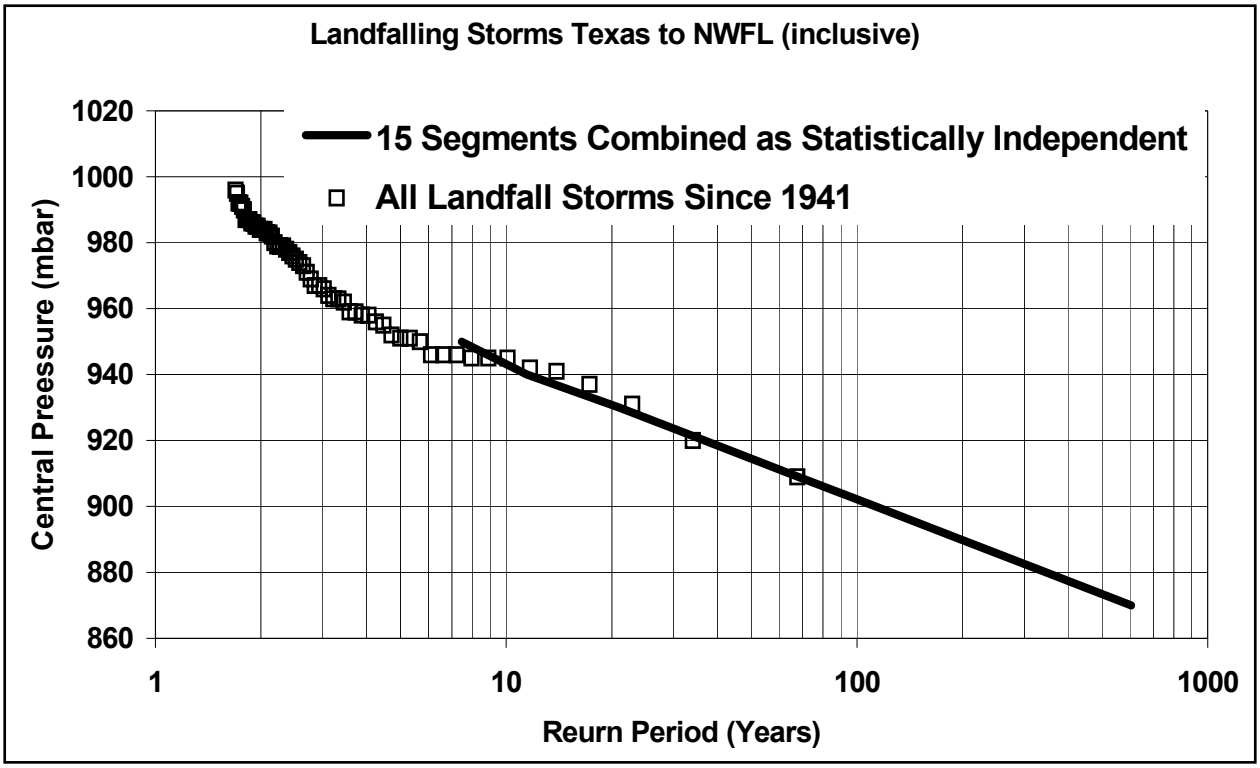

Figure 7a. Comparison of Vickery's analysis of the combination of distributions for landfalling central pressures from all coastal segments (taken from the NOAA results shown in Figure 6) compared to the distribution of all (NOAA) landfalling central pressures within the Gulf of Mexico.

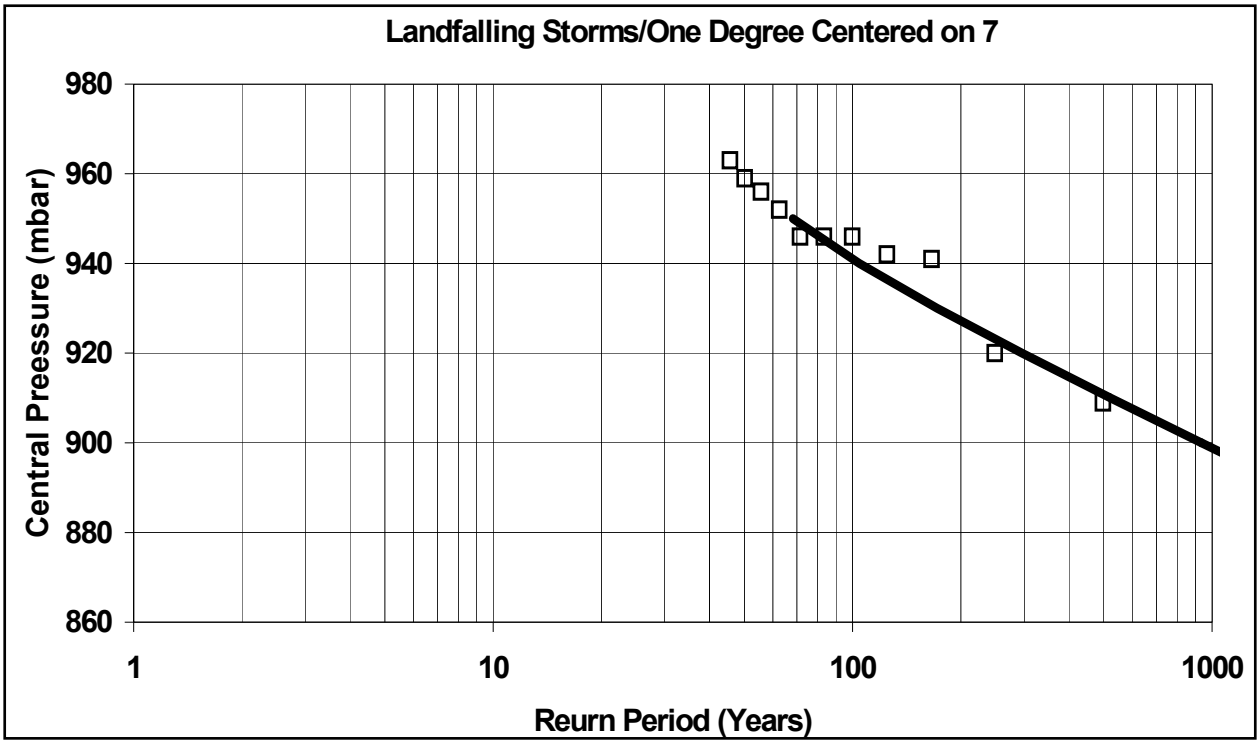

Figure 7b. Same as Figure 7a except specific to the 1-degree increment centered on 7.

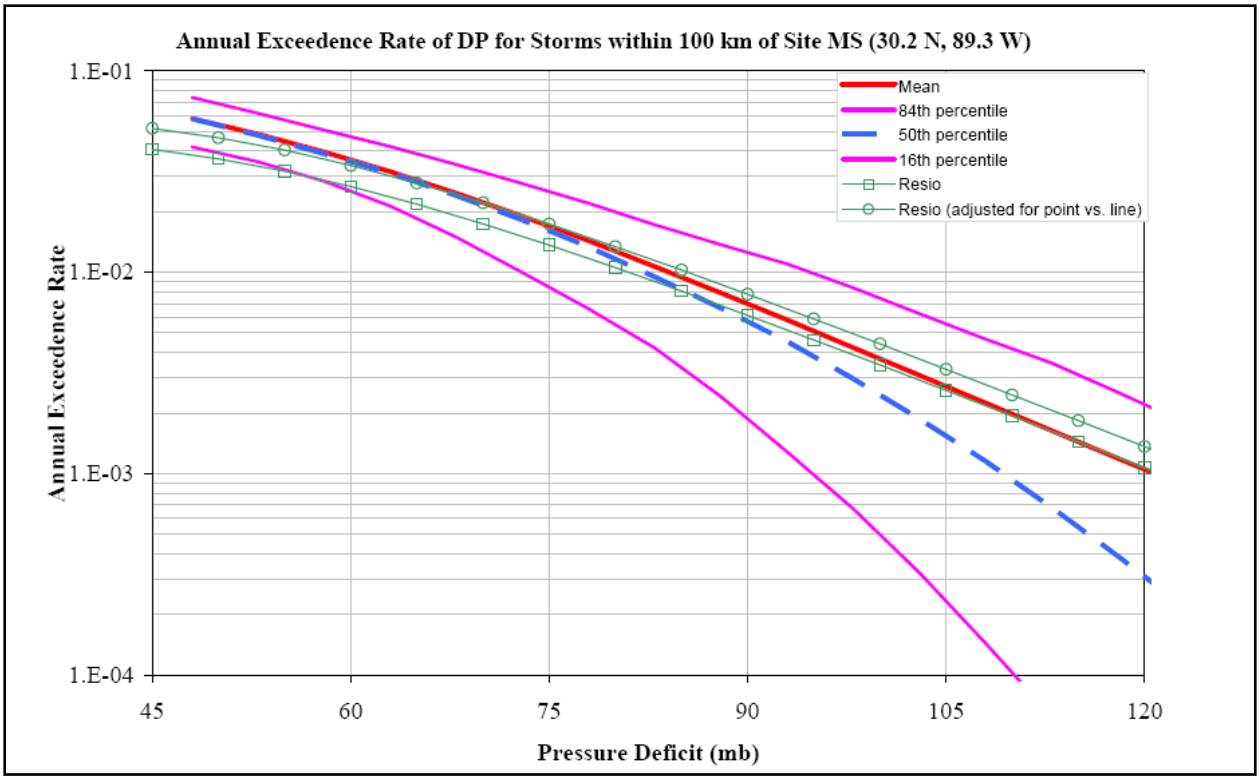

Figure 7c. Independent estimate of storm probabilities in the Mississippi coastal area by Gabriel Toro (for FEMA Region 4) compared to estimate based on Gumbel segments developed in this White Paper. As can be seen here the mean curve is in very good agreement with Toro's results.

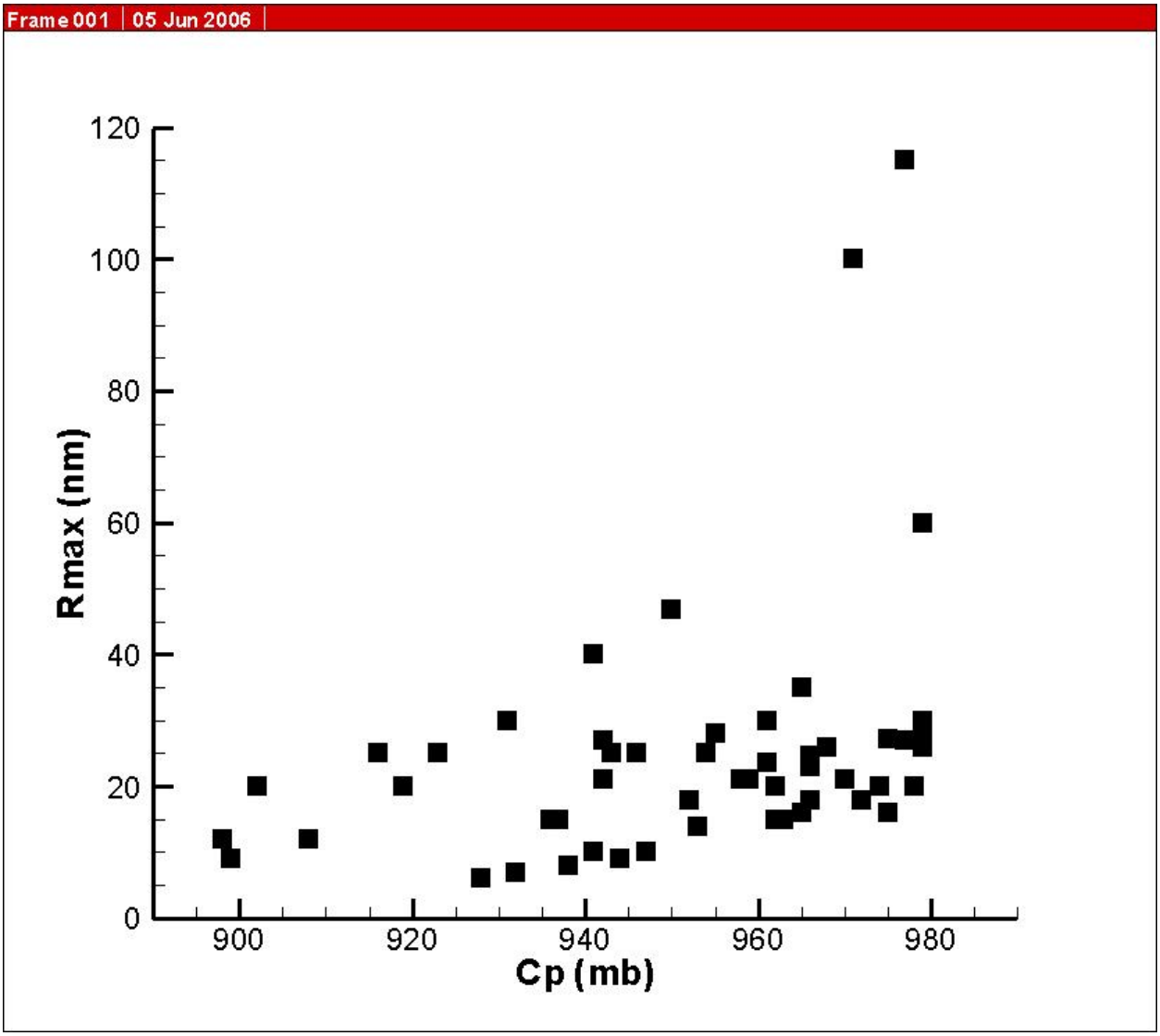

Figure 8a. Relationship between size scaling parameter (Rp) versus Central Pressure for 52 storm set in Gulf of Mexico (offcoast; all storms > Cat 2).

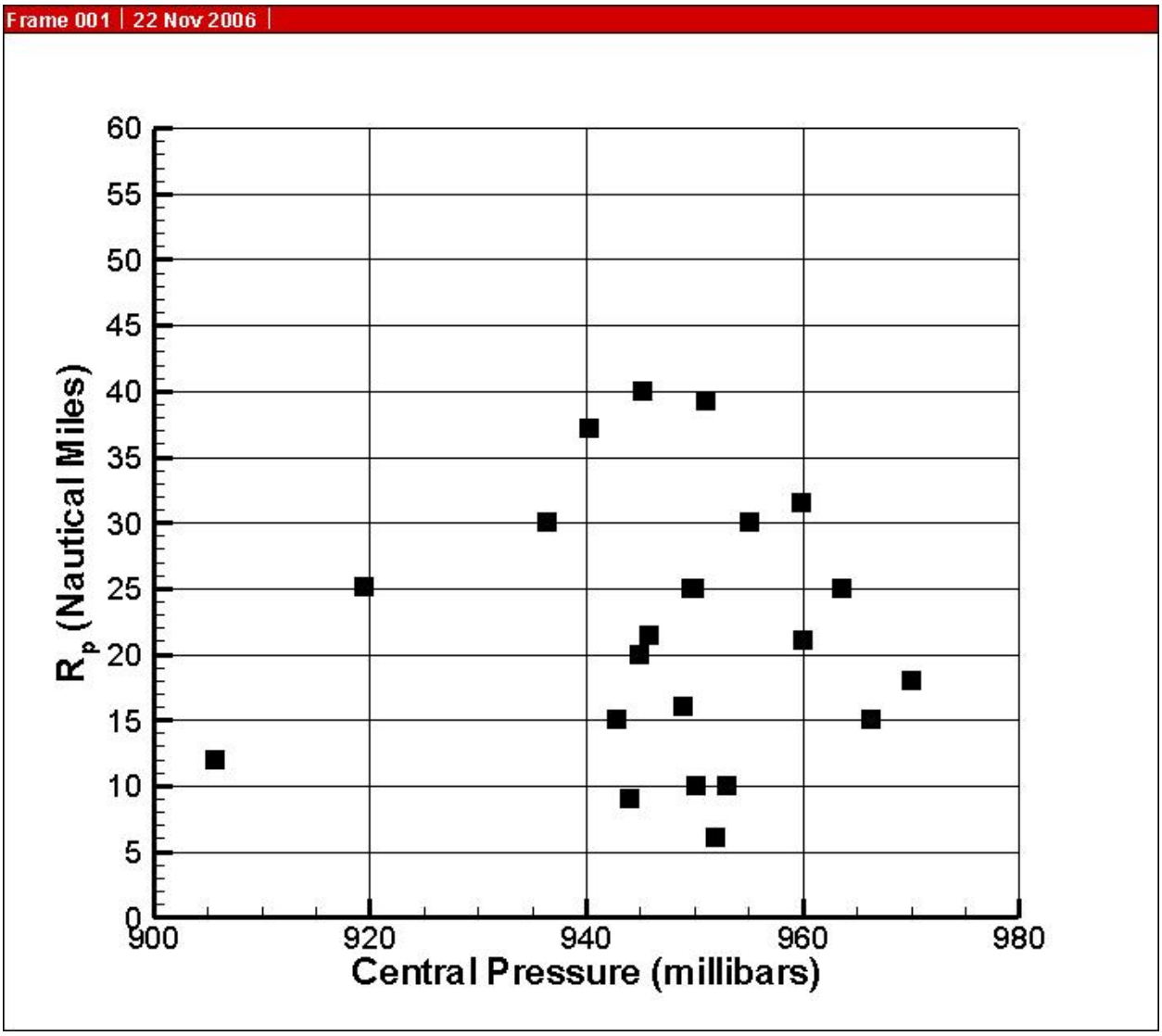

Figure 8b. Relationship between size scaling parameter (Rp) at landfall versus Central Pressure for 22 storm set in Gulf of Mexico (offcoast; all storms with central pressure < 955 at time of minimum pressure in the Gulf of Mexico).

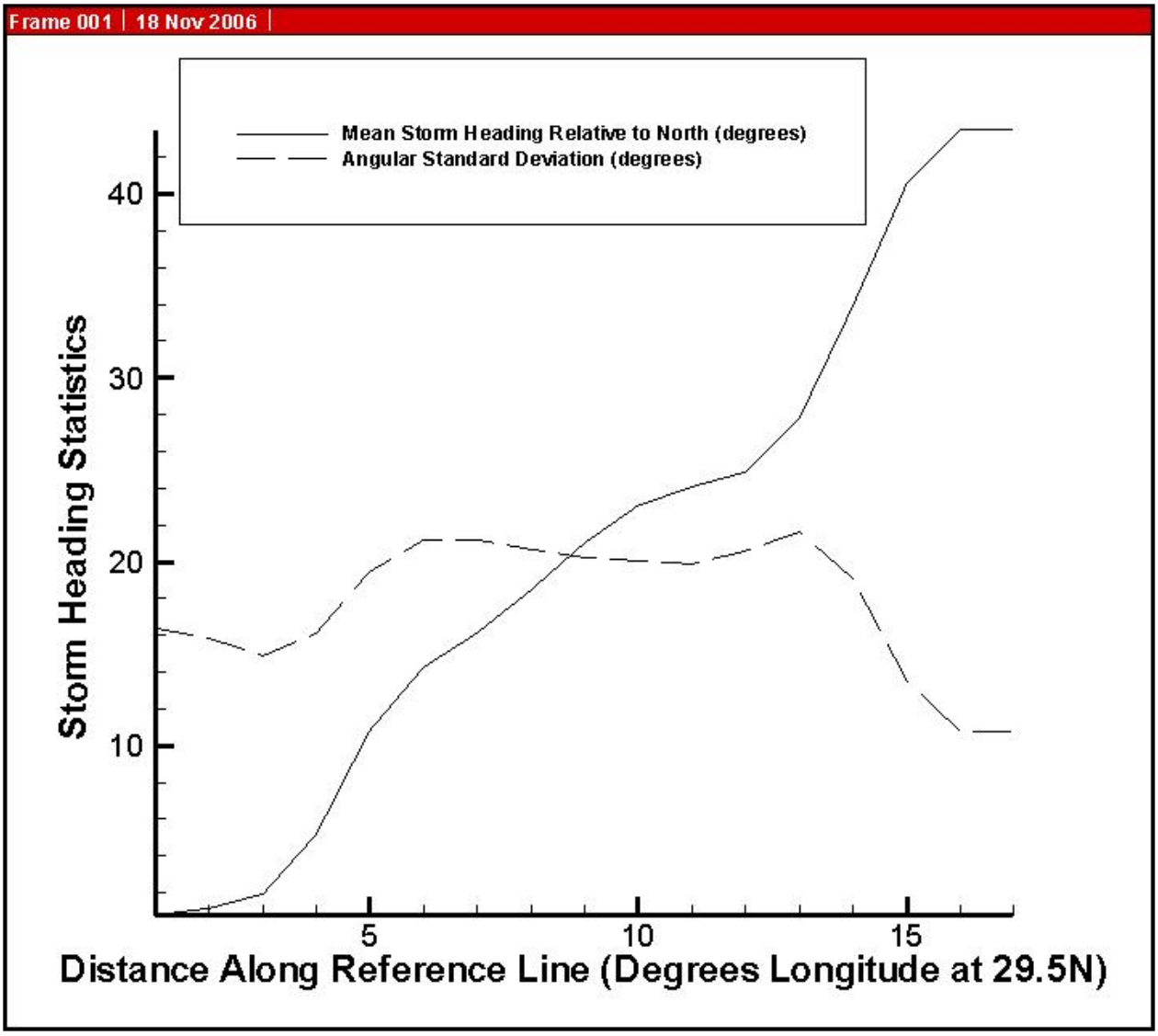

Figure 9. Plot of mean storm heading angle and standard deviation around this angle as a function of location along reference line. Distance along the x-axis can be taken as equivalent to 1-degree increments along the coast, with the New Orleans area falling within increment 7.

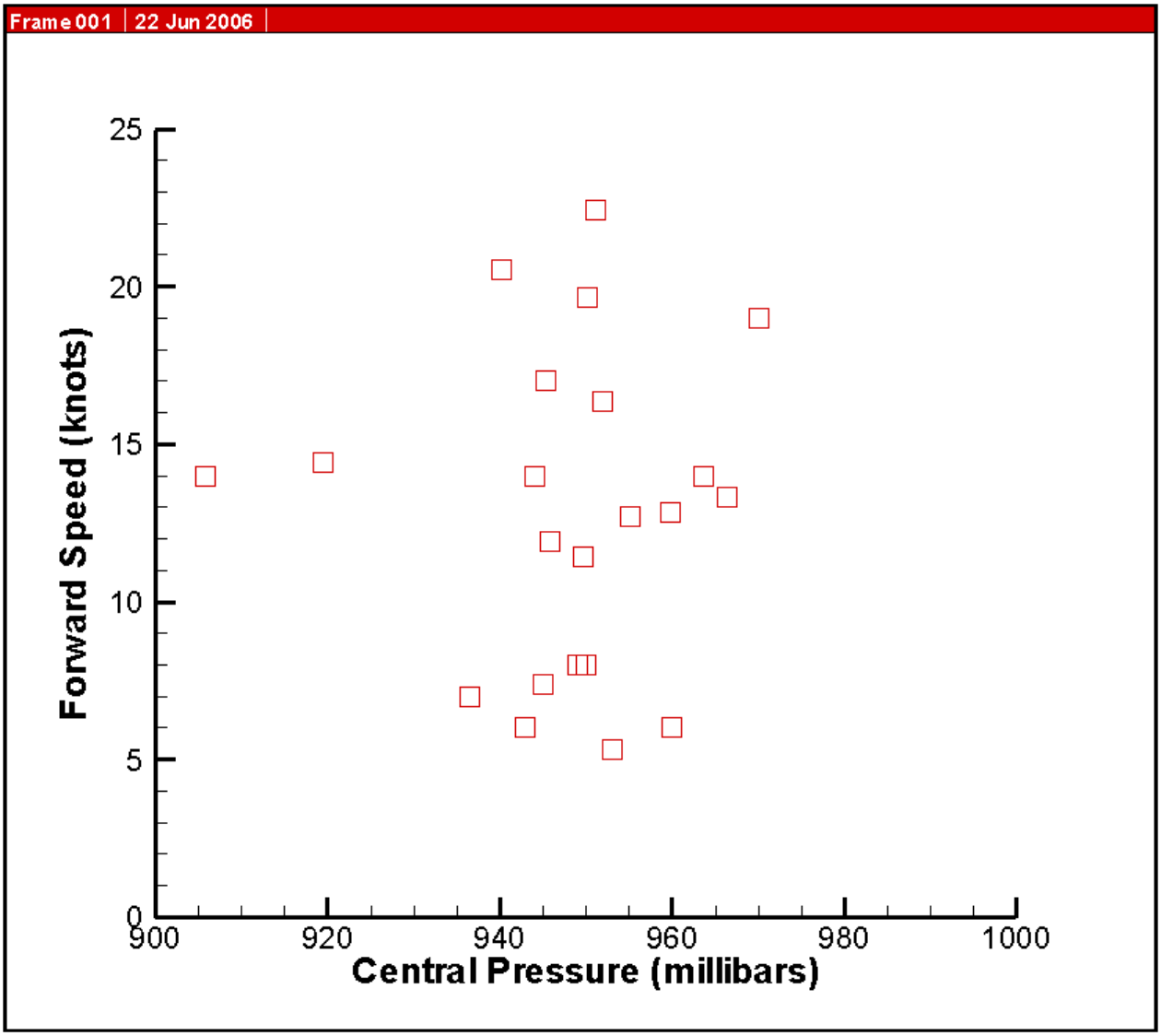

Figure 10. Plot of forward speed of storm at landfall versus central pressure at landfall.

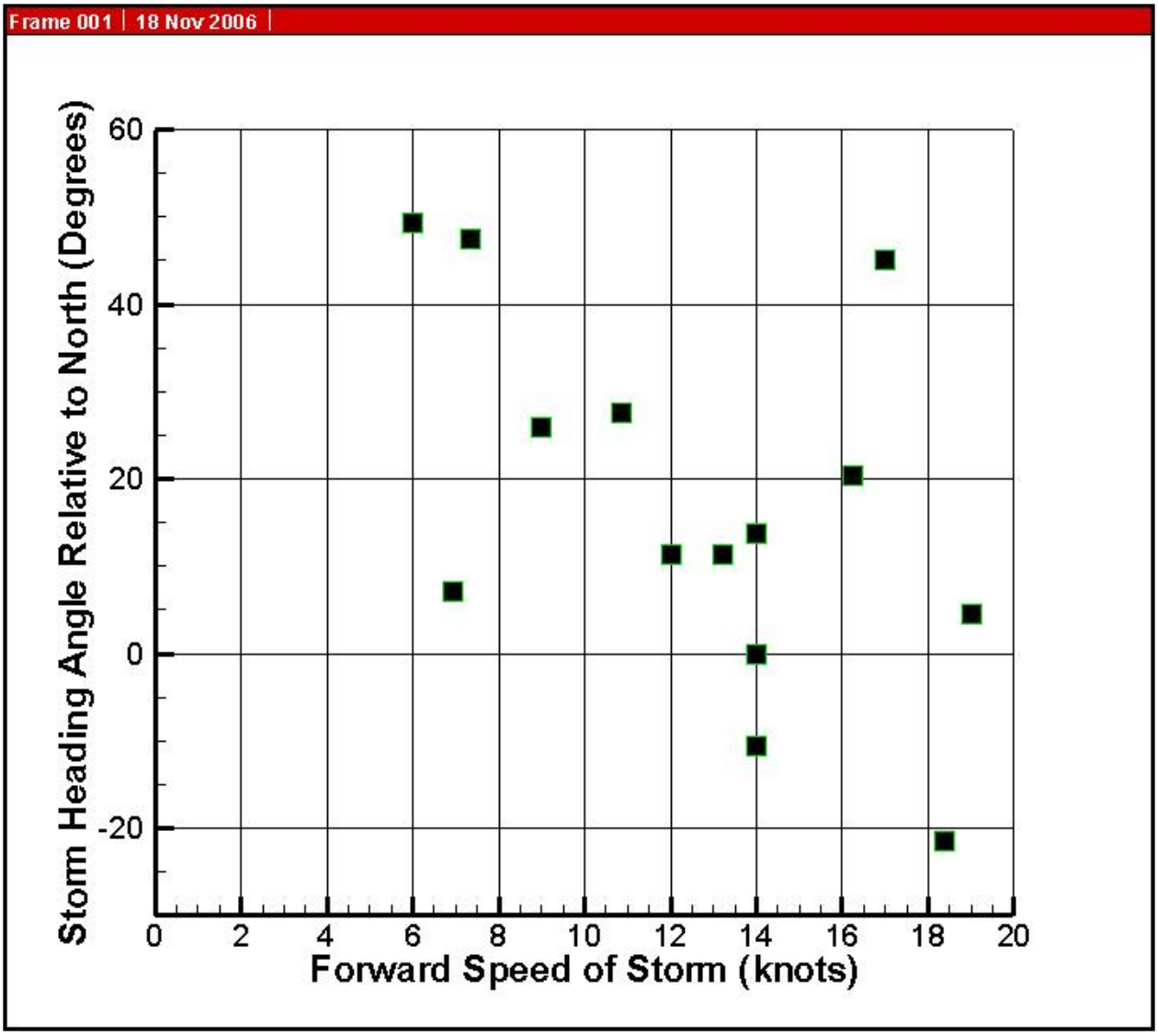

Figure 11a. Plot of storm heading and forward speed at time of landfall for only central Gulf landfalling storms.

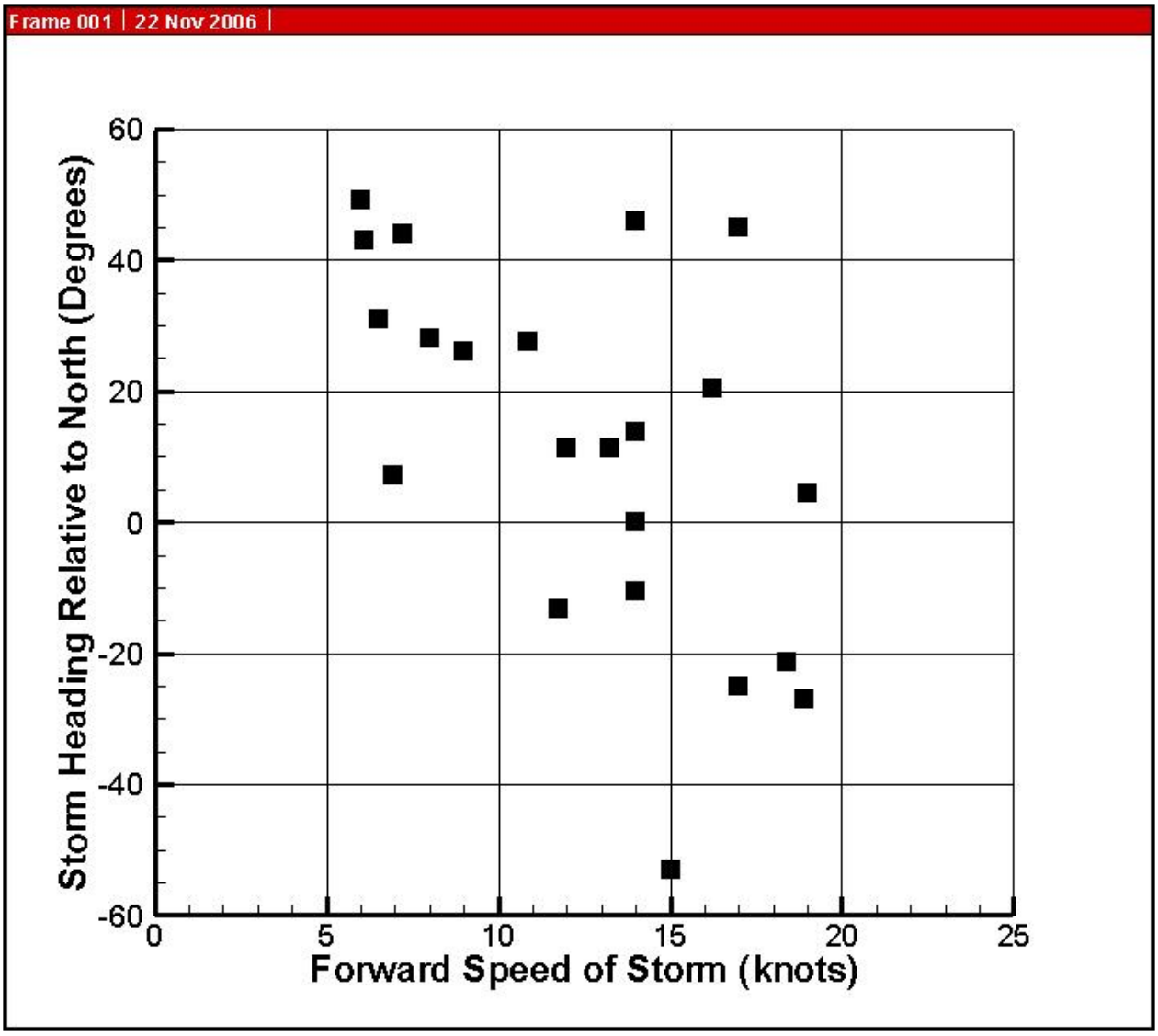

Figure 11b. Plot of storm heading and forward speed at time of landfall for the entire 22-storm sample.

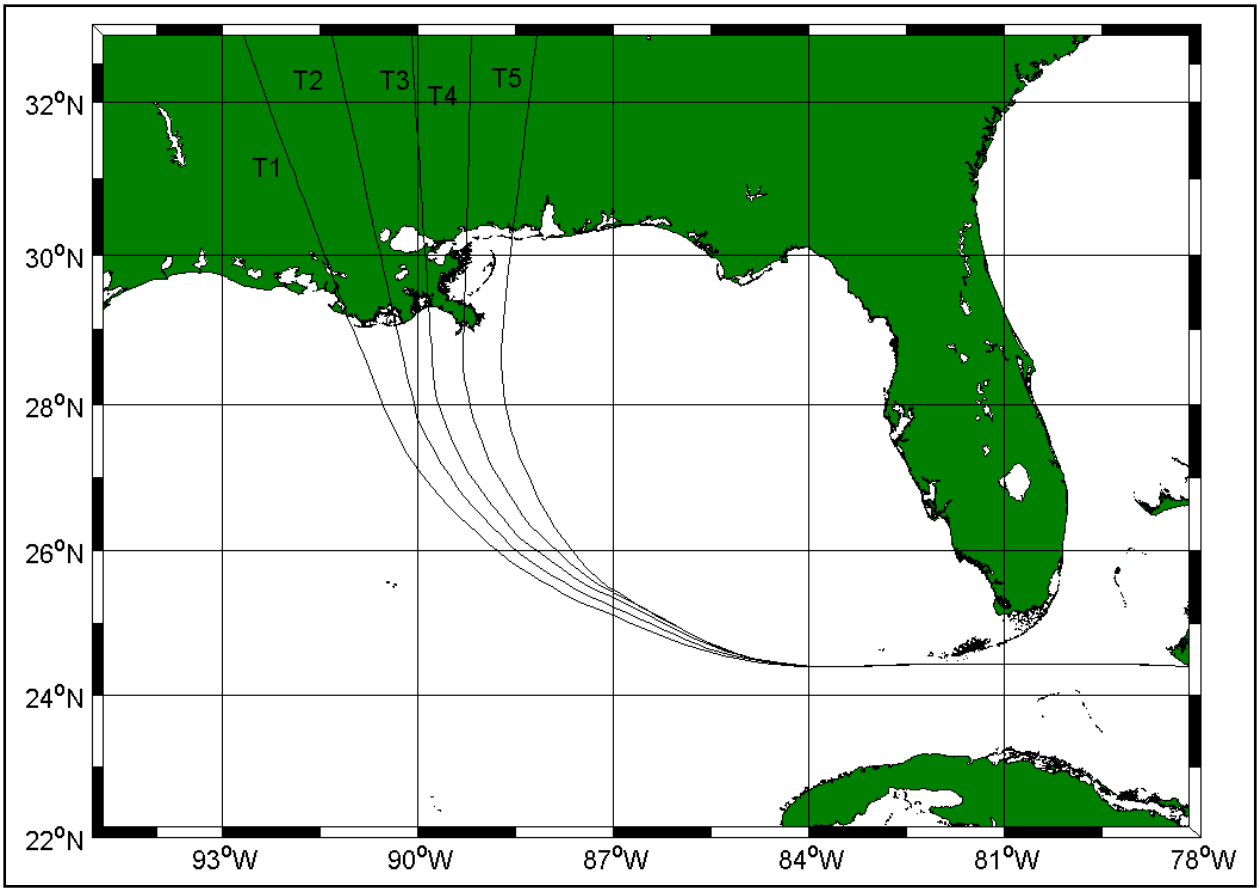

Figure 12. Central angle tracks (RICK-fan set).

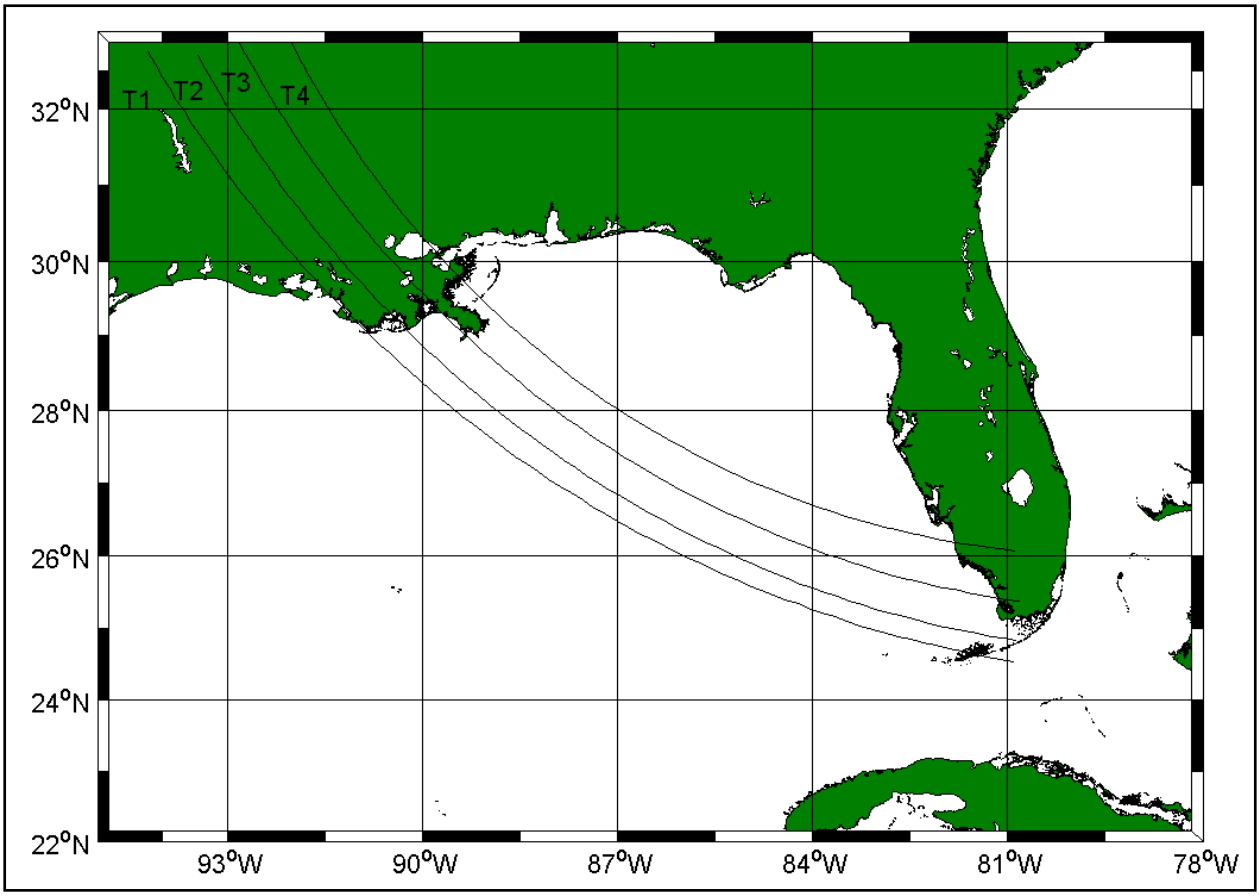

Figure 13. Tracks from southeast at 45-degree angle to RICK-fan set.

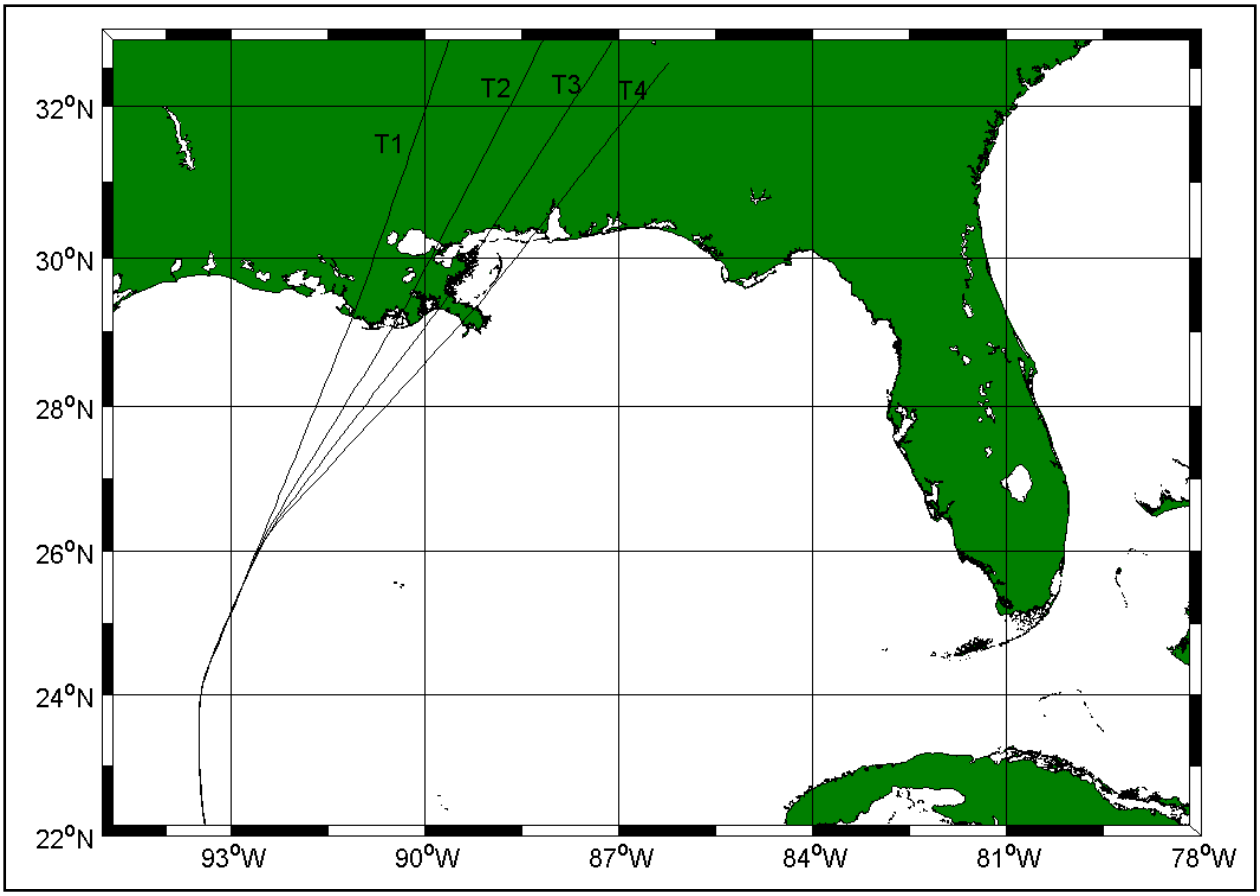

Figure 14. Tracks from southwest at 45-degree angle to RICK-fan set.

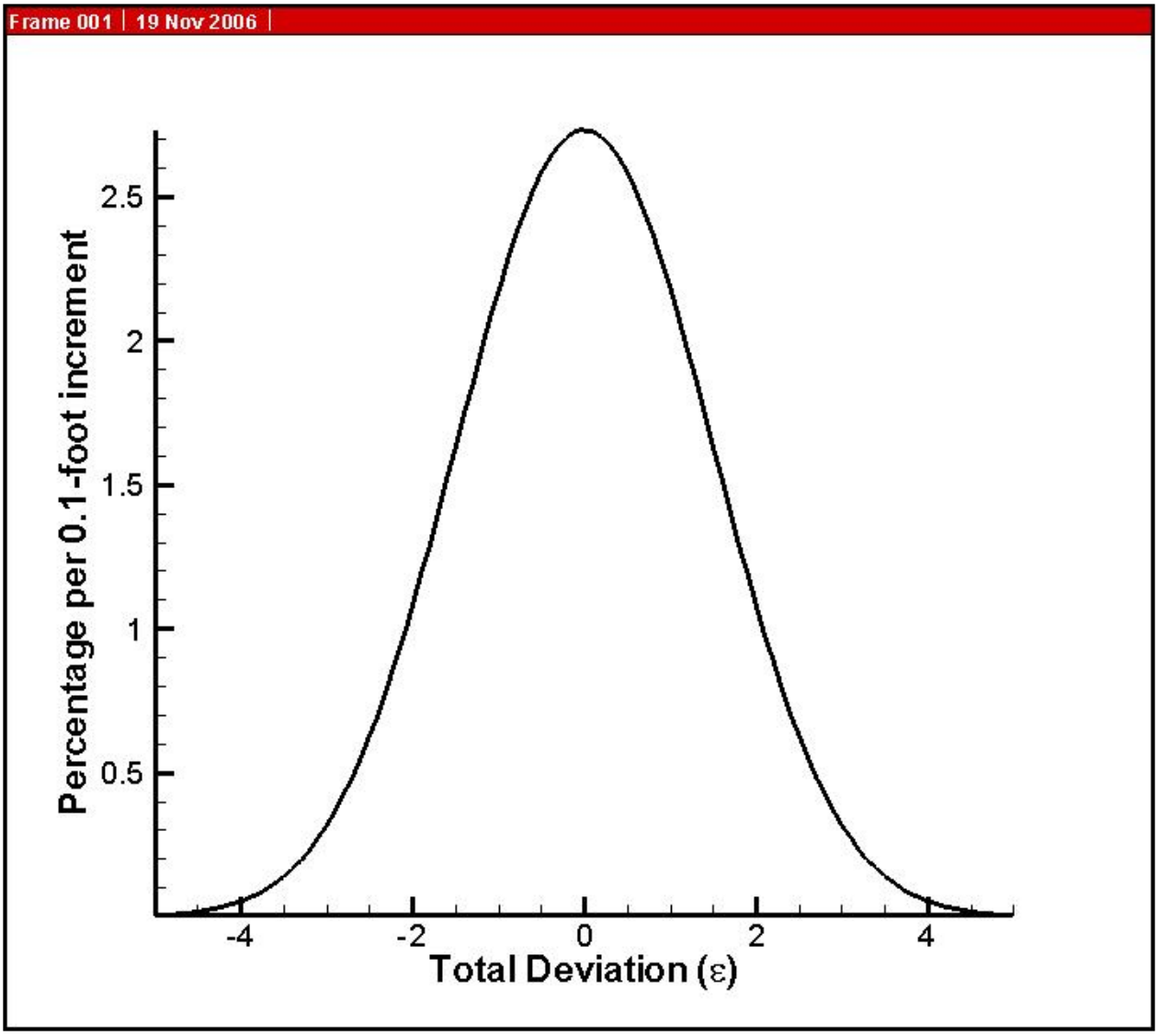

Figure 15. Percentage of deviations per 0.1-foot class as a function of deviation in feet.

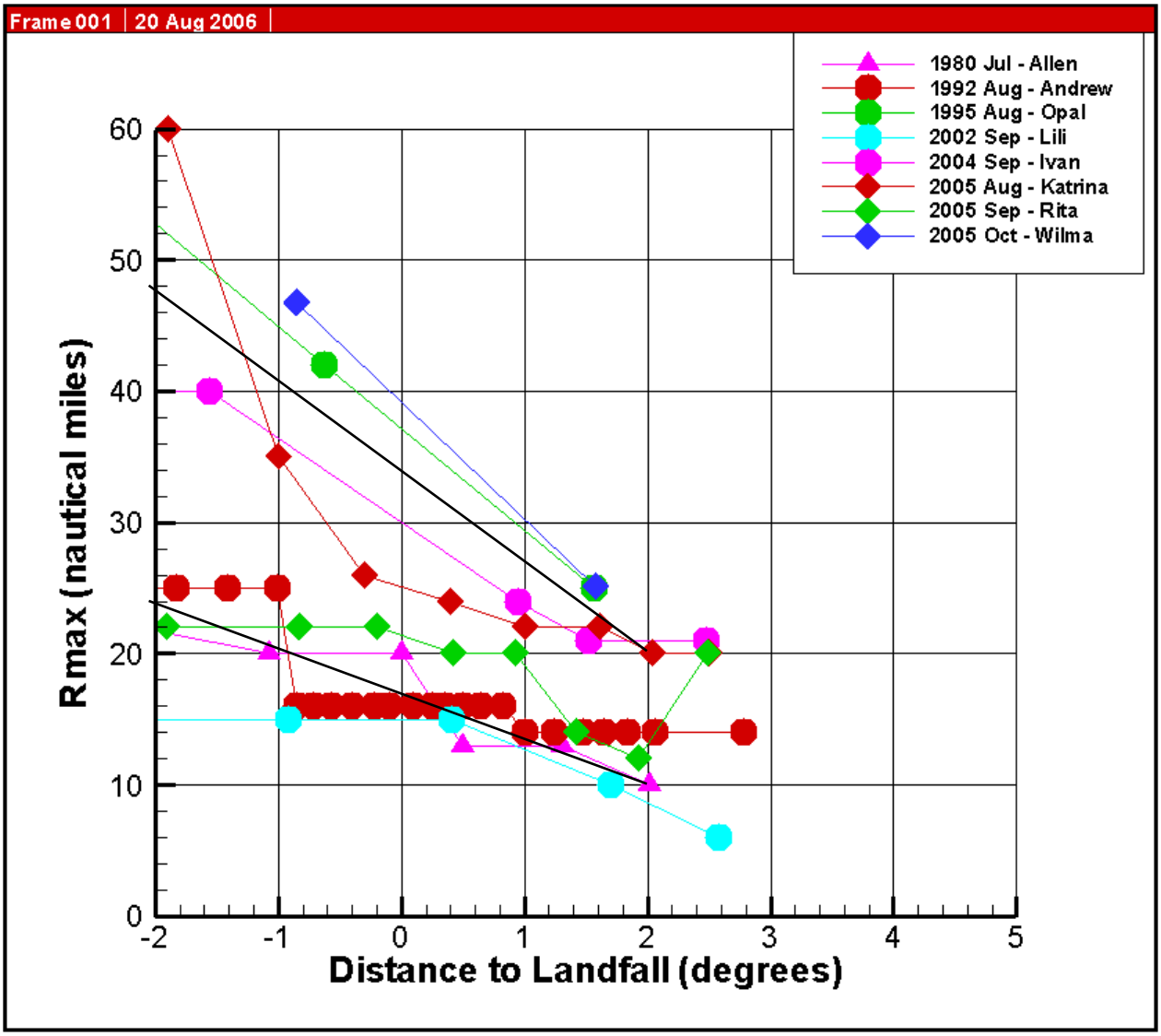

Figure 16. Increase in hurricane size during approach to coast, as seen in recent, well-documented storms.

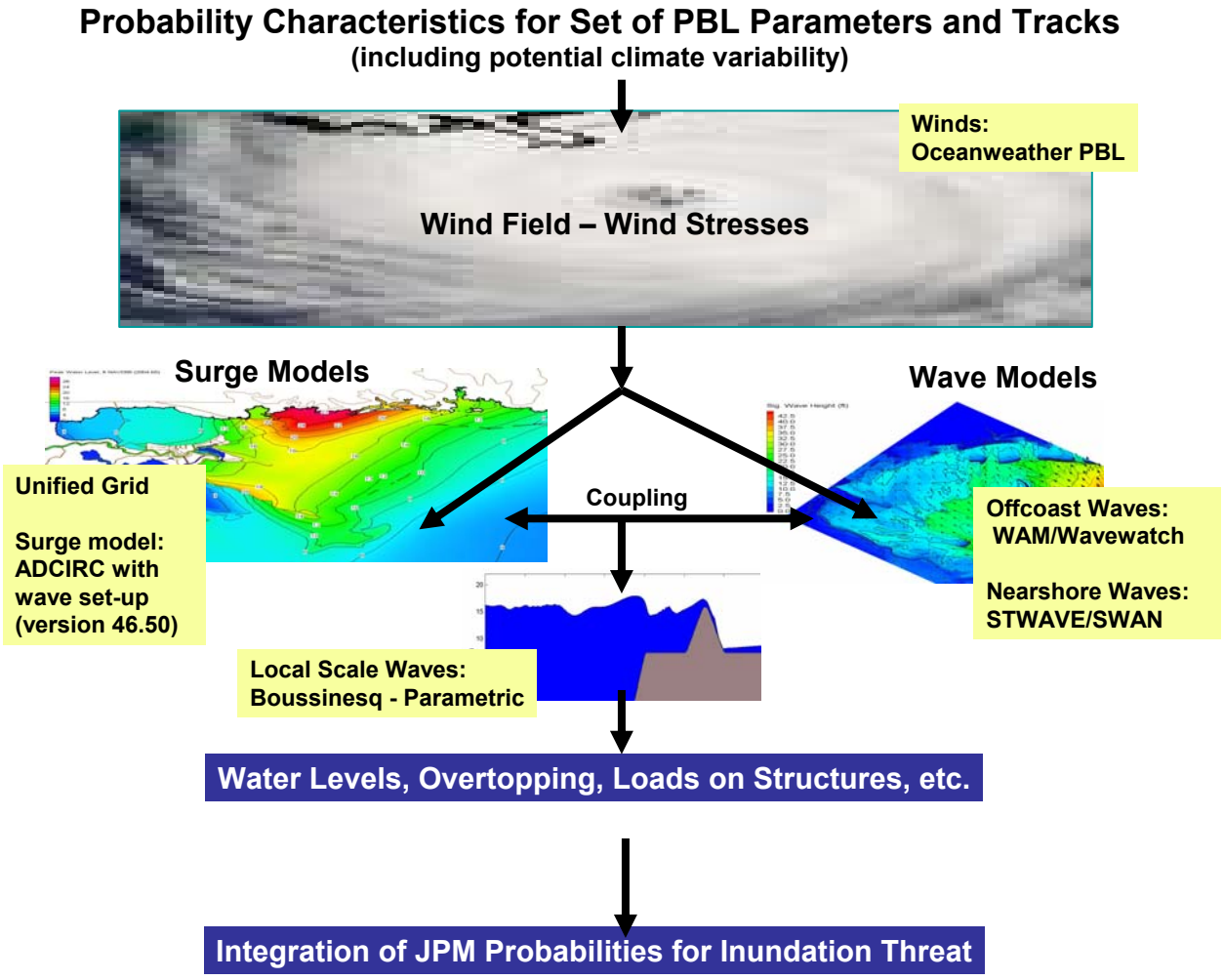

Figure 17. Schematic diagram of “production” modeling system for coastal inundation applications.

APPENDIX A of R2007
Expedient Estimation of Return Periods for Specific Historical Storms

On one hand, the most accurate characterization of the return period for a specific storm water level is to wait until the stage-frequency relationships have been developed and see where the water levels from that storm fall on this curve. Inspection of such an approach would show that water levels from a specific storm would fall at different return periods at different locations. A different, albeit more approximate approach which does not have to wait until the final results of simulations are complete, is to treat the storm water level potential in terms of the primary parameters affecting peak surge levels, typically storm intensity, storm size, angle of approach to the coast, forward storm speed, the geometry of the coast, and the offshore bathymetric slope.

Application to Hurricane Katrina

Figure A1, taken from Irish et al. (submitted for journal publication), shows the dependence of peak surge on storm intensity (peripheral pressure minus central pressure) and size (scaling radius for the pressure field). These values were generated from ADCIRC simulations using the Oceanweather Planetary Boundary Layer (PBL) model for wind fields. In these runs, storms were held at constant intensity and size during the approach to the coast. This figure is appropriate for a very shallow offshore slope (1:10000), found to be approximately representative of the continental shelf east of the Mississippi River in this area. Sensitivity studies of the effects of storm speed and storm approach angle showed that these factors were of secondary influence on surges at the coast, at least within the ranges of expected values for large, intense storms. Sensitivity studies also showed that although the coastal geometry in the New Orleans area (the presence of the Mississippi River Delta and river levees) tends to modify local storm surge levels, this factor did not change the relative ranking of the different storms.

Assuming that we can neglect the secondary factors, the relative ranking, and thus the return period for a specific event, can be deduced from a combination of Figure A1 and a specification of the joint probability structure of storm intensity and storm size. The estimation of the latter is a key part of the same methodology being used in the JPM-OS application in this area.

The frequency of storms along a coast has units of number of storms per year per length of coastline. For our application, we will assume that a storm within 1/2 degree longitude is the relevant parameter for our purpose here. This is equivalent to assuming that the surge within ±1/2 degree remains sufficiently close to the peak value that is can be considered approximately equal to the peak (within 10%). Although a continuous method can be used for this estimation method, the results were quite similar and the discretized method is easier to explain. Figure A2 shows a line along the Gulf of Mexico coastline that will be taken as the "sample line" for landfalling conditions in our analysis. A centered, running average of landfalling conditions over a distance of 6 degrees along this line was used to estimate the frequency of storms and to accumulate samples for extremal analysis within contiguous 1-degree (longitude – at 29.5 degrees) increments along the coast. The New Orleans area is located in Increment 7 along the coast in this scheme.

The storm sample used in this analysis is the 22-storm sample shown in Figures A3-A5 (essentially all storms with central pressures less than 955 mb during their transit through the Gulf of Mexico since 1941). Eleven of these storms fell within ±3 degrees of the center of the New Orleans section of coast. Since this is not a very large number, we restrict our analysis to a 2-parameter (Gumbel) distribution here. The conditional Gumbel distribution of hurricane pressure differential was found to be given by

$$\text{A1. } F(\Delta p \mid hurricane) = e^{-e^{-z}}$$

where F is the condition cumulative distribution function (i.e. the expected CDF given a hurricane) and z is given by the best 2-parameter fit

$$z = \frac{\Delta p - a_0}{a_1}$$

where a_0 and a_1 are the distribution parameters and Δp is the pressure differential. For Increment 7 along the coast, the value of a_0 and a_1 are 56.557 and 16.463, respectively. The frequency of occurrence of hurricanes for this coastal segment is 0.0486 per year per degree (or once per every 20.6 years, or so).

Since, the contours in Figure A1 denote lines of equal surge, The probability of a storm capable of generating a storm surge equal to or greater than that produced by Hurricane Katrina can be estimated by the sum of the probabilities in regions A, B, and C, delineated by different R_p limits in Figure A6 or

$$F(\eta) = \int A + \int B + \int C$$

It can be shown that all three of these integrals can be written in a common form

$$\text{A2. } \int (A,B,C) = \int_{R_1}^{R_2} \int_{\Delta p(R)}^{\infty} \frac{\partial F(\Delta p)}{\partial \Delta p} P(R_p \mid \Delta p) d\Delta p dR_p$$

where the limits of the first integral are made to match the region shown in Figure A6. The conditional probability for size is given by a Gaussian distribution of the form

$$P(R_p \mid \Delta p) = \frac{1}{\sigma(\Delta p)\sqrt{2\pi}} e^{-\frac{x^2}{2}}$$

A3. *where*

$$x = \left(\frac{R_p - \overline{R}_p(\Delta p)}{\sigma(\Delta p)} \right)$$

In this equation a linear regression ($\overline{R}_p = 14. + 0.3 * (110. - \Delta p)$ – with units for R_p and $\overline{R}_p$ in nautical miles and units for Δp in millibars implied) was used to represent the conditional mean for storm size and the standard deviation was taken as $\sigma(\Delta p) = 0.44\overline{R}_p(\Delta p)$. The sum of all three integrals is 0.0518, which can be interpreted as slightly more than 1 hurricane in 20 can produce a surge of Katrina's level in the New Orleans area. When 1 is divided by the product of the two frequency parameters, it yields an estimate of 397.6 years for the return period of a storm capable of producing a surge of comparable magnitude to Katrina. For practical purposes, Katrina would seem to fall in the range of a 400-year storm, in terms of storm surge generation. It should be noted that the methodology described here pertains to the area of maximum surges within a storm; consequently, the surges at some distance from area of maximum surge will certainly not be 400-year surges for those points.

Application to Hurricane Rita

The same procedure outlined above, modified to consider the different offshore slope, was applied to Hurricane Rita, with a landfall in Increment 10 of our analysis. A slope of 1:1000, which is characteristic of the shelf region in the area west of the Mississippi River, was adopted here in the idealized surge modeling referenced here. The return period for this storm from this analysis is 89.7 years. Again, for practical purposes, this can be taken to imply that Rita was somewhere in the neighborhood of a 90-year storm, in terms of storm surge.

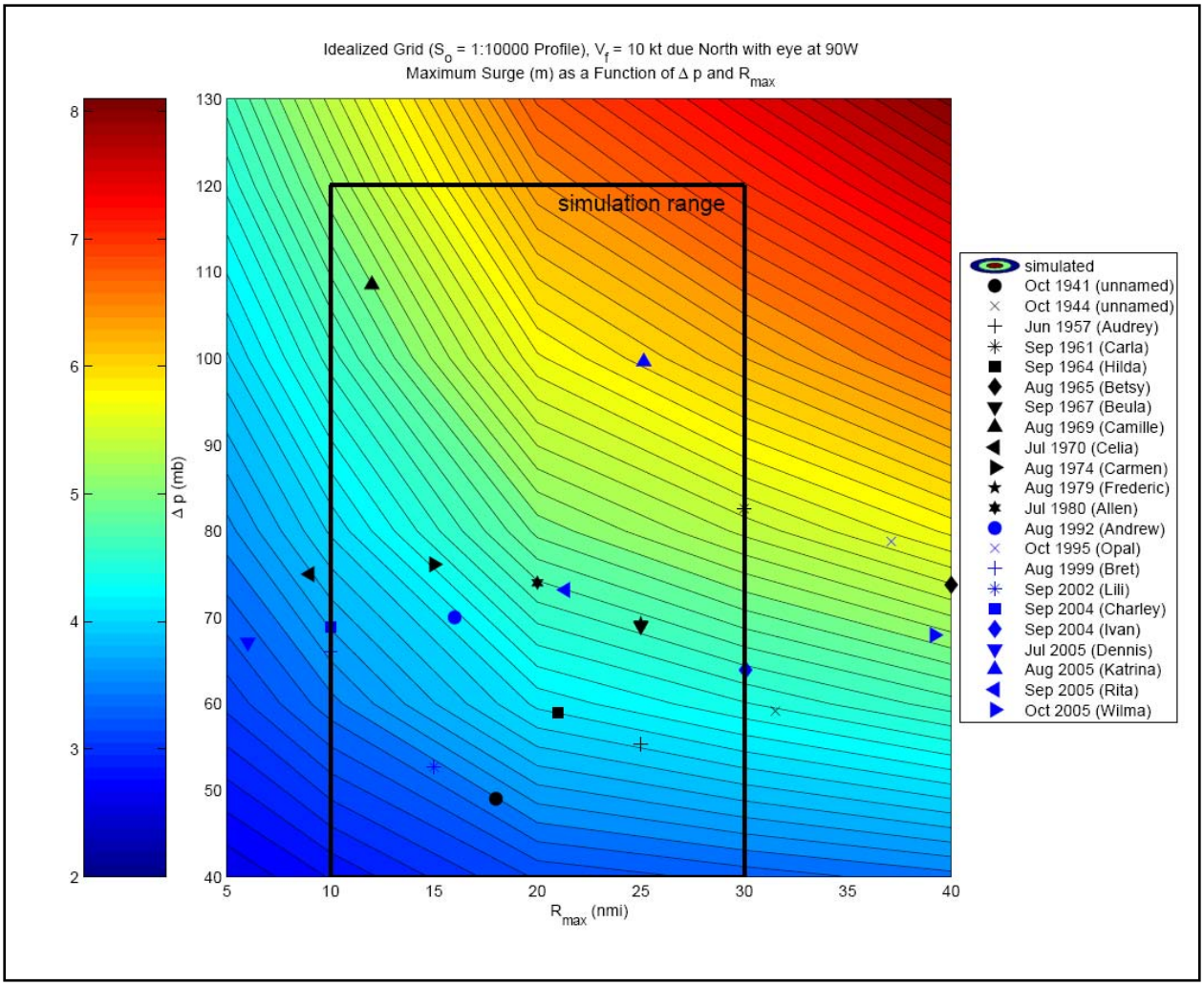

Figure A1. Contour plot of peak surge levels along a straight coast with a constant offshore slope as a function of storm size (R_{max} = R_p in our terminology) and storm intensity (peripheral pressure minus central pressure). The storm values used in this plot are the offshore conditions, rather than the conditions at the coast.

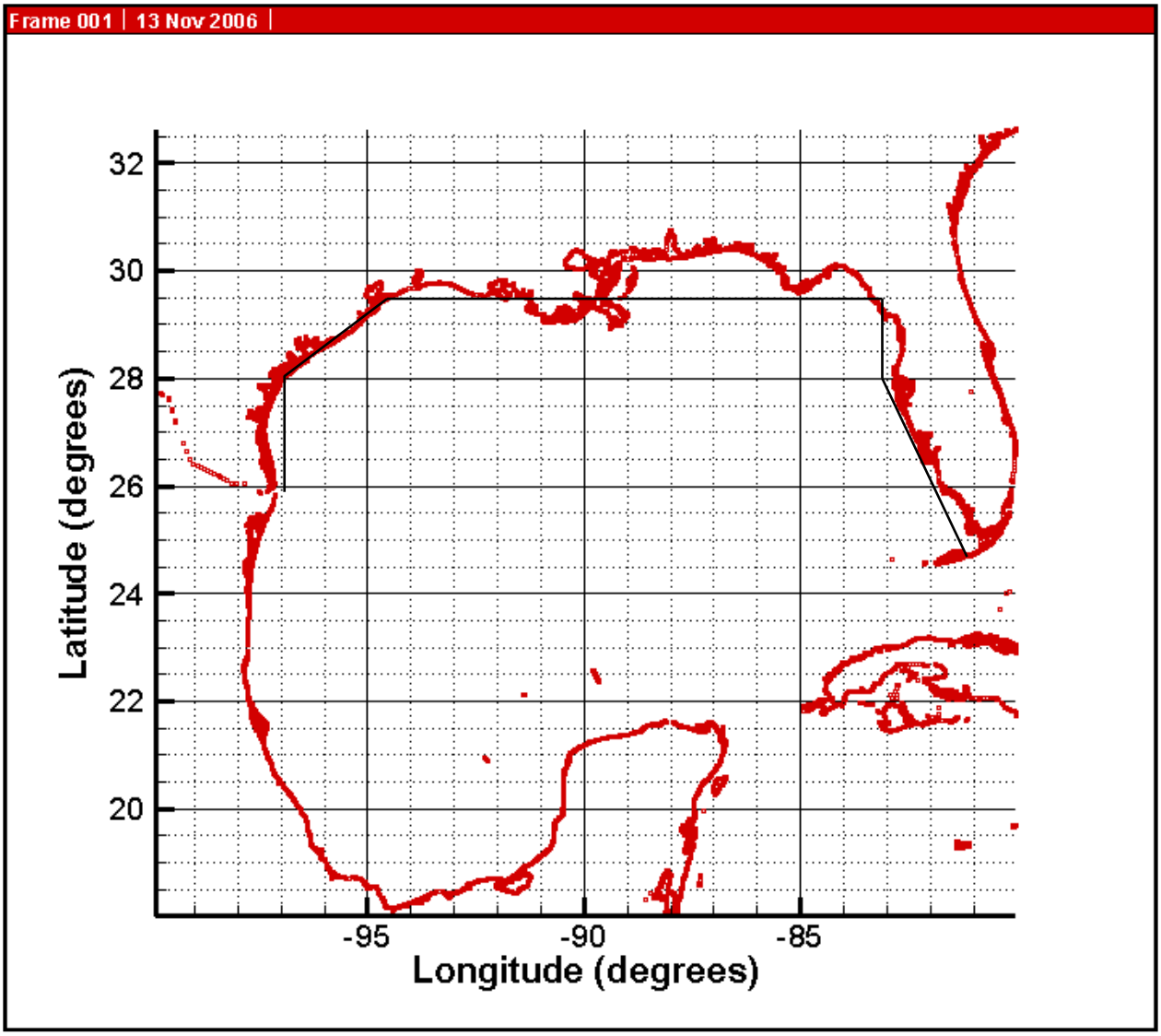

Figure A2. Location of line for analysis of hurricane landfalling characteristics. Throughout this white paper, one-degree increments of distance along this line from east to west, with the "zero-value" taken at -83 degrees longitude, will be used as a locator for discretized sections of coast. In this convention, the increment number for any section being analyzed is given by $N_{increment}$ = *Integer* (-83-*longitude*). For example, any point with a longitude less or equal to -83 and greater than -84 would fall in increment 0, any point with a longitude less than or equal to -85 and greater than -85 would fall in increment 1, etc.

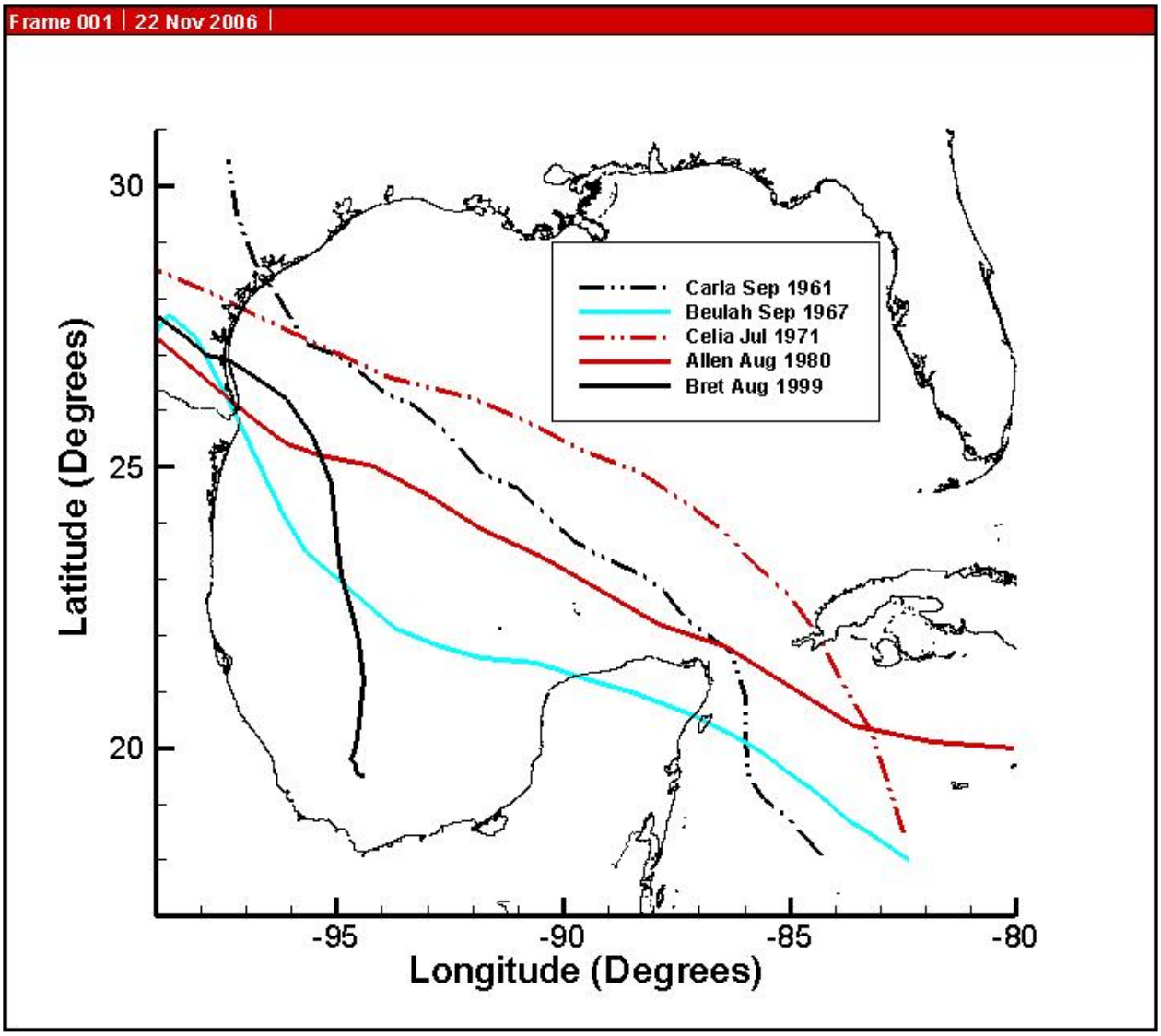

Figure A3. Tracks of all hurricanes (1941-2005) making landfall in the Western Gulf of Mexico for storms that attained a central pressure of 955 millibars or lower during its transit through the Gulf of Mexico.

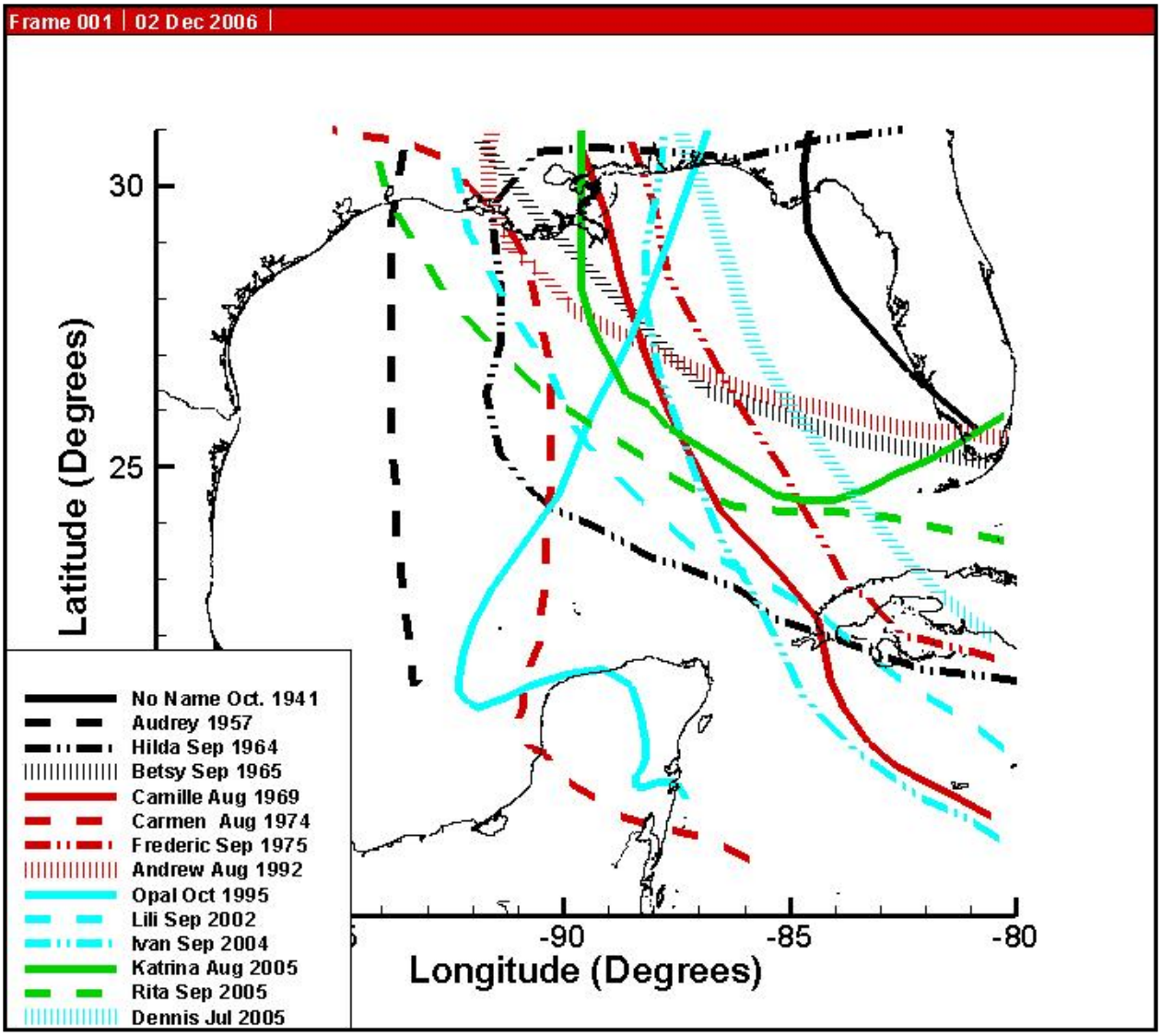

Figure A4. Tracks of all hurricanes (1941-2005) making landfall in the Central Gulf of Mexico for storms that attained a central pressure of 955 millibars or lower during its transit through the Gulf of Mexico.

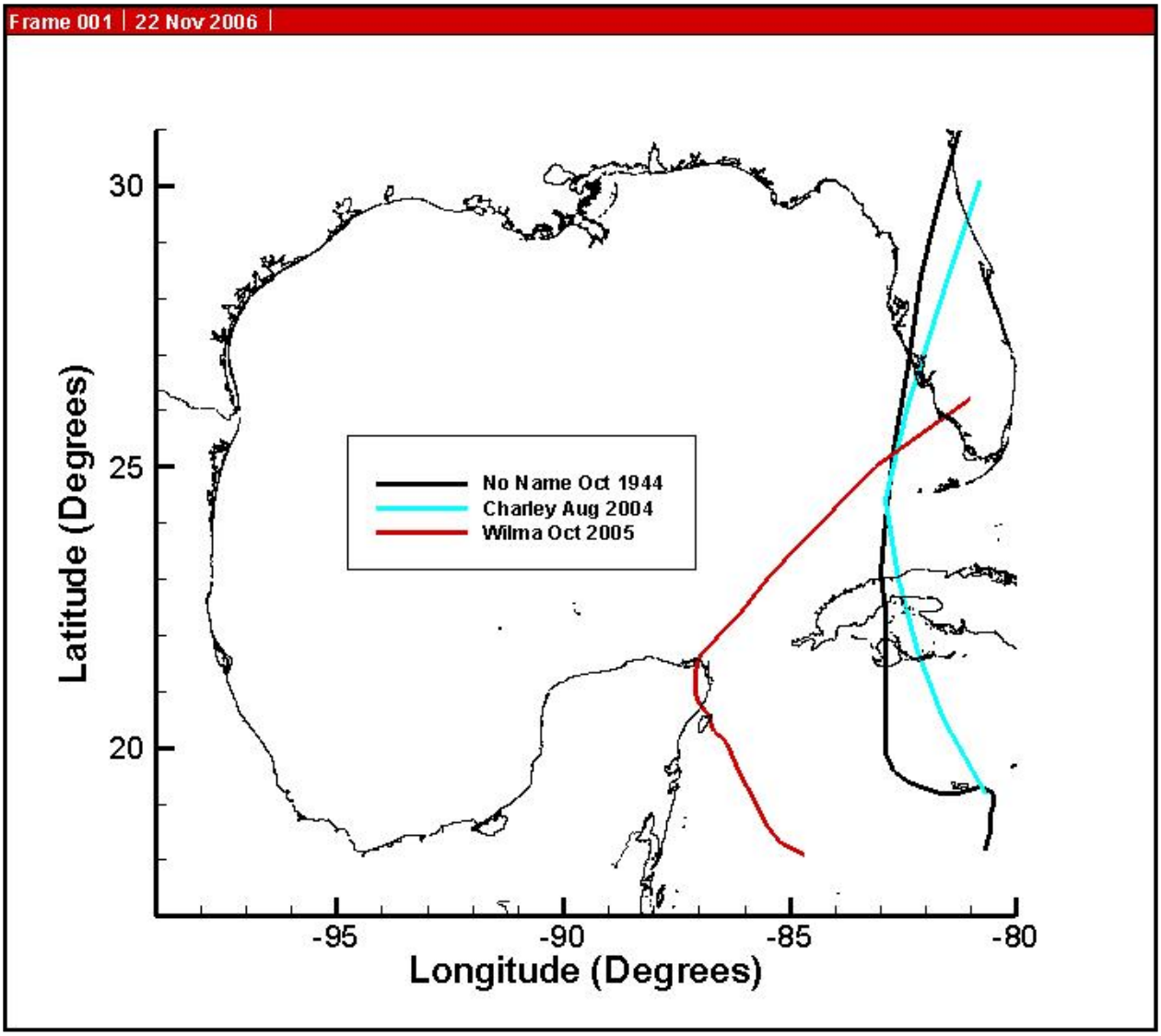

Figure A5. Tracks of all hurricanes (1941-2005) making landfall in the Eastern Gulf of Mexico for storms that attained a central pressure of 955 millibars or lower during its transit through the Gulf of Mexico.

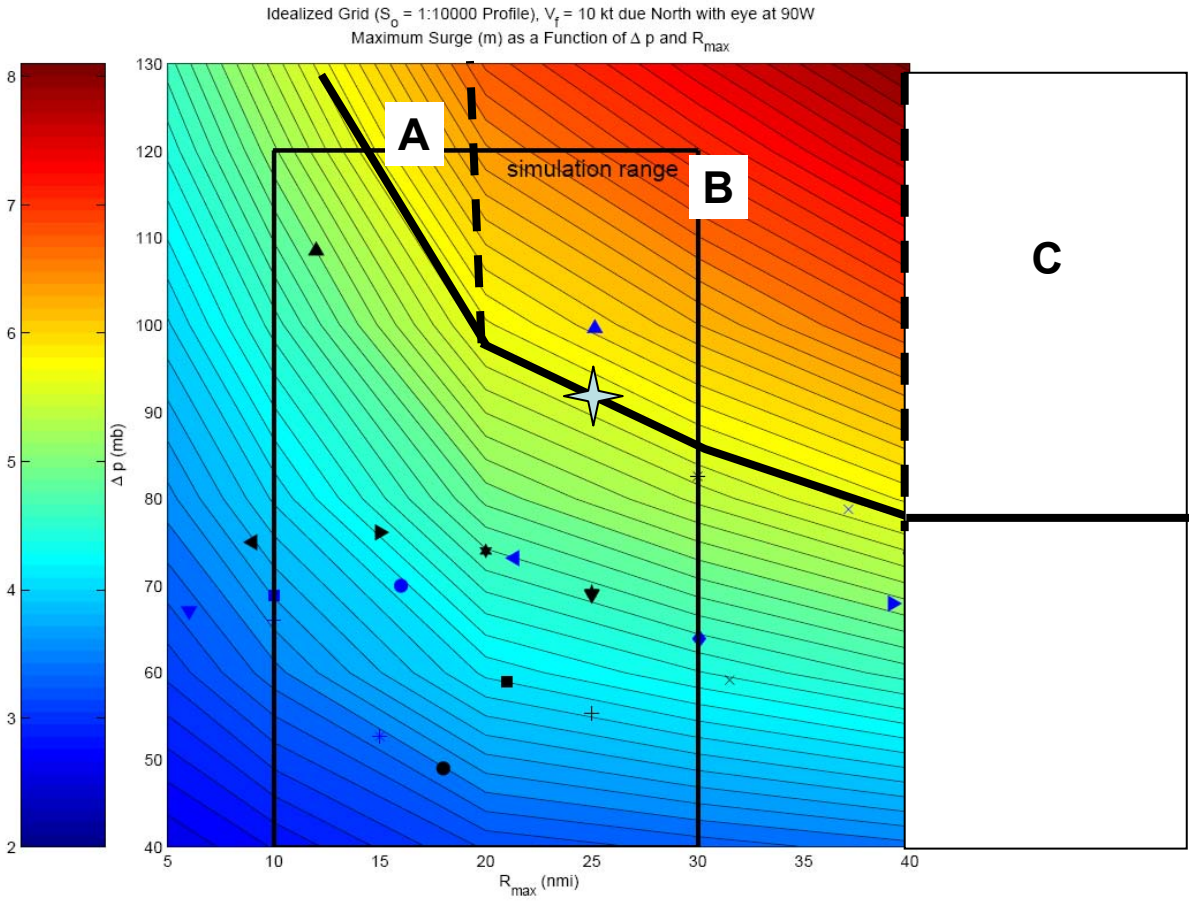

Figure A6. Regions of size-intensity domain expected to contribute to surges greater than or equal to that of Hurricane Katrina. The Blue "star" represents Katrina's characteristics at time of landfall, with a somewhat lower intensity than shown in Figure A1.

APPENDIX B of R2007
Selection of Wind Model for Coastal Surge Estimation

Ocean response models for waves and surges require winds at a constant reference level with some suitable averaging interval (typically around 20-30 minutes) and a specified drag law to convert these winds into estimates of momentum fluxes from the atmosphere to the ocean. Two different models (Thompson and Cardone, 1996; Vickery *et al.*, 2000) were investigated for application to coastal surge modeling as part of a general investigation of modeling for coastal inundation.

The dynamic (Planetary Boundary Layer – PBL) model of Thompson and Cardone (1996) has been selected for use in estimating hurricane wind fields. In older storms, the "best-estimate" wind fields will be virtually identical to the initial guess wind fields due to the lack of information available for assimilation into the PBL wind fields. Comparisons of Oceanweather and Vickery PBL winds from Hurricane Katrina, along east-west and north-south transects through the center of the storm, to Oceanweather's "best-estimate" winds are shown in Figures B1 and B2, respectively. Figure B3 shows a similar set of comparisons for both the east-west and north-south transects for Hurricane Betsy. As can be seen in these figures, Oceanweather's PBL winds capture most of the broad-scale structure of the wind fields.

The Vickery PBL model does not perform as well as the Oceanweather PBL model in comparisons with the Oceanweather "best-estimate" winds. This is not too surprising, since the Oceanweather analysis "best-estimate" analysis is likely to have been considered in deriving the PBL parameters. The abrupt drop-off of wind speeds in the Vickery wind is an artifact of the version of the Vickery code that was available for testing during the time of this comparison. This problem is being remedied and is not a property of the general solution capabilities inherent to the Vickery model.

Since the relaxation time for coastal surge is on the order of hours rather than 10's of hours, as for the generation of waves, offshore complexities of storm tracks tend to affect wave fields much more than they affect coastal surges. Since tracks of major storms tend to lack the complexity exhibited by minimal hurricanes and tropical storms and since wave generation tends to produce a wave field that represents the integrated effects of winds over many hours, the effect of track variation on wave fields should be rather minimal. It should also be recognized that PBL winds have long been shown to be capable of providing accurate wind field estimates for purposes of hindcasting waves in hurricanes (Cardone et al., 1976).

The use of PBL winds is also consistent with the approach of Vickery et al. (2000) or estimating wind hazards in U.S. coastal areas, which were found to provide very reasonable wind estimates when compared to both onland and offshore wind observations. Given all of the problems associated with using historical wind fields with indefinite degrees of freedom in their formulation, it would seem that a very careful study of the differences between PBL-driven surges and "best-estimate"-driven surges should be undertaken for a small set of hurricanes before any clear advantage to using "best-estimate" wind fields for surge prediction can be claimed.

A very important improvement pertinent to PBL wind field estimation is the availability of carefully estimated size parameters for all historical storms (from Oceanweather). These parameters were compiled specifically for driving ocean response models (e.g. wave and surge models) and allow improved estimation of the joint probability of intensity-size relationships in Gulf of Mexico hurricanes.

As a final element of this Appendix, the Holland B parameter will be briefly described. This description is excerpted from the section on Meteorology in the *Coastal Engineering Manual* (Resio, Thompson, and Bratos), which can be found online for reference.

Myers (1954), Collins and Viehmann (1971), Schwerdt *et al.* (1979), and Holland (1980) all present descriptions and justifications of various parametric approaches to wind-field specification in tropical storms. Cardone *et al.* (1992) use a modified form of Chow's (1971) moving vortex model to specify winds with a gridded numerical model. However, since this numerical solution is driven only by a small set of parameters and assumes steady-state conditions, it produces results which are of similar form to those of parametric models. The Holland model differs from previous parametric models in that it contains a parameter (the Holland B parameter) which allowed the peakedness of winds in a hurricane to vary. This model will be described here to demonstrate the role of the Holland B parameter in this model.

In the Holland model, hurricane pressure profiles are normalized via the relationship

$$\text{B1.}\quad \beta = \frac{p - p_c}{p_n - p_c}$$

where

p is the surface pressure at an arbitrary radius (r);
p_c is the (surface) central pressure in the storm; and
p_n is the ambient surface pressure at the periphery of the storm.

Holland showed that the family of β-curves for a number of storms resembled a family of rectangular hyperbolas and could be represented as

$$r_p^B \ln(\beta^{-1}) = A$$

or

$$\text{B2.}\quad \beta^{-1} = \exp\left(\frac{A}{r_p^B}\right)$$

or

$$\beta = \exp\left(\frac{-A}{r_p^{-B}}\right)$$

where

A is a scaling parameter with units of length; and

B is a dimensionless parameter which controls the peakedness of the wind speed distribution.

This leads to a representation for the pressure profile as

$$\text{B3. } p = p_c + (p_n - p_c)\exp\left(\frac{-A}{r_p^B}\right)$$

which then leads to a gradient wind approximation of the form

$$\text{B4. } U_{gr} = \left[\frac{AB(p_n - p_c)\exp\left(\frac{-A}{r_p^B}\right)}{\rho_a r^B} + \frac{r^2 f^2}{4}\right]^{1/2} - \frac{rf}{2}$$

where

U_{gr} represents the gradient approximation to the wind speed.

In the intense portion of the storm, this equation reduces to a cyclostrophic approximation (a flow in which the pressure gradient force is balanced only by centrifugal acceleration) given by

$$\text{B5. } U_c = \left[\frac{AB(p_n - p_c)\exp\left(\frac{-A}{r_p^B}\right)}{\rho_a r^B}\right]^{1/2}$$

where

U_c represents the cyclostrophic approximation to the wind speed; which yields explicit forms for the radius to maximum winds as

$$\text{B6. } R_{\max} = A^{\frac{1}{B}}$$

where R_{max} is the distance from the center of the storm circulation to the location of maximum wind speed, compared to r_p which is the pressure-scaling radius.

The maximum wind speed can then be approximated as

B7. $$U_{\max} = \left(\frac{B}{\rho_a e} \right)^{1/2} (p_n - p_c)^{1/2}$$

where

$U_{\max}$ is the maximum velocity in the storm; and

e is the base of natural logarithms, 2.718.

If B is equal to 1 in this model, the pressure profile and wind characteristics become similar to results of Myers (1954), Collins and Viehmann (1971), Schwerdt et al. (1979), and Cardone et al. (1976). In the case of the Cardone et al. model this similarity would exist only for the case of a storm with no significant background pressure gradient. Although the Cardone et al. PBL model initially did not consider the effects of the Holland B parameter, it now does include this term in its formulation (Thompson and Cardone, 1996). The Vickery et al. (2000) model also includes the Holland B term in its formulation.

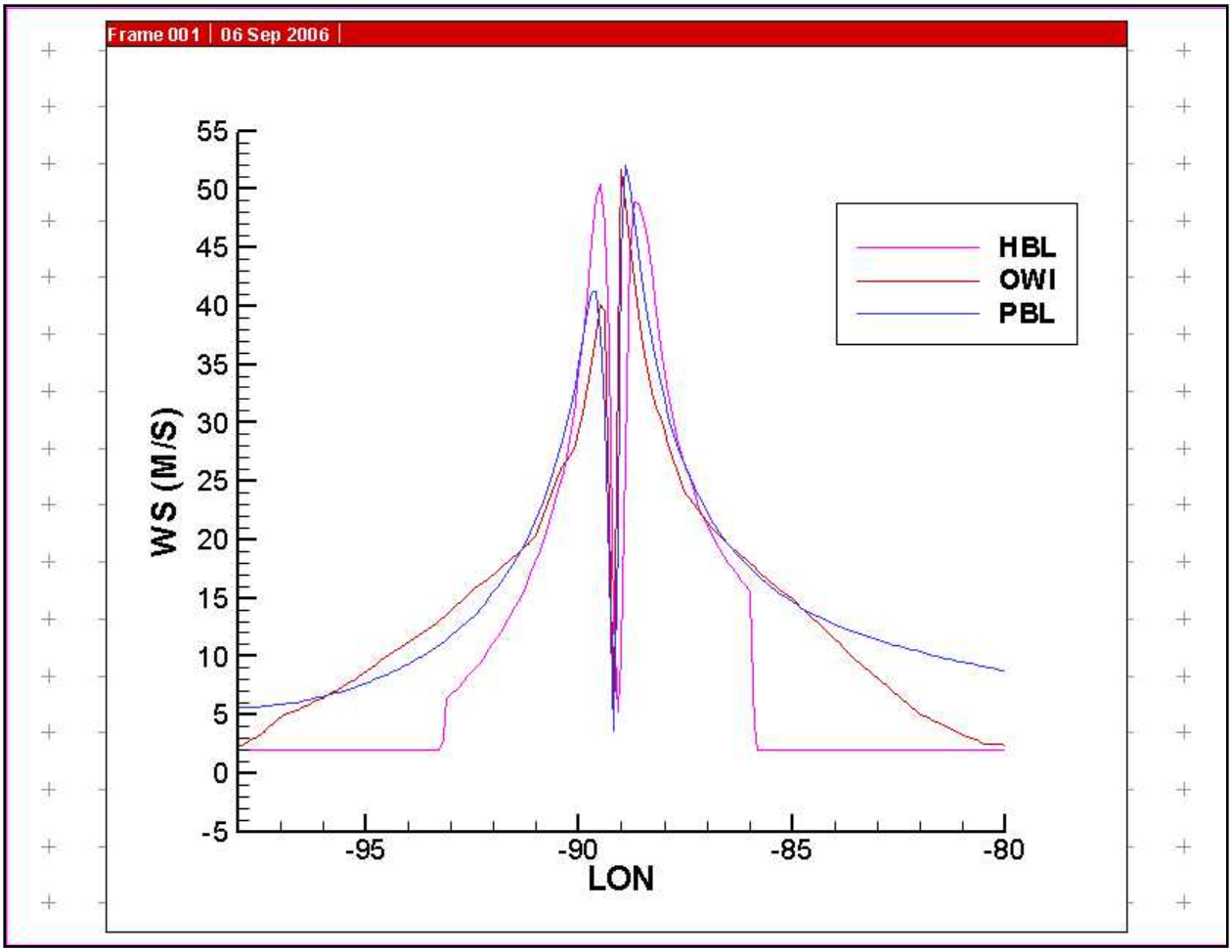

Figure B1. Plot of wind speeds (in meters per second) along east-west transects through Hurricane Katrina. HBL denotes wind speeds from the Vickery et al. (2000) hurricane boundary layer model. PBL denotes wind speeds from the Thompson and Cardone (1996) planetary boundary layer (PBL) model; and OWI denotes wind speeds from the "best-available" wind speeds from analysts at Oceanweather, Inc., which include the HWIND inputs from Mark Powell in NOAA's Hurricane Research Division.

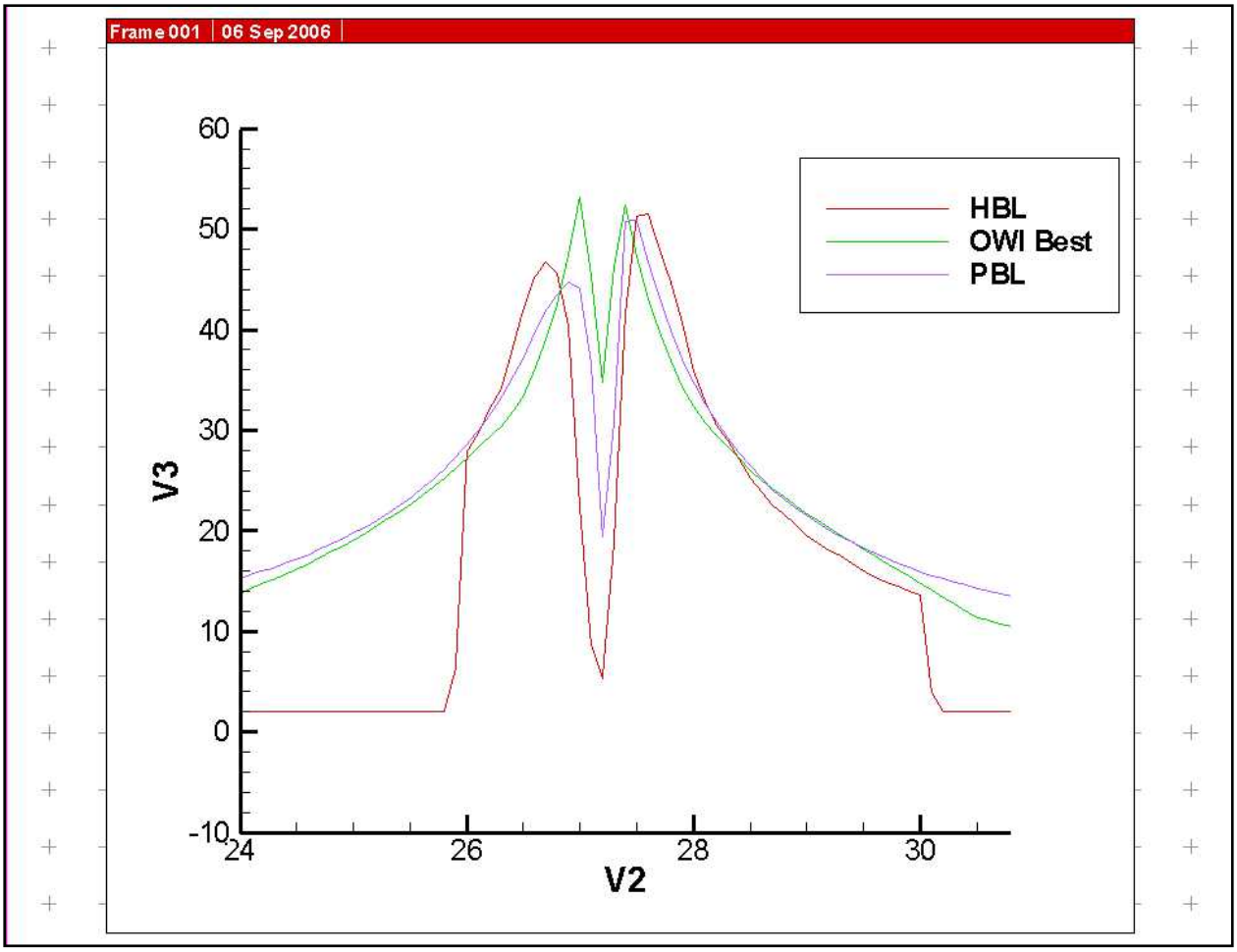

Figure B2. Plot of wind speeds (in meters per second) along north-south transects through Hurricane Katrina. HBL denotes wind speeds from the Vickery et al. (2000) hurricane boundary layer model. PBL denotes wind speeds from the Thompson and Cardone (1996) planetary boundary layer (PBL) model; and OWI denotes wind speeds from the "best-available" wind speeds from analysts at Oceanweather, Inc., which include the HWIND inputs from Mark Powell in NOAA's Hurricane Research Division.

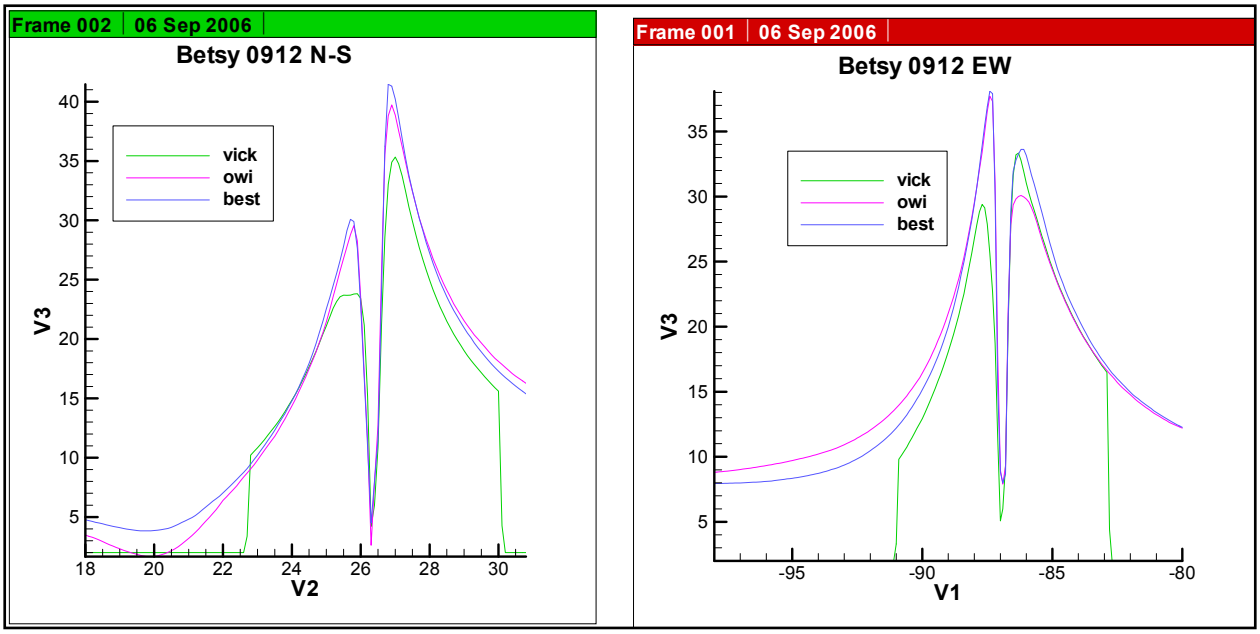

Figure B3. Plot of wind speeds (in meters per second) along north-south (N-S) and east-west (E-W) transects through Hurricane Betsy. Vick denotes wind speeds from the Vickery et al. (2000) hurricane boundary layer model. OWI denotes wind speeds from the Thompson and Cardone (1996) planetary boundary layer (PBL) model; and "best-available" denotes wind speeds from the "best-available" wind speeds from analysts at Oceanweather, Inc.

APPENDIX C of R2007
Selection of Period of Record for Surge Estimation and Consideration of the Effects of Climatic Variability on Surge Extremes

An analysis of climatic variability was undertaken by Resio and Orelup (submitted for publication to J. Climate). Enclosed here are some of the findings relevant to the selection of the period of record and the estimated effects of climatic variability on expected surge extremes. Three fundamental data sets are used in this study: 1) sea-level pressures (SLP's) from the NOATL-tropic data set (a sub-domain of the total NCEP SLP data set that covers from 0^o to 40^o N latitude and from 5^o to 110^o W longitude); 2) sea surface temperature (SST) data downloaded from Extended Reconstructed Sea Surface Temperature (ERSST); and 3) information on hurricane characteristics taken from Oceanweather, Inc files, now available in the public domain. Details on these data sets are available on appropriate web sites.

Empirical Orthogonal Functions (EOF's) have long been recognized as a powerful tool for encapsulating natural patterns within the atmosphere. In this study we used data from the 1950-2005 period (56 years) and defined five-day mean sea level pressure (SLP) fields on a 2.5^o by 2.5^o grid. This resulted in 73 five-day intervals for every year without a leap year. Leap year was handled by adding that day into the time interval starting on February 25^{th}, which created one element encompassing six days once in every four years. Given that we were not interested in the seasonality of hurricane but rather in inter-annual and longer variability, we defined mean pressure fields for each five-day interval throughout the year, with the average taken over the 56 years included in this analysis. Calculated mean pressure fields for each five-day interval were subtracted from individual mean five-day pressure fields to produce a set of 73 x 56 pressure fields that were input into an EOF analysis.

The SST data used here represent a subset of the total ERSST data set and covers from 18^o to 30^o N latitude and from 58^o to 98^o W longitude on a 2^o by 2^o grid, with a land mask that restricts the data to only water points. Although SST patterns within the Gulf exhibit considerable spatial variability, it is not clear that the variations in the spatial characteristics of these patterns play a major role in the inter-annual variability of hurricane genesis and/or development. Consequently such variations are not considered here. Instead, mean monthly data for the entire Gulf of Mexico region for July through October were averaged together to provide a single measure of sea surface temperature for each hurricane season from 1950 through 2005.

The data set for hurricane characteristics includes estimates of six-hourly storm position, along with several parameters that relate to hurricane shape, size and intensity. Unlike previous data sets which have focused on short-duration (typically 1-minute maximum) wind speeds from flight level, this new data set also contains estimates of the highest sustained (30-minute average) surface-level (10-meter) wind speeds along the path of the storms. Since these are the appropriate winds for driving ocean response models, they provide a much more direct measure of hurricane surge and wave production. In the earlier storms in this data set (prior to 1990) these wind estimates were derived primarily from simulated wind fields based on a "slab model" of the lowest region of the atmosphere combined with a planetary boundary layer model (Thompson

and Cardone, 1996). For most of the later storms these wind fields have been extensively reworked by analysts to assimilate available measurements.

Most past studies of climatic variability have used storm frequency (sometimes stratified by Saffir-Simpson scale) to categorize storm activity in each year. However, for our purposes we will define a single parameter that incorporates both intensity and frequency into one measure of hurricane activity. This measure of annual hurricane activity is obtained by calculating the estimated kinetic energy for each storm passing through the Gulf of Mexico at the time of its maximum intensity and then adding all maxima within a given year. At a fixed time, the total kinetic energy in a hurricane can be related to storm size and storm intensity as

$$E_k \sim \iint V^2(x,y)dxdy = \iint V^2(r,\theta)rd\theta dr$$

C1. given that $V(r,\theta) = V_{\max}\phi_1\left(\frac{r}{R_{\max}}\right)\phi_2(\theta-\theta_0)$ then

$$E_k \sim V_{\max}^2 R_{\max}^2$$

where V_{max} is the maximum (30-minute average, 10-m) wind speed within the storm and R_{max} is the radius to maximum winds at the same time. The value of the parameter E_k at the time of maximum wind speed during a storm's passage through the Gulf of Mexico provides a good integrated measure of the storm intensity and size at the time of the storm's maximum intensity. Summing all values of E_k for a season yields a surrogate for combined number, size, and intensity of storms in a year.

Figure C1 shows the cumulative hurricane kinetic energy per season as defined previously in this paper, smoothed over a running five-year period. Since we are trying to extend the data as long as possible, the "smoothed" data at either end of this record is defined only in terms of the existing data within the five-year window. For example, the 2005 data considers only data from 2003, 2004, and 2005 in its average. Thus as the ends are approached, a slight bias is created in terms of the mean position of the years contributing to this mean, culminating in a one-year displacement at the beginning and end of the analysis along with a reduced averaging window. This Figure shows two very notable peaks, one that commenced in the late-1950's and persisted until about 1970 and a second that began around 2000 and has persisted through 2005, with a broad trough in Gulf hurricane activity between these two peaks. There does not appear any strong secular signal within this record. The first of these periods coincides with the very active hurricane seasons that included Hurricanes Carla, Hilda, Betsy, Beulah and Camille that devastated much of the Gulf coast during the 1960's; while the second contains the recent set of intense hurricanes, including Lili, Charley, Ivan, Dennis, Katrina, and Rita.

Figure C1 shows that there are two intervals of high hurricane activity separated by an interval of relatively low hurricane activity in the years from 1950 to 2005. If this cycle is real, it seems advisable to use a sampling scheme that preserves the expected long-term ratio of high-activity and low-activity years. Since we obviously want to retain both the early (1960-1970) interval of high activity latest (partial?) interval (2000-2005) of high activity in our sample, we should include about 2/3 of the 30-year low-activity interval preceding 1960 in order to achieve

this balance. This suggests that including approximately 20 years of the 30-year low-activity interval (1941-1960) is appropriate. Thus, the total record sample length recommended for surge estimation in the Gulf of Mexico is 1941-2005.

Figure C2 shows estimated return periods for central pressures for the total sample within the Gulf of Mexico for different estimation methods. The estimation methods examined are 1) analysis of only quiescent years (Group1); 2) analysis of only active years (Group 2); 3) analysis of both quiescent-year and active-year samples, treated as though they are drawn from separate populations (Equation 4 from the Resio and Orelup manuscript, reproduced below); and 4) analysis of both quiescent-year and active-year samples as though they are a single population.

Eq. 4 from Resio and Orlup:

$$T(x) = \frac{1}{1 - \sum \lambda_n \beta_n F_n(x)}$$

where

$T(x)$ is the return period for x;

C2. λ_n is the frequency of storms in Group n;

$F_n(x)$ is the cumulative distribution function (CDF) for storms in Group n; and

β_n is the proportion of years in Group n.

These results combined with integrations of the full probability integral for surges along a straight coast from the Irish *et al.* computer runs yields the results shown in Table C1 for the expected variations in wave and surge extremes within the Gulf of Mexico, given a doubling of the high-activity years (from ¼ of the total time to ½ of the total time). There is nothing in the Gulf of Mexico record that suggests such a scenario is imminent, so this prediction should probably be taken as an upper limit of what could happen rather than what will happen.

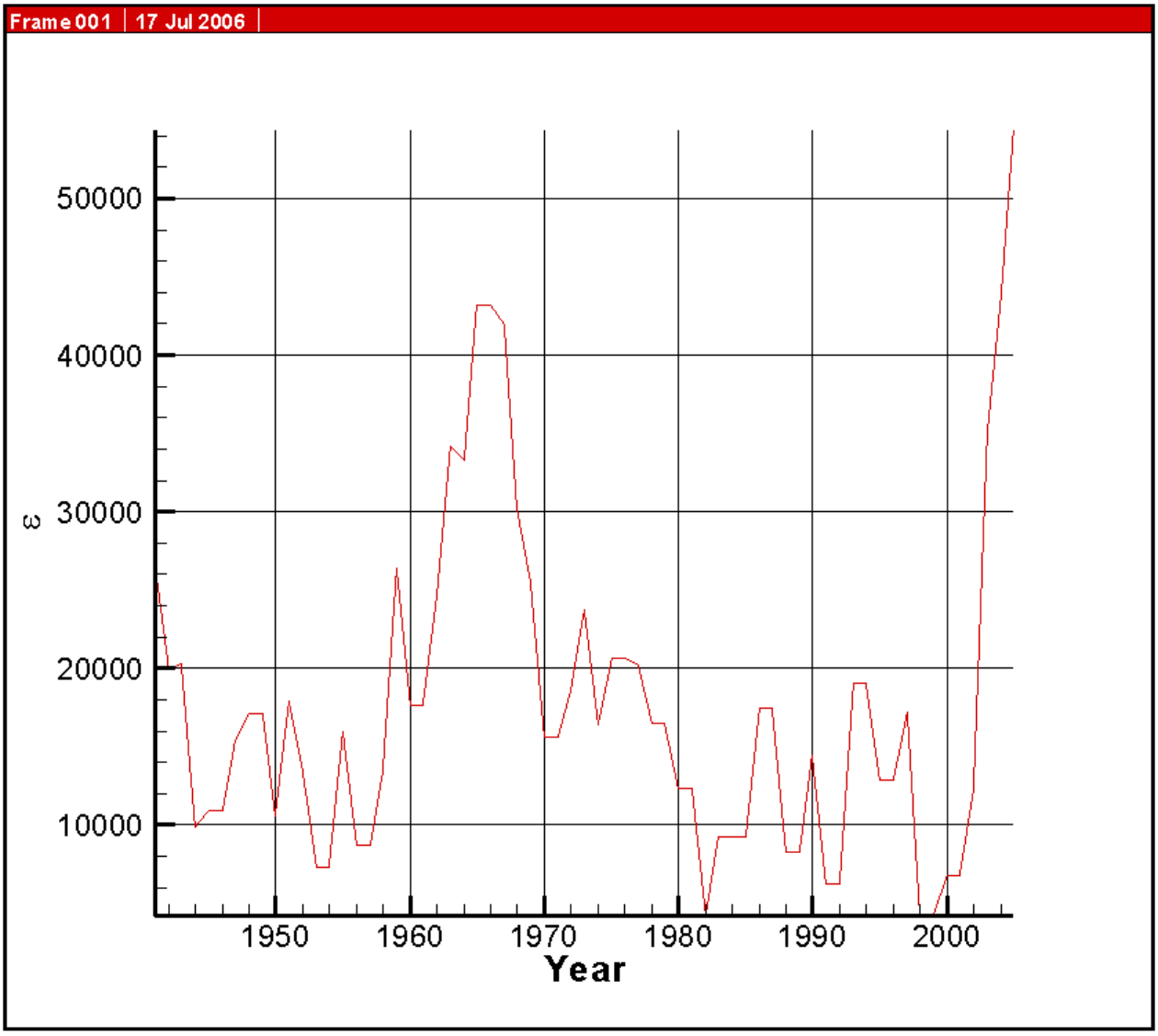

Figure C1. Plot of estimated cumulative kinetic energy for all storms at time of maximum surface winds within each year: 1941-2005. The units of ε are l^4/t^2, since we have factored out the mass term (consistent with equation C1). Note: ε is termed E_k in Appendix C.

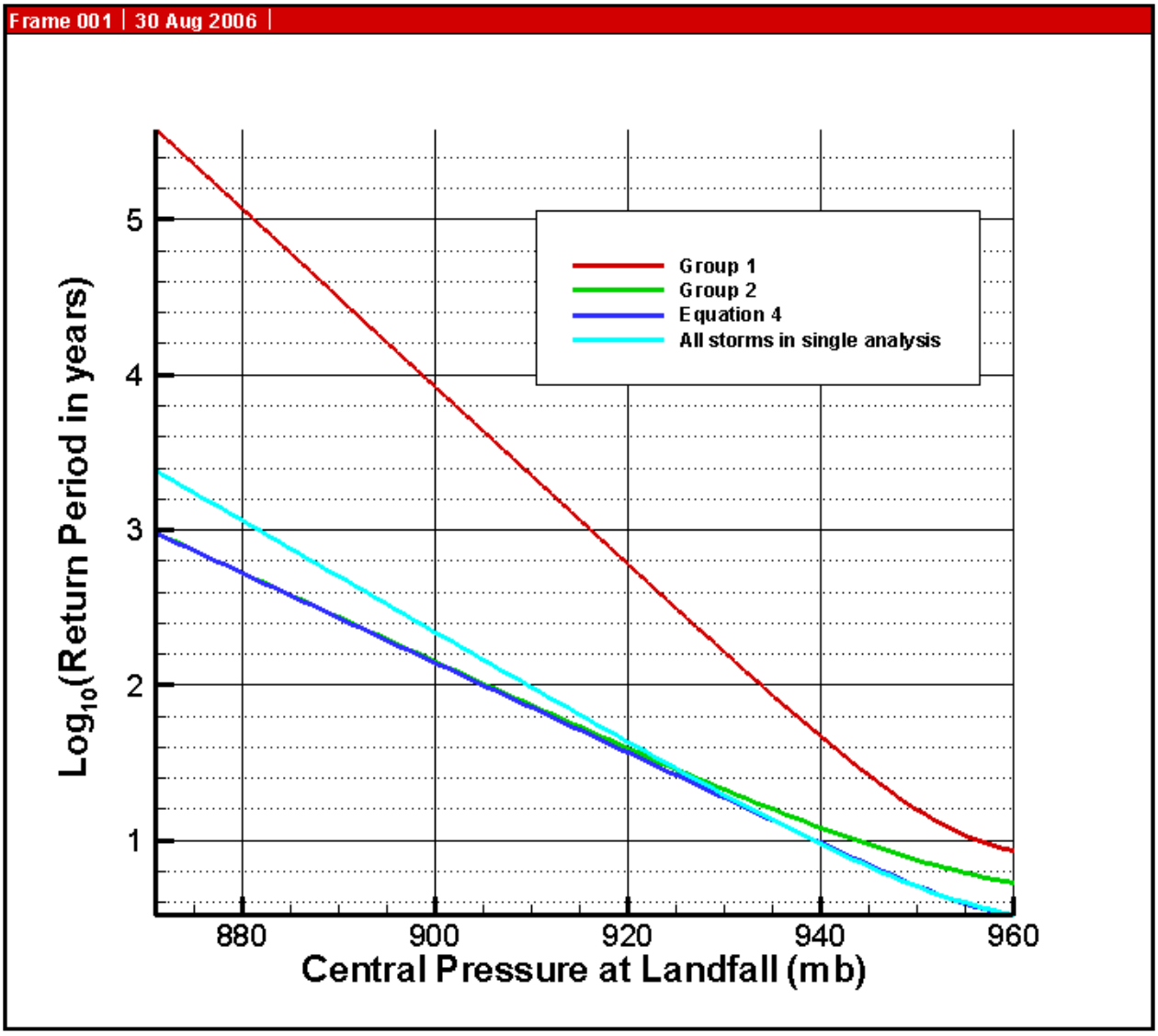

Figure C2. Estimated return periods for 4 separate analyses: Low-Activity years only (Group 1 – red line); High-Activity Years only (Group 2 – green line); All years into a single analysis (light blue line); and estimate based on combined analysis of two populations (equation 4 from Resio and Orelup - dark blue line).

Table C1.
Estimated changes in extreme waves heights and surges for selected return periods, given a doubling of years with high hurricane activity.

Return Period (years)	Change in Wave Height (percent)	Change in surge (percent)
25	+15	+18
50	+13	+16
100	+12	+15
250	+11	+12
500	+10	+9

APPENDIX D of R2007
Selected Storm Sample for Simulations

In this Appendix, the terms $R_{\max}$ (storm-size scaling radius) and C_p (central pressure) should be taken as equal to R_p and C_p, as defined elsewhere in this white paper. Tracks 1-5 are defined as shown in Figure 12 of the main text. This set of tracks has been nicknamed the "RICK-fan" since it mimics the tracks of Rita, Ivan, Camille, and Katrina. Track 1 is the westernmost and Track 5 is the easternmost track in this set. Tracks 1b-4b fall midway between the five primary tracks. One primed track 4' is located about 40 nm north of the landfall point for Track 4 to allow for storms entering the N-S aligned portion of the coast in this area.

One of the issues affecting our storm selection is implicit in the spacing of the tracks shown in Figure 12. This spacing is approximately 0.6 degrees longitude at a latitude of 29.5 degrees, equivalent to a distance of about 31 nautical miles in the along-coast direction. Studies of surge response on idealized, open coasts have shown the distribution of surges along the coast scale quite nicely with this parameter for a wide range of storm sizes and offshore slopes (Figures D1-D3). Figure D4 provides a plot with all three of the storm sizes plotted together. A second factor which influences along-coast surge variations is the presence of large geometric features in the coastal configuration, such as the Mississippi River, its deltas, and the river levees south of New Orleans. Figure D5-A shows a general set-up for a numerical study to examine this effect. Figure D5-B shows the distribution of surges along the coast. It is apparent in this figure that the effect of the land protrusion is to add a second scale to the along-coast surge distribution. In the New Orleans area, this scale is likely to be of more significance than the simple open coast scaling. In the New Orleans area, this effect will tend to dominate the second source of along coast variation for storm within about 30 nm or so of the eastern edge of the land protrusion. In this context, the storm track spacing for the New Orleans area should be quite reasonable.

In the more general case of storms along a straight coast, any single storm will produce a patter with a shape similar to those shown in Figures D1-D3. Figure D6 shows a plot of where surges from two storm tracks might fall if they were separated by 31 nautical miles on each of these figures. This represents the worst case in which neither of the simulated storms captures the peak condition that could be generated by these hurricanes. This case is the worst possible since it has the maximum distance from the peak on both sides. Since tracks are assumed to be distributed uniformly along the coast, the expected value would be the mean of all points between the two lines. The bias introduced into the estimated extreme from this set of tracks can be estimated as

$$\text{D1.}\quad \frac{E(\eta_1+\eta_2)}{E(\eta_{1-2})} = \frac{\dfrac{\eta_1+\eta_2}{2}}{\dfrac{1}{(x_2-x_1)}\displaystyle\int_{x_1}^{x_2}\eta(x)dx}$$

which can be calculated numerically for each of the different radii to maximum winds considered. For the three cases shown, the calculated values are 0.794, 0.907, and 0.959 for the

10 nm, 20 nm, and 30 nm cases, respectively, which translates into low biases of approximately 20%, 9% and 4% in these "worst-case" situations. It should be noted that the sampling pattern itself should not introduce a bias in either direction (high or low); consequently, in other sections of the coast, where the exact peak is attained, the simulated value is actually higher than the denominator in this equation. Historically, this problem of low and high values along the coast has been addressed by some sort of smoothing along the coast. The smoothing interval of approximately $\frac{R_{\max}}{2}$ should work relatively well for this purpose.

Along each of the tracks modeled, the central pressure is allowed to vary during a simulated intensification interval until its intensity reaches a plateau. This plateau is maintained until the storm comes within 90 nautical miles of the coast at that time, the pressures decay according to the (linear interpolation) relationship

D2.
$$C_p(s) = \lambda_0 C_p(s_0) - (1-\lambda_0)\Delta P_{decay}$$
where
C_p is the central pressure at s
s is the distance along the storm track, with s_0 located 90 nm from landfall
λ_0 is an interpolation multiplier (=1 at 90 nm from landfall and =0 at landfall)
ΔP_{decay} is the total change in central pressure over 90 nm approach to landfall

The pressure decay term is somewhat dependent on storm size, so the following relationship was used to represent this term

D3.
$\Delta P'_{decay} = R_p - 6$ (with R_p given in nautical miles)
constrained by $\Delta P_{decay} = Max(\Delta P'_{decay}, 18); Min(\Delta P'_{decay}, 5)$

Once a storm is one hour past landfall the pressure decay factor due to Vickery is applied

D4.
$$C_p = P_\infty - \delta P$$
where
$$\delta P = \delta P_0 e^{-a\Delta t}$$
where
δP is the local pressure differential
δP_0 is the pressure differential one hour after landfall
a is an empirical constant
Δt is time after landfall minus 1 hour

As noted in the main section of this white paper, Rmax and the Holland B parameter are allowed to vary linearly over the same distance as Cp for all storms except the smallest storm class used in this application. For that class (Rmax = 6nm), the storm is assumed to retain its intensity, its size, and its Holland B parameter all the way to landfall. Figure D6 shows a typical variation of storm parameters for a storm in which the characteristics vary during their approach to the coast. This figure shows the characteristic "spin-up" time for the hurricane (based on historical times required to reach peak storm intensities) and the variations during its approach to the coast.

Four different Cp – Rp (central pressure – size scaling radius) combinations are defined as

A. 3 Cp and 3 Rmax values

Cp=960 Rmax = (21.0, 35.6, 11.0)
Cp=930 Rmax = (17.7, 25.8, 8.0)
Cp=900 Rmax = (14.9, 21.8, 6.0)

The loop structure for JPM run sequencing is (from inner loop working outward)

- Rmax
- Cp
- Track

Thus, the sequence of runs for any track using Combination A is

	Cp	Rmax
1.	960	15.4
2.	960	21.0
3.	960	35.6
4.	930	11.7
5.	930	17.7
6.	930	25.8
7.	900	6.0
8.	900	14.9
9.	900	21.8

B. 2 Cp and 2 Rmax values

Cp=960 Rmax=(18.2,24.4)
Cp=900 Rmax=(12.5,18.4)

The sequence of runs for any track using Combination B will be

	Cp	Rmax
1.	960	18.2
2.	960	24.4
3.	900	12.5
4.	900	18.4

C. 2 Cp and 1 Rmax values

Cp=960 Rmax=17.7
Cp=900 Rmax=17.7

The sequence of runs for any track using Combination C will be

	Cp	Rmax
1.	960	17.7
2.	900	17.7

D. 1 Cp and 1 Rmax value

Cp=930 Rmax=17.7

Defining three angles as the central angles in the RICK-fan +/- 45 degrees should cover most of the important range for estimating the response surface of the surges. With the secondary variables (tidal phases, Holland B variations, wind field variations around the PBL central estimate, etc.) added to the integral, this should provide a very reasonable estimate of the surge CDF. Figures 13 and 14 in the main text provide the geographic information on these tracks. The tracks approaching the New Orleans area from the southeast are extremely similar to the tracks of the 1947 Hurricane, Betsy, and Andrew in this area. During the 1941-2005 interval, no tracks approached New Orleans from the southwest; however, other storms such as the 1893 storm did approach New Orleans from this direction. In fact, the 1893 track is fairly similar to one of the hypothetical tracks out of the southwest. A track from this direction represents the fact that these storms have to become caught up in the more westerly flow (winds blowing toward the east). For a storm to maintain its strength it cannot move too far west or too close to land; consequently, the track of a major storm is constrained somewhat to come from the region from which all the hypothetical (+45 degree) tracks emerge in order for these storms to strike the New Orleans area.

The effect of storm heading angle on surges at the coast appears to be twofold. First, the overall along-coast pattern is broadened; since the storm moves along the coast at the same time that it moves toward landfall. Second, there is a relatively slow variation in the maximum surges produced by a storm as a function of the angle of the storm track with the coast; however, as seen in Figure D8, maximum surge is relatively weakly dependent on the angle of storm intersection with the coast. In general, the hurricane approaching slightly (15-30 degrees) from west of straight onto a straight east-west coast produce a somewhat higher surge (5% or so) than hurricanes moving perpendicularly to the coast. On the other hand, hurricanes approaching the straight east-west coast from a more easterly direction will tend to produce lower surges than produced by hurricanes moving perpendicular to such a coast. This appears to be a fairly broad pattern that can be represented via interpolation.

The effect of forward storm speed is addressed by considering three different forward velocities Vf=(11,6,17) knots, where 11 is around the mean and the 6-kt and 17-kt speeds span almost the entire range of Vf values at landfall for storms with Cp's less than 950. Note that a few of the track-angle combinations are dropped due to either their very oblique angle with respect to the shore or they were exiting storms from the New Orleans area moving toward the

northeast. Increased forward storm speed contributes to higher wind speeds in the hurricane PBL model. Consequently, one effect of increasing forward storm velocity is to increase the surge at the coast by a factor which similar to increasing the wind speeds within the hurricane, i.e.

$$\eta_1 = \eta_2 \left(\frac{v_{\max} + 0.5 v_{f_1}}{v_{\max} + 0.5 v_{f_2}} \right)^2$$

where

D5. η_1 is the surge at the coast in storm 1, with forward speed = v_1

η_2 is the surge at the coast in storm 2, with forward speed = v_2

$v_{\max}$ is the maximum wind speed of a stationary storm

v_{f_i} is the forward storm velocity of the i^{th} storm

A second effect of storm speed is to change the duration that a flood wave has to propagate inland. Thus, a slowly moving storm may produce more extensive inland flooding than a faster moving storm. By covering essentially the entire range of forward storm speeds observed in major storms within the Gulf (see Figures 11a and 11b), we should be able to quantify the range of the effects of storm speed on surges in the New Orleans area.

The information below provides information on the variation parameter combinations used in the New Orleans 152-storm study.

Primary Tracks

	Track						
(Vf=11)	1	2	3	4	4’	5	
Mean angle	9	9	9	9		9	(use Cp-Rmax combination set A) – storms 1-45
-45	4	4	4		4		(use Cp-Rmax combination set B) – storms 46-61
+45	4	4	4	4			(use Cp-Rmax combination set B) – storms 66-81

TOTAL = WAS 81 — NOW 77

	Track						
(Vf= 6)	1	2	3	4	4’	5	
Mean angle	2	2	2	2		2	(use Cp-Rmax combination set C) – storms 82-91
-45	1	1	1		1		(use Cp-Rmax combination set D) – storms 92-95
+45	1	1	1	1			(use Cp-Rmax combination set D) – storms 97-100

TOTAL = 19

	Track						
(Vf=17)	1	2	3	4	4’	5	
Mean angle	1	1	1	1		1	(use Cp-Rmax combination set D) – storms 101-105
-45	1	1	1		1		(use Cp-Rmax combination set D) – storms 106-109
+45	1	1	1	1			(use Cp-Rmax combination set D) – storms 111-114

TOTAL = WAS 14 – NOW 13

Secondary Tracks

	Track				
(Vf = 11)	1b	2b	3b	4b	
Mean angle	2	2	2	2	(use Cp-Rmax combination set C) – storms 115-122
-45	2	2	2		(use Cp-Rmax combination set C) – storms 123-128
+45	2	2	2		(use Cp-Rmax combination set C) – storms 131-136

TOTAL = 20

	Track				
(Vf = 6)	1b	2b	3b	4b	
Mean angle	2	2	2	2	(use Cp-Rmax combination set C) – storms 137-144
-45	1	1	1		(use Cp-Rmax combination set D) – storms 145-147
+45	1	1	1		(use Cp-Rmax combination set D) – storms 149-151

TOTAL = 14

	Track				
(Vf = 17)	1b	2b	3b	4b	
Mean angle	1	1	1	1	(use Cp-Rmax combination set D) – storms 152-155
-45	1	1	1		(use Cp-Rmax combination set D) – storms 156-158
+45	1	1	1		(use Cp-Rmax combination set D) – storms 160-162

TOTAL = 10

GRAND TOTAL = 152

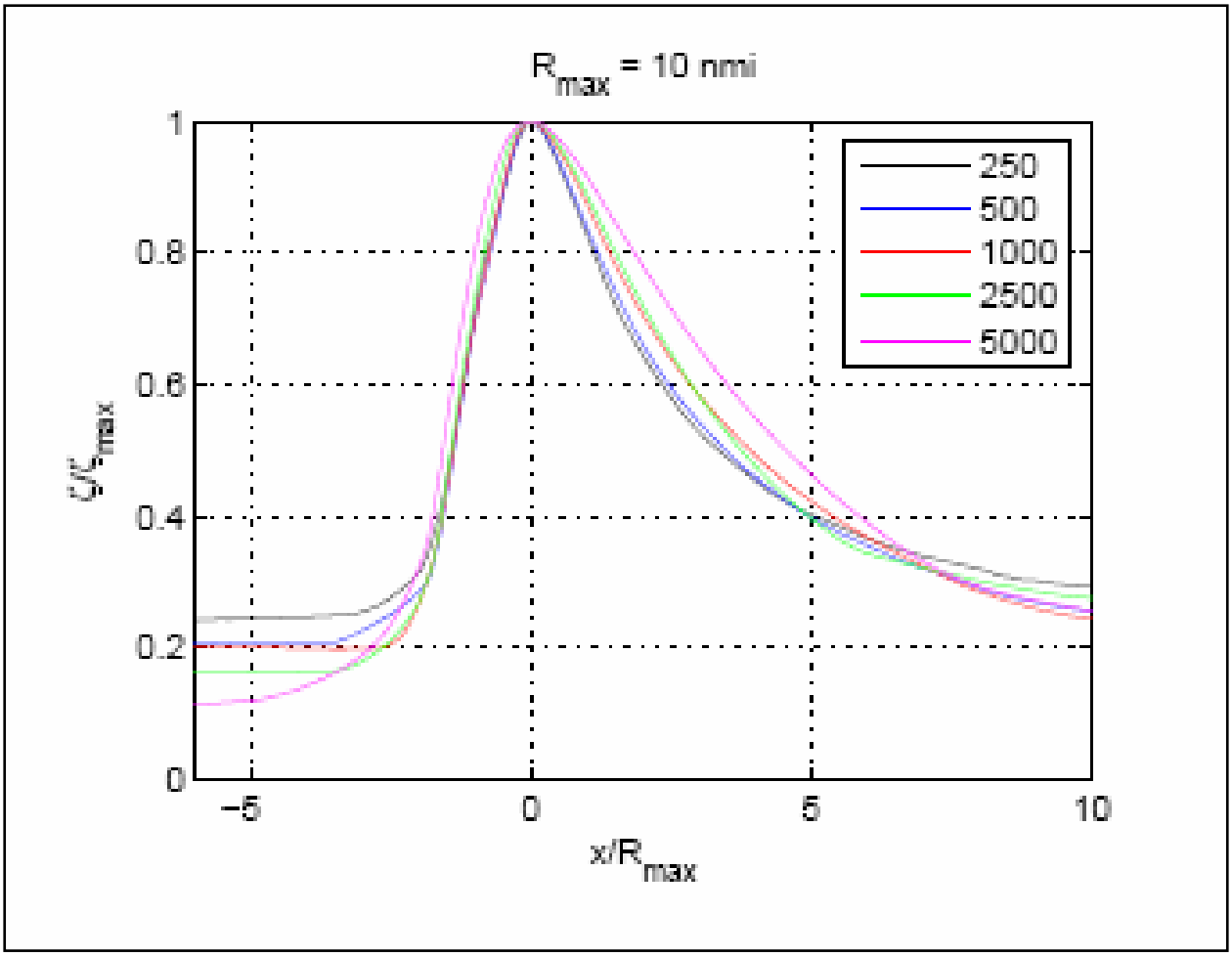

Figure D1. Distribution of normalized maximum surges along the coast (local surge maximm (ζ) divided by the maximum surge within the entire storm (ζ_{max}) versus normalized distance along the coast (distance from storm peak divided by radius scaling parameter, R_{max}, for offshore slopes in the range of 1:250 to 1:5000. Results are from numerical simulations on an idealized, straight coast for hurricanes for relatively small storm: R_{max} (= R_p scaling radius in Cardone PBL model) = 10 nm.

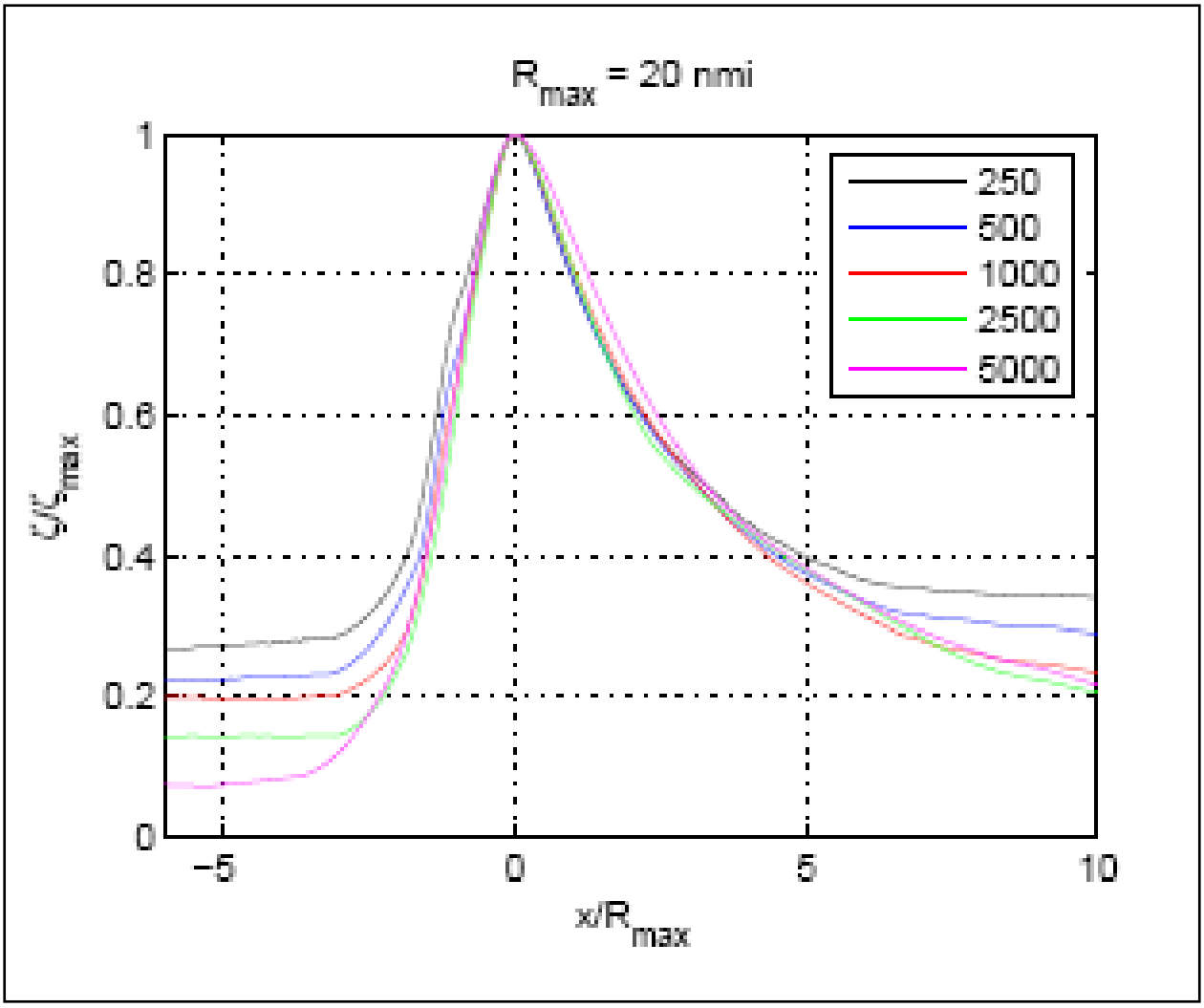

Figure D2. Distribution of normalized maximum surges along the coast (local surge maximm (ζ) divided by the maximum surge within the entire storm (ζ_{max}) versus normalized distance along the coast (distance from storm peak divided by radius scaling parameter, R_{max}, for offshore slopes in the range of 1:250 to 1:5000. Results are from numerical simulations on an idealized, straight coast for hurricanes for relatively small storm: R_{max} (= R_p scaling radius in Cardone PBL model) = 20 nm.

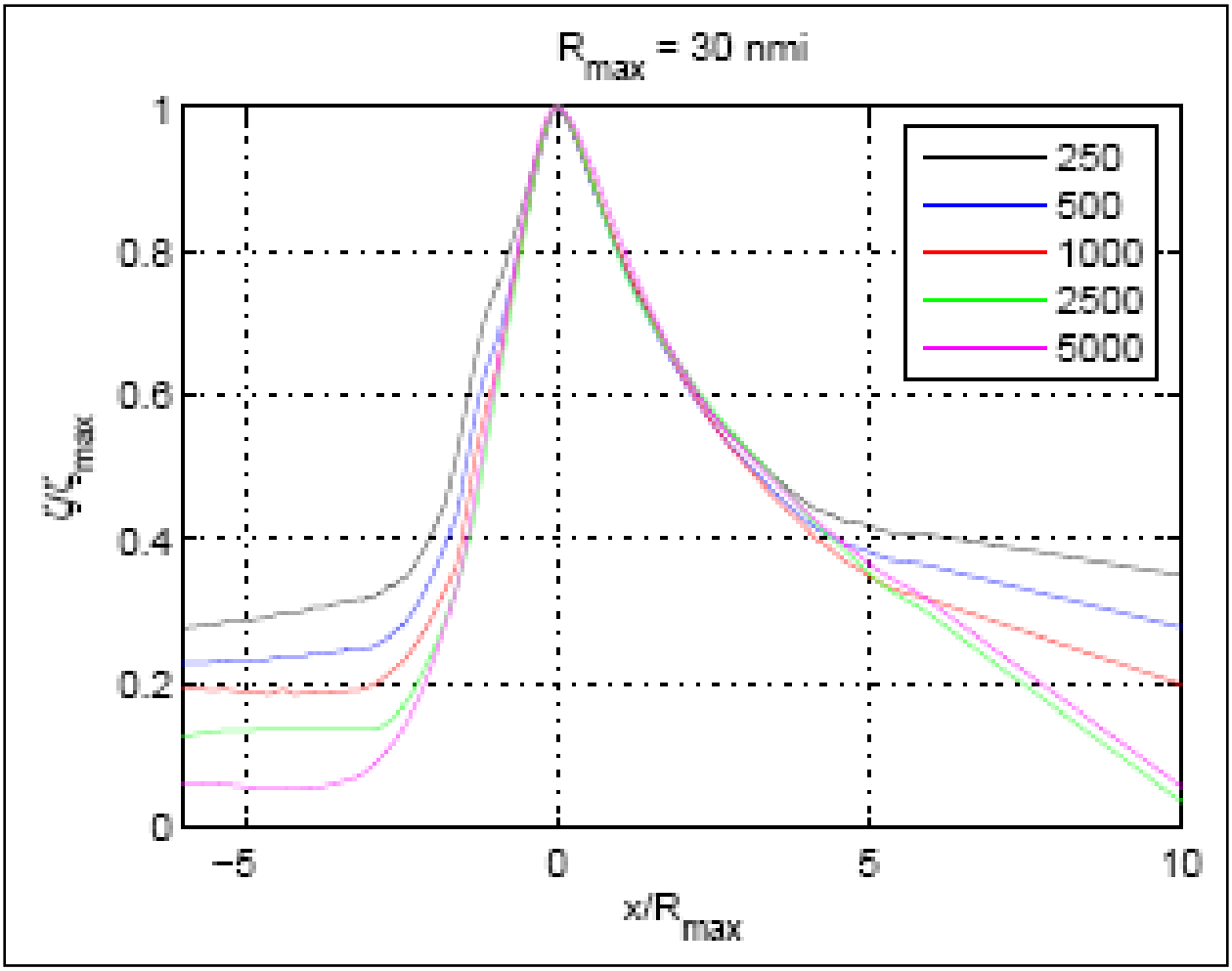

Figure D3. Distribution of normalized maximum surges along the coast (local surge maximm (ζ) divided by the maximum surge within the entire storm (ζ_{max}) versus normalized distance along the coast (distance from storm peak divided by radius scaling parameter, R_{max}, for offshore slopes in the range of 1:250 to 1:5000. Results are from numerical simulations on an idealized, straight coast for hurricanes for relatively small storm: R_{max} (= R_p scaling radius in Cardone PBL model) = 30 nm.

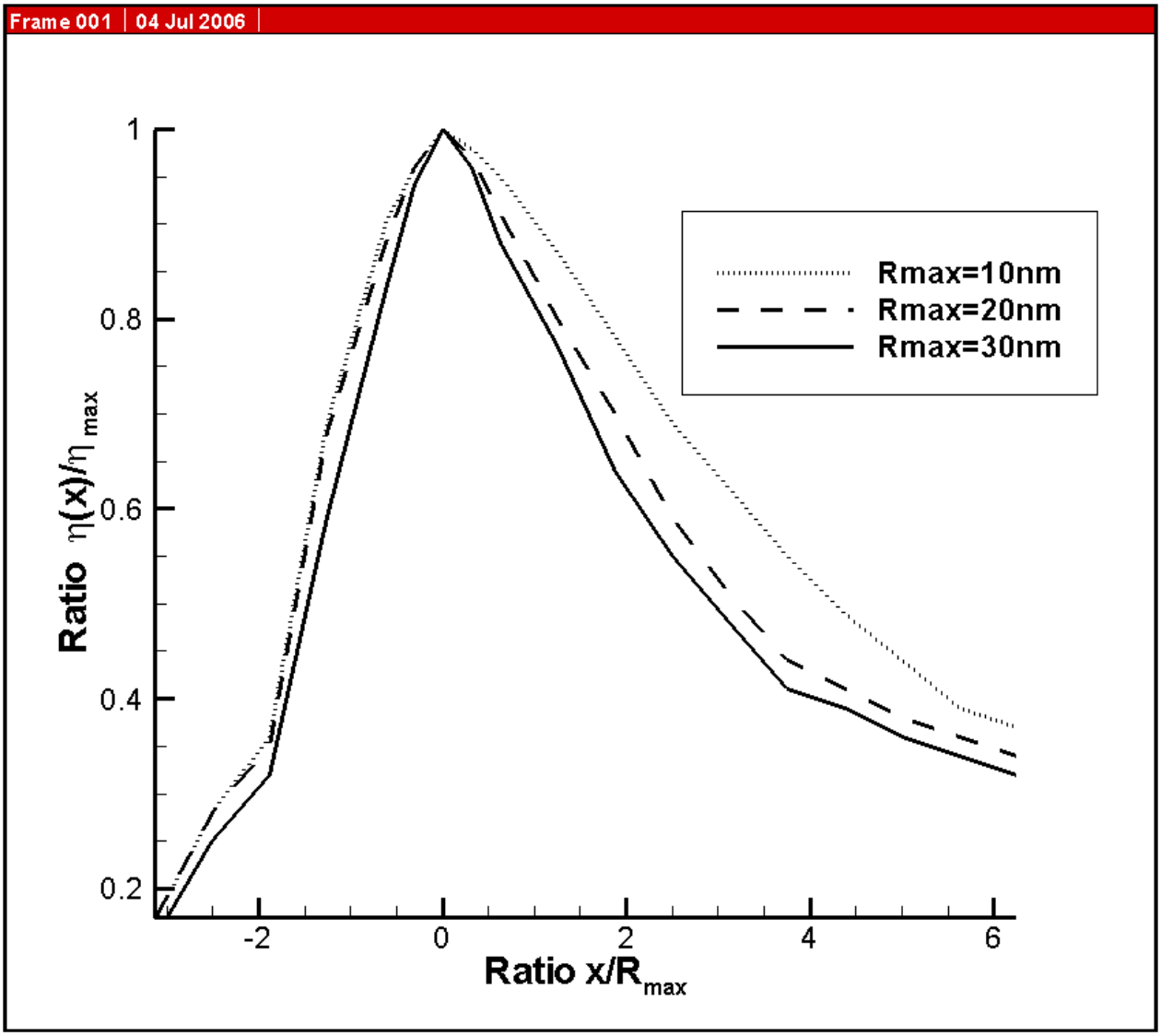

Figure D4. Distribution of normalized storm surge (local maximum ([$\eta(x)$]) divided by maximum over entire storm (η_{max}) as a function of normalized distance along the coast.

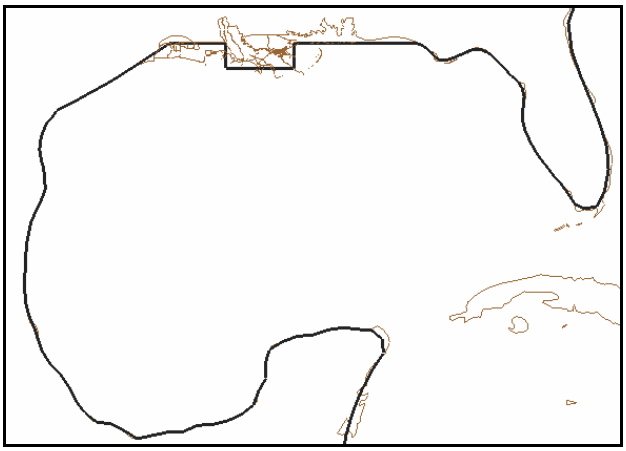

A. 1:10000

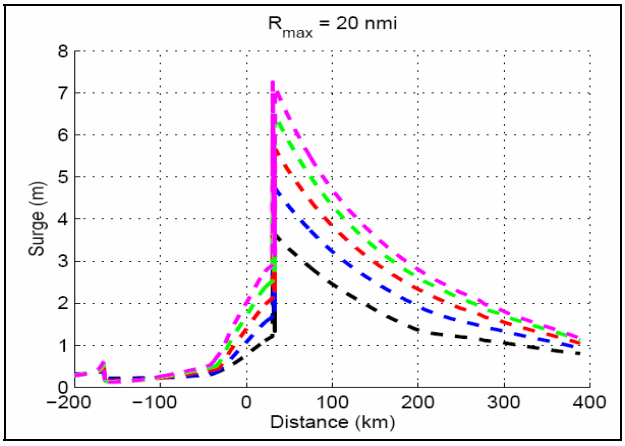

B.

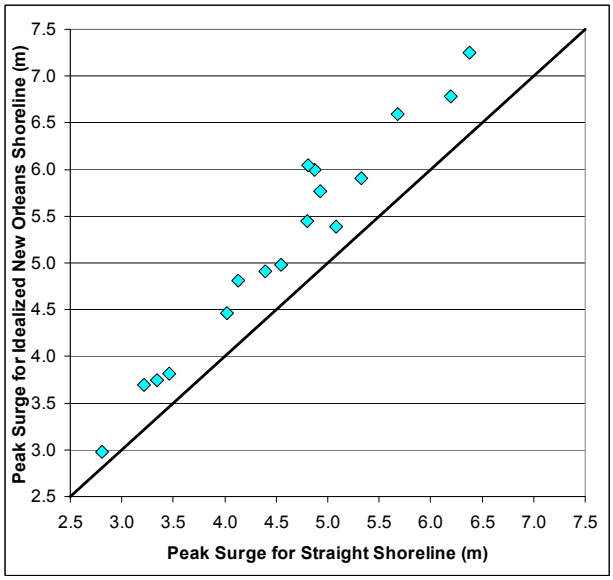

C.

Figure D5(A-C). Figure D5-A shows an idealized representation of the New Orleans coastal area, with a section of land protruding from a generalized straight-line coast. Figure D5-B shows that the resulting surge distributions along the coast. Figure D5-C shows that surge values for this coastal configuration tend to be about 10-20% higher than the corresponding surges on a straight-line coast.

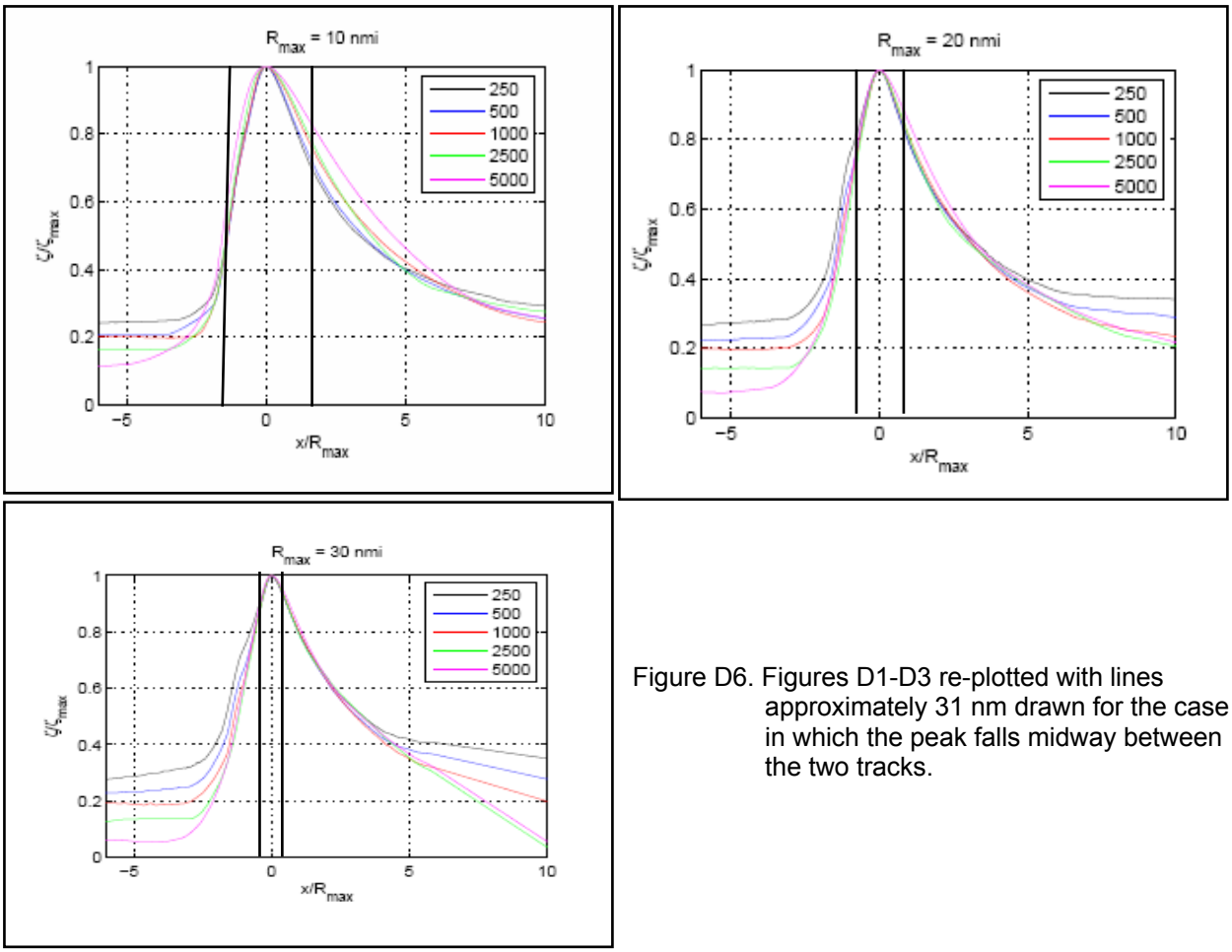

Figure D6. Figures D1-D3 re-plotted with lines approximately 31 nm drawn for the case in which the peak falls midway between the two tracks.

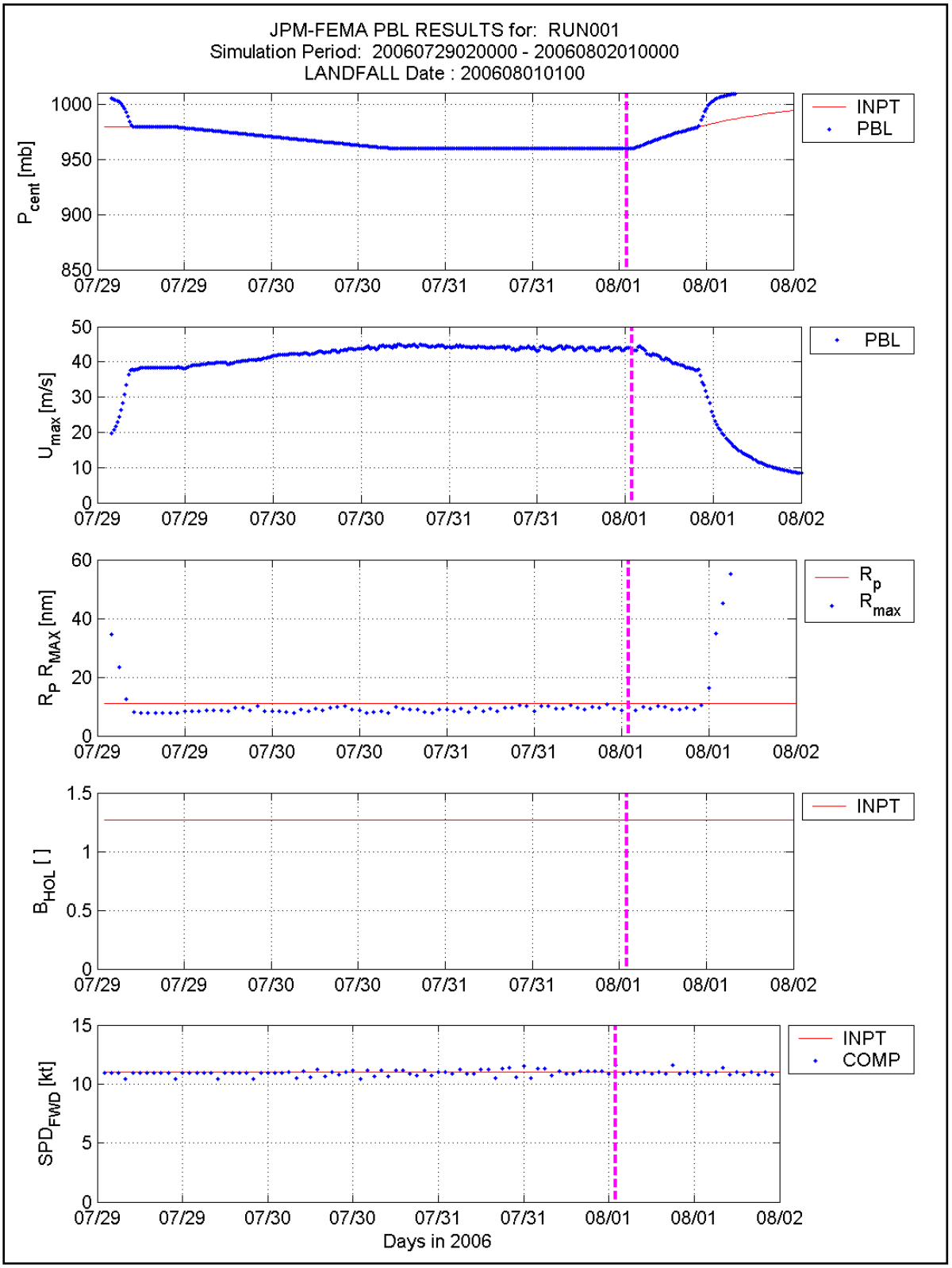

Figure D7. Sample time plot of the variation in central pressure, maximum wind speed, R_p, and forward storm speed used in quality control check of storm parameter behavior for first storm in JPM sequence.

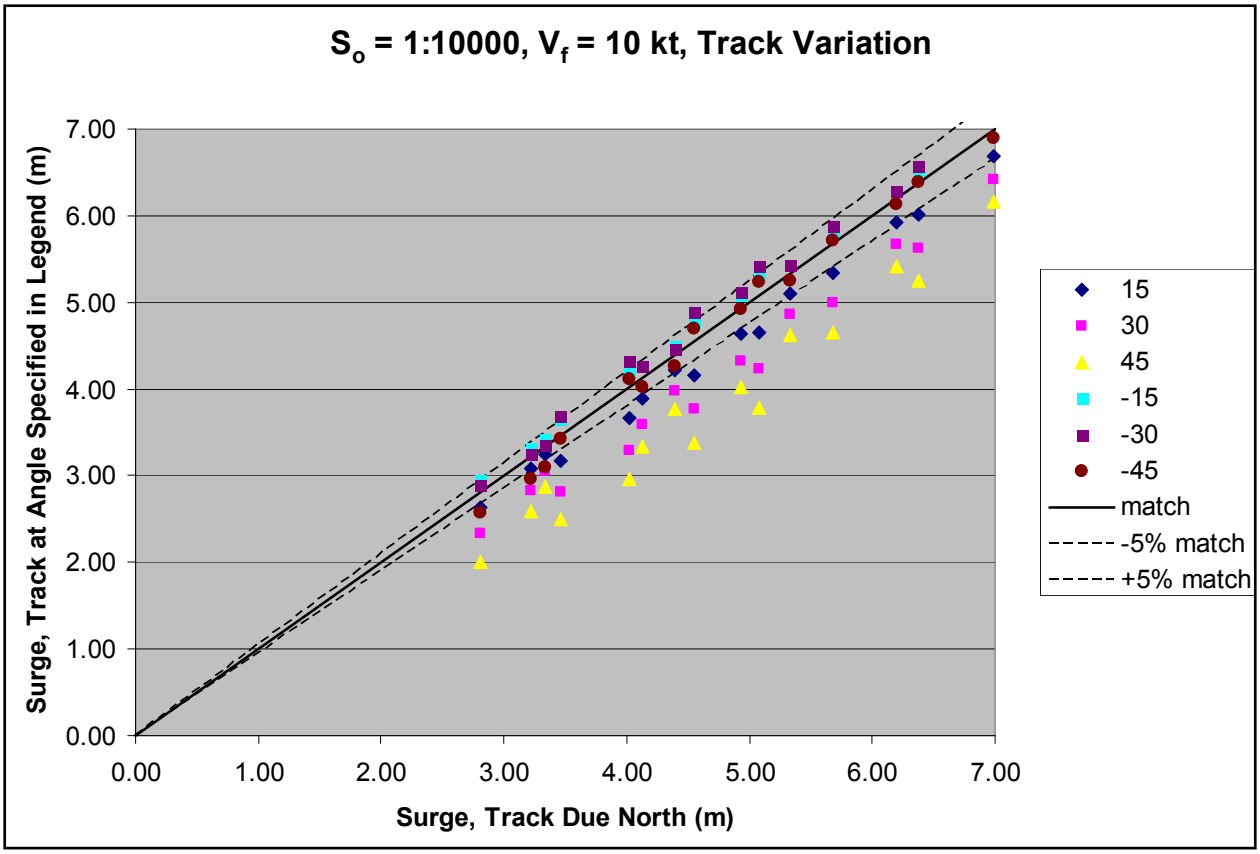

Figure D8. Variation in maximum storm surge produced by hurricanes approaching a straight, shallow-sloping (1:10,000) coast relative to the maximum surge produced by a storm moving perpendicularly to the coast.

APPENDIX E of R2007
The Characteristics of the Holland Pressure Profile Parameter and the Radius to Maximum Winds for Gulf of Mexico and Atlantic Hurricanes as Determined from an Analysis of Flight Level Pressure Data and H*Wind Surface Wind Speed Data

Introduction

Using pressure data collection during hurricane reconnaissance flights, coupled with additional information derived from the Hurricane Research Division's H*Wind snapshots of hurricane wind fields, an analysis of the radius to maximum winds and the Holland *B* parameter was performed. The reconnaissance data incorporates flights encompassing the time period 1977 through to 2001, but the analysis was limited to include only those data collected at the 700 mbar or higher level.

The Holland *B* parameter was found to be inversely correlated with both the size of a hurricane and the latitude of a hurricane. A weak positive correlation of *B* with central pressure deficit and sea surface temperature was also observed. A statistical relationship between the Holland B parameter and a non-dimensional parameter incorporating central pressure, radius to maximum winds, sea surface temperature and latitude was developed.

A qualitative examination of the variation of *B*, central pressure and radius to maximum winds as a function of time suggests that along the Gulf of Mexico coastline (excluding Southwest Florida), during the final 6 hrs to 24 hrs before landfall the hurricanes weaken as characterized by both an increase in central pressure and the radius to maximum winds, and a decrease in the Holland *B* parameter. This weakening characteristic of landfalling storms was not as evident for hurricanes making landfall elsewhere along the United States coastline.

Flight Level Data Analysis Methodology

Upper level aircraft data available at NOAA site were used to estimate Holland's pressure profile parameter (*B*). The upper level aircraft dataset used here contains a total of 4546 radial profiles from 62 Atlantic storms. For every storm, data has been organized based on the different flights that passed through the storm. For each flight, the airplane traversed through the hurricane a number of times in different directions. For every pass the data was collected from the center of the storm to a certain radius (usually 150 km). Available data is then organized according to their radial distance from the center of the storm. For each bin (based on the radius from the center of the storm) flight level pressure, flight altitude, dew point temperature, wind speed and air temperature are available. Each profile from every flight and every storm is treated as an independent observation. Holland, (1980) describes the radial distribution of surface pressure in a hurricane in the form:

$$p(r) = p_0 + \Delta p \cdot \exp - \left[\frac{A}{r^B} \right] \quad (1)$$

where $p(r)$ is the surface pressure at a distance r from the storm center, p_0 is the central pressure, Δp is the central pressure difference, A is the location parameter and B is the Holland's pressure profile parameter. Holland (1980) showed that $RMW = A^{1/B}$ where RMW is the radius to maximum winds, and thus Equation (1) can be expressed as:

$$p(r) = p_0 + \Delta p \cdot \exp - \left[\frac{RMW}{r} \right]^B \tag{2}$$

The surface pressure and radial distance are transformed to the form of Equation (2). The missing quantities in Equation (2) are RMW and B. First estimate of RMW is made from the recorded wind speed profile i.e. RMW is the radius to the measured maximum wind speed. From here on, the radius corresponding to the maximum wind speed in a profile is referred to as RMW. To estimate the optimum values of B and RMW, RMW and B are varied over the range [0.5RMW, 1.5RMW] and [0.5, 2.5] respectively. The algorithm calculates an optimum B value by minimizing the mean of the square differences between the measured and the modeled surface pressure in a range of 0.5RMW to 1.5RMW for different B and RMW values. Mathematically, the mean square error between the measured and the modeled surface pressure can be written as:

$$\varepsilon^2 = \frac{\sum_{i=0.5RMW}^{1.5RMW} \left(P_{obs_i} - P_{theo_i} \right)^2}{n} \tag{3}$$

where P_{obsi} is the measured pressure, P_{theoi} is the theoretical pressure calculated using equation (2) and n is the number of data points in the range [0.5RMW, 1.5RMW]. The values of B and RMW chosen correspond to those yielding the minimum mean square error, ε^2. The corresponding r^2 value for the fit is given by:

$$r^2 = 1 - \frac{\varepsilon^2}{\sigma^2} \tag{4}$$

where σ is the standard deviation of the measured pressure data in the range of [0.5RMW, 1.5RMW].

Quality control criteria

A quality control criterion was used to filter out profiles. Each of the filtered profiles has at least one of the following characteristics associated with it, (a) Flight level pressure is less than 700 mbar i.e. height greater than 3000 m, (b) Central pressure difference is less than 25 mbar, (c) Radius to maximum winds is greater than two-third of the sampling domain, (d) the distance of aircrafts closest approach to the center is greater than half of the radius to maximum winds, (e) Data is available for less than one third of the sampling range i.e. less than 50 km, (f) visual inspection which involved eliminating profiles with a considerable amount of data missing in the

range of interest [0.5*RMW*, 1.5*RMW*]. The rationale for using criteria (a) is that higher the measurement height, less representative measurements are of the surface observations. Criteria (b) results in the data associated with Category 1 or higher hurricanes only. The rationale for using criteria (c), (d), (e) and (f) is to ensure that there is a sufficient number of measurements on both sides of the radius to maximum winds to have a clear representation of the shape of the profile.

The use of the quality control criteria eliminated a total of 2291 profiles from a set of 4556 profiles. Table 1 presents the count of the eliminated pressure profiles based on the filtering criteria. It is clear that criteria (a) and (b) are the most common reasons for profile elimination. Storm by storm percentage of the retained profiles is given in Table 2. For some storms, no profiles were retained as all the profiles either had a central pressure difference of less than 25 mbar (e.g. Chantal 1995) or a flight level pressure of less than 700 mbar (e.g. Hugo 1989). Figure 1 presents a few examples of pressure profiles that were eliminated from the analysis. Both the measured pressure data and the corresponding fit to Holland's equation are shown. It is observed that each of the subplots in Figure 1 is compromised by at least one of the above mentioned quality control criteria.

Figure 2 presents examples of pressure profiles that were retained for analysis. Each row in Figure 2 corresponds to a complete airplane traverse in one direction. The shaded regions in Figure 2 represent the error minimizing range of 0.5*RMW* to 1.5*RMW*. The fit parameters i.e. the *B* value, the central pressure difference and the *RMW* are also provided in the title of every profile. For a given traverse through a hurricane, differences in the *B* values for two different profiles is due to the change in the radius to the maximum winds and the central pressure difference. The geographical distribution of the filtered profiles, based on the storm center, is shown in Figure 3. The filtered profiles have a wide geographical distribution and provides with a wide domain of hurricane climatic characteristics. The filtered dataset has an average *RMW* of 46 km (standard deviation of 22 km), an average central pressure difference of 51 mbar (18 mbar) and an average location of 25.84°N (5.74°N) and 74.78°W (12.82°W). 71% of the fits yield r^2 values greater than 0.95 and 80% of the fits have a mean square error less than 2.5 mbar. The maximum mean square error was 24.6 mbar which occurred for one of Hurricane Opal's profiles where Holland's equation overestimated the pressures at all points.

Table 1.
Distribution of filtered pressure profiles based on filtering criteria.

Filter criteria	Number of profiles eliminated
(a)	459
(b)	1180
(c)	121
(d)+(e)+(f)	531
Total number of filtered profiles	2291

Table 2.
Percentage of flight level pressure profiles retained.

Storm	Year	Total	Retained	%Retained	Comments
no-name	1938	5	5	100.00	Data extracted manually from Myers & Jordan (1956)
Anita	1977	20	20	100.00	
David	1979	24	17	70.83	
Frederic	1979	62	38	61.29	
Allen	1980	125	43	34.40	
Gert	1981	78	1	1.28	Δp<25mb for all the cases, except one.
Alicia	1983	50	39	78.00	
Arthur	1984	22	0	0.00	Δp <25mb for all the cases.
Diana	1984	128	67	52.34	
Danny	1985	26	0	0.00	Δp <25mb for all the cases.
Elena	1985	122	99	81.15	
Gloria	1985	42	24	57.14	
Isabel	1985	48	0	0.00	Δp <25mb for all the cases.
Juan	1985	36	6	16.67	
Charley	1986	28	0	0.00	Δp <25mb for all the cases.
Emily	1987	56	1	1.79	40 out of 56 profiles have flight level pressure <700mb.
Floyd	1987	22	0	0.00	Δp <25mb for all the cases.
Florence	1988	20	11	55.00	
Gilbert	1988	50	39	78.00	
Joan	1988	6	5	83.33	
Dean	1989	12	1	8.33	
Gabrielle	1989	12	10	83.33	
Hugo	1989	40	0	0.00	Flight level pressure <700mb for all the cases
Jerry	1989	17	5	29.41	
Gustav	1990	84	82	97.62	
Bob	1991	92	34	36.96	
Claudette	1991	73	71	97.26	
Andrew	1992	141	95	67.38	
Debby	1994	10	0	0.00	Δp <25mb for all the cases.
Gordon	1994	83	8	9.64	57 out of 83 profiles have Δp <25mb.
Allison	1995	39	3	7.69	35 out of 39 profiles have Δp <25mb.
Chantal	1995	72	0	0.00	Δp <25mb for all the cases.
Erin	1995	97	66	68.04	
Felix	1995	130	59	45.38	
Gabrielle	1995	16	0	0.00	Δp <25mb for all the cases.
Iris	1995	132	41	31.06	
Luis	1995	130	77	59.23	
Marilyn	1995	116	96	82.76	
Opal	1995	76	21	27.63	
Roxanne	1995	141	52	36.88	
Bertha	1996	78	56	71.79	
Cesar	1996	34	0	0.00	Δp <25mb for all the cases.
Edouard	1996	178	135	75.84	
Fran	1996	143	102	71.33	
Hortense	1996	109	59	54.13	
Josephine	1996	23	1	4.35	

Storm	Year	Total	Retained	%Retained	Comments
Kyle	1996	8	0	0.00	Δp <25mb for all the cases.
Lili	1996	68	28	41.18	
Marco	1996	67	1	1.49	Δp <25mb for all the cases, except two.
Erika	1997	56	36	64.29	
Bonnie	1998	193	113	58.55	
Danielle	1998	133	48	36.09	
Earl	1998	32	3	9.38	
Georges	1998	202	125	61.88	
Mitch	1998	86	57	66.28	
Bret	1999	102	49	48.04	
Dennis	1999	158	83	52.53	
Floyd	1999	163	103	63.19	
Keith	2000	50	40	80.00	
Leslie	2000	29	0	0.00	Δp <25mb for all the cases.
Michael	2000	21	11	52.38	
Humberto	2001	46	13	28.26	
Michelle	2001	89	61	68.54	

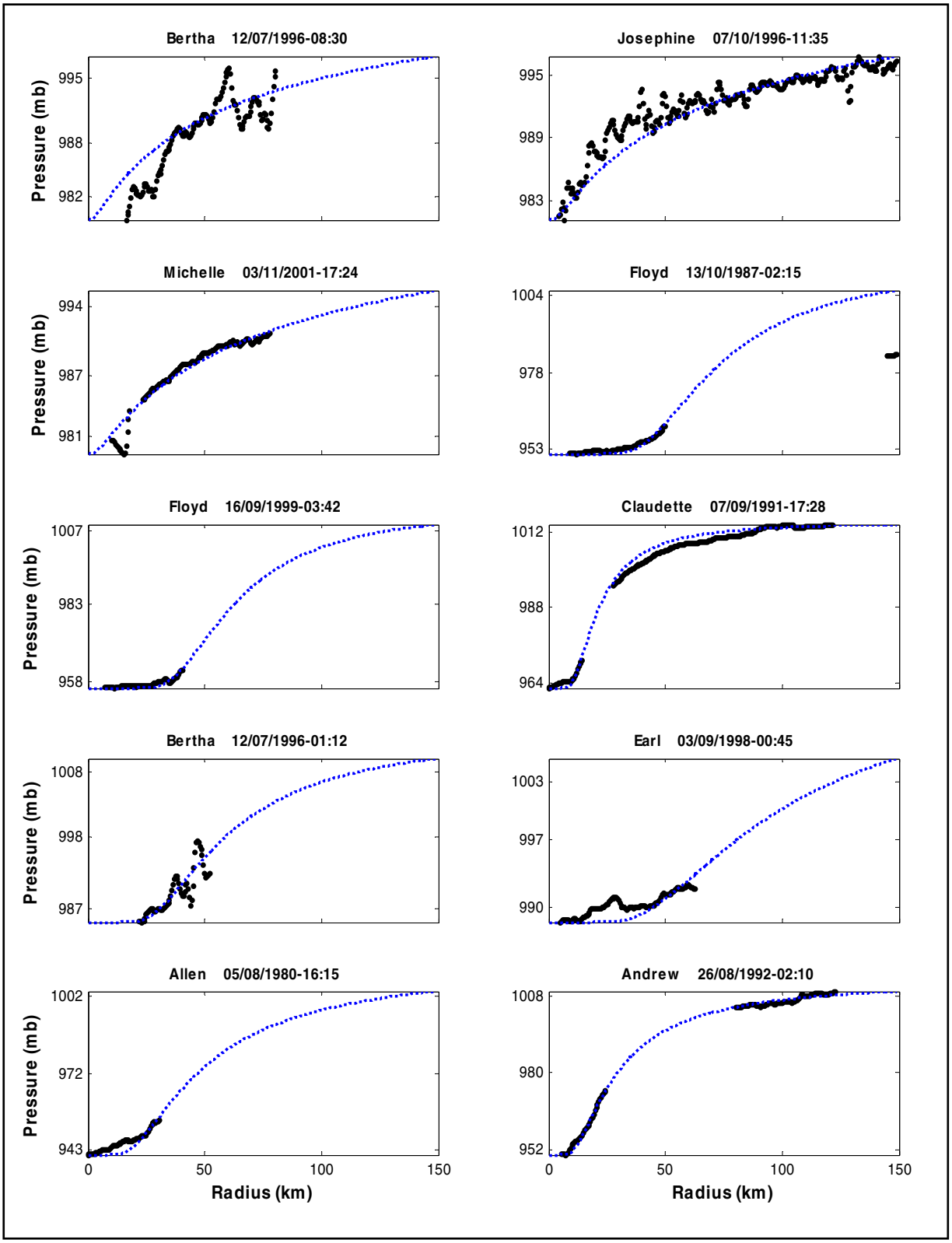

Figure 1. Examples of the eliminated profiles.

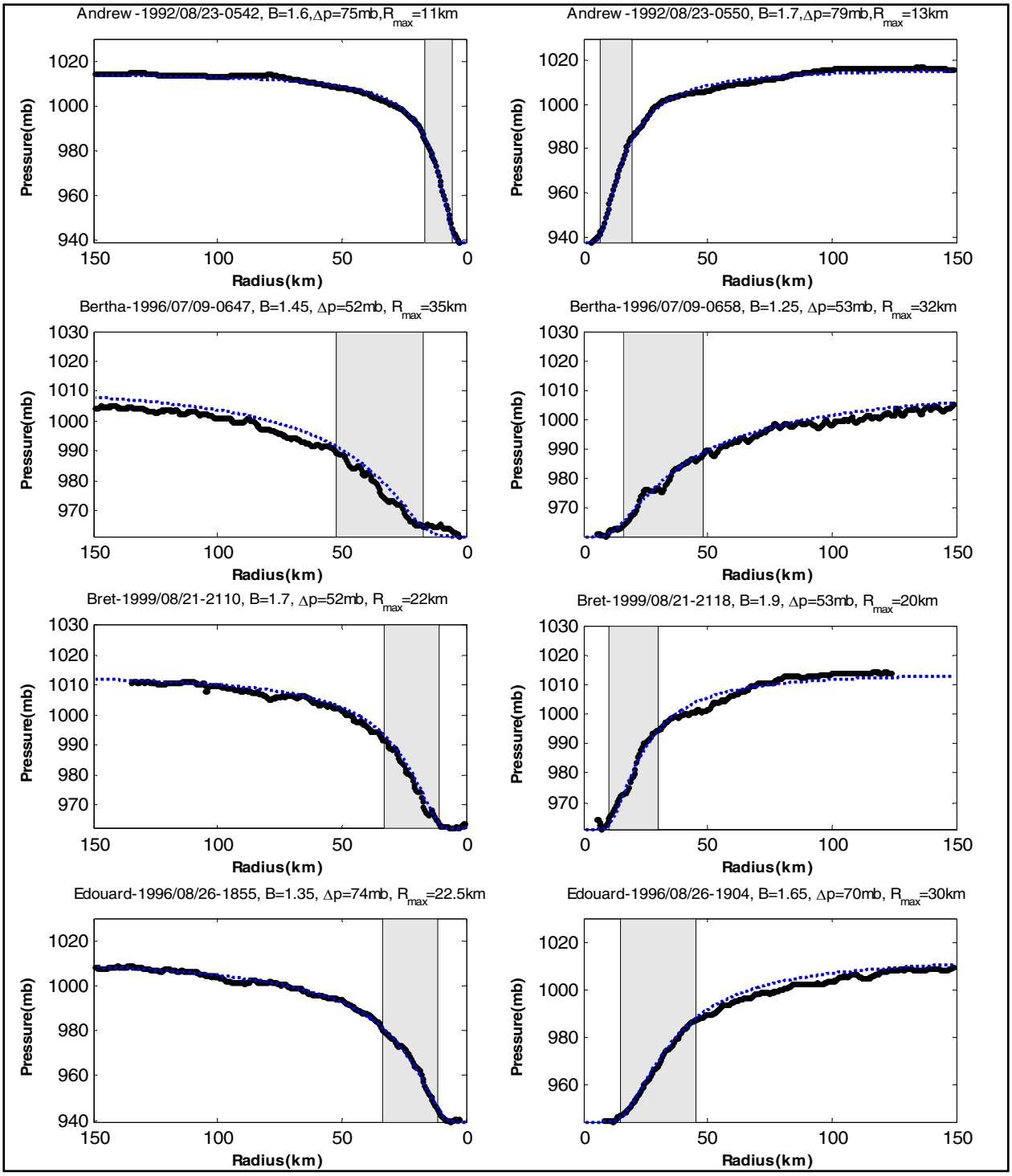

Figure 2. Examples of surface pressure profiles for a traverse across a given hurricane.

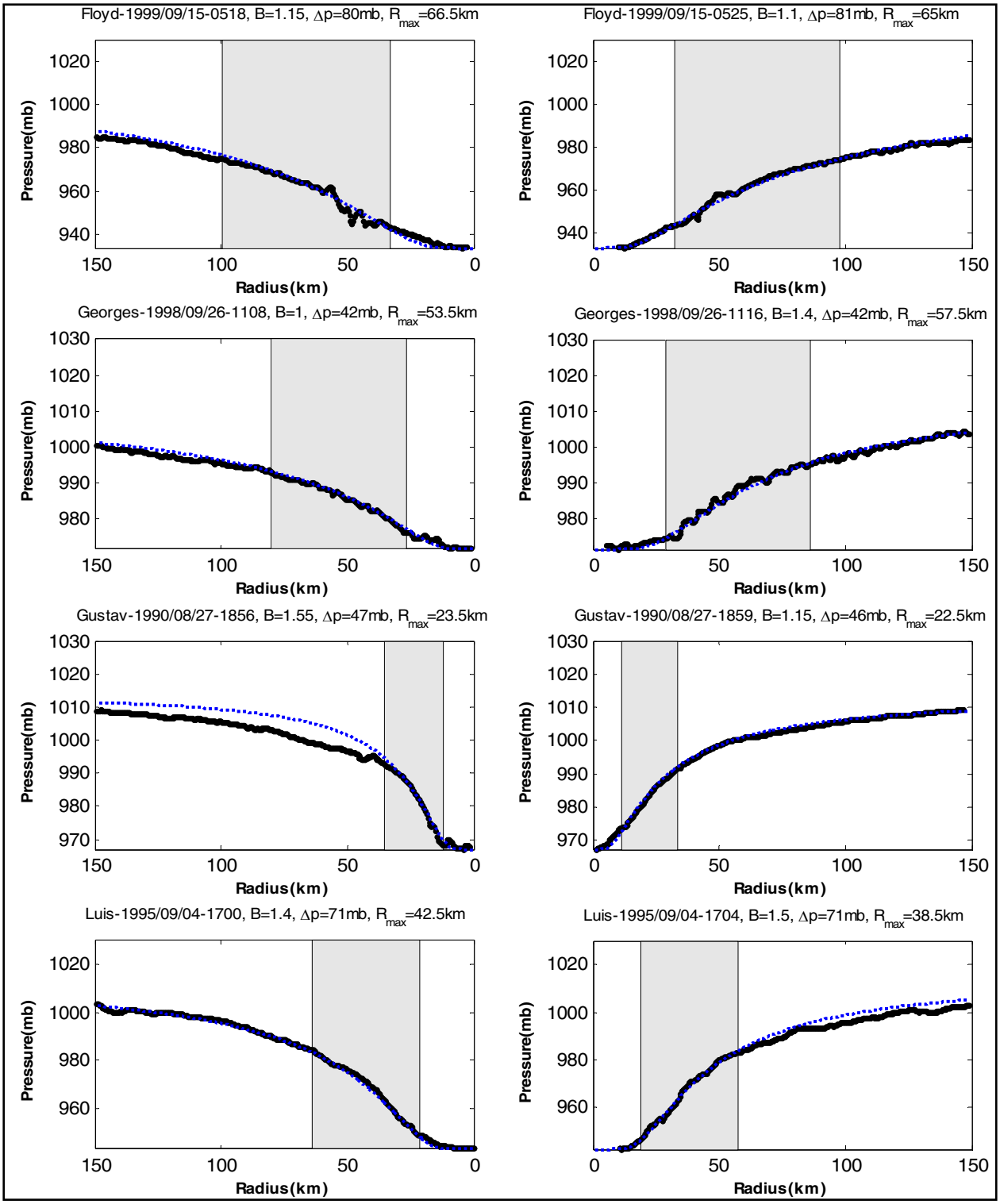

Figure 2. (continued) Examples of surface pressure profiles for a traverse across a given hurricane.

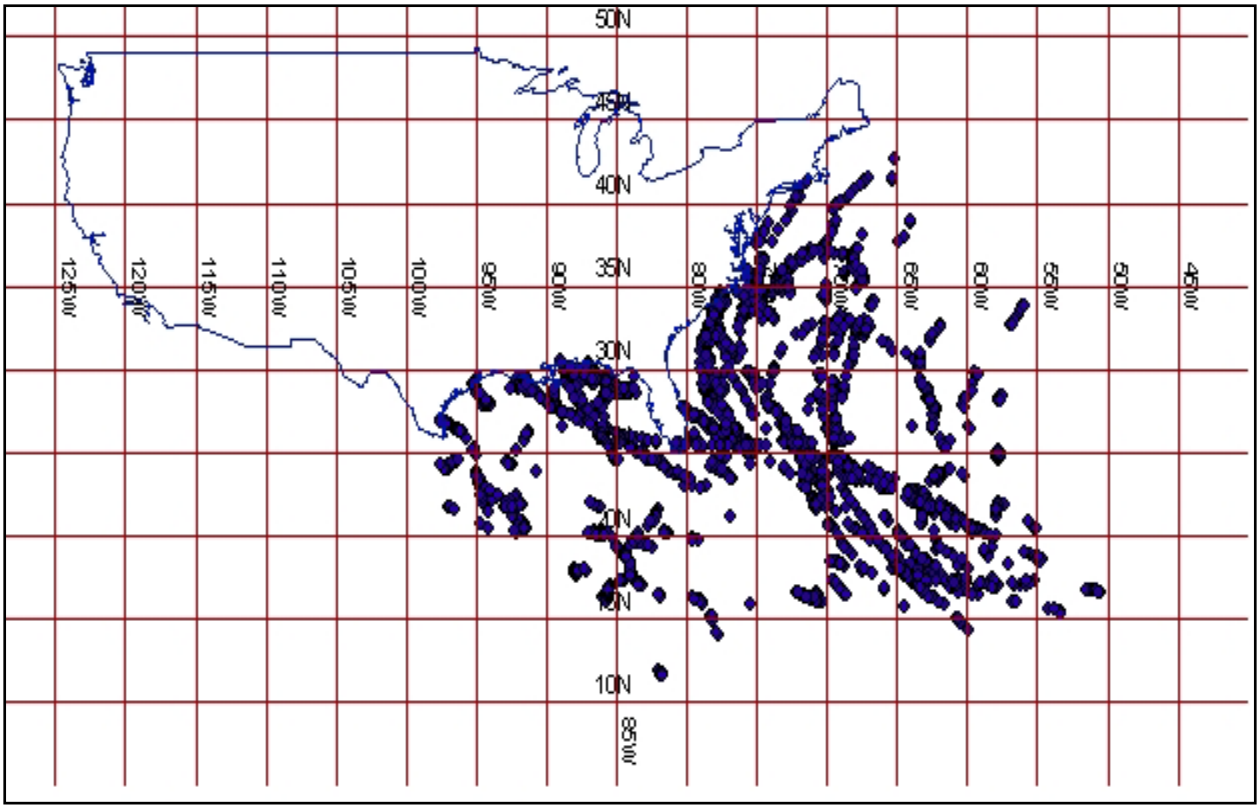

Figure 3. Geographical distribution of all the filtered profiles.

The approach for analyzing the *B* and *RMW* data involved the estimation of *RMW* and *B* from each single pass of a flight through the storm, and then smoothing the variations in *B* and *RMW* as a function of time. Figure 4 presents ten examples of both the single flight (point estimates) and the smoothed estimates of *B* and *RMW* plotted vs. time, for landfalling hurricanes. The landfall time is indicated with a vertical line in each plot. Using the smoothed data, values of *B* and *RMW* were extracted at intervals of approximately 3 hrs and retained for use in the statistical analyses. The mean values of *B* and *RMW* for the smoothed data set are 1.21 and 47 km respectively. The corresponding standard deviations are 0.29 and 21 km respectively. Note that in only one of the 11 landfall's indicated in Figure 4, does the Holland *B* parameter appear to increase as a hurricane approaches land (Hurricane Floyd near the NC coast). Table 3 summarizes, qualitatively, the tendency in the changes of *B* over the final few hours before landfall.

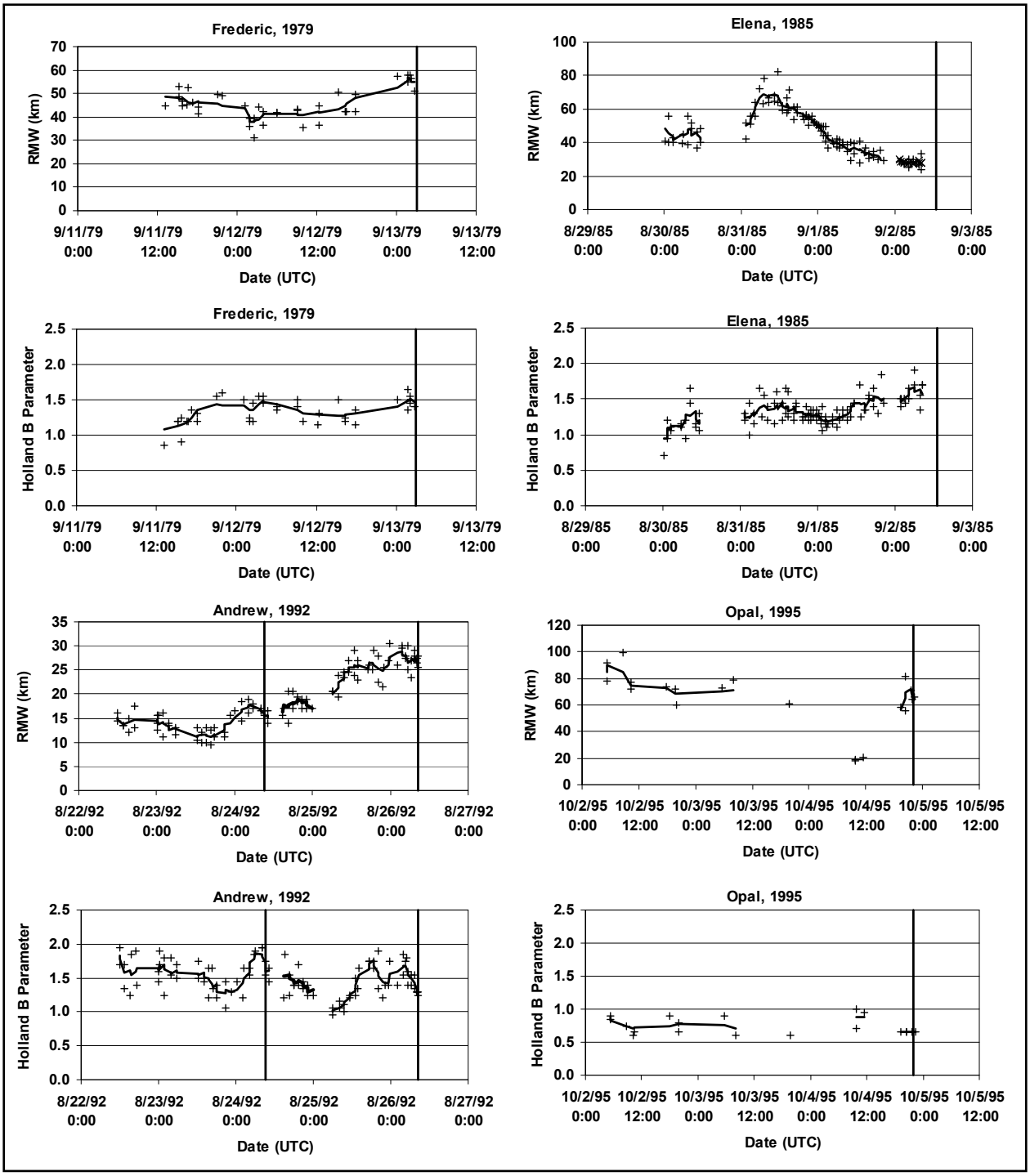

Figure 4. Examples of Smoothed (line) and Point Estimates (symbols) of *RMW* and *B* derived from 700 mbar level pressure data. Vertical line(s) represent time of landfall.

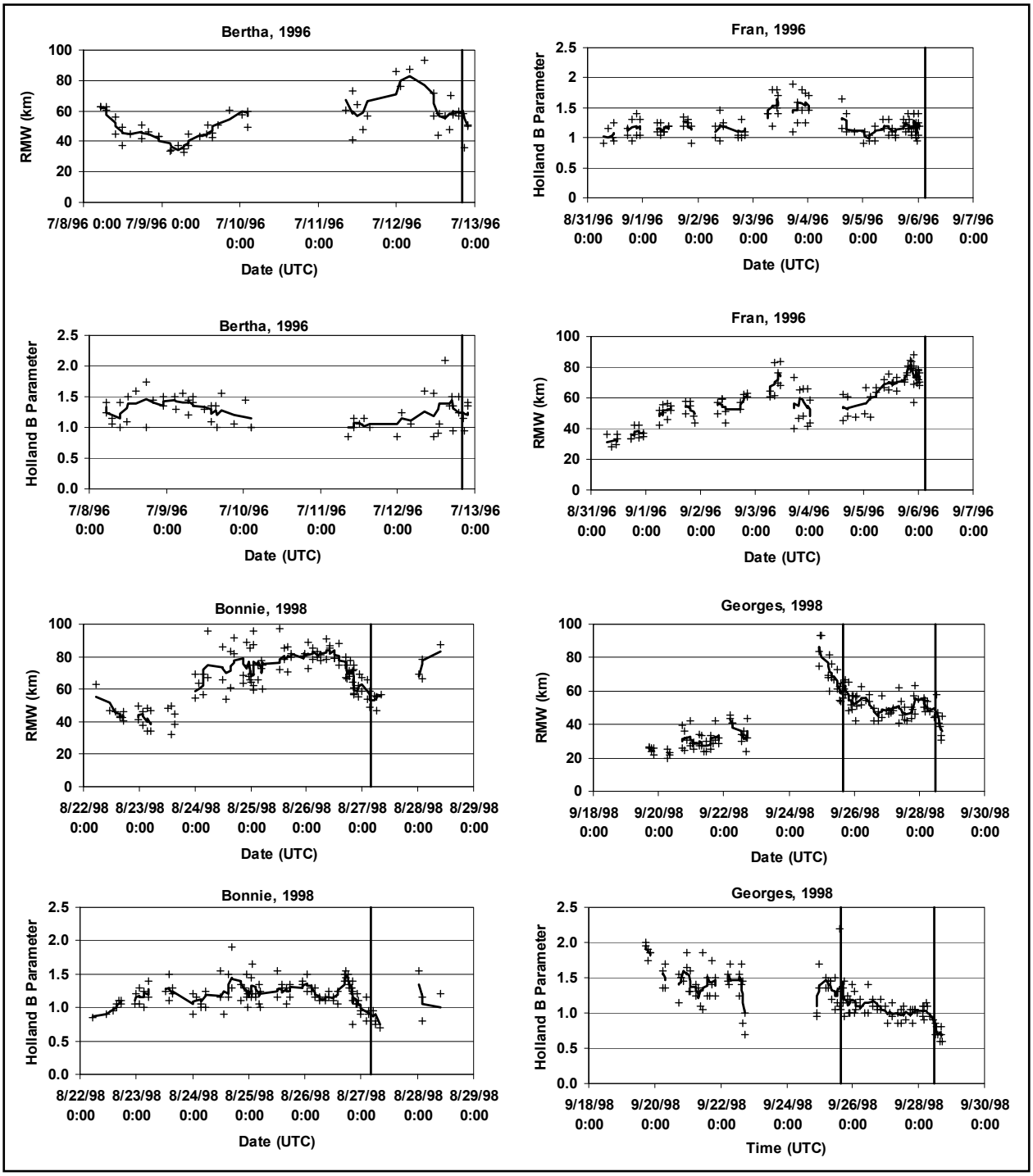

Figure 4. (continued) Examples of Smoothed (line) and Point Estimates (symbols) of *RMW* and *B* derived from 700 mbar level pressure data. Vertical line(s) represent time of landfall.

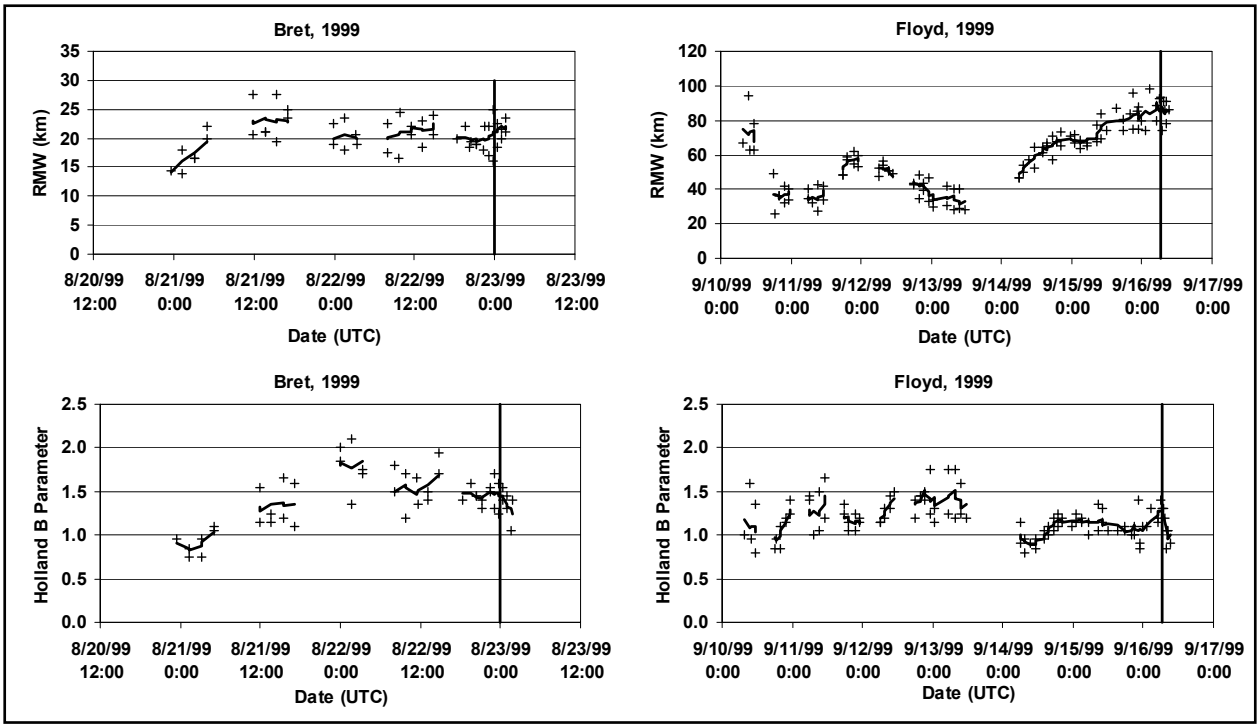

Figure 4. (concluded) Examples of Smoothed (line) and Point Estimates (symbols) of *RMW* and *B* derived from 700 mbar level pressure data. Vertical line(s) represent time of landfall.

Table 3.
Tendency of Holland B Parameter for Landfalling Storms

Hurricane and Landfall Location	*B* Tendency at landfall
Frederic (Alabama)	~ constant
Elena (Mississippi)	~ constant
Andrew South Florida	~constant to ~negative
Andrew Louisiana	negative
Opal (North West Florida)	constant
Bertha (North Carolina)	negative
Fran (North Carolina)	~constant
Bonnie (North Carolina)	negative
Georges (Mississippi)	negative
Bret (Texas)	~constant
Floyd (North Carolina)	positive

Supplemental H*Wind Data

The flight level data encompasses storms through to 2001, and thus to supplement the data set with more recent storms, some additional storms analyzed using the H*Wind methodology were added. The only storms added were the intense storms from the 2004 and 2005 seasons that had been re-analyzed using the most recent SFMR calibrations. The intense storms that have been reanalyzed include Hurricanes Katrina (2005) and Hurricane Ivan (2004). Hurricane Rita was added to the data set even though it had not been re-analyzed, because at its most intense, the storm had a minimum central pressure of less than 900 mbar. Using the wind field model described in Vickery, et al. (2007)., and the values of central pressure, *RMW,* storm translation speed*,* and the maximum sustained wind speed, a *B* value chosen so that the maximum surface level wind speed (one minute sustained value) obtained from the model match the H*Wind estimate of the maximum wind speed. Thus the estimated *B* values are obtained through an indirect measure, matching the maximum wind speed rather than the shape of the entire wind field.

Figure 5 presents plots of *RMW*, maximum one minute surface level wind speed, the derived *B* parameter and central pressure as a function of time for the three aforementioned hurricanes, in addition to the data derived for hurricanes Dennis (2005), Bret (1999) and Lili (1999). These three additional storms are given to examine the change in the characteristics of the storms as they approach land. Each plot also presents the central pressure(s) at land fall as given in the NHC hurricane reports.

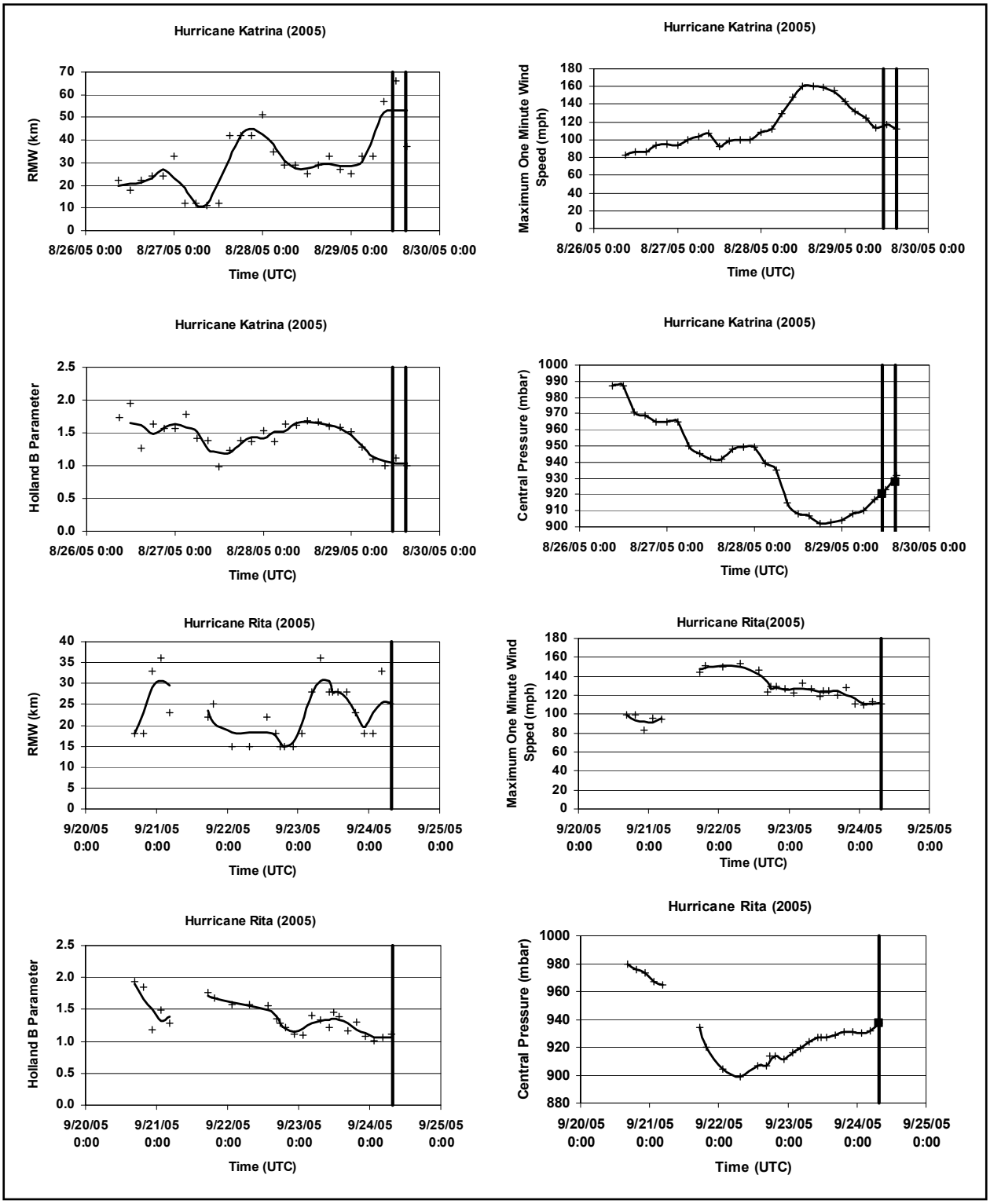

Figure 5. Smoothed (line) and Point Estimates (symbols) of *RMW* and *B* derived from H*Wind data. Vertical line(s) represent time of landfall. Solid square point at time of landfall represents NHC landfall pressure value.

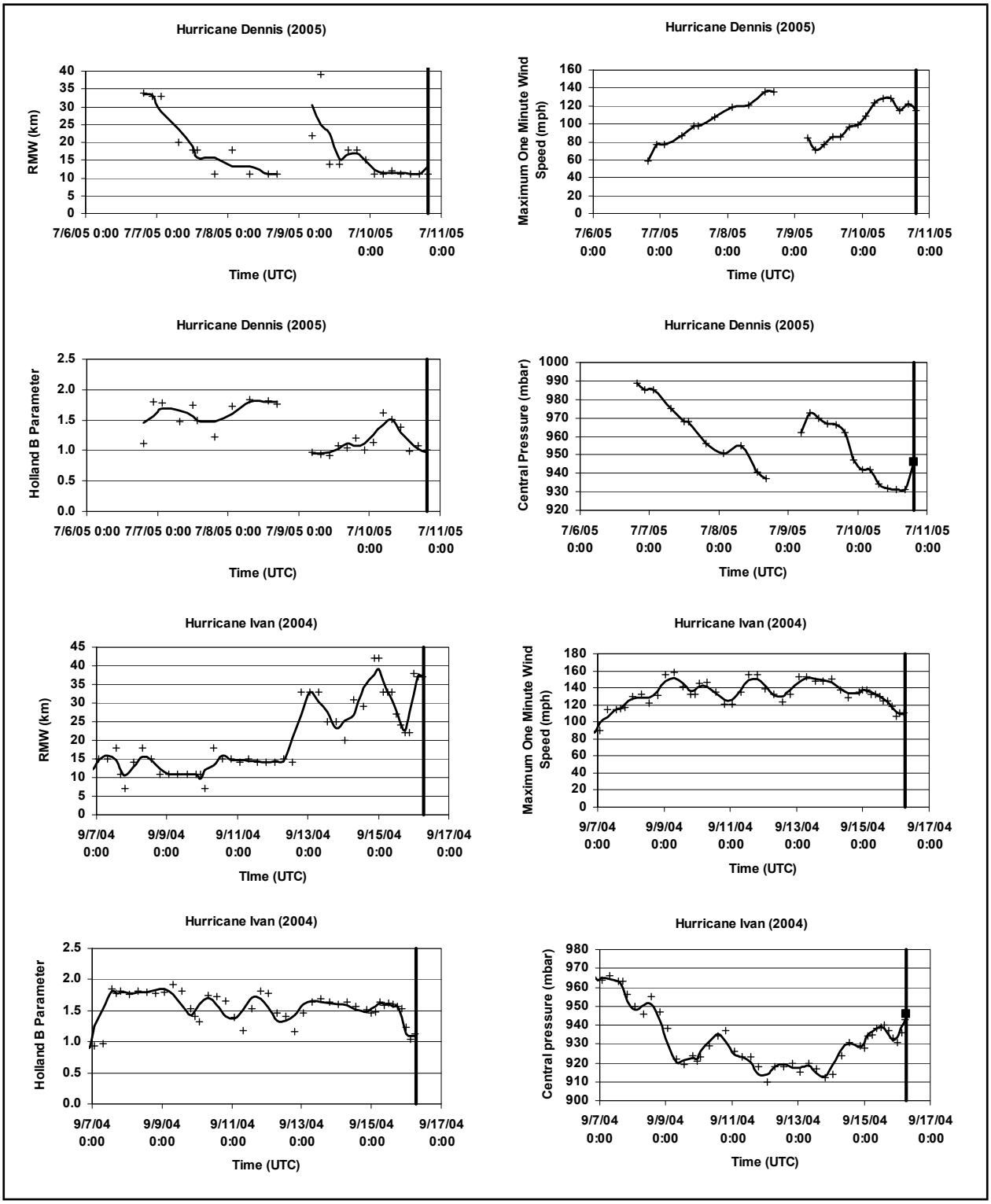

Figure 5. (continued) Smoothed (line) and Point Estimates (symbols) of *RMW* and *B* derived from H*Wind data. Vertical line(s) represent time of landfall. Solid square point at time of landfall represents NHC landfall pressure value.

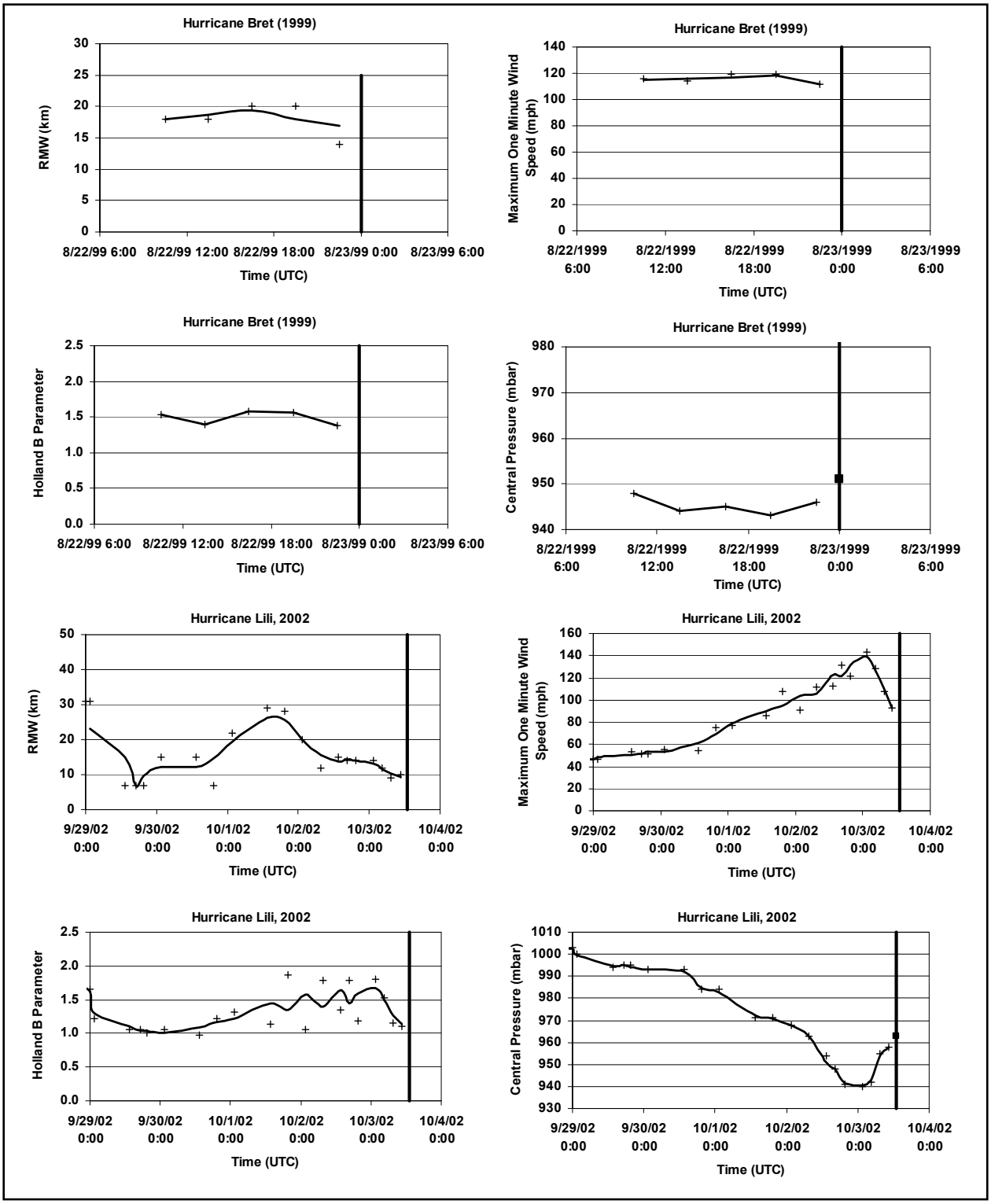

Figure 5. (concluded) Smoothed (line) and Point Estimates (symbols) of *RMW* and *B* derived from H*Wind data. Vertical line(s) represent time of landfall. Solid square point at time of landfall represents NHC landfall pressure value.

These six hurricanes represent all the Gulf of Mexico landfalling hurricanes in the H*Wind database that include information on both wind speeds and central pressure in each of the H*Wind snapshots. Additional storms are given in the H*Wind database that do not have central pressures provided on the H*Wind snapshots. All of the six hurricanes show an increase in central pressure and a decrease in the magnitude of the Holland *B* parameter as they approach the Gulf Coast. An increase in the radius to maximum winds as the hurricanes approach landfall is also evident in five of the six cases examined.

A similar analysis of hurricane characteristics for hurricanes making landfall in regions other than along the Gulf of Mexico coast did not indicate that there is a strong tendency for the storms to weaken and enlarge before landfall.

Statistical Model for Radius to Maximum Winds

All Hurricanes. The *RMW* for all points (flight level data plus H*Wind data) in the data set having a central pressure of less than 980 mbar were modeled as a function of central pressure difference and latitude in the form:

$$\ln(RMW) = 3.559 - 7.229\times10^{-5}\,\Delta p^2 + 5.296\times10^{-4}\,\Psi^2\,;\; r^2=0.266,\; \sigma_{\ln RMW} = 0.449 \qquad (4)$$

An analysis of the errors (difference between the regression model estimates and the data) indicates that the model error reduced with increasing Δp, as indicated in Figure 6.

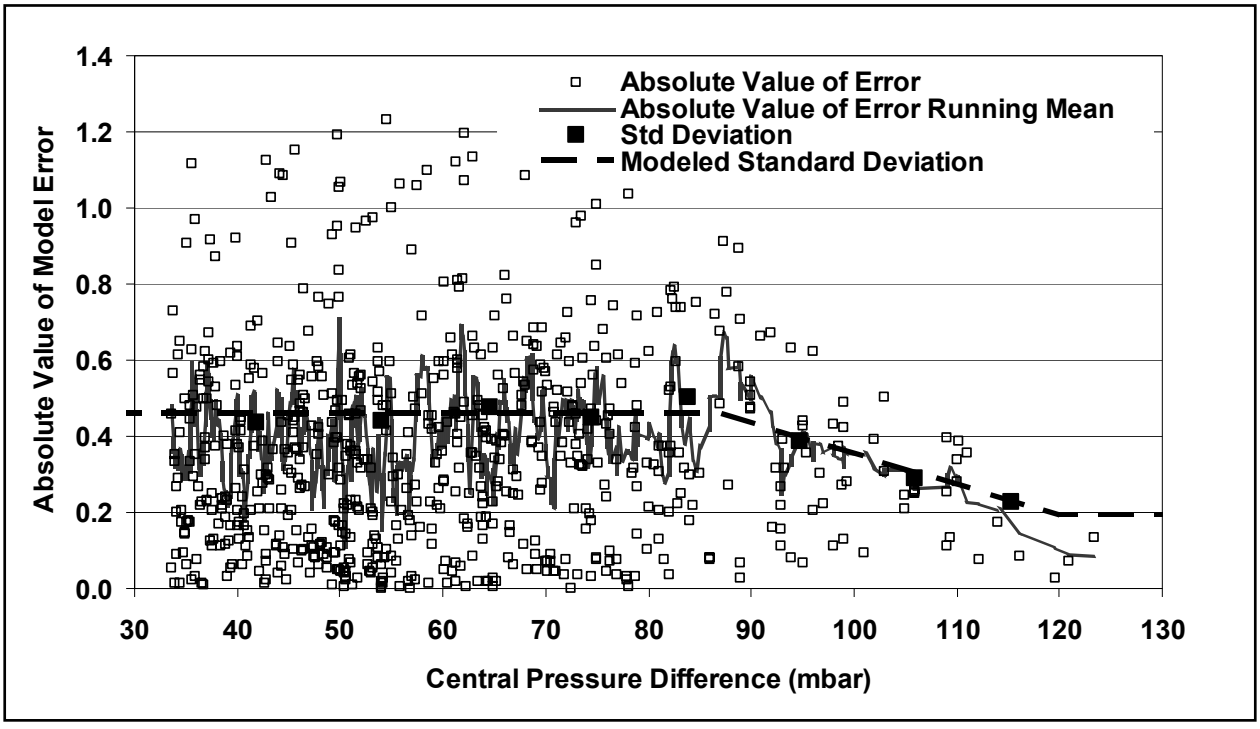

Figure 6. Absolute value of *RMW* model error vs. Δp

The error, $\sigma_{\ln RMW}$, is modeled in the form:

$$\sigma_{\ln RMW} = 0.460 \quad \Delta p \leq 87 \text{ mbar} \tag{5a}$$

$$\sigma_{\ln RMW} = 1.1703 - 0.00817\Delta p \quad 87 \text{ mbar} \leq \Delta p \leq 120 \text{ mbar} \tag{5b}$$

$$\sigma_{\ln RMW} = 0.190 \quad \Delta p > 120 \text{ mbar} \tag{5c}$$

Figure 7 presents the modeled and observed values of *RMW* plotted vs. Δp. The modeled data are given as the median estimates and the range defined by $\pm 2\sigma_{\ln RMW}$. The modeled range reflects the reduction in $\sigma_{\ln RMW}$ as a function of Δp.

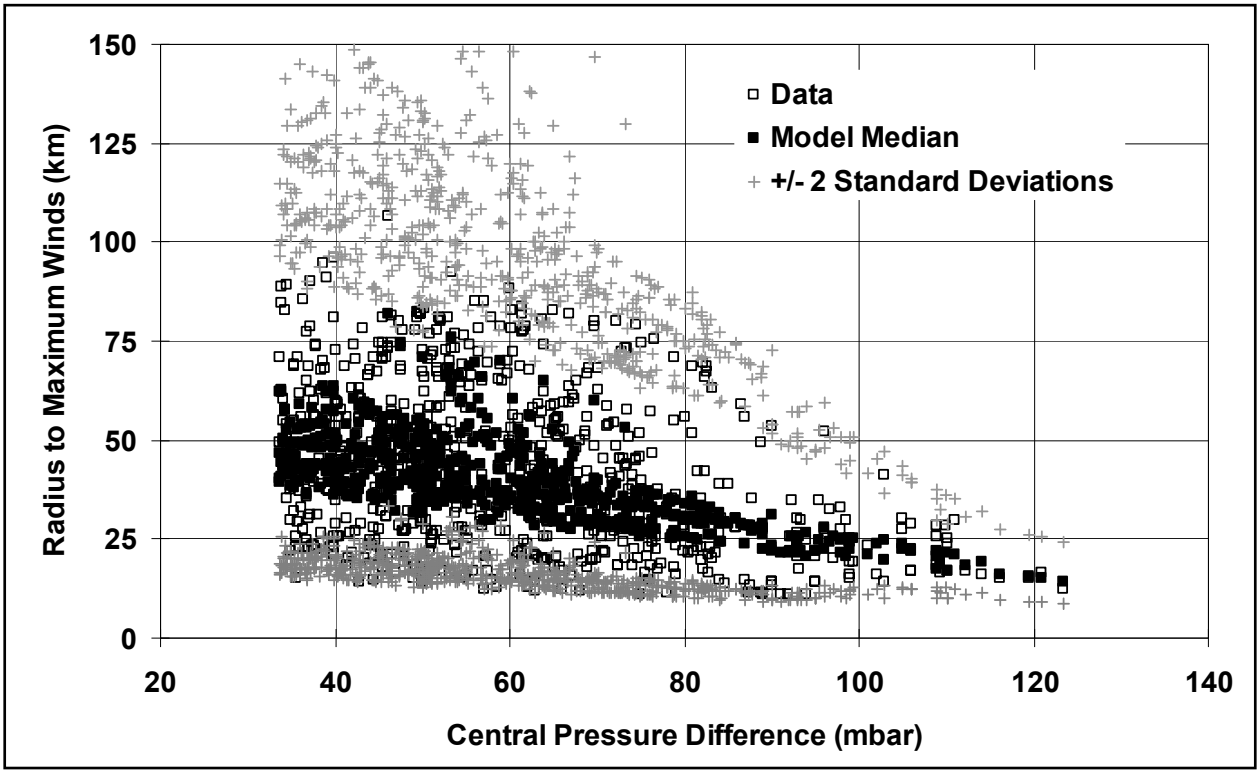

Figure 7. Modeled and observed *RMW* vs. Δp for all hurricanes

Gulf of Mexico Hurricanes. In order to determine if the characteristics of the *RMW* associated with the Gulf of Mexico storms differed from that obtained using the all storm data, the *RMW* –Δp and *RMW*-ψ relationships were re-examined. For this analysis the Gulf of Mexico storms included all hurricanes west of 81°W and north of 18°N. The *RMW* for all storms (flight level data plus H*Wind data) in the Gulf of Mexico data set with central pressures less than 980 mbar were modeled as a function of central pressure difference in the form:

$$\ln(RMW) = 3.859 - 7.700 \times 10^{-5} \Delta p^2 \quad r^2 = 0.290,\ \sigma_{\ln RMW} = 0.390 \tag{6}$$

The *RMW* was found to be independent of latitude. As in the all storm case, the model error reduces with increasing Δp, as indicated in Figure 8.

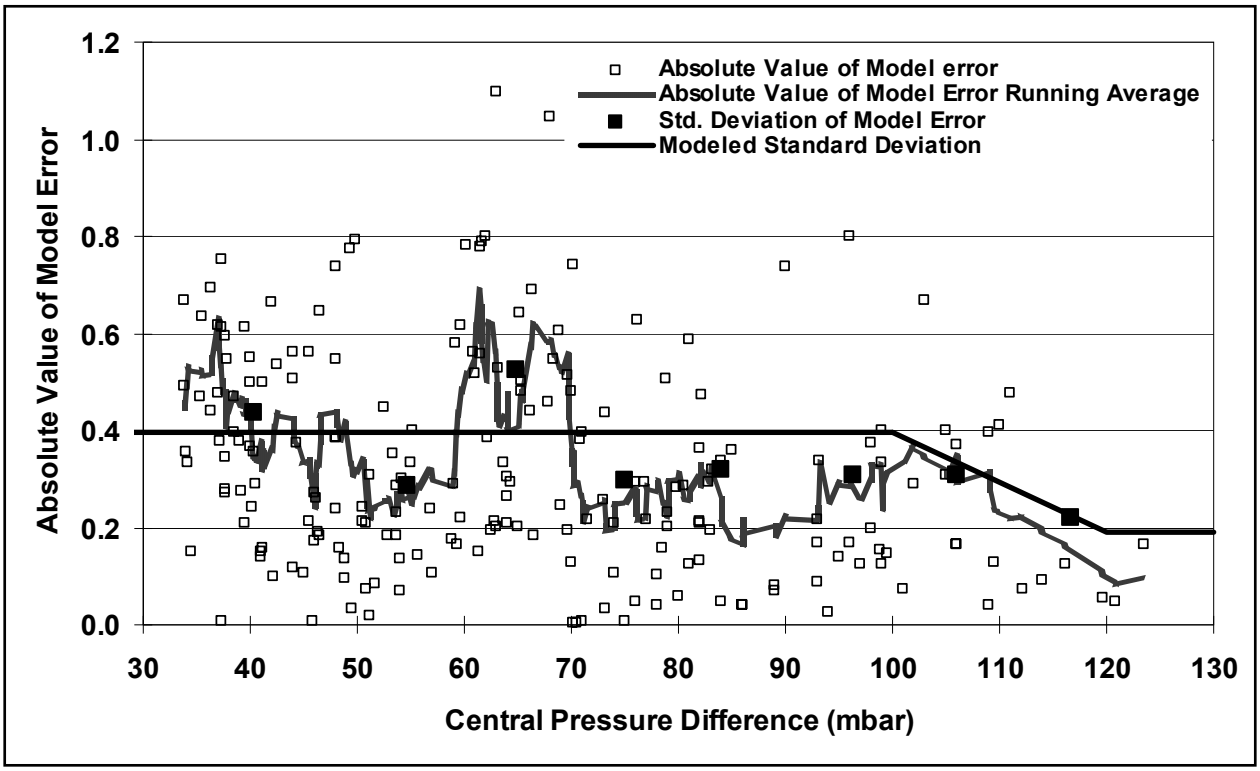

Figure 8. Absolute value of *RMW* model error vs. Δp for Gulf of Mexico hurricanes

The error, $\sigma_{\ln RMW}$, for Gulf of Mexico hurricanes is modeled in the form:

$$\sigma_{\ln RMW} = 0.396 \quad \Delta p \leq 100 \text{ mbar} \tag{7a}$$

$$\sigma_{\ln RMW} = 1.424 - 0.01029\Delta p \quad 100 \text{ mbar} \leq \Delta p \leq 120 \text{ mbar} \tag{7b}$$

$$\sigma_{\ln RMW} = 0.19 \quad \Delta p > 120 \text{ mbar} \tag{7c}$$

Figure 9 presents the modeled and observed values of *RMW* plotted vs. Δp for the Gulf of Mexico hurricanes. The modeled data are given as the median estimates and the range defined by $\pm 2\sigma_{\ln RMW}$. The modeled range reflects the reduction in $\sigma_{\ln RMW}$ as a function of Δp.

Figure 10 presents the median values of the *RMW* computed using Equation 4 (all hurricane *RMW* model) computed for latitudes of 25°N (Southern Gulf of Mexico) and 30°N (Northern Gulf of Mexico), where it is seen that for the Northern Gulf of Mexico storms, the all hurricanes *RMW* model over estimates the size of the Gulf of Mexico hurricanes, indicating that Gulf of Mexico hurricanes, are smaller than Atlantic hurricanes.

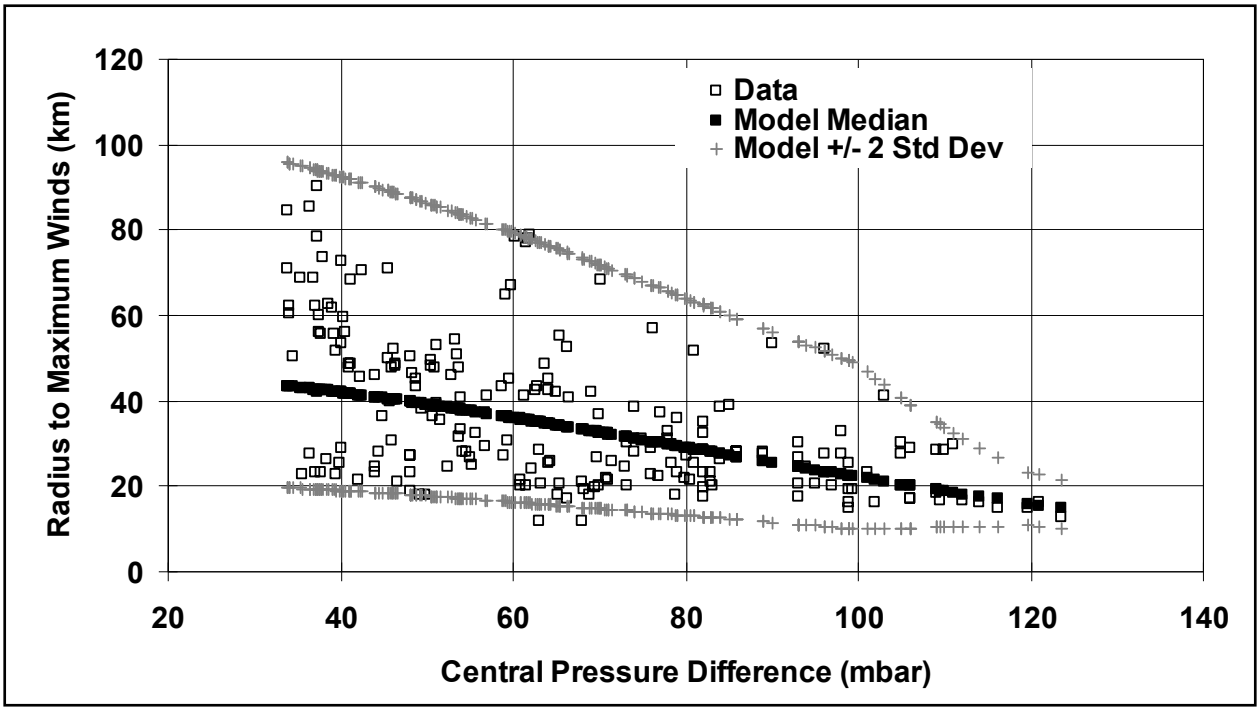

Figure 9. Modeled and observed *RMW* vs. Δ*p* for Gulf of Mexico hurricanes.

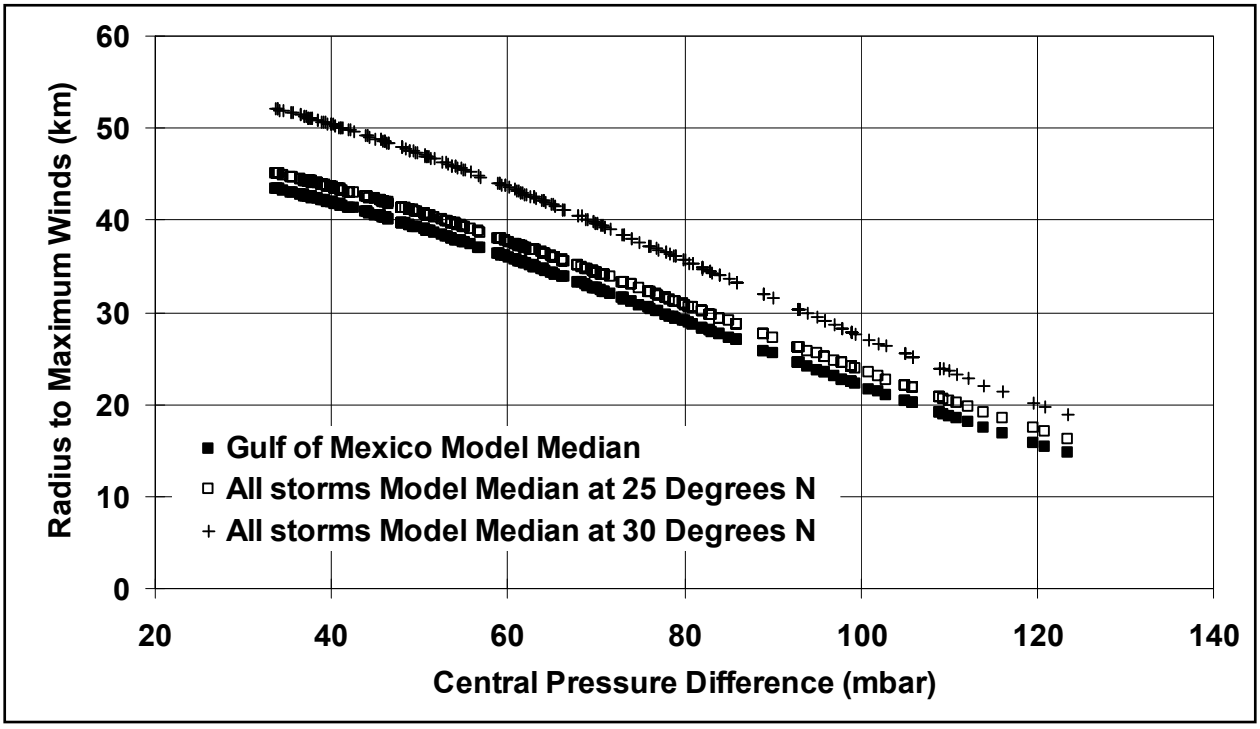

Figure 10. Comparison of all hurricanes model predicted median *RMW* to Gulf of Mexico model median *RMW*.

RMW for Landfalling Storms

Figure 11 presents the values of the *RMW* for storms making landfall along the Gulf and Atlantic coasts of the United States. In the case of Gulf Coast storms, no statistically significant correlation exists between the *RMW* and either latitude or Δp. In the case of hurricanes making landfall along the Atlantic coast, the *RMW* is positively correlated with latitude, and negatively correlated with the Δp^2. As a group (i.e. both Atlantic and Gulf Coast landfalling hurricanes), the *RMW* is also positively correlated with latitude, and negatively correlated with the Δp^2. Using only landfall values of *RMW* the following statistical models best define the relationship between *RMW*, Δp and latitude.

1. Gulf of Mexico landfalling hurricanes:

$$\ln(RMW) = 3.558 \qquad \sigma_{\ln RMW} = 0.457 \tag{8a}$$

2. Atlantic Coast landfalling hurricanes:

$$\ln(RMW) = 2.556 - 5.963 \times 10^{-5} \Delta p^2 + 0.0458\psi \; ; \qquad r^2 = 0.336, \; \sigma_{\ln RMW} = 0.456 \tag{8b}$$

3. Gulf and Atlantic Coast landfalling hurricanes:

$$\ln(RMW) = 2.377 - 4.825 \times 10^{-5} \Delta p^2 + 0.0483\psi \; ; \qquad r^2 = 0.203, \; \sigma_{\ln RMW} = 0.457 \tag{8c}$$

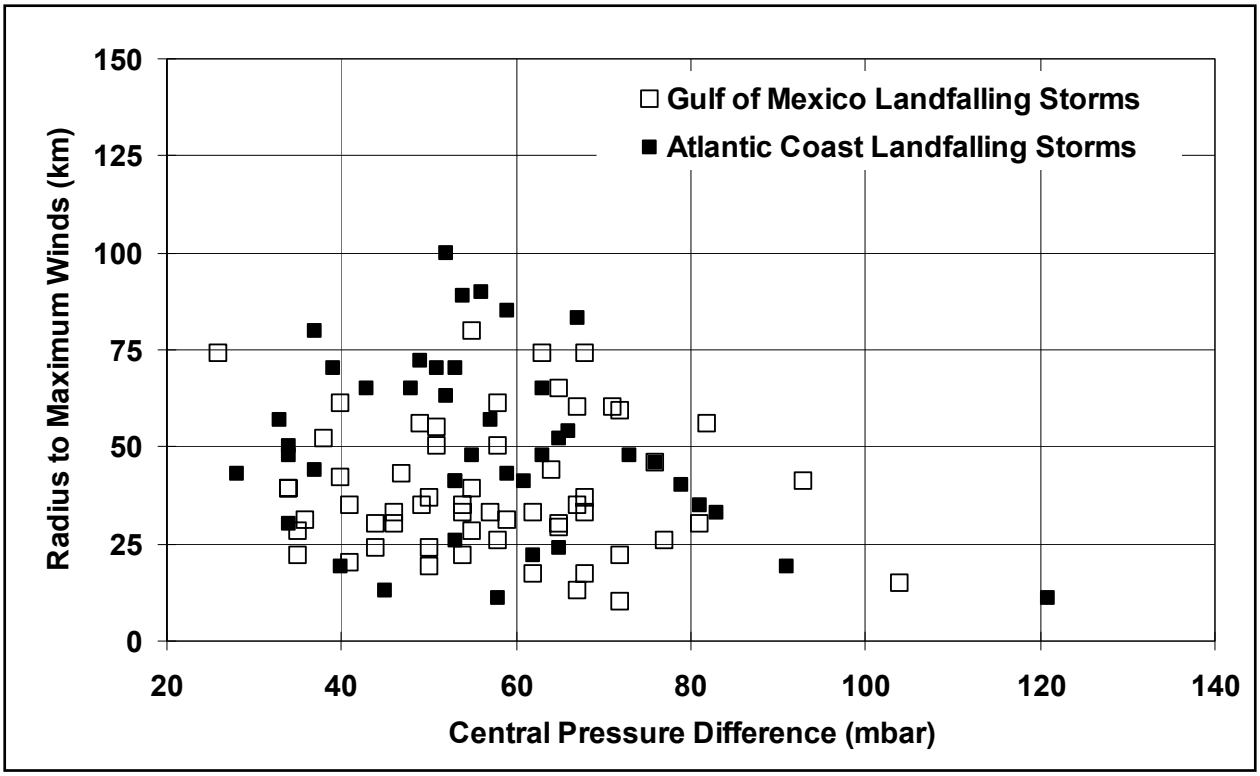

Figure 11. *RMW* for landfalling storms along the Gulf and Atlantic Coasts of the US

The ability of the *RMW* models developed using the flight level and H*Wind data (primarily open ocean data) to model the landfalling hurricane *RMW* was tested by computing the mean errors (in log space) and the resulting standard deviations and r^2 values using the landfall *RMW* data and the flight level/H*Wind derived *RMW* models. The error, $\mu_{\ln RMW}$, is defined as model *RMW* minus observed *RMW*, thus a mean positive error indicates the model overestimates the size of the landfalling hurricanes. The comparisons yield the following findings:

1. Gulf of Mexico landfalling hurricanes with GoM *RMW* model:

   $\mu_{\ln RMW} = 0.032$; r^2=-0.008 $\sigma_{\ln RMW} = 0.459$

2. Atlantic Coast landfalling hurricanes with the all hurricane *RMW* model:

   $\mu_{\ln RMW} = 0.058$; r^2=0.356 $\sigma_{\ln RMW} = 0.450$

3. Gulf and Atlantic Coast landfalling hurricanes with the all hurricane *RMW* model for the Atlantic Coast and GoM *RMW* model for the Gulf Coast:

   $\mu_{\ln RMW} = 0.043$; r^2=0.219 $\sigma_{\ln RMW} = 0.453$

A comparison of the model errors noted above to those resulting from the statistical analyses of the landfalling storms alone indicates that the models derived from the flight level and H*Wind data can be used to define the characteristics of landfalling hurricanes. In the case of landfalling Gulf of Mexico hurricanes, the use of the GoM *RMW* model which contains the negative correlation between *RMW* and Δp^2, is not statistically significantly different from the uncorrelated *RMW*-Δp relationship derived from the landfalling hurricanes alone. This observation suggests that there are an insufficient number of landfalling intense storms in the historical data to discern such a relationship.

Statistical Model for Holland's Parameter (*B*)

The *B* values computed as discussed above were found to be correlated to the radius to maximum winds, central pressure difference, latitude and sea surface temperature. Only points associated with central pressures of less than 980 mbar are included in the analysis. Figure 12 presents the variation of *B* as separate linear functions of the *RMW*, Δp, latitude (ψ) and the mean sea surface temperature T_s. It is clear from the data presented in Figure 12 that *B* decreases with increasing *RMW* and increasing latitude. A weak positive correlation of *B* with Δp is seen as is a weak positive correlation with sea surface temperature.

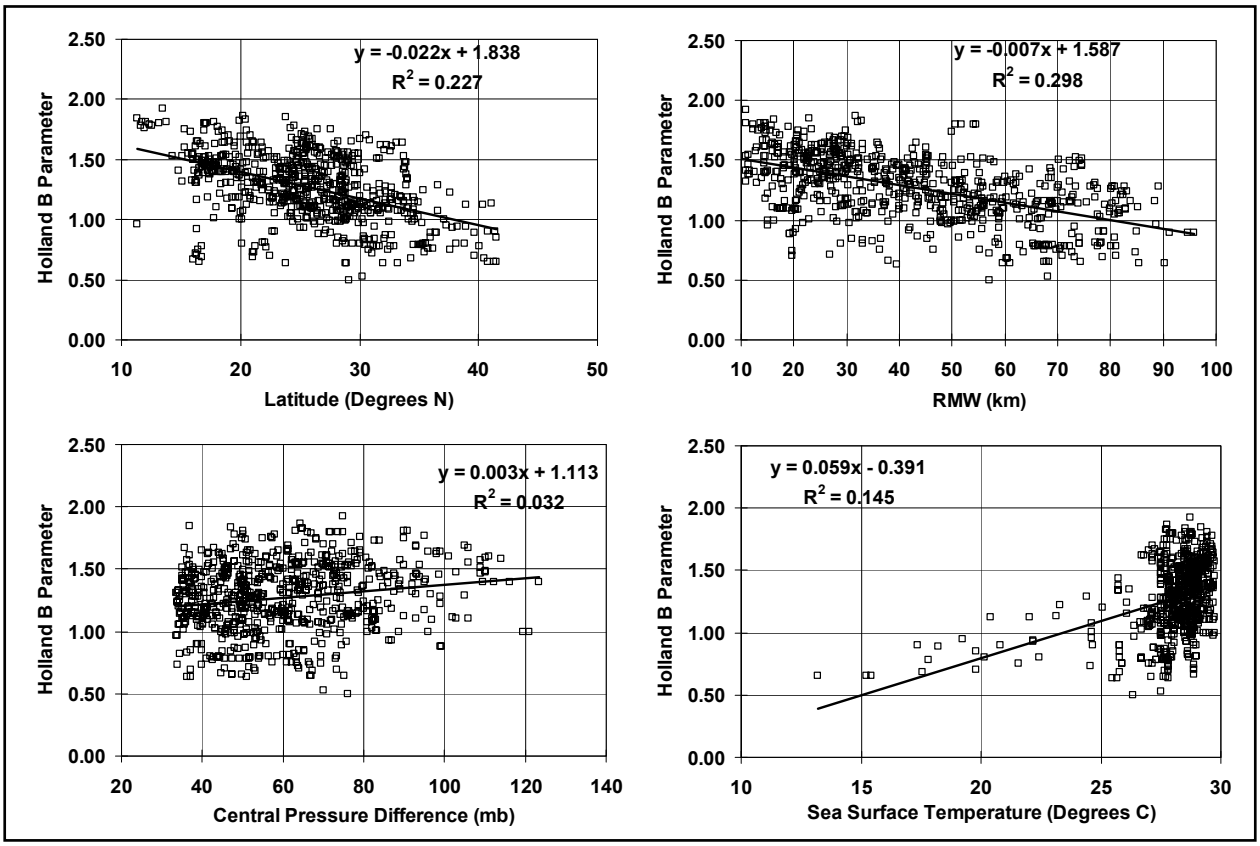

Figure 12. Relationships between the Holland *B* parameter, latitude, *RMW*, Δp, and T_s

In order to incorporate the effects of *RMW*, Δp, latitude (ψ) and T_s into a single model, new non-dimensional variable, *A*, was developed defined as:

$$A = \frac{RMW \cdot f_c}{\sqrt{2R_d T_s \cdot \ln\left(1 + \frac{\Delta p}{P_c \cdot e}\right)}} \tag{9}$$

The numerator of *A* is the product of the *RMW* (in meters) and the Coriolis force, defined as $2\Omega\sin\varphi$ and represents the contribution to angular velocity associated with the coriolis force. The denominator of *A* is an estimate of the maximum potential intensity of a hurricane. From Emanuel (1988), the maximum wind speed in a tropical cyclone is:

$$V_{\max} = \sqrt{2R_d T_s \ln\left[\frac{p_{\max}}{p_c}\right]} \tag{10}$$

where $V_{\max}$ is the maximum wind speed, R_d is the gas constant for dry air, $p_{\max}$ is the pressure at r=*RMW*, T_s is the sea surface temperature in degrees K and p_c is the pressure at the storm center.

Using Holland's Equation it can be shown that

$$\frac{p_{\max}}{p_c} = 1 + \frac{\Delta p}{p_c e} \tag{11}$$

Hence, both the numerator and denominator of *A* have the units of velocity, and thus *A*, is non-dimensional. Modeling *B* as a function of the square root of A yields a linear model (Figure 13) with *B* negatively correlated with $\sqrt{A}$ and has an r^2 of 0.34, with a the standard deviation of the error equal to 0.225. The relationship between *B* and $\sqrt{A}$ is expressed as:

$$B = 1.732 - 2.237\sqrt{A}\,; \quad r^2 = 0.336,\ \sigma_B = 0.225 \tag{12}$$

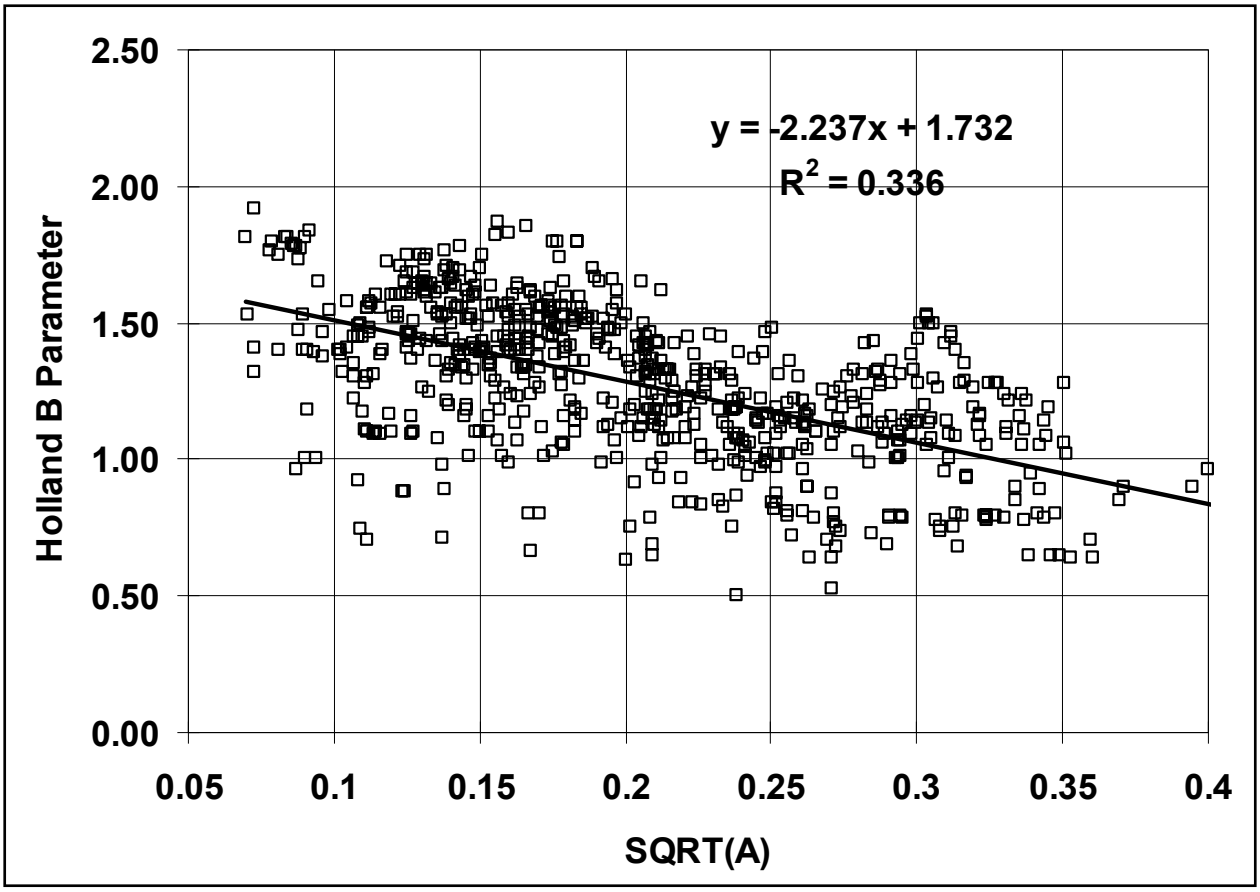

Figure 13. Relationship between the Holland *B* parameter dimensionless parameter, *A*.

In order to determine if the relationship between *B* and *A* is valid for intense storms, the point values of *B* and the model values of *B* were plotted as a function of *RMW* for strong hurricanes (i.e. storms with a central pressure of < 930 mbar) as shown in Figure 14. The data presented in Figure 14 indicates that in the case of strong storms with large *RMW* (*RMW* > 40 km) the relationship between *B* and *A* described earlier breaks down, with the true values of *B* being less than those predicted by the model. Although only two storms with large *RMW* and low central pressures exist in the data analyzed (Hurricane Katrina in the Gulf of Mexico and Hurricane Floyd in the Atlantic), the data indicate that the likelihood of a storm with a central pressure less than 930 mbar, a *RMW* greater than 40 km, combined with a *B* value greater than about 1.1 is remote. The mean value of *B* for these large, strong hurricanes is 1.01, and the estimated standard deviation is 0.082. In cases where these strong storms are simulated, *B* should be constrained to lie within the range of 0.85 to 1.18 (i.e. mean ±2σ).

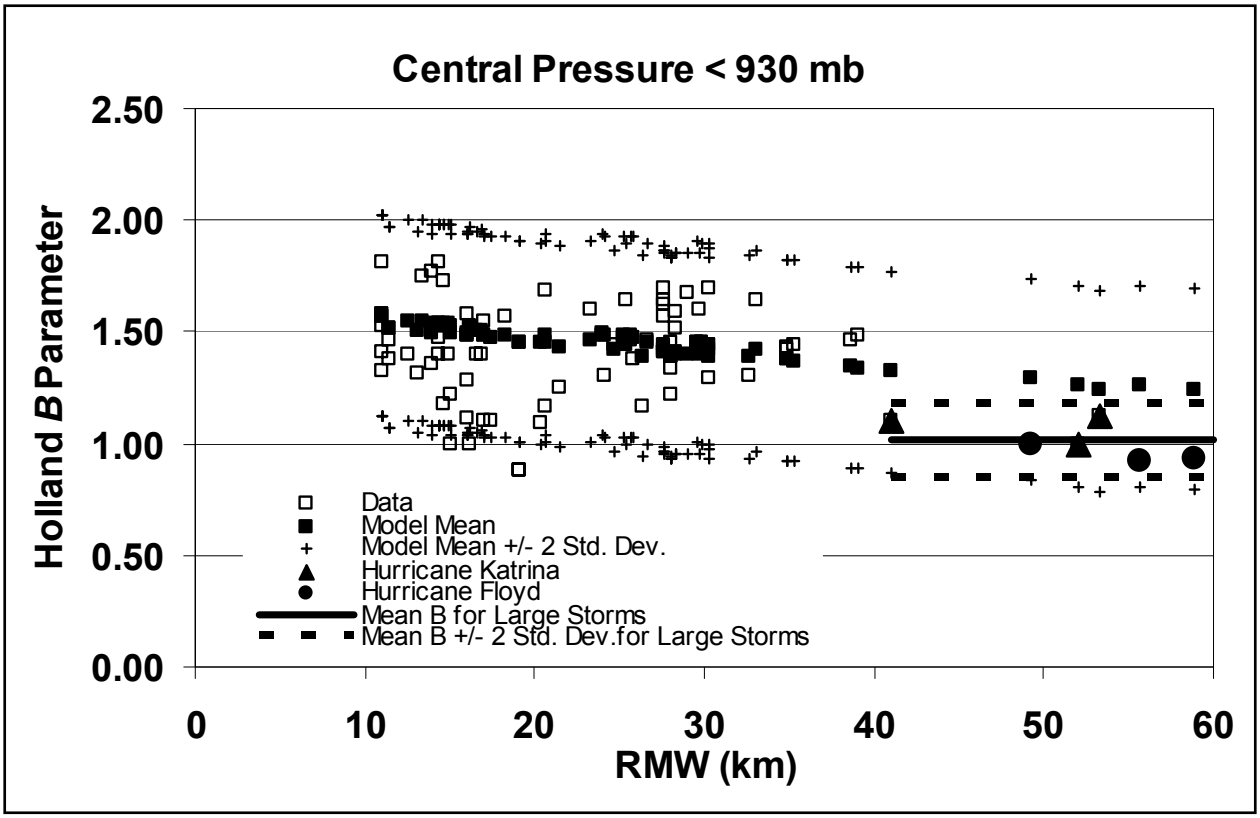

Figure 14. Holland *B* parameter vs. *RMW* for storms with central pressure < 930 mbar

As in the case of the analysis of Gulf of Mexico (GoM) hurricanes with respect to the behavior of *RMW* with Δp and latitude, *B* values for all hurricanes within the Gulf of Mexico were extracted and analyzed alone. Unlike the results seen for the *RMW* where the GoM hurricanes were found to be smaller than the other hurricanes, the variation of *B* with *A* for the GoM hurricanes is essentially identical to that seen in the all hurricane case. Figure 15 presents the individual *B* values for the GoM and Atlantic hurricanes along with the model predicted mean values of *B* where it is clearly evident that there is, for practical purposes, no difference in the variation of *B* with *A* between the two regions.

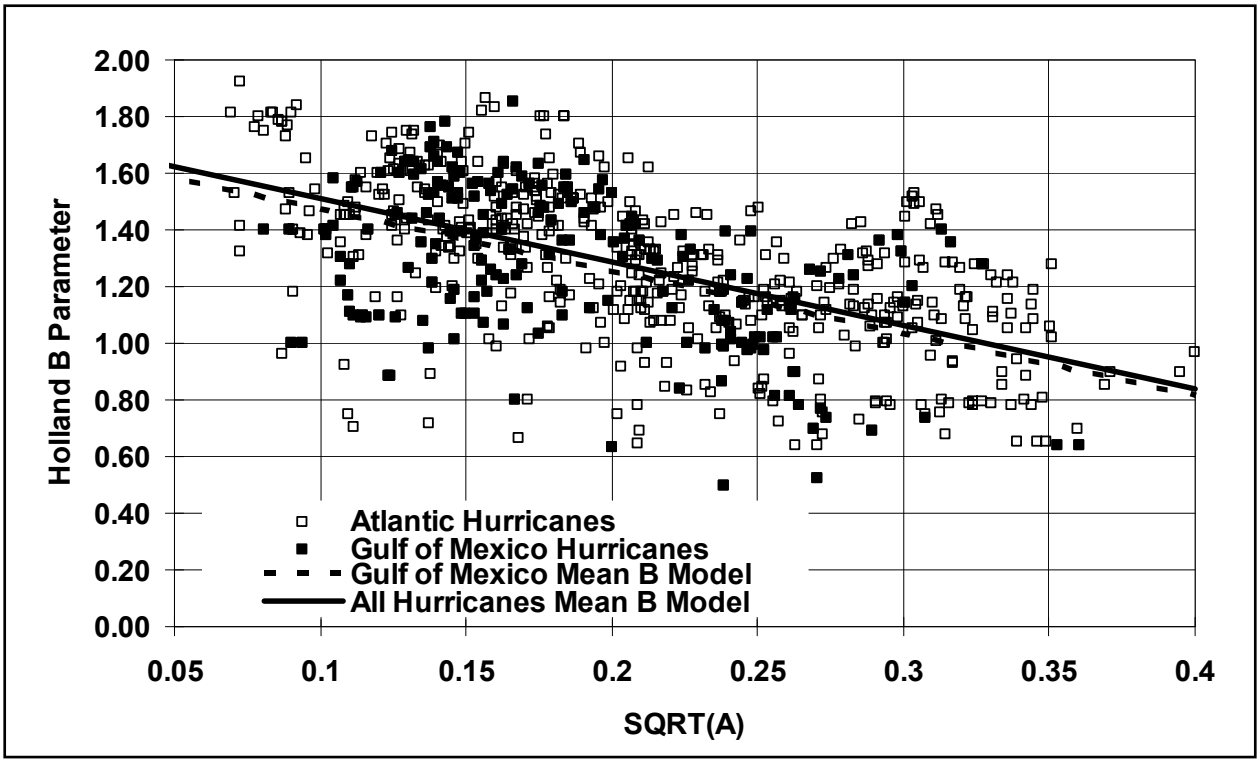

Figure 15. Relationship between the Holland *B* parameter and the dimensionless parameter, *A,* comparing the all hurricane data with the GoM hurricane data.

Note that two simpler, but less elegant models, relating *B* with *RMW* and latitude were examined modeling *B* as a function of $f_c RMW$ and *B* as a function of $\sqrt{C}$, where *C* is defined as:

$$C = \frac{RMW \cdot \sin\psi}{\sqrt{T_s \cdot \ln\left(1 + \frac{\Delta p}{P_c \cdot e}\right)}} \tag{13}$$

Where in Equation (13) T_s is expressed in degrees C rather than degrees K.

The regression model relating *B* to $\sqrt{C}$ is given in the form:

$$B = 1.756 - 0.194\sqrt{C}\,; \quad r^2 = 0.368,\ \sigma_B = 0.220 \tag{14}$$

The regression model relating *B* to $f_c RMW$ is given in the form:

$$B = 1.793 - 0.326\sqrt{f_c RMW}\,; \quad r^2 = 0.357,\ \sigma_B = 0.221 \tag{15}$$

Both of these models yield marginally improved r^2 values than does the model relating B to the non-dimensional relative intensity parameter, but have the small disadvantage in that the independent variable is not non-dimensional. The limitations of these models when applied to large intense storms are the same as those evident in the case of the non-dimensional model. The reduction the r^2 value seen when changing the independent variable in the non-dimensional parameter given in Equation (9) to the dimensional parameter given in Equation (13) is due solely to the conversion of the sea surface temperature from degrees C (Equation 13) to degrees K (Equation 9). For practical purpose, any of the three linear regression models given in Equations 12, 14 or 15 can be used to model the Holland B parameter, with Equation 15 requiring the least computational effort.

Comparisons of Flight Level *B* Values with Landfall Analysis *B* Values

Figure 16 presents a comparison of the Holland B parameters derived from the flight level data to those used in the wind field model described in Vickery, et al. (2007) used for estimating the wind speeds associated with land falling storms. Overall, the comparisons indicate that the two values of B are similar, with the B values used within the windfield model in post storm analyses being slightly lower that those derived from the flight level data. The largest difference between the two estimates of the Holland B parameter occurs in the case of Hurricane Erin for the landfall along the Florida Panhandle.

Figure 17 presents the same information as Figure 16, but is limited to hurricanes with central pressures of 964 mbar or less. The comparisons indicate that the B values used within the hurricane wind field model to match the surface observations of wind speeds and pressures is about 7% less than those derived from the flight level data. This difference could be due to either changes in the characteristics of the pressure field between the 700 mbar level and the surface, or biases in the windfield model. Note that a 7% reduction in B corresponds to approximately a 3.5% reduction in the maximum modeled wind speed. However, comparisons of modeled and observed peak gust wind speeds and time series of the surface level pressures suggests that there is no such bias in the wind model.

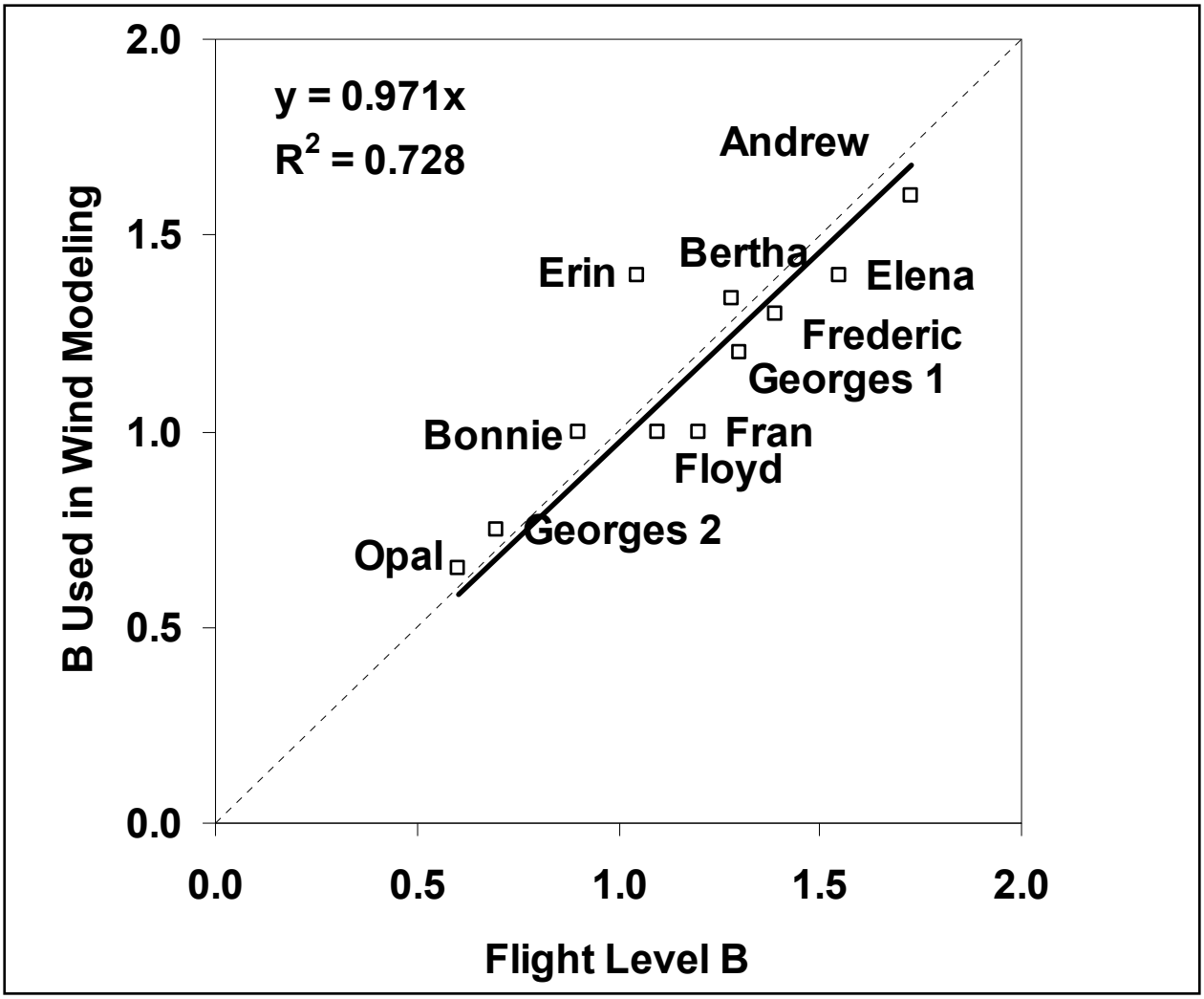

Figure 16. Comparison of Holland *B* parameters derived from flight level data to those derived using a post landfall windfield analysis.

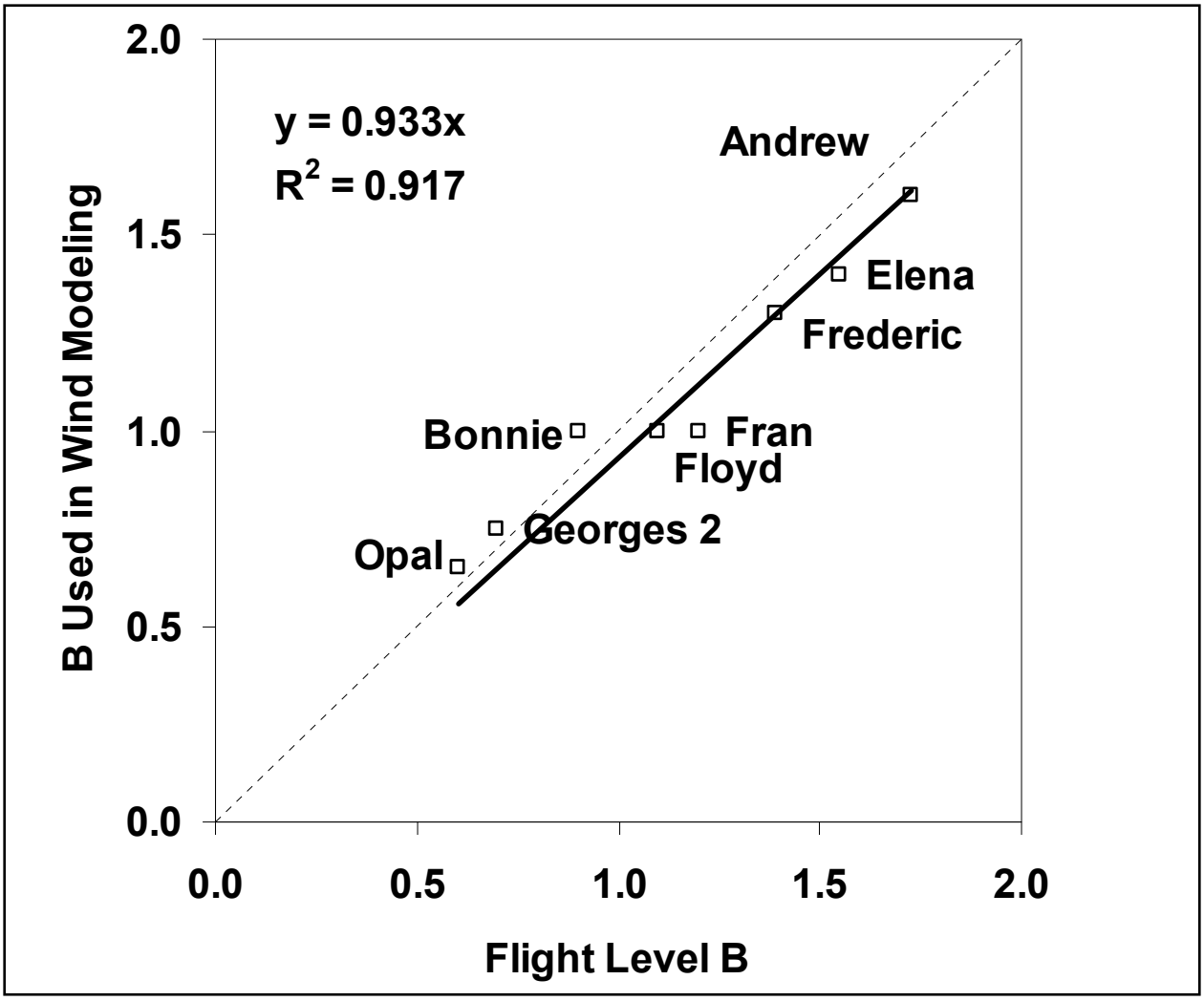

Figure 17. Comparison of Holland *B* parameters derived from flight level data to those derived using a post landfall windfield analysis for hurricanes with central pressures <= 964 mbar.

Summary

The Holland pressure profile parameter, *B*, was found to decrease with increasing latitude and increase with decreasing *RMW*. A weak positive correlation between *B* and both Δp and sea surface temperature was also observed. The effect of all four of these parameters was accounted for by defining a new non-dimensional parameter, *A*, defined by Equation 12, however; a two parameter model (with dimensions) relating *B* to the *RMW* and the coriolis parameter is an equally good predictor of *B*.

The limited data for large (as defined by *RMW*) hurricanes, having low central pressures (p_c<930 mbar) indicates that *B* has an upper limit of ~1.2. The relationship between *B* and *A* was found to be the same in the Atlantic Basin and in the Gulf of Mexico.

A qualitative examination of the characteristics of intense hurricanes making landfall along the coast of the Gulf of Mexico (excluding Southwest Florida) suggests that these hurricanes

weaken in the last 6 – 24 hours, with this weakening characterized by an increase in the central pressure, and increase in the radius to maximum winds and a decrease in the Holland *B* parameter. The reason for this weakening is beyond the scope of this investigation.

The few cases where flight level data were available up to the time a hurricane makes landfall indicates that in most cases, *B*, tends to decrease as the hurricane approaches land. Recognizing that the data set is limited, this observation suggests that using the statistical model for *B* derived using open ocean (or open Gulf) data may result in an overestimate of *B* for landfalling storms. This potential overestimate of the magnitude of the Holland *B* parameter along the Gulf Coast associated with the use of a statistical model developed using open water hurricane data may be further exaggerated because of the decrease in the Holland *B* parameter just before landfall observed in the limited number of landfalling cases examined.

Appendix F of R2007
Integration Method

There are several ways that one could approach the integration of the storm probabilities within the JPM. Each of these can be justified under a particular set of assumptions. Three of these will be discussed here; but before we proceed to examine these, a brief overview of the integration procedure is in order.

The integration is performed by summing discretized probabilities to approximate equation 6 in the main text of this white paper (with ε now included within the same probability function as the other five parameters), i.e.

$$F(\eta) = \sum\sum....\sum p(c_p, R_{\max}, v_f, \theta_l, x, \varepsilon) H[\Psi(c_p, R_{\max}, v_f, \theta_l, x) - \eta + \varepsilon] \Delta(c_p, R_{\max}, v_f, \theta_l, x, \varepsilon)$$

where

$F(\eta)$ is the CDF for surge levels (η)

$p(c_p, R_{\max}, v_f, \theta_l, x, \varepsilon)$ is the probability density function for the multivariate set of parameters;

H[z] is the Heaviside function (=1 if z ≥ 0, = 0, otherwise);

$\Psi(c_p, R_{\max}, v_f, \theta_l, x)$ is the result of the numerical simulation for a particular parameter combination;

$\Delta(c_p, R_{\max}, v_f, \theta_l, x, \varepsilon)$ is the increment of parameter space encapsulated within a discritization.

F1.

There are three primary aspects of this equation that contribute to the accuracy of approximations to $F(\eta)$:

1. The accuracy in the specification of $p(c_p, R_{\max}, v_f, \theta_l, x, \varepsilon)$;

2. The accuracy in the numerical simulations, $\Psi(c_p, R_{\max}, v_f, \theta_l, x)$; and

3. The influence of the discretization size on the approximation.

The first two of these are fairly intuitive, but the third is often more difficult to explain and quantify, since the size of the discrete increments required for a given accuracy is dependent on the behavior of the probability function itself. We shall now proceed to examine three approaches to the integration.

1. The Case of Simple Models Combined with Many Simulations

One approach to estimating coastal hazards would be to utilize simple models with many, many simulations. In this context, one could discretize the each parameter in the hurricane parameterization considered here (c_p, $R_{\max}$, v_f, θ_l, x) and even add some additional probabilistic attributes to the storms (for example: variations in the Holland B parameter, variable storm decay during approach to the coast, suite of variations in offshore storm tracks associated with

each landfalling storm, etc.). Given n parameters with m categories used to represent each parameter, n^m simulations would be required in this approach. For example, for the five-dimensional representation, with 5 categories in each parameter, 3125 simulations would be required to populate the JPM integral.

This approach would produce a very accurate discretization of the probability function; however, inaccuracies in the simulations do not vanish by simply increasing the number of simulations. For example, if simplified models predict values that are 30% too high or too low at a given point along the coast for the portion of the parameter space that contains the primary contribution to surges at the 1 $F(\eta) = 0.01$ level (the range of the nominal "100-year" surge event), no increase in the number of simulations will converge to the correct answer for this range, nor will the addition of uncertainty make the error vanish.

For the case of wind fields, Vickery *et al.* (2002) have shown that a parametric wind field approach, which includes physical effects captured within an accurate planetary boundary layer model, can provide reasonable representations of wind speeds in coastal areas. This method also allows many simulations to be run and, therefore, represents a good application of this type of approach. Coastal surge generation requires that wave fields, direct wind-driven surges, and the interaction between these two driving mechanisms be modeled correctly. Parametric wave models for hurricanes have been known to be quite inaccurate for a number of years and are not used by any major wave modeling group in the world today, even in offshore areas. In nearshore areas, refraction, wave breaking, sheltering and other physical mechanisms cannot be captured by parametric models. Also, surge models such as ADCIRC include much improved capabilities for depicting critical shallow-water physics and for representing small-scale coastal features. Because of this, the methodology described in the main text, which relies on state of the art models to ensure unbiased estimates of coastal surges is recommended; however, it is practical limitations related to computer run time (even on the largest supercomputers available today) presently preclude the execution of multiple thousands of runs using this complete prediction system.

2. The Case of Optimized Category Definition

Given that *a priori* information is available for the variation and co-variation of the variables used in the probability function, as well as for the sensitivity of coastal surges to variations in each of the variables, it is possible to construct an optimized set of discrete samples to simulate surges from the overall multivariate distribution. This approach is presently under development by Toro for applications within FEMA Region 4. As shown in Figure 7c in the main text, Toro's independent check on the pressure distribution used here showed very good agreement. Similarly, preliminary comparisons between the two statistical methods appear to show good agreement for JPM applications.

3. The Case of Structured Interpolation on a Response Surface

Numerical studies using ADCIRC have shown that coastal surge response is very dependent on pressure differential (peripheral pressure minus central pressure), storm size (R_{max}), and storm

location relative to a site, as discussed in Appendix D. Storm surge is less sensitive to forward storm speed and angle of the storm relative to the coast. Figure F1 shows the characteristic variation of surge elevations at coastal stations as a function of variations in pressure differential ($p_0 - c_p$), based on SLOSH tests along the coast of Mississippi. As noted in Appendix B, the maximum wind speed in a slowly varying, stationary hurricane can be approximated as

$$U_{\max} = \left(\frac{B}{\rho_a e} \right)^{1/2} (\Delta P)^{1/2}$$

where

B is the Holland B parameter;

ρ_a is the density of air;

e is natural logarithm base (= 2.718...); and

ΔP is the pressure differential between the storm periphery and its center.

Since surges tend to be proportional to the wind stress, which for a capped coefficient of drag is proportional to the wind speed squared, it follows that the linear relationship between ΔP and surge is consistent with our theoretical expectation for this relationship.

Since a major portion of the surge response to hurricanes is captured by the variation of Δ_P and R_p, the integration method selected for application here is based on the estimation of $\Delta_P - R_p$ planes within the 5 dimensional parameter space used in the JPM. Thus, for a fixed value of storm landfall location (x), storm track angle relative to the coast (θ_l), and storm speed (v_f), we can define a response function,

$$\eta_{\max}(x, y) = \phi_{kmn}(\Delta P, R_p, x, y) \qquad \text{F2.}$$

where φ_{kmn} is the surge response function and the subscripts "k, m and n" denote a specific track angle, storm speed, and landfall location, respectively. This notation reflects the fact that this response function must be defined for each spatial (x, y) point in the computations. Figure F2 shows an example of such a response function. As expected, the surge values increase essentially linearly with increasing pressure differential and also increase with increasing values of R_p.

Figures F3 and F4 show the characteristic variations of coastal surges as a function of storm angle relative to the coast (θ_l) and forward storm speed (v_f), respectively. As can be seen here, the variations tend to be quite smooth with either linear or slightly curved slopes in these figures. The JPM integration method employed here makes use of the "smoothness" of these functions to interpolate between discretized storm parameters.

An advantage of the approach used here is that the surge response is characterized with some level of detail in the important $\Delta P - R_p$ plane. To drive the relevance of this point home, let us examine the effects of discretization on a probability integral along the "pressure-differential"

axis. Given the linear variation of surge elevation with pressure differential, surge elevation can been written as

$$\eta = \lambda \Delta p \qquad \text{F3.}$$

where λ is a site-specific constant, and hence

$$F(\eta) = F(\lambda \Delta p) \qquad \text{F4.}$$

If we assume that the pressure differential probability follows a Gumbel distribution, we can calculate this probability directly. Figure F5 shows a comparison of the CDF's for three different approximations to the return period as a function of surge level, given the value of $\lambda = 0.2$ in equation F4 (just for an example here). As can be seen in this figure, for a fixed return period deviations between the 3-category approximation (categories with a width of 30-millibars) and the continuous function can be as large as ±3.0 feet. For the 3-millibar categories, the deviations are, as expected, only about ±0.3 feet. Although this pattern will be smoothed and obscured by the addition of many categories of storms, it is clear that the smaller categories provide an improved representation for the probabilities. Also, due to the physical basis for the pressure differential scaling used here, we can extrapolate to larger storms than those actually utilized in the storms. This will provide a somewhat conservative estimate if there is substantial levee overtopping; but since the level of extrapolation used here is only about 18% (ΔP = 113 mb to ΔP = 133 mb), this should not present a serious problem.

In this approach, we do not treat the set of 9 storms simulated for a given track, forward storm speed, and track angle as a discrete set of storms each with its own associated probability increment, since this would give only a relatively crude representation of the actual probability structure. Instead, we interpolate between simulated values and extrapolate over relatively short distances in Δp and ($R_{\max}$). For the integration used in the New Orleans area, the 3 Δp and 3$R_{\max}$ values were interpolated to increments of 1-mile in $R_{\max}$ and 3 millibars in Δp, over the range of 960 mb to 882 mb for offshore pressures (i.e. before they begin to decay) and 5 nm to 40 nm for $R_{\max}$ values. This provides a very smooth response surface for the primary storm tracks in this area (the so-called RICK-fan tracks). For the ±45-degree tracks, the 2 values of Δp and $R_{\max}$ are likewise used to develop a finely discretized (1 nm by 3 mb) set of values over the Δp-$R_{\max}$ plane. At this point, we have finely discretized categorizations within the Δp-$R_{\max}$ plane for the five primary (RICK-fan) tracks and the eight additional ±45-degree tracks. Thus, we have a set of response functions [φ_{kmn} (ΔP, R_p, x, y)] that are quite well defined for the central storm speed (11 knots) for these tracks.

Since the effect of variations in storm speed is fairly small and tends to have fairly linear slopes that are roughly independent of ($R_{\max}$) and Δp, only a small number of storms can be used to modify the functional form of [φ_{kmn} (ΔP, R_p, x, y)] as a function of forward storm speed. This retains the overall structure of the response function for the alternative speeds, rather than assigning only a single surge value to all the responses for that storm speed. For the New Orleans area, two storms (with different combinations of Δp and $R_{\max}$) were used to estimate the impact of a slower storm speed on the surge response function [φ_{kmn} (ΔP, R_p, x, y)] compared to the

primary (central) speed category (11 knots) for the RICK-fan set of tracks. Single storms were also used to estimate the impact of varying the forward speed from 11 knots to 6 knots, along the ±45-degree tracks and to estimate the effects of varying the forward speed from 11 knots to 17 knots for all storms. In the approach used here, the value of [φ_{kmn} (ΔP, R_p, x, y)] for different speeds is obtained from the relationship

$$\phi_{kmn}(\Delta P, R_p, x, y) = \phi_{k_0 m_0 n}(\Delta P, R_p, x, y)\Psi_{kmn}(\Delta P, R_p, x, y)$$

where

The subcript "0" refers to the central speed and angle categories

for a specific landfall location; and

$$\Psi_{kmn}(\Delta P, R_p, x, y) = \frac{\partial \phi_{kmn}(\Delta P, R_p, x, y)}{\partial v_f}\delta v_f$$

For the cases in which a single storm is used to infer the variation with forward speed Ψ_{kmn} (ΔP, R_p, x, y) reduces to a constant.

This now provides a suitable set of interpolated, finely-discretized values of surge heights as a function of Δp and $R_{\max}$ for all forward storm speeds, storm angles and storm tracks and the summation in Equation F1 can be rewritten as

$$F(\eta) = \sum\sum....\sum p(\Delta p_i, R_{\max_j}, v_{f_k}, \theta_{l_l}, x_m, \varepsilon_n)H[\Lambda(\Delta p_i, R_{\max_j}, v_{f_k}, \theta_{l_l}, x_m) - \eta + \varepsilon]\Delta(\Delta p_i, R_{\max_j}, v_{f_k}, \theta_{l_l}, x_m, \varepsilon_n)$$

where

F(η) is the CDF for surge levels (η)

$p(\Delta p_i, R_{\max_j}, v_{f_k}, \theta_{l_l}, x_m, \varepsilon_n)$ is the probability density function for the multivariate set of parameters;

H[z] is the Heaviside function (=1 if z ≥ 0, = 0, otherwise);

$\Lambda(\Delta p_i, R_{\max_j}, v_{f_k}, \theta_{l_l}, x_m)$ is the interpolated value between simulations with a particular parameter combination;

$\Delta(\Delta p_i, R_{\max_j}, v_{f_k}, \theta_{l_l}, x_m, \varepsilon_n)$ is the increment of parameter space encapsulated within a discretized category.

One concern addressed briefly in Appendix D is the sensitivity of the probability estimates to track spacing. The sufficiency of the spacing used here can be investigated by comparing results from the runs on the set of tracks that fell between the 5 major RICK-fan tracks to results of interpolations based on only the 5 initial tracks. Figures F6-F9 show the results of these comparisons. In general little or no bias is introduced into the probability integration, even if only the information from the primary tracks is used. Only at Track 4a, where the sites are switching from the “right-hand” (onshore winds) side of the storm to the “left-hand” (offshore winds) side of the storm in the are east of the Mississippi River does the variability exceed 10% of the surge values for surges greater than 10 feet.

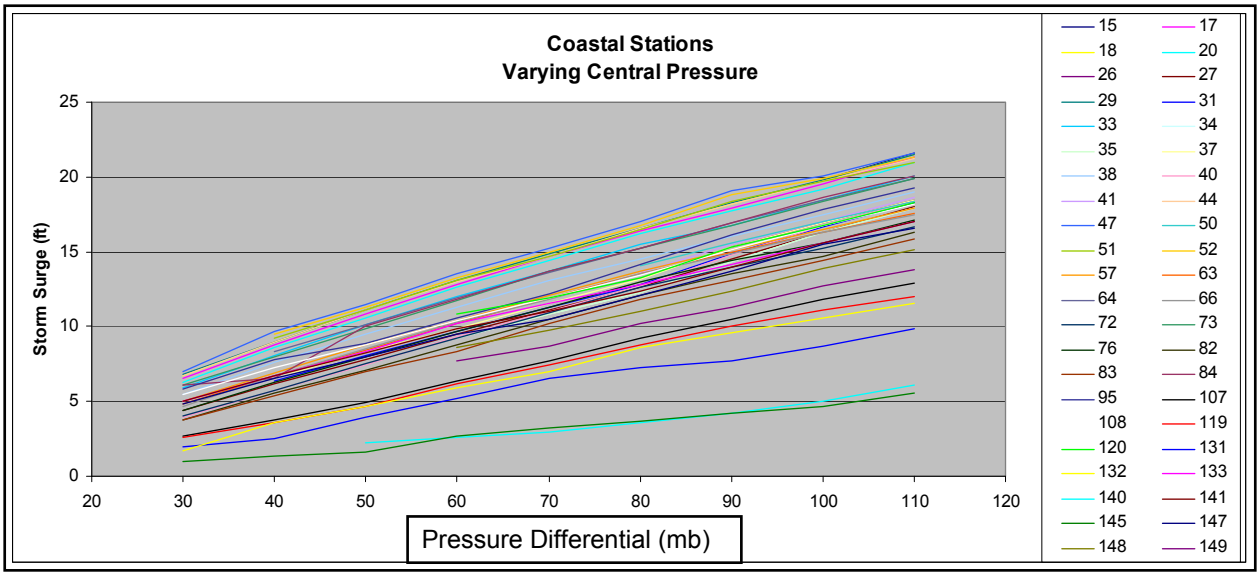

Figure F1. Surge levels (feet) at coastal stations (Station Numbers denoted on right hand side of chart) along Mississippi coast as a function of pressure differential (mb).

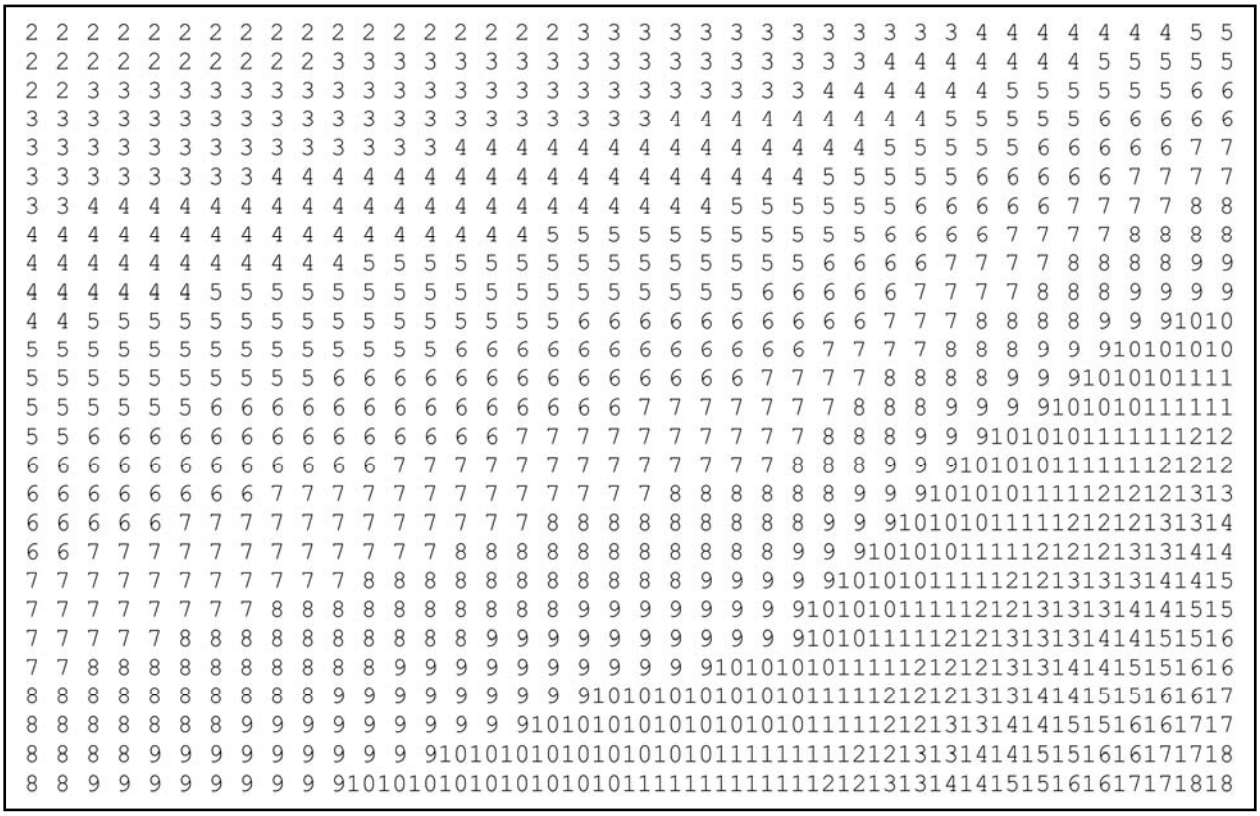

Figure F2. Response surface showing integerized surge values in feet as a function of row from top to bottom (ΔP from 53 to 133 mb in increments of 3 mb) and column from left to right (R_p from 1 nm to 40 nm in increments of 1 nm).

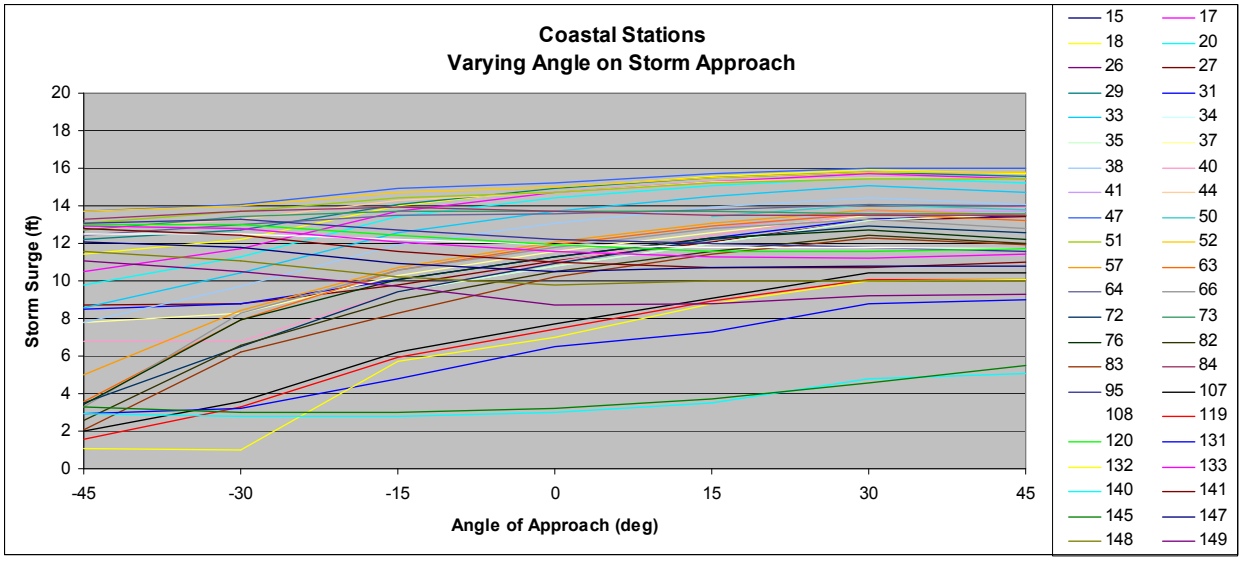

Figure F3. Surge levels (feet) at coastal stations (Station Numbers denoted on right hand side of chart) along Mississippi coast as a function of angle of storm approach to land.

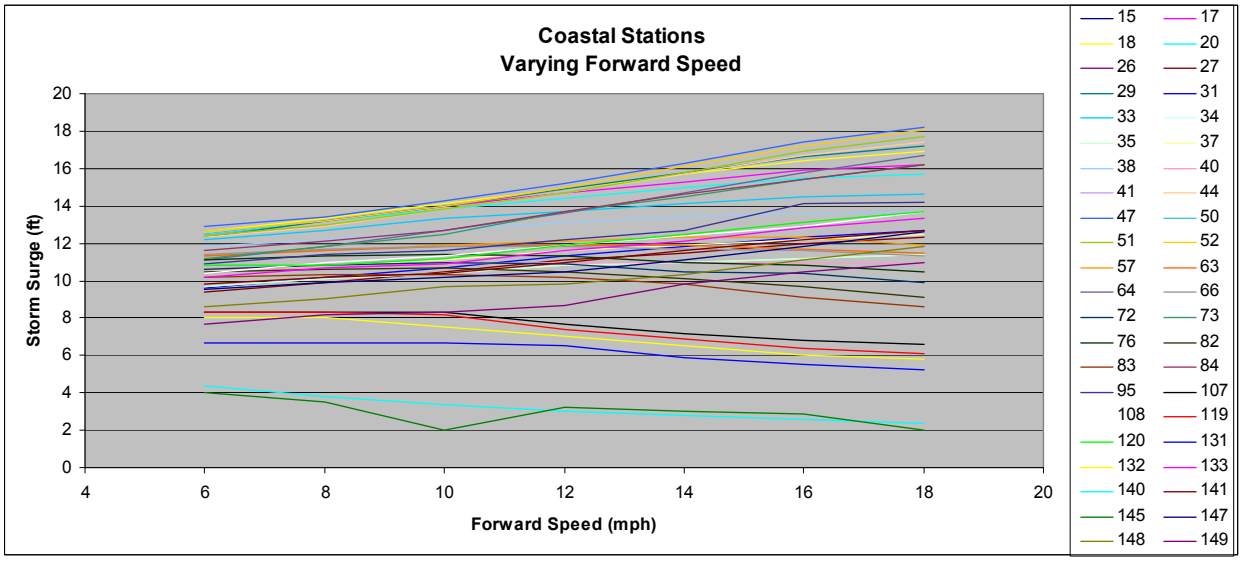

Figure F4. Surge levels (feet) at coastal stations (Station Numbers denoted on right hand side of chart) along Mississippi coast as a function of forward speed of storm (mph).

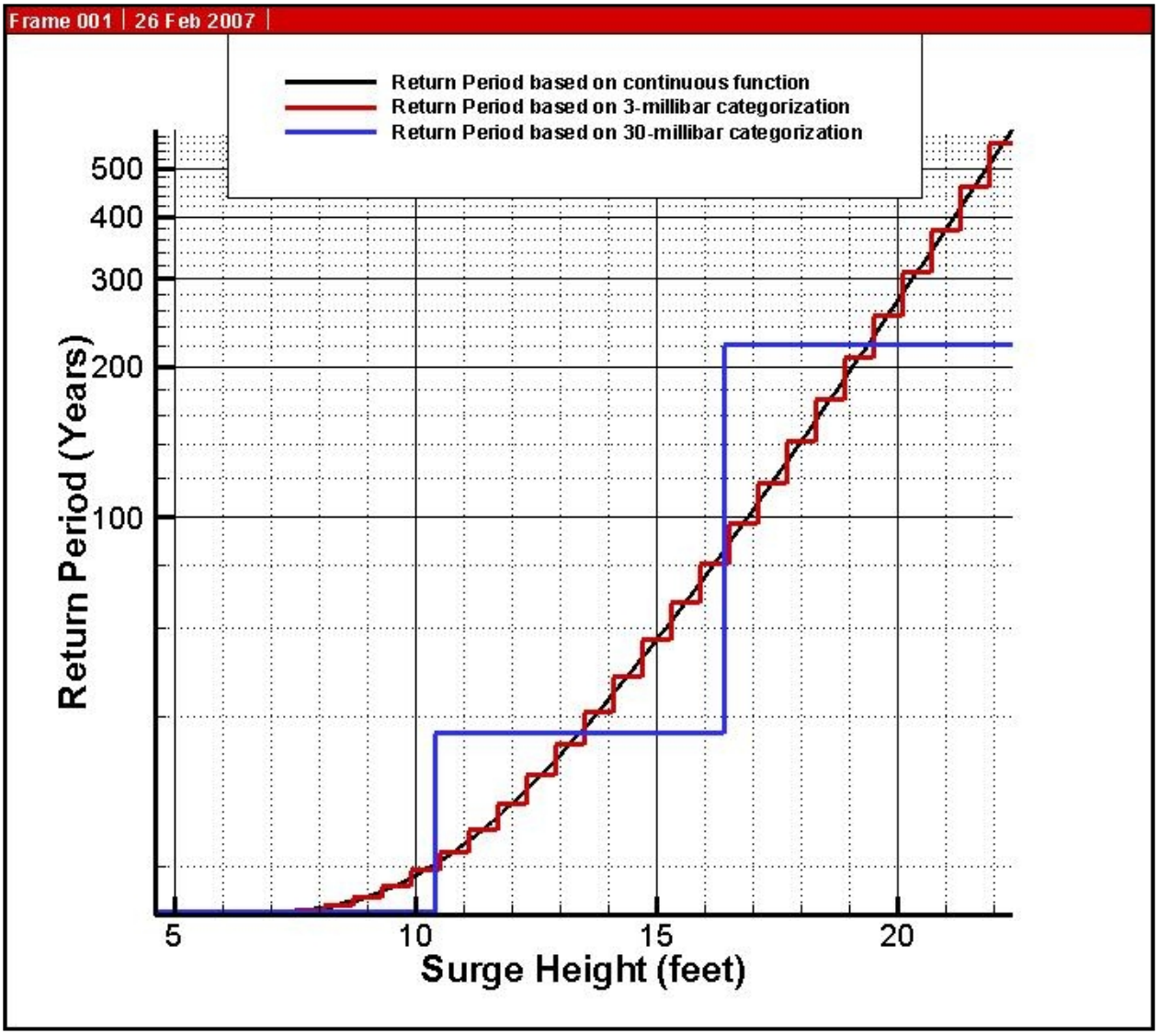

Figure F5. Comparison of Return Periods for surges estimated from 3-millibar and 30-millibar categories compared to a continuous function.

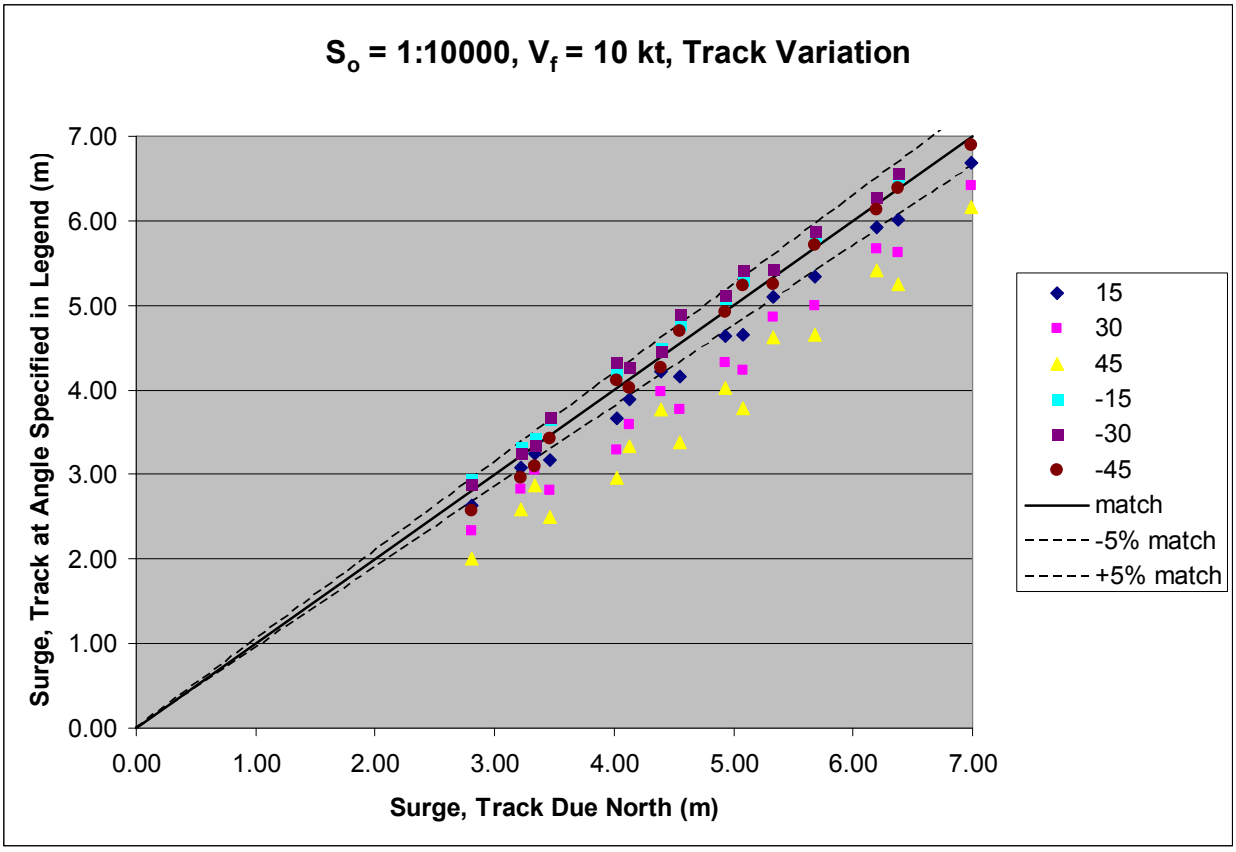

Figure F6. Maximum surges produced along a straight east-west coast by storms approaching the coast at variable angles compared to storms approaching perpendicular to the coast (tracking due north).

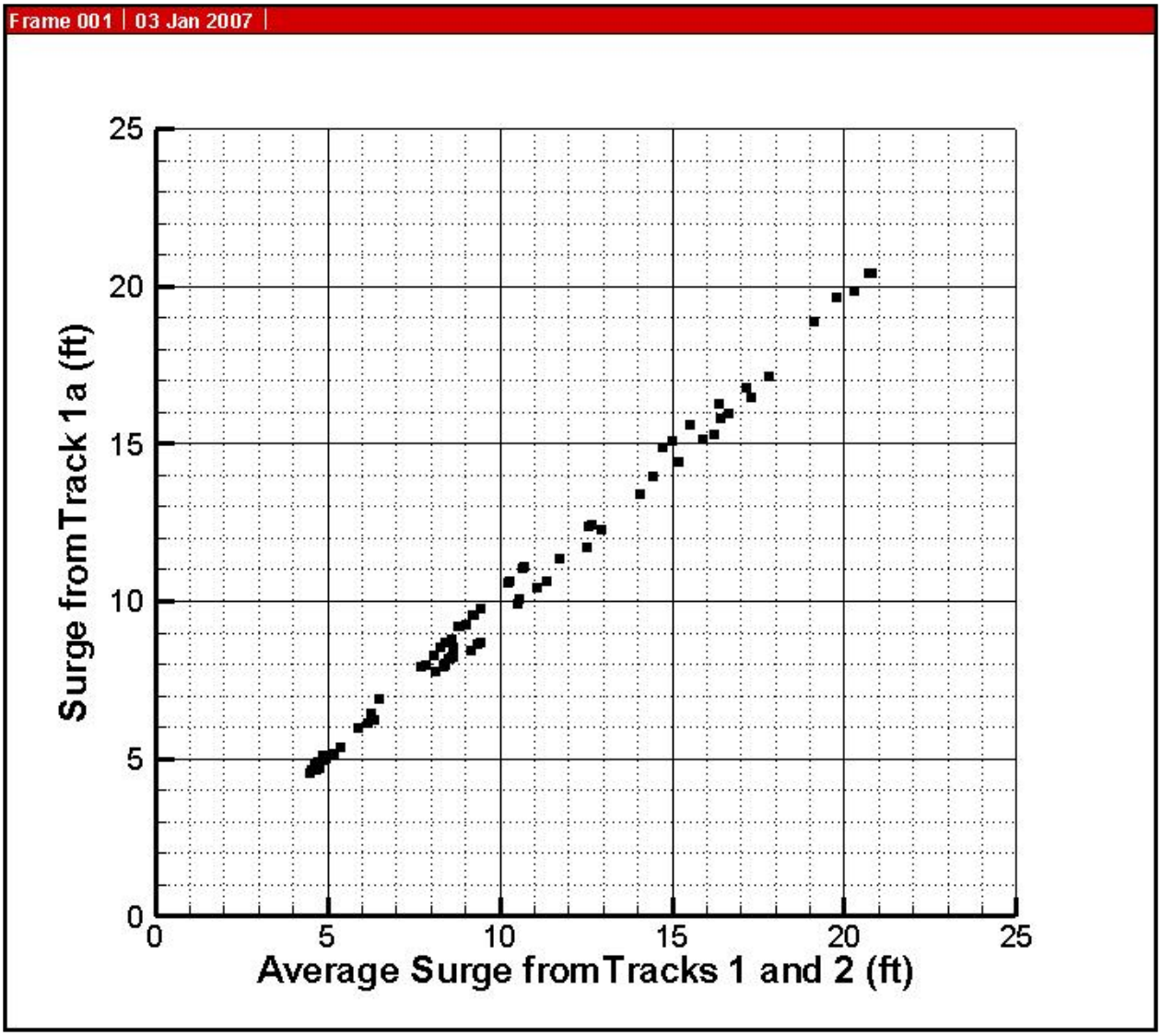

Figure F7. Comparison of results from Track 1a (midway between Tracks 1 and 2) to interpolated values using information from Tracks 1 and 2 for a set of points spread throughout the entire New Orleans region.

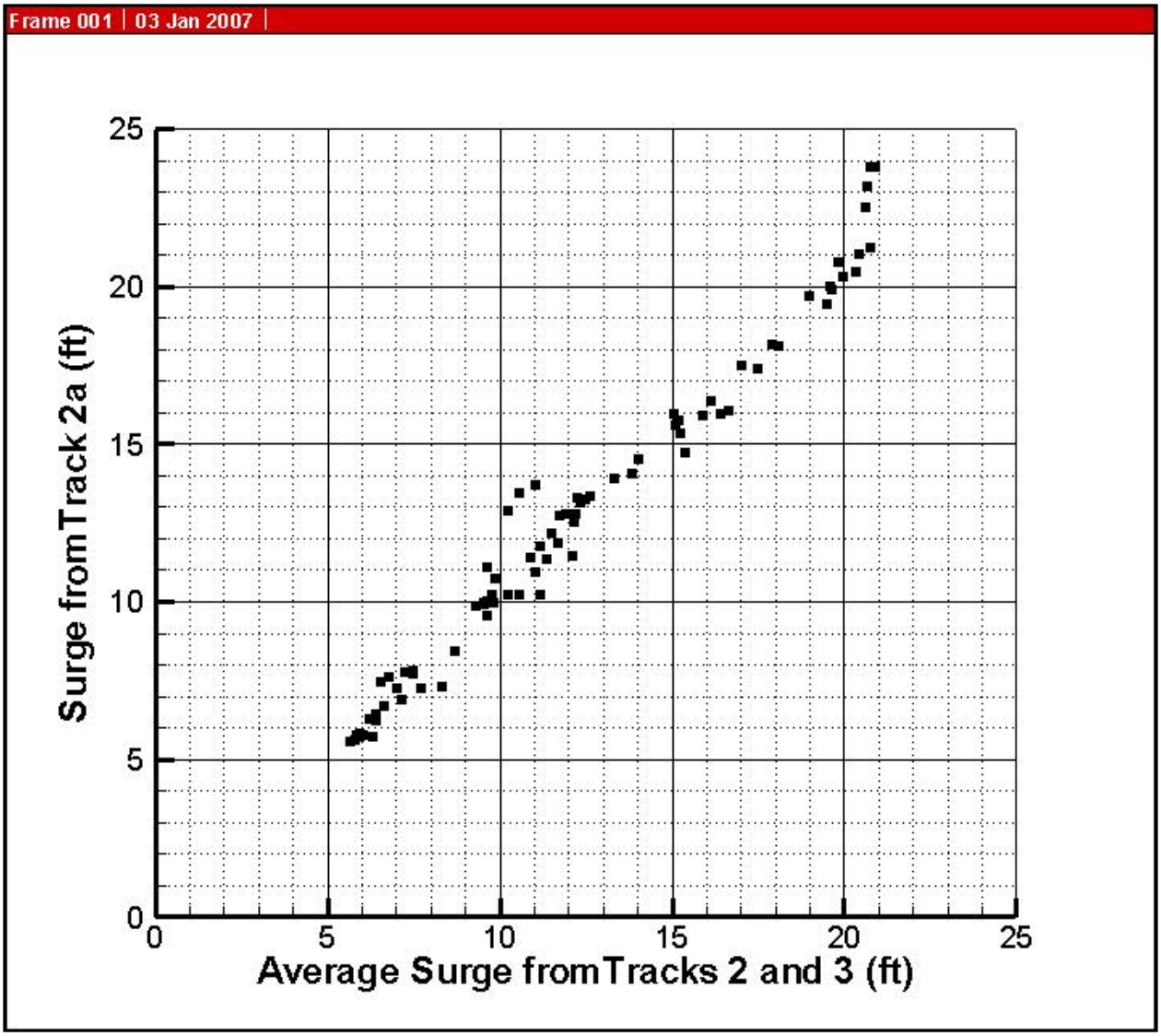

Figure F8. Comparison of results from Track 2a (midway between Tracks 2 and 3) to interpolated values using information from Tracks 2 and 3 for a set of points spread throughout the entire New Orleans region.

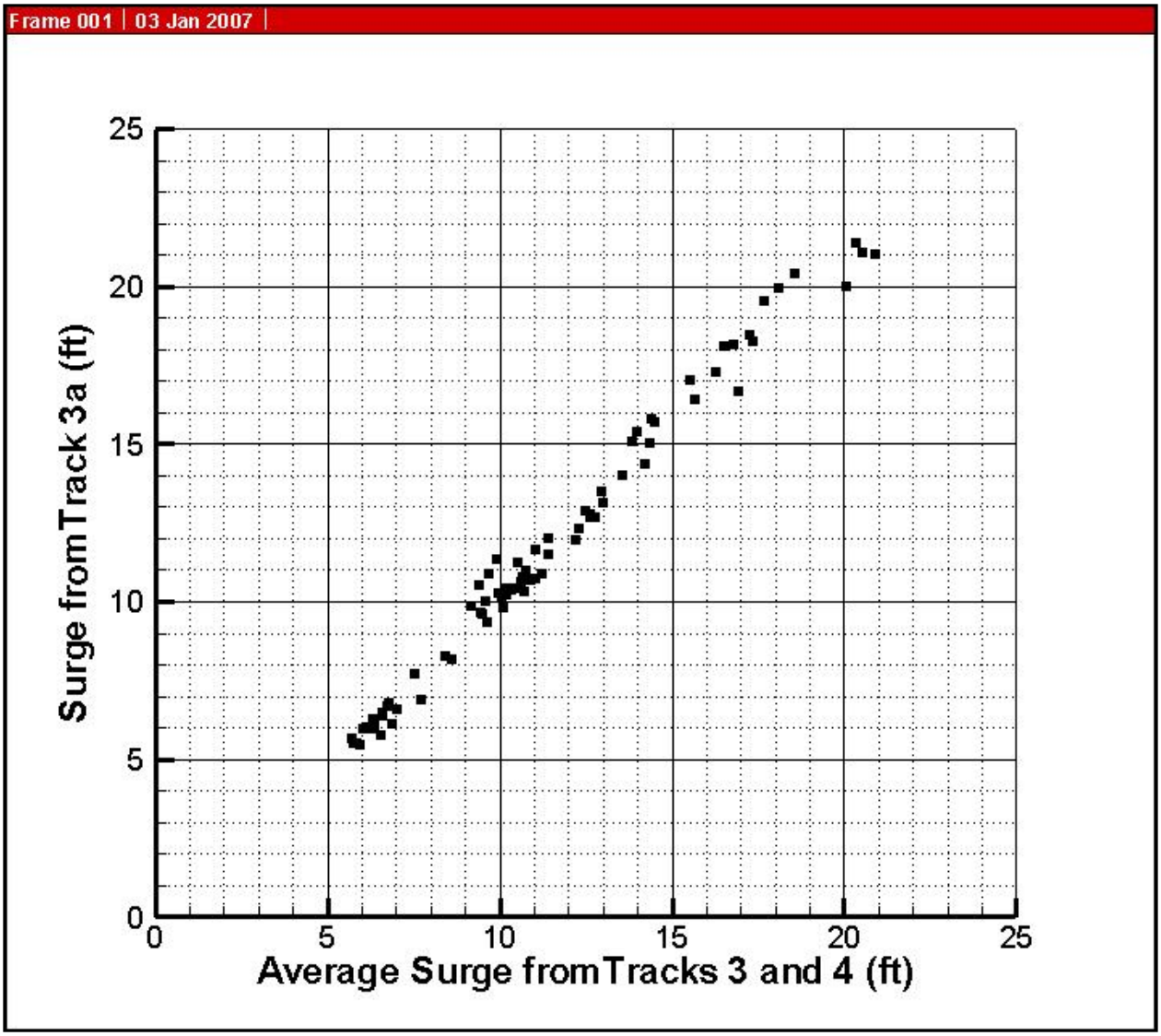

Figure F9. Comparison of results from Track 3a (midway between Tracks 3 and 4) to interpolated values using information from Tracks 3 and 4 for a set of points spread throughout the entire New Orleans region.

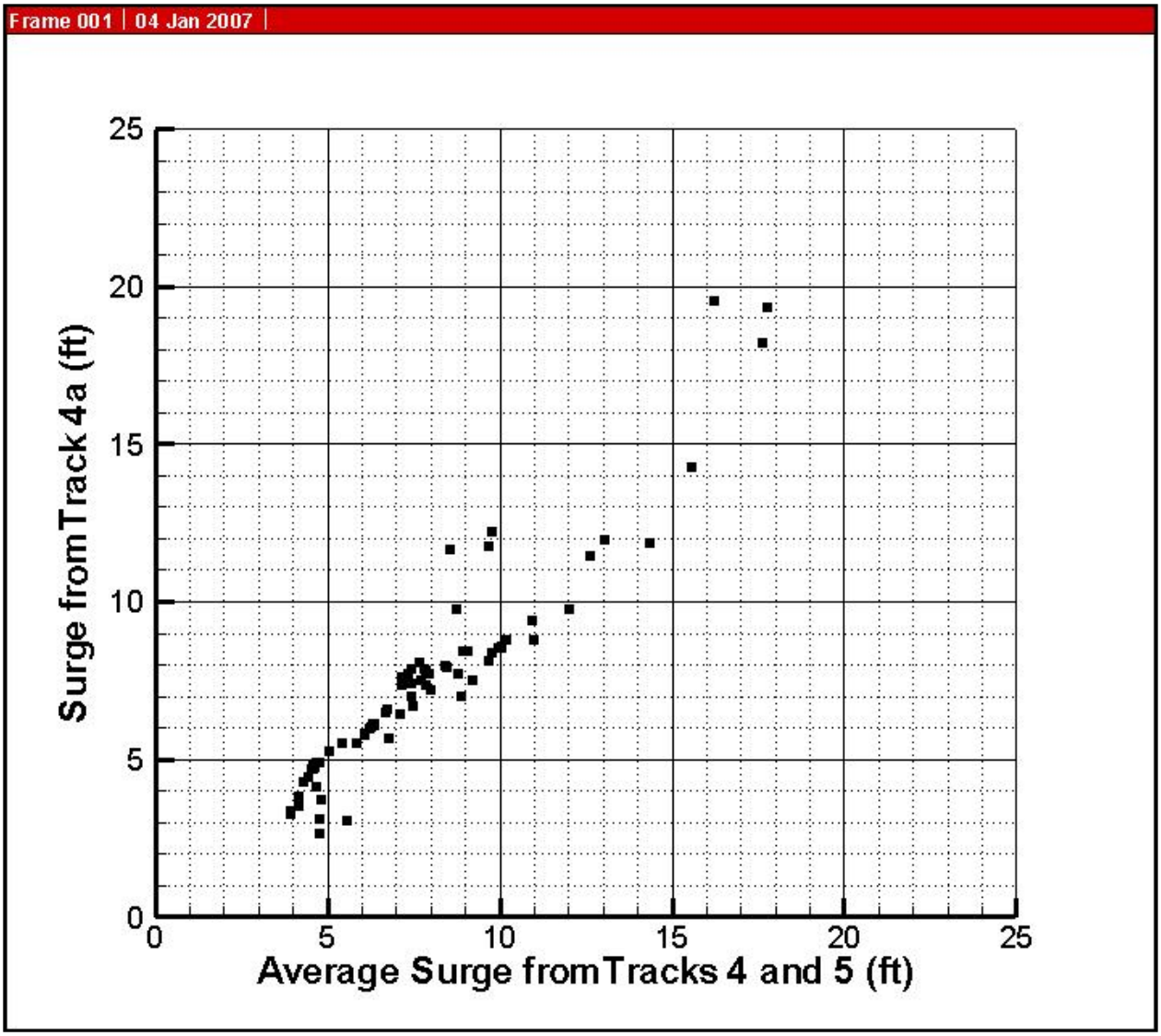

Figure F9. Comparison of results from Track 4a (midway between Tracks 4 and 5) to interpolated values using information from Tracks 4 and 5 for a set of points spread throughout the entire New Orleans region.

Appendix G of R2007
Estimation of Confidence Bands for Surge Estimates

Three main types of uncertainty with respect to the estimation of extremes are relevant to understanding hurricane hazards along coasts. First, there is uncertainty that the actual sample of storms is representative of the "true" climatology today. Second, there is uncertainty in the events within future intervals of time, even if the "true" climatology is known exactly. And, third, there is uncertainty that some non-stationary process (sea level rise, subsidence, climate change, new development patterns, man-made alterations to the coasts, marsh degradation, etc.) will affect future hazards. The first of these has traditionally been addressed via sampling theory. The second can be addressed via re-sampling or "bootstrap" methods. And, the third must be estimated from ancillary information, often not contained within the initial hazard estimates themselves.

The first type of uncertainty listed above pertains to what used to be termed confidence bands (or control curves) for estimates of extremes. It cannot be estimated using re-sampling techniques, since these techniques use the initial sample as the basis for their re-sampling and implicitly assume that the initial sample represents the actual population characteristics. Thus, some parametric method must be used to obtain this information. There are many classes of distributions which can be used to fit the data. Since we are only using the parametric fits to estimate uncertainty and not to replace the non-parametric estimates obtained from the JPM, we are somewhat free to use any distribution for which the sampling uncertainty is known. Gringorten (1962, 1963) has shown that the expected root-mean-square (rms) error of an estimated return period in a two-parameter Fisher-Tippett Type I (Gumbel, 1959) distribution is given by

G1.

$$\sigma_T = \sigma\sqrt{\frac{1.1000y^2 + 1.1396y + 1}{N}}$$

where

σ is the distribution standard deviation;

σ_T is the rms error at return period, T;

N is the number of samples used to estimate the distribution parameters; and

y is the reduced Gumbel variate given by

$$y = (\eta - a_0) / a_1;$$

η is the variate of interest (surge level in this case); and

a_0 and a_1 are the parameters of the Gumbel distribution.

The reduced variate and return period are related by

$$y = -\ln\left[\ln\left(\frac{T}{T-1}\right)\right] \qquad \text{G2.}$$

which for T >7 approaches an exponential form given by

$$\left(T - \frac{1}{2}\right) \rightarrow e^{y} \qquad \text{G3.}$$

Equation G1 shows that the rms error at a fixed return period is related to the distribution standard deviation and the square root of a nondimensional factor involving the ratio of different powers of y (y^2, y^1, and y^0) to the number of samples used to define the parameters. By the method of moments, the Gumbel parameters can be show to be given by

$$a_0 = \gamma a_1 - \mu \qquad a_1 = \frac{\sqrt{6}}{\pi}\sigma \qquad \text{G4.}$$

where γ is Euler's constant (= 0.57721...) and μ is the distribution mean.

Thus, the distribution standard deviation is related to the slope of the line represented by equation G3.

Although equation G1 was initially derived for applications to annual maxima, it can be adapted to any time interval for data sampling in a straightforward manner. For the case of hurricanes, the average interval between storms (the inverse of the Poisson frequency used in the compound Gumbel-Poisson distribution) can be used to transform equation G1 into the form

$$\sigma'_T = \sigma\sqrt{\frac{1.1000y'^2 + 1.1396y' + 1}{N'}}$$

where

σ is the distribution standard deviation; G5.

σ'_T is the rms error at return period, T′

(T/$\hat{T}$, where $\hat{T}$ is the average years between hurricanes); and

N′ is the number of samples used to estimate the distribution parameters (N/$\hat{T}$).

Since the form of equation G3 is logarithmic, the slope is not affected by a multiplicative factor, and thus, the distribution standard deviation remains the same. N' in equation G5 can be estimated from the equivalent total number of years in the sample divided by $\hat{T}$. The total number of years for this case is 65 (1941-2005, inclusive) times a factor, Z, which relates the spatial area covered by the sample used to the spatial extent of a hurricane surge. For relatively intense storms capable of producing surges that are exceeded only every 100 years or more, the along-coast extent of very high surges at least 60% of the peak value is about 60 nm for a storm

with a 20-nm radius to maximum winds (se Figure D4 in Appendix D). The parameter estimation used to derive the values shown in Figure 5 of the main text covered ±3.5 degrees longitude along 29.5 north latitude. The value of Z is given by

$$Z = \frac{\text{Distance along coast}}{\text{Width of a single sample}} \qquad \text{G6.}$$

which in this case is 365.5 nm divided by 60 nm, or approximately 6.1. Thus, the effective number of years is 396.

Appendix 8-3
Rainfall Analysis

Rainfall Intensity

Rainfall is an additional mechanism that contributes to the inundation of the sub-basins. While rainfall is not of primary concern for the hurricane protection system, it is a contributor to the frequency of low-level flood losses. Hence it was decided that a relatively coarse model of hurricane-induced rainfall would suffice.

Prior to NASA's Tropical Rainfall Measuring Mission (TRMM) (Simpson et al., 1988), information on hurricane rainfall was scanty. The TRMM mission, which started in November 1997, produced significant rainfall data for tropical storms and hurricanes at a spatial scale of about 5 km in various tropical regions, including the Atlantic basin. These rainfall products have been analyzed statistically by Lonfat et al. (2004) and Chen et al. (2006). The model proposed below is based primarily on those two studies and on discussions with Dr. Shuyi Chen at the University of Miami.

Mean Rainfall Intensity

Hurricane rainfall intensity I (mm/hr) varies with distance r from the hurricane center and azimuth β relative to the direction of motion. Moreover, the mean intensity field $m_I(r, \beta)$ varies with the central pressure deficit ΔP, the radius of maximum winds R_{max}, the storm velocity V, and the vertical wind shear S (in the above quoted references, S is measured as the difference between the horizontal wind fields at the 200 and 850 hPa levels). Finally, rainfall intensity displays strong fluctuations at different scales around the mean value $m_I(r, \beta)$.

The azimuthal average of $m_I(r, \beta)$, $m_I(r)$, gives the symmetrical component of the mean rainfall field. This component has a maximum at a distance from the hurricane center close to R_{max} and decays in an approximately exponential way at larger distances. This decay is contributed by the approximately exponential decay of both the fraction of rainy area and the mean rainfall intensity at the rainy locations. The rate of exponential decay $m_I(r)$ is inversely proportional to the size of the hurricane; hence, in good approximation, it is inversely proportional to R_{max}.

The value of $m_I(r)$ for $r = R_{max}$ increases with increasing ΔP, approximately doubling from a Cat2 to a Cat4-5 event. Considering the Cat12 and CAT3-5 results in Lonfat et al. (2004) as representative of the Cat1-2 boundary and of Cat4, respectively, assuming linear dependence of the mean rainfall intensity at R_{max} on Δp, and fitting an exponential decay with distance as mentioned above, one obtains

$$m_I(r) = \begin{cases} 1.14 + 0.12\Delta P, & for\ r \le R_{\max} \\ (1.14 + 0.12\Delta P)\, e^{-0.3\left(\frac{r - R_{\max}}{R_{\max}}\right)}, & for\ r > R_{\max} \end{cases} \quad (10)$$

where m_I is in mm/h and ΔP is in mb.

The asymmetric component of the mean rainfall field, i.e. the way $m_I(r, \beta)$ depends on the azimuth β, is affected mainly by the storm velocity V and the vertical wind shear S. This influence is complex, as the asymmetric pattern and its strength vary with the absolute and relative values of V and S, the relative direction of wind shear and storm motion, the distance r from the center, and the geographic location. For hurricanes in the Atlantic region, there is a general tendency for rainfall to intensify in the front-east quadrant relative to the direction of storm motion and de-intensify in the rear-west quadrant. This tendency is especially evident for fast-moving storms and away from the hurricane center, reaching about 30-40% of $m_I(r)$ for $r \approx 3R_{\max}$. The effect is stronger over land than over water.

Variability of Rainfall Intensity

For each TRMM observation of each hurricane, Lonfat et al. (2004) extracted the average rainfall intensity $\overline{I}^+(r, r+10)$ at rainy locations inside annular regions of 10 km width. Using these values, they found the empirical distribution of $\overline{I}^+(r, r+10)$ for different r and different storm intensity classes. A consistent result is that $\overline{I}^+(r, r+10)$ varies by a factor of about 7 above and below the median value. The standard deviation of $\log\left(\overline{I}^+(r, r+10)\right)$ corresponds to a factor of about 2-2.5. Hence the variability of this average rainfall intensity is very large.

In addition, there is variability in the fraction of rainy area. The latter variability is not given in Lonfat et al. (2004), but it can be bounded and roughly estimated as follows. The mean fraction of rainy area, m_{F+}, is given by Lonfat et al. as a function of r and storm intensity range. Given m_{F+}, an upper bound to the variance of F^+ is obtained by assuming that F^+ is either 0 (no rain in the region) or 1 (it rains everywhere in the region). In this case $Var\left[F^+\right] = m_{F^+}\left(1 - m_{F^+}\right)$, with a coefficient of variation $V_{F^+} = \sqrt{\frac{1}{m_{F^+}} - 1}$. A more realistic estimate of the coefficient of variation is perhaps one half of this theoretical upper bound, or

$$V_{F^+} \approx 0.5\sqrt{\frac{1}{m_{F^+}} - 1} \quad (11)$$

For distances r up to 150 km, which are those that contribute the most to intense rainfall, m_{F+} is around 0.9 irrespective of hurricane intensity and Eq. 11 gives $V_{F+} \approx 0.17$. This coefficient of

variation is much smaller than the coefficient of variation of rainfall intensity inside the rainy area, which is on the order of 1.0. Therefore, the variability of the rainy area may be neglected.

Assessment of Rainfall Intensity inside the Sub-basins

Based on the above considerations, the following simplified model of rainfall inside the sub-basins was adopted. First, the mean rainfall contribution from the symmetric component of the mean rain field, $m_I(r)$ is specified; then the asymmetric component is discussed, and finally an assessment of the variability of rainfall around the mean is given.

Denote by $m_{I_k}(r,t)$ the temporal variation of $m_I(r)$ for hurricane k (in this model, temporal variation is due to the variations of ΔP). The contribution of $m_{I_k}(r,t)$ to the mean rainfall intensity in subbasin j is evaluated as $m_{I_k}\left(r_{jk}(t),t\right)$, where $r_{jk}(t)$ is the distance to a representative point of subbasin j from the center of hurricane k at time t. The appropriate distance was taken to be the instantaneous distance between the eye of the storm and the centroid of the subbasin.

For hurricanes that pass to the right or near the subbasin, one may conservatively neglect the azimuthal dependence of the rainfall field. For hurricanes that pass to the left of the sub-basin centroid, the asymmetric component has been accounted for by multiplying the above symmetric mean rainfall values by 1.5. This factor includes intensification due to land effects.

Uncertainty may be expressed by a lognormal random variable with mean value 1 and log standard deviation 0.69, which corresponds to an uncertainty factor of 2. This random factor should be applied to the entire mean rainfall time history. In reality, rainfall intensity inside a subbasin would display significant fluctuations in time and space, which locally could far exceed a factor of 2. However, the above random factor should adequately reflect uncertainty on the total precipitation in a sub-basin during the passage of a hurricane.